

**PIECES TO THE PUZZLE OF
HIGH-REDSHIFT GALAXIES FALLING
INTO PLACE**

STEFAN JOHANNES GEIER

**DISSERTATION
SUBMITTED FOR THE DEGREE**

PHILOSOPHIÆ DOCTOR

**DARK COSMOLOGY CENTRE
NIELS BOHR INSTITUTE
THE PHD SCHOOL OF SCIENCE
FACULTY OF SCIENCE**

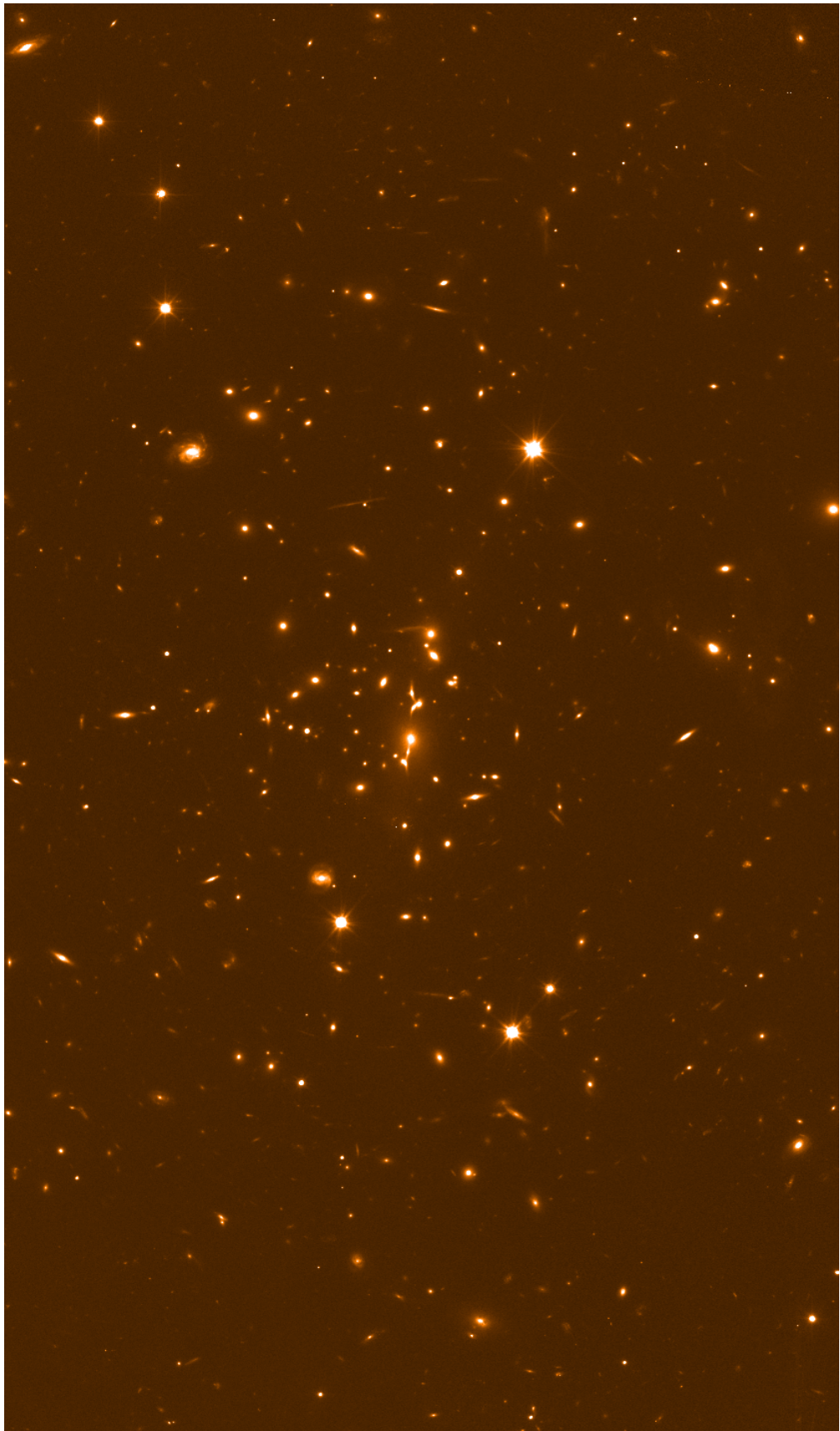
UNIVERSITY OF COPENHAGEN

Submission: *September 3rd, 2013*

Defense: *December 2nd, 2013*

Supervisor: *Prof. Johan Peter Uldall Fynbo*

Opponents: *Prof. Emanuele Daddi*
Prof. Páll Jakobsson



The picture on the previous page is a composite of images of the strong lensing cluster MACSJ2129-0741, taken with the Hubble Space Telescope in 17 filters ranging from UV to NIR. It shows one of the “biggest telescopes” in the Universe, so-to-say.

CONTENTS

Contents	v
Abbreviations and Acronyms	ix
List of Figures	xi
List of Tables	xvii
Acknowledgments	xix
Abstract	xxi
Abstrakt	xxiii
1 Introduction	1
1.1 Structure formation in the universe since the Big Bang	3
1.2 Cosmology	5
1.3 Dark Matter and the build-up of structure	7
1.4 Classification and morphologies of galaxies	8
1.4.1 Active Galactic Nuclei and Quasars	11
1.5 Damped Lyman α Absorbers	13
1.6 Galaxy formation	16
1.6.1 Growth of perturbations	16
1.6.2 Object formation	20
1.6.3 Making real galaxies	22
1.7 Stellar populations as main constituents of galaxies	23
1.8 Gamma Ray Bursts and their host galaxies	29
1.9 Galaxy populations at high redshifts	30
1.10 Gravitational Lensing as a tool to study quiescent high redshift galaxies	32
2 VLT/X-Shooter Near-Infrared Spectroscopy and HST Imaging of Gravitationally-Lensed $z \sim 2$ Compact Quiescent Galaxies	37
2.1 Introduction	37
2.2 Object selection, data reduction and SEDs	40

2.2.1	Target selection	40
2.2.2	Spectroscopic data	41
2.2.3	Spectroscopic Data Reduction	42
2.2.4	Flux calibration, combination and 1d extraction	42
2.2.5	HST imaging data	43
2.2.6	Spitzer imaging data	44
2.3	Data analysis	44
2.3.1	Redshift determination and spectral energy distribution analysis	44
2.3.2	Profile fits to the de-lensed images	48
2.4	Discussion and conclusions	51
2.4.1	Redshifts and derivation of intrinsic magnitudes	51
2.4.2	Constraints on line-fluxes and star formation	51
2.4.3	Stellar population properties	52
2.4.4	Morphologies	53
2.4.5	Stellar masses and sizes	55
2.4.6	Prospects for future detailed studies	57
2.5	Acknowledgments	57
2.6	Appendix material	57
3	The Galaxy Counterparts of the two high-metallicity DLAs towards Q 0918+1636	61
3.1	Introduction	61
3.2	Observations and data reduction	62
3.2.1	HST imaging	62
3.2.2	NOT imaging	63
3.2.3	VLT/X-Shooter spectroscopy	64
3.3	The $z = 2.583$ DLA galaxy	65
3.3.1	HST imaging	65
3.3.2	NOT/Alfosc imaging	66
3.3.3	NOT/NOTCam imaging	68
3.3.4	SED fitting	68
3.3.5	VLT/X-Shooter spectroscopy	70
3.4	The $z = 2.412$ DLA Galaxy	72
3.4.1	Absorption line analysis	72
3.4.2	The galaxy counterpart	73
3.5	Discussion	77
3.5.1	The $z = 2.583$ DLA Galaxy	77
3.5.2	The nature of DLA galaxies	78
3.5.3	Outlook	81
3.6	Acknowledgments	81

4	The metal-enriched host of an energetic γ-ray burst at $z \approx 1.6$	83
4.1	Introduction	84
4.2	Observations and data reduction	86
4.2.1	Space-based imaging	86
4.2.2	Ground-based imaging	87
4.2.3	X-shooter optical/NIR spectroscopy	88
4.3	Results	89
4.3.1	Host galaxy system and afterglow position	89
4.3.2	Emission line profile	90
4.3.3	Host SED	90
4.3.4	Emission line fluxes	91
4.3.5	Balmer decrement	93
4.3.6	Electron density	94
4.3.7	Star-formation rate	94
4.3.8	Metallicity	96
4.4	Discussion	98
4.4.1	The host of GRB 080605 within the sample of GRB hosts	98
4.4.2	Afterglow versus host properties	101
4.4.3	The mass-metallicity relation at $z \sim 2$	101
4.4.4	The non-detection of $\text{Ly}\alpha$	102
4.5	Conclusions	103
4.6	acknowledgements	104
	Coauthorstatements	105
	Coauthorstatements	105
	Bibliography	133

ABBREVIATIONS AND ACRONYMS

2dF	Two Degree Field Galaxy Redshift Survey
ACS	Advanced Camera for Surveys
AGB	Asymptotic Giant Branch
AGN	Active Galactic Nucleus
Alfosc	Andalucia Faint Object Spectrograph and Camera
ALMA	Atacama Large Millimeter Array
CDM	Cold Dark Matter
CMD	Color-Magnitude Diagram
CMB	Cosmic Microwave Background
COBE	COsmic Background Explorer
DEC	Declination
DLA	Damped Lyman α Absorber system
DRG	Distant Red Galaxy
SDSS	Sloan Digital Sky Survey
ESO	European Southern Observatory
EW	Equivalent Width
FoV	Field of View
FWHM	Full Width at Half Maximum
GCN	Gamma-ray Burst Coordinates Network
GMASS	The Galaxy Mass Assembly ultra-deep Spectroscopic Survey
GRB	Gamma-ray Burst
GR	General Relativity
Gyr	Gigayears
HDM	Hot Dark Matter
HRD	Hertzsprung-Russel Diagram
HST	Hubble Space Telescope
IDL	Interactive Data Language (programming language)
IGM	Inter-Galactic Medium
IMF	Initial Mass Function
IRAF	Image Reduction and Analysis Facility (reduction and analysis software)
IR	Infrared
ISAAC	Infrared Spectrometer And Array Camera (IR instrument at VLT)

ISM	Inter-Stellar Medium
kpc	kilo-parsec
NIR	Near-Infrared
LBG	Lyman Break Galaxy
LoCuSS	Local Cluster Substructure Survey
Le PHARE	Photometric Analysis for Redshift Estimate
LIRIS	Longslit Intermediate Resolution Imager and Spectrograph (NIR instrument at WHT)
MACS	MAssive Cluster Survey
mas	milli-arcseconds
MIPS	Multiband Imaging Photometer
MOS	Multi Object Spectroscopy
Mpc	Mega-parsec
MW	Milky Way
Myr	Megayears
NOT	Nordic Optical Telescope (Roque de los Muchachos Observatory, La Palma)
NOTCam	Nordic Optical Telescope Near-Infrared Camera and spectrograph
NTT	New Technology Telescope (La Silla, Chile)
Photo-z	Photometric redshift
PSF	Point Spread Function
QSO	Quasi-stellar Object
RA	Right Ascension
SDSS	Sloan Digital Sky Survey
SED	Spectral Energy Distribution
SFH	Star-formation history
SFR	Star-formation rate
sSFR	Specific star formation rate
S/N	Signal to Noise
SNR	Signal-to-Noise Ratio
SOFI	Son OF ISAAC (NIR instrument at the NTT)
SPSF	Spectral Point Spread Function
SSP	Single stellar population
ToO	Target-of-Opportunity
UT	Universal Time
UV	Ultra-violet
WIRC	Wide field IR Camera (NIR instrument on Palomar 200inch telescope)
WFC3	Wide Field Camera 3
VLA	Very Large Array (New Mexico)
VLT	Very Large Telescope (Paranal/Chile)
WHT	William Herschel Telescope (Roque de los Muchachos Observatory, La Palma)
WMAP	Wilkinson Microwave Anisotropy Probe
z	redshift
Z	metallicity

LIST OF FIGURES

1.1	The map of the anisotropies in the cosmic microwave background, as observed by the Planck satellite.	4
1.2	An illustration how structure grows out of tiny fluctuations.	4
1.3	The relative contributions of baryonic matter, dark matter, and dark energy to the total energy density of the universe, as determined from CMB observations by the Planck satellite.	6
1.4	Left Panel: A sketch illustrating the top-down scenario of structure formation. Right Panel: An illustration of the bottom-up scenario, also called hierarchical structure formation.	8
1.5	The classical Hubble “tuning fork” diagram.	9
1.6	A composite spectrum (de-redshifted to rest-frame wavelengths) combined from low-resolution spectra of QSOs and Seyfert 1s, taken from Meusinger et al. (2003).	12
1.7	The $Ly\alpha$ absorption profiles of the two DLAs imprinted in the spectrum of Q0918+1636 from Fynbo et al. (2013b).	14
1.8	Examples of spectral energy distributions for typical galaxies: An old elliptical galaxy (red line), two types of spiral galaxies (Sb in green and Sd in blue), an AGN (Markarian 231, solid black line), a QSO (dotted black line), and a merging star-bursting galaxy (Arp 220, violet line). The spectra are taken from Polletta et al. (2007).	24
1.9	$J_s - K_s$ colors as a function of redshift for single-age stellar populations with ages of 0.25, 0.5, and 1Gyr are shown as solid lines. It can be seen that the Balmer/4000Å break causes very red colors of $J - K_s > 2.3$ exclusively for $z > 2$. Dotted and dashed lines show models with on-going star-formation with ages of 1Gyr and 100Myr and reddenings of $E_{B-V} = 0.15$ and $E_{B-V} = 0.5$, respectively. The dash-dotted line demonstrates the color evolution of a single-burst stellar population with a formation redshift of $z_f = 5$, which also satisfies the DRG color cut for redshifts $z > 2$. Figure taken from Franx et al. (2003).	32

1.10	HST image of the strong lensing cluster MACS2248 with the overlaid FoV of SOFI (red square) and the 0.5mag magnification contour (green). The inner contours indicate magnifications of 1mag (red), 1.5mag (blue) and 2mag (magenta).	36
2.1	Upper panel: Cutout images of the gravitationally-lensed galaxy A1413-1 in the (WIRC) K_s - and J -bands, and in the HST/ACS F775W band. Lower panel: Cutout images of the gravitationally-lensed galaxy MACS2129-1 in the (ISAAC) K_s - and J -bands, and in the HST/ACS F606W band. .	41
2.2	Upper panel: Spectro-photometric SED of the gravitationally-lensed galaxy A1413-1, together with HST/ACS and Palomar/WIRC photometry. Overplotted is the best-fit BC03 model, a 2.4 Gyr passively evolving population with little dust and a stellar mass of $M_\star = 7.6 \cdot 10^{10} M_\odot$. Lower Panel: Probability distribution of the photometric redshift for A1413-1.	48
2.3	Upper panel: Spectro-photometric SED of the gravitationally-lensed galaxy MACS2129-1. Overplotted in red is the best-fit BC03 model with a Chabrier IMF, a 1.7 Gyr population with a stellar mass of $M_\star = 1.1 \cdot 10^{11} M_\odot$. Lower panel: Probability distribution of the photometric redshift for MACS2129-1.	49
2.4	The 2D and 1D X-Shooter NIR spectrum of A1413-1. We overplot the expected positions of several spectral lines at the redshift of $z = 1.71$. Little black lines above the 1D spectrum indicate skylines. The wavelength regions in the gaps between the J- and H-bands and the H- and K-bands are plotted in grey to avoid distraction by the high noise (and absence of information) there.	52
2.5	The 2D and 1D X-Shooter NIR spectrum of MACS2129-1. We overplot the expected positions of several spectral lines at the redshift of $z = 2.15$. The blue line indicates the error spectrum. Little black lines above the 1D spectrum indicate skylines. The wavelength regions in the gaps between the J- and H-bands and the H- and K-bands are plotted in grey to avoid distraction by the high noise (and absence of information) there.	53
2.6	Left panel: Zoom-in on the wavelength region around the expected position of the $H\alpha$ line in the 2D and 1D spectrum of A1413-1. Right panel: Zoom-in on the wavelength region around the expected position of the $H\alpha$ line in the 2D and 1D spectrum of MACS2129-1. The cutouts show that there is no detectable emission line.	54
2.7	Left panel: The de-lensed image of the gravitationally-lensed distant massive quiescent galaxy A1413-1, reconstructed from the HST F850LP image, based on the derived redshift of $z = 1.71$. Middle panel: A Sersic profile fit to the de-lensed image, obtained with GALFIT. For further information about the fit results, see Table 2.3. Right panel: Residuals from the Sersic fit.	54

2.8	Left panel: The de-lensed image of the gravitationally-lensed distant massive quiescent galaxy MACS2129-1, reconstructed from the HST F160W image, based on the derived redshift of $z = 2.15$. Middle panel: A Sersic profile fit to the de-lensed image, obtained with GALFIT. For further information about the fit results, see Table 2.3. Right panel: Residuals from the Sersic fit. We recognize a bright core, which is not aligned with the disk and leaves a residual. Furthermore, there is another additional component in the northern part of the galaxy. In the lower panels we show the multi-component fit described in section 2.3.2 which include those extra components.	55
2.9	Effective (circularized) radii of the lensed $z \sim 2$ galaxies A1413-1 and MACS2129-1 plotted against their stellar masses. For comparison we overplot the values for a sample of $1.5 < z < 2.5$ passive galaxies compiled from Toft et al. (2012), van de Sande et al. (2011), Kriek et al. (2009); van Dokkum et al. (2009), van Dokkum & Brammer (2010), Onodera et al. (2010), Muzzin et al. (2012), Mancini et al. (2010), and Cimatti et al. (2008). The local stellar mass-size-relations for early-type (red color) and late-type (blue color) galaxies from Shen et al. (2003) are also overplotted, with their intrinsic scatter in dashed lines. The compactness criterion of Barro et al. (2012) is indicated by the bold black line.	56
3.1	The <i>HST</i> /WFC3 F160W image and with all the X-Shooter slit orientations indicated with dashed lines for the observations presented in Fynbo et al. (2011) and full-drawn lines for the new observations presented here (see also Table 3.1).	66
3.2	Top 9 panels: 5×5 arcsec ² sections centred on the QSO in F606W, F105W and F160W (from left to right). The DLA galaxy is seen south-west of the QSO at an impact parameter of $2''$. The top row shows the science images, the middle row shows the GALFIT model and the bottom row shows the residuals after subtracting the model (QSO PSF and galaxy models) from the science images. The field size is 5×5 arcsec ² and the images are oriented with North up and East to the left. The arrow in the lower left panel indicates the possible signature of the $z = 2.412$ DLA galaxy. The tail extending below the QSO is a result of Charge Transfer Inefficiency. Bottom panel: 19×19 arcsec ² sections centred on the QSO in the u-, g-, and Ks-bands after PSF-subtraction. Also shown to the right is the <i>HST</i> /F160W band image on the same scale for comparison. The position of the $z = 2.583$ DLA galaxy is marked with a dotted circle. Again the images are oriented with North up and East to the left.	67

3.3	The broad-band SED of the $z = 2.583$ DLA galaxy, comprising of the Alfosc u- and g-bands, HST/WFC3 F606W-, F105W- and F160W-bands and the NOTCam K_s -band, is shown as black points. The best-fit model is shown with a full-drawn line.	69
3.4	The [O III] $\lambda 5007$ emission line of the $z = 2.583$ DLA galaxy. The top panel shows the 2D spectrum and the bottom panel shows the 1D spectrum. The vertical dashed line indicates the predicted position of the line based on the absorption line redshift of the DLA. The observed line has a centroid that is blue shifted by 36 km s^{-1} relative to the absorption redshift. The FWHM of the line based on a Gaussian fit is $256 \pm 23 \text{ km s}^{-1}$ (uncorrected for the spectroscopic resolution of 45 km s^{-1}).	71
3.5	A wider region around the [O III] $\lambda 5007$ line of the $z = 2.583$ DLA galaxy after subtraction of the QSO SPSF (the boundaries of where the QSO continuum has been subtracted can be seen at each end of the figure). As seen here, there is no evidence for [O III] $\lambda 5007$ emission at small impact parameter. A [O III] $\lambda 5007$ line 3 times fainter than the detected line would have been detected even if superposed on the QSO trace.	72
3.6	Voigt profile fits to the two DLA lines. For the $z = 2.583$ DLA at $\lambda = 4355 \text{ \AA}$ the fit is from Fynbo et al. (2011). The derived column density for the $z = 2.412$ DLA is $\log N/\text{cm}^{-2} = 21.26 \pm 0.06$	72
3.7	Voigt-profile fits to metal lines from the $z = 2.412$ DLA. The zero-point for the velocity scale is defined from the centroid of the [OIII] $\lambda 5007$ emission line. Data are shown in black and the model-fits in red. In the left column we list a weak and a strong low-ionization line (Si II and Fe II) and a medium- and high-ionization line (Al III and C IV) to illustrate the very different ionization states of the different sub-components. The vertical dotted lines mark the velocities for the sub-components in the fit to the low-ionization lines. In the right column we show the low-ionization lines from Zn II, Cr II, Fe II and Mg I. The zeropoint for the velocity scale is defined by the centroid (first moment) of the Si II 1808 line.	75
3.8	The region around the position in the spectrum where the [O III] $\lambda 5007$ emission line from the $z = 2.412$ DLA galaxy is expected to be observed. The upper panel is based on a stack of all the data taken up to and including 2012 and the lower panel is based on the 3 hr observation from March 2013. The QSO continuum can be seen in the left and right extremes of the figures, but in between it has been subtracted. Regions with sky-lines from airglow have been marked with a double-hatched pattern. The [O III] $\lambda 5007$ emission line from the $z = 2.412$ DLA galaxy is marked with a dashed circle in the upper panel.	77

4.1	Finding chart (8×8) for the host of GRB 080605 as imaged with HST/WFC3. The afterglow position and its uncertainty are indicated by a red circle, and the different components are labeled A and B. The barycenter of each component is indicated by a white cross. The geometry of X-shooter's UVB slit with width of $1''.0$ is illustrated by dashed black lines. The VIS and NIR slit have the same orientation but a width of $0''.9$. Logarithmically spaced contours are shown in white lines.	86
4.2	Two-dimensional cutouts of the X-shooter NIR spectrum centered on the observed wavelength of [O III]($\lambda 5007$) and $H\alpha$. Skylines are indicated with grey shading. Linearly spaced contours are shown in red lines.	89
4.3	Continuum-subtracted emission lines used to determine the gas-phase metallicity in the X-shooter spectrum, as well as the [S II] doublet. The black line shows the raw spectrum including errors, and the red-shaded areas denote the 90% confidence region of the fit of the emission lines using Gaussians. Grey shaded areas denote wavelength regions that have been omitted in the fitting due to skyline contamination.	91
4.4	The continuum-subtracted [O II] ($\lambda\lambda 3726 3729$) doublet. Lines and shadings are the same as in Fig. 4.3.	95
4.5	Metallicity of the host of GRB 080605 (star). Other GRB host metallicities are shown with black circles and upward/downward triangles as compiled and in the scale of Savaglio et al. (2009) (top panel) and Mannucci et al. (2011) (bottom panel). Field galaxies are shown as grey dots (Savaglio et al., 2005; Pérez-Montero et al., 2009; Mannucci et al., 2009; Hayashi et al., 2009; Richard et al., 2011), and in similar metallicity scales as the GRB measurements. Absorption metallicities from GRB afterglows (Rau et al., 2010; D'Elia et al., 2010; Savaglio et al., 2012; Thöne et al., 2011, and references therein) and QSOs (Prochaska et al., 2003) are plotted as black and grey diamonds, respectively. Errorbars for individual events in the comparison samples are omitted to enhance clarity. The error bars at the bottom right corner of each panel illustrate uncertainties of 0.2 dex., which are typical for both, GRB-DLA (e.g., Rau et al., 2010; Thöne et al., 2011) and GRB host metallicity (e.g., Mannucci et al., 2011) measurements.	100

4.6 The host of GRB 080605 with respect to the mass-metallicity relation at $z \sim 2$. Different colored symbols represent the averaged galaxy distribution from Erb et al. (2006) in black, as well as individual sources from Förster Schreiber et al. (2006, 2009) in green, from Law et al. (2009) in blue and gravitationally lensed galaxies from Yuan & Kewley (2009) and Erb et al. (2010) in cyan and grey, respectively. Upper limits are shown with downward triangles with the same color-coding. All measurements are in the N2 scale of Pettini & Pagel (2004). The horizontal dashed-dotted line marks the solar oxygen abundance. The dashed line is the local $M - Z$ relation (Tremonti et al., 2004), which is also shown shifted (solid line) to the observations at $z \sim 0.7$ (Savaglio et al., 2005). Approximate systematic errors on the N2 metallicity scale and the mass determination are indicated in the top left corner. 102

LIST OF TABLES

2.1	Coordinates, magnitudes and colors of the two target galaxies. ^(a) Observed magnitude. ^(b) Estimated intrinsic magnitude inferred from the lensing magnification at $z \approx 2$	41
2.2	LePhare fitting results for the lensed galaxies A1413-1 and MACS2129-1	49
2.3	GALFIT fitting results for the reconstructed images of the lensed galaxies A1413-1 and MACS2129-1	50
2.4	Spectro-photometric measurements for A1413-1. ^(a) Effective wavelength calculated as in Eq. 3. ^(b) Short and long wavelength ends of the spectro-photometric bins. ^(c) Observed AB magnitude. ^(d) Intrinsic AB magnitude inferred from the lensing magnification.	58
2.5	Spectro-photometric measurements for MACS2129-1. ^(a) Effective wavelength calculated as in Eq. 3. ^(b) Short and long wavelength ends of the spectro-photometric bins. ^(c) Observed AB magnitude. ^(d) Intrinsic AB magnitude inferred from the lensing magnification.	59
3.1	Log of observations	63
3.2	Results from the GALFIT fits and NOT photometry. b/a is the ratio of the minor and major axis radii and n is the Sersic index. The magnitudes in the HST filters were computed by GALFIT, whereas aperture photometry was done on the NOT images.	68
3.3	Results from the SED fitting	69
3.4	Ionic column densities in the 6 individual line components of the DLA system at $z_{\text{abs}} = 2.412$	74
3.5	Measured emission line fluxes	76
3.6	Comparison of the two DLA galaxies studied here with DLA galaxies at similar redshifts from the literature. In the table we refer to the $z = 2.412$ and $z = 2.583$ DLA galaxies as DLA0918+1636-1 and DLA0918+1636-2, respectively.	79
4.1	Photometric measurements.	88
4.2	Host parameters from stellar population synthesis modeling.	90
4.3	Emission lines in the X-shooter spectrum.	93

4.4	Oxygen abundances based on different strong-line indicators	97
-----	-----------------------------------------------------------------------	----

ACKNOWLEDGMENTS

Another finished PhD thesis in astrophysics may be a small step for mankind but a giant leap for the one who did it (me!). However, when becoming aware of the unimaginably tremendous huge gigantic distances and timescales we are dealing with in this area of research, it becomes more than just obvious that this was only doable because “I have stood on the shoulders of giants”. These giants are, in general, all the scientists who, over (at least) the last four centuries paved the way for not only our current state of knowledge, but also the highly sophisticated technology which enables us to go further and further.

The past almost 4 years have been a intense and often incredible time, and I could clearly feel how I grew with the challenge. Here I would like to honor those people who made a difference (in the positive sense!) to me during this time.

First, let me praise my first flatmate in Copenhagen, Cristiano Sousa, who turned out to be a true comrade and who was always on the spot when adversity took over. It was a great shame that he was forced to leave Denmark for incomprehensible reasons.

Next I would like to say a thousand thanks to my other close friends who emerged during those years: Teddy Frederiksen, Daniele Malesani, and Radek Wojtak were those who I would exclusively confide in. It was also them who were willing to stand by me when serious conflict with some formally high-level people was looming.

Having said this, comes the point where I can only be fulsome in my praise of the man who backed me in those tense times: Johan Fynbo had not only turned out to be an “astronomical soulmate” of mine, but also had the guts to deal with my contemnners. I consider myself very fortunate that I had the opportunity to this exhilarating experience. In this context I also feel especially obliged to Bjarne Andresen, who was a great advocate for my case: he figuratively shot at anything that moved.

And it came even better when my dream to work at a real telescope came true: I am very grateful to Johannes Andersen and Thomas Augusteijn for getting me to the Nordic Optical Telescope on La Palma for more than a year, and especially that they were willing to “wait for me” until the way was cleared. It has been an amazing time, especially as I happened to get involved in more than one breakthrough discovery.

At this point I gratefully acknowledge the support I got by Anlaug Amanda Djupvik, who always had a sympathetic ear for me.

Moreover, I want to thank Yeisson Osorio who assisted me as a native Spanish speaker

when I fulfilled myself one of my biggest dreams: my first own BMW.

Let me conclude these acknowledgements by saying how much I appreciated the help and assistance I received from various people when I was looking for new accommodation in Copenhagen, a situation which happened several times during the past years: Warm thanks to Esther Teresa Porras for giving me shelter for one month where I would otherwise been "homeless", and to Allison Man and Simon Challet for doing the same one year later. I would also like to convey my thanks to Vladimir Nielsen for renting is "fancy" apartment to Radek and me, and to Leif Røerbæk and Jorun Christoffersen, my last landlords in Copenhagen before I moved to La Palma, for selecting me among the hundreds of candidates for the apartment they rented out, and for letting me out of the contract ahead of time. Having written about all those, I of course also have to thank those who helped with the practicalities of moving (like carrying boxes, etc.), namely Antonio de Ugarte Postigo, Ia Kochiashvili, Teddy Frederiksen, Radek Wojtak, Daniele Malesani, and Cristiano Sousa.

Right now I'm awaiting the opportunity to defend my PhD thesis, which will be the point where this mission will be really accomplished. And then ... freedom!

ABSTRACT

Our Universe is filled with a mind-blowing diversity and different types and appearances of galaxies. Finding out about how they formed and evolved is one of the most challenging tasks in astronomy. When looking about 10 billion years back, to an epoch about 3 billion years after the big bang, we can see galaxies at earlier stages of their lives. In this thesis studies of different kinds of galaxies in the early universe are presented. Two examples of the very intriguing population of massive quiescent $z \sim 2$ galaxies were analyzed in terms of their stellar populations and morphologies. Although during the past decade big steps forward have been made in the study of this particular population of galaxies, key questions about their formation and evolution remain unsolved and the observational sample is still small, especially for galaxies at the faint end of the luminosity function. To make spectroscopic investigations easier for those typically very faint objects we make use of the biggest available “telescopes” in the universe: We search for red $z \sim 2$ galaxies whose apparent brightnesses have been boosted by the Gravitational Lensing effect of intermediate redshift galaxy clusters with available mass models. Our findings indicate older ages for these galaxies than expected. Also, their remarkable compactness was corroborated. Further conclusions such as about the validity of the downsizing paradigm are not possible given the very small sample of just two such galaxies. Furthermore, we present a study of another class of high-redshift galaxies which came into the limelight during the last decade: Star-forming galaxies with relatively small stellar masses but large surrounding hydrogen reservoirs, which can only be found and studied against the background light of a luminous quasar in the line of sight. We studied a special case of these so-called Damped Lyman α Absorbers (DLAs), with two intervening galaxies in the line of sight of a higher-redshift QSO, which is also one example of only about a dozen known galaxy counterparts of a DLA. It fits into the emerging paradigm that galaxies which are responsible for higher metallicity DLAs are more massive and luminous than typical DLA galaxies. Finally, we present a study of another star-forming galaxy, which was selected as the host of a Gamma Ray Burst (GRB). It revealed a relatively high metallicity, contrary to the common perception of GRB hosts as metal-poor galaxies, indicating that GRBs are less biased tracers of star-formation at higher redshifts than previously thought. Each of the presented studies of high-redshift galaxies constitutes pioneering work, opening a window through which we might one day see a coherent

picture of the formation and evolution of galaxies in the history of the universe. We can also conclude that although we gained valuable insights into both the star-forming as well as quiescent population of galaxies at high redshifts, new questions have emerged, which we will have to tackle in future studies.

ABSTRAKT

Universet er fyldt med en overvældende mangfoldighed af galakser. Afklaringen af, hvordan de blev dannet og udviklede sig er en af de mest krævende problemer i astronomien. Når vi ser omkring 10 milliarder år tilbage til en tid ca. 3 milliarder år efter big bang, så kan vi se galakserne i tidligere udviklingstrin. I denne PhD afhandling præsenteres studier af forskellige typer af galakser i det tidlige univers. Jeg har studeret to eksempler på den forbløffende population af massive, uvirksomme galakser omkring $z \sim 2$ og har karakteriseret deres stjernepopulationer og deres morfologi. Selvom der i det seneste tiår er sket store fremskridt i studiet af denne population af galakser, så forbliver centrale spørgsmål omkring deres dannelse og udvikling ubesvarede og antallet af studerede galakser er småt, særligt i den svagere end af luminositetsfordelingen. For at bedre muliggøre spektroskopiske studier af disse typisk meget lyssvage objekter gør vi brug af de største tilgængelige "teleskoper" i universet: Vi undersøger røde $z \sim 2$ galakser hvis tilsyneladende lysstyrke er blevet forstærket af den gravitationelle linseffekt fra foranliggende galaksehobe med allerede udarbejdede massemodeller. Mine resultater indikerer højere end forventede aldre for disse galakser. Endvidere bekræfter jeg den forbløffende store kompakthed af disse objekter. For at drage yderligere konklusioner fra dette studie, f.eks. omkring gyldigheden af downsizing paradigmet, må flere end to galakser undersøges. Ydermere, præsenteres et studie af en anden klasse af højrødforskydningsgalakser som er kommet frem på scenen i det seneste årti: stjernedannende galakser med relativt små stellare masser, men omgivet af store brinthaløer som kun kan findes og studeres v.h.a. lyset fra bagvedliggende kvasarer langs sigtelinien. Jeg har studeret et specielt tilfælde af disse såkaldte Dæmpede Lyman- α Absorbere (DLA), nemlig en sigtelinie med to DLA'er mod den samme bagvedliggende kvasar. For begge DLA er den absorberende galakse identificeret, hvilket er interessant da kun omkring et dusin sådanne systemer er kendte. Resultaterne fra dette studie passer med det billede, der er ved at danne sig, hvori de galakser, der forårsager de mest metalrige DLA'er er mere massive og lysstærke end typiske DLA galakser. Endelig præsenterer jeg et studie af en anden stjernedannende galakse som er udvalgt fordi den var vært for et gammaglimt (engelsk: Gamma-ray Burst, GRB). Undersøgelsen klarlægger et relativt højt metalindhold i modsætning til den vante forestilling af GRB værtsgalakser som værende metal-fattige galakser. Dette indikerer, at GRB værtsgalakser er mere repræsentative for generelt stjernedannende galakser end

man hidtil har troet. Hvert af disse tre studier af højrødforskydningsgalakser er ved forskningens frontlinie og er med til at åbne vinduer gennem hvilke vi forhåbenlig en dag kan se et komplet billede af galaksernes dannelse og udvikling i universet. Det kan konkluderes, at selvom vi har indhentet værdifuld ny indsigt i såvel stjernedannende som uvirksomme populationer af galakser ved høj rødforskydning, så er der stadig ubesvarede spørgsmål som vi må besvare i fremtidige studier.

1

INTRODUCTION

If you wish to make an apple pie from scratch, you must first invent the universe.

Carl Sagan

It is the goal of the oldest of all natural sciences, astronomy, to unravel the nature, origin, and evolution of all kinds of objects which the Universe comprises. For a long time, even up to the beginning of the 20th century, it looked like the main content of the universe was simply stars. At that time it was also thought that they were mostly uniformly distributed in the universe, and it was even not known how they worked, i.e. how the energy is released which makes them shine, let alone their ages and lifetimes. It is also worthwhile to mention that the age of the universe as a whole was not well constrained (or better say, unknown), with the only constraint being a lower limit set by the current knowledge about the age of the Earth. On the other hand, astronomers, with the first one being Galileo Galilei, had realized that a very prominent feature on the night sky, which because of its visual appearance is known as “Milky Way”, is actually made of millions and millions of stars, forming a distinct structure. The technical term “galaxy” originates from the Greek word for Milky Way. At those times it was still believed that the Milky Way would constitute the whole universe.

Nevertheless, in the 18th century, I. Kant had already come up with the idea about galaxies, when he wrote in his book “Allgemeine Naturgeschichte und Theorie Des Himmels oder Versuch von der Verfassung und dem mechanischen Ursprunge des ganzen Weltgebäudes, nach Newtonischen Grundsätzen abgehandelt” (Kant, 1755): “I am coming to that part of the proposed theory which makes it most particularly attractive because of the sublime picture it presents of creation’s plan. The series of ideas which has led me to it is short and natural. It consists of the following. If a system of fixed stars, all spatially related to a common plane, just as have sketched out the Milky Way, is so far distant from us that all perception of individual stars making up the system is no longer possible, even with a telescope, if the distance of this system has exactly the same relationship to the distance of the stars in the Milky Way as the latter have to the distance of the sun from us, in short, if such a world of fixed stars is seen at such an immeasurable distance from the eye of the observer located outside this

world, then this world will appear in a small angle as a tiny and weakly lit area, with a circular shape if its plane is oriented directly in the line of sight and elliptical if it is viewed from the side. The weakness of the light, the shape, and the recognizable extent of its diameter will clearly distinguish such a phenomenon, when present, from all the stars which are seen individually.”¹

Let us contrast this with the quote from Miss Agnes Clerke from 1906: “No competent thinker, with the whole of the available evidence before him, can now, it is safe to say, maintain any single nebula to be a star system of coordinate rank with the Milky Way.” (quoted from the book: “The expanding Universe - Astronomy’s great debate 1900-1931” Smith, 1982) The reason why Clarke came to this wrong conclusion is that distance measurements to nebulae at that time were flawed and gave way too small distances, which then led to the conclusion that the nebulae were objects much smaller than the Milky Way.

It is still less than a century ago that it was realized by the leading astronomers of their time, that some of the fuzzy patches of light which for their visual appearance were simply called nebulae, and which were up to that time thought to be located within our galaxy, are in fact galaxies in their own right (Hubble, 1926).

And it was only back then, as a consequence of that insight, that it became clear that the Universe is much bigger (by many orders of magnitude) than was thought when it looked like that our galaxy, the Milky Way, was the only such entity in the universe.

Around the same time, astronomers began to determine how fast galaxies were moving with respect to each others, by measuring the redshifts (or blueshifts) of their spectral lines. V. Slipher, K. Lundmark, W. Wirtz, E. Hubble, among others (Trimble, 2013), realized that these velocities increased linearly with their distances. G. Lemaître, A. Friedmann and others realized that this was consistent with a solution of General Relativity, where space itself expands, thus increasing distances between objects. The redshift can be imagined as light waves being “stretched” by the same factor as space expands. Formally it is defined as relative change of wavelength, i.e. $z = \frac{\delta\lambda}{\lambda}$. Another conclusion of these revolutionary findings was that when counting back in time, the universe must have been much more dense, and so the picture emerged that the universe is not static and infinitely old, but rather began in a very dense and hot initial state (“Big Bang”), and has since then been expanding, thus cooling down and allowing for stars and galaxies to form and build up the universe as we see it today.

The prevailing astronomical worldview was shaken once again soon after, when F. Zwicky found that galaxies in a cluster were moving faster than allowed by the virial theorem, if one assumes that the visible matter contains all mass, so it was concluded that there must be another kind of matter which does not emit light (Zwicky, 1933). When in the decades after that it was also found that the rotation curves of spiral galaxies were especially in their outskirts faster than expected by Kepler’s laws (Rubin et al., 1977; Rubin, 1983), which in combination with the stability of rotating galaxies could

¹taken from <http://www.calstatela.edu/faculty/kaniol/a360/Kant.Island.Universe.Theory.htm>

only be explained by the presence of more invisible mass, the existence of the so-called “dark matter”, which must be of different nature than the matter of our every day world, became widely accepted. It became clear that dark matter constitutes a clear majority of all matter in the Universe. An expanding Universe with an age of roughly 14 billion years, which contains more dark than “normal” matter, became the standard picture of cosmology, the science of the universe as a whole. Against this background, we can study and try to understand the origin of galaxies, and how they came to be what they are in today’s universe.

This thesis is about galaxies in the early universe, at times between 2 and 4 billion years after the Big Bang (corresponding to redshifts $1.5 < z < 3.5$), an epoch in cosmic time in which crucial steps in the evolution of galaxy populations took place.

In this introduction I will first introduce and explain the most important technical terms and concepts, mainly the formation of large scale structure and especially galaxies, and the different populations of galaxies, as well as some important methods for studying them.

1.1 STRUCTURE FORMATION IN THE UNIVERSE SINCE THE BIG BANG

The notion that the Universe began with a very hot and dense initial state led to the prediction that there should be an afterglow which permeates the whole universe (Gamow, 1948). Indeed this “cosmic microwave background” (CMB) radiation was discovered in the 1960s (Penzias & Wilson, 1965; Dicke et al., 1965). It originates from a time roughly 380000 years after the Big Bang when the plasma in the early universe had cooled down to about $3000K$ and protons and electrons could combine to form neutral hydrogen atoms, after which photons could travel unimpeded through space (before that, the plasma was opaque because of Compton scattering).

Actually not only hydrogen was present after the Big Bang, but also helium, the second element on the periodic table, had already been “produced”, with a mass fraction of about 24% (Audouze, 1981; Tytler et al., 2000; Izotov et al., 2013). Heavier elements (apart from negligible traces of Lithium) did not exist yet (there is however a problem with the primordial lithium abundance: The measured Lithium abundance in metal poor stars is a factor of 3 lower than the prediction for the Big Bang nucleosynthesis Spite et al., 2012). This was the reason why for all the other chemical elements a technical term was coined: they are simply called “metals” (i.e. this term has a completely different meaning than in chemistry).

Measurements with the satellites COBE and WMAP showed that the signal of the CMB looks almost identical in every direction. It thus seems that right after the Big Bang, matter in the universe was distributed very homogeneously. Structures like galaxies and galaxy clusters did not exist yet. This homogeneity raised a big question, the so-called “horizon problem”: how could it be that regions which in today’s universe are

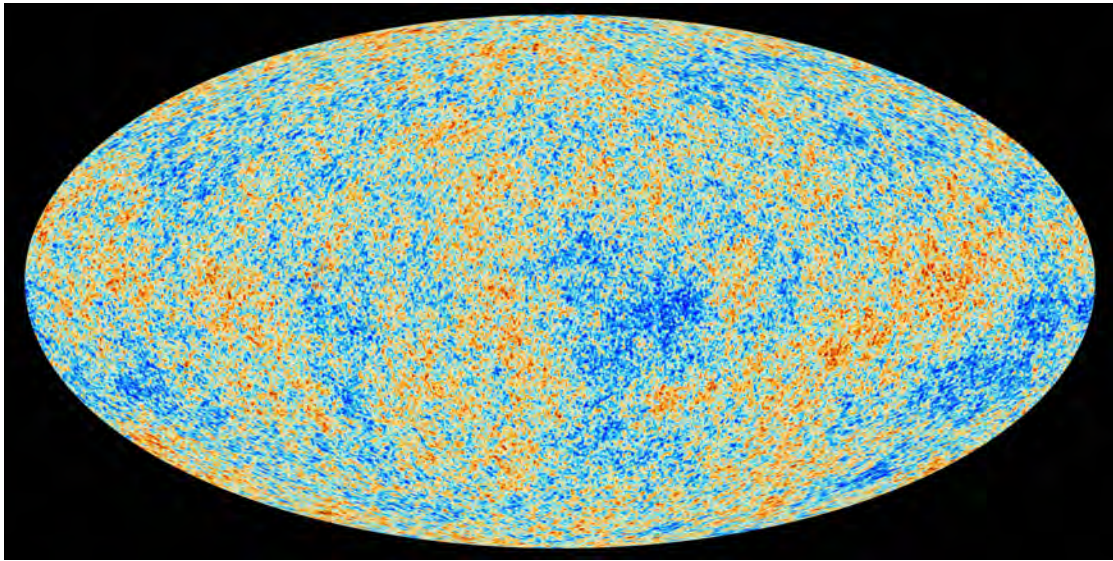


Figure 1.1 The map of the anisotropies in the cosmic microwave background, as observed by the Planck satellite.

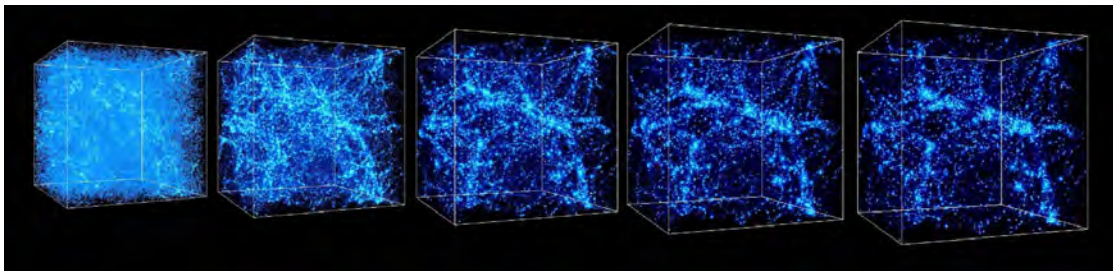


Figure 1.2 An illustration how structure grows out of tiny fluctuations.

not causally connected could “know” about each others temperature? The most popular answer to this riddle is the theory of Inflation, i.e. that space expanded by an enormous factor (somewhere between 10^{30} and 10^{50}), a scenario which solves the horizon problem and also explains that the universe seems to be flat, i.e. its curvature is consistent with zero. What is today’s observable universe must have been very small before inflation. Quantum fluctuations which occur on microscopic levels were also inflated, causing anisotropies in the density and thus temperature of the primordial plasma. Indeed these anisotropies were detected by the COBE satellite (Smoot et al., 1992), which was probably one of the most important astronomical discoveries ever, and measured with higher accuracy by WMAP (Jarosik et al., 2011) and Planck (Planck Collaboration et al., 2013). The CMB anisotropy map obtained by Planck is shown in Fig. 1.1.

These tiny fluctuations are at a level of $\frac{\delta\rho}{\rho} \sim 10^{-5}$. They are the origin of the fact that today’s universe is not structureless but exhibits a huge network of galaxies, clusters, and superclusters, arranged in so-called “filaments”, with huge empty voids in

between. Looking at this so-called “cosmic web” (Braun, 2013), one might say that galaxies are simply “quantum mechanics written to the sky”.

In the general framework of the theory of structure formation, the slightly denser regions, by means of their stronger gravity, attracted more matter than the lower density regions, thus growing. This process reinforces itself and thus the contrast between highest and lowest density grows.

In order to discuss structure formation in more detail, I will first introduce some important concepts of cosmology, which plays an important role in the global picture of structure formation in the universe in general.

1.2 COSMOLOGY

One cornerstone of modern cosmology is the theory of General Relativity, the leading theory of gravity, because gravity is the one dominating force on large scales and long distances. The expansion of space itself since the Big Bang is easily explained within its framework, and its form is a consequence of the so-called cosmological principle. The cosmological principle states that the Universe is isotropic in every point in space, which in combination with the Copernican principle (which states that we are not at a special position in space) means that it is also homogeneous. It is an assumption which is justified especially by the above-mentioned properties of the CMB, but also by the observation that galaxies are (despite them constituting inhomogeneities themselves) on large scales homogeneously distributed. In order to keep a once homogeneous universe homogeneous at all times, the expansion velocity of space has to scale linearly with distance, a relation which is named Hubble law after Edwin Hubble who already discovered this in his measurements of recession velocities: $v = H_0 \cdot D$ where v is the expansion velocity, D the distance, and the proportionality factor H_0 the so-called “Hubble constant”. The latter is the current value of the Hubble parameter $H(t)$ which evolves with time, according to the Friedmann equations.

Another important ingredient of cosmological models are the densities of different components of the universe, relatively to the so-called critical density $\rho_{crit} = \frac{3 \cdot H^2}{8 \cdot \pi \cdot G}$ which corresponds to a flat universe. One defines $\Omega = \frac{\rho}{\rho_{crit}}$, and $\Omega_{crit} = 1$. The individual components are the matter density Ω_M , the radiation density Ω_r , the energy density associated with curvature Ω_k , and the energy density from the cosmological constant Ω_Λ . As we seem to live in a flat universe, $\Omega_k = 0$. In the early universe, photons (or radiation in general, including also neutrinos) made up a significant fraction of the total energy density (about 15% at the time of recombination), but as it scales down with the fourth power of the scale factor, is almost negligible today. In contrast, Ω_Λ grows with expansion, because the space density of the cosmological constant is constant, making up about 70% of today’s energy density. Matter, both ordinary (baryonic) matter ($\Omega_b \sim 0.05$) as well as dark matter ($\Omega_{DM} \sim 0.25$) make up about 30% of the content of today’s universe. The relative fractions of the different components, as measured by the Planck satellite, are shown in Fig. 1.3.

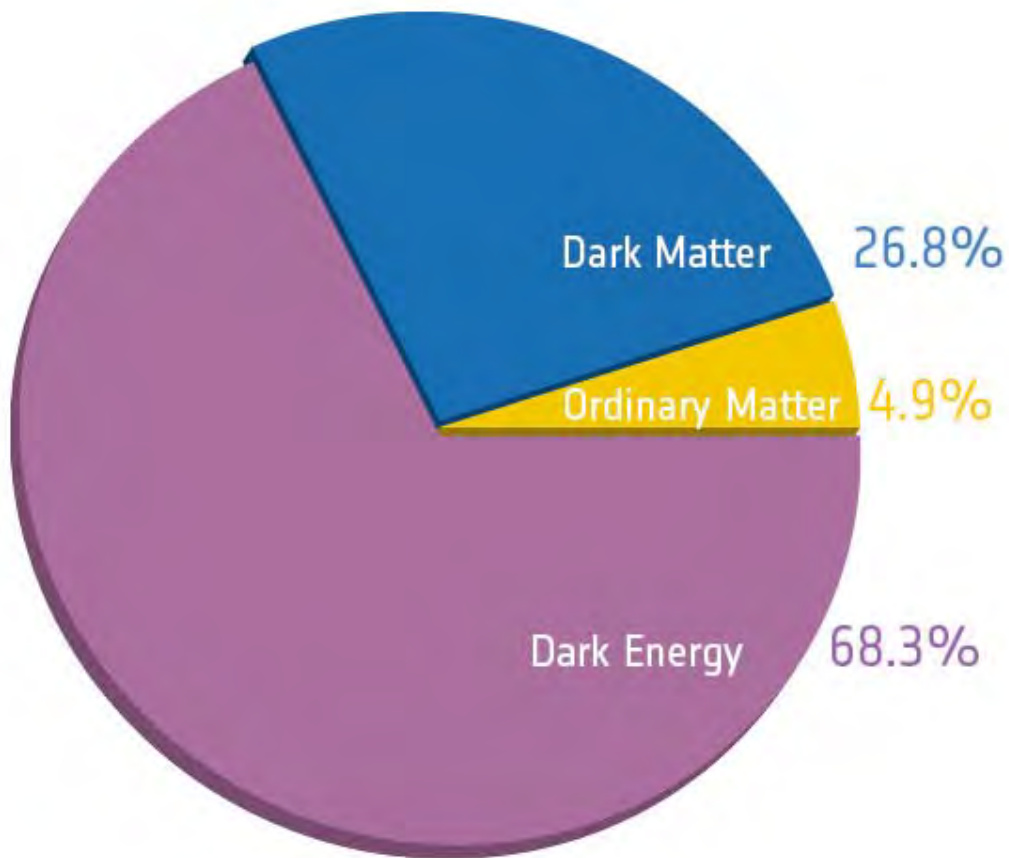


Figure 1.3 The relative contributions of baryonic matter, dark matter, and dark energy to the total energy density of the universe, as determined from CMB observations by the Planck satellite.

Furthermore, luminous matter, i.e. mostly stars, only accounts for a fraction of baryonic matter, whose majority is rather “hidden” in hot ionized plasma in between galaxies, the so-called inter-galactic medium (IGM, Jakobsen, 1998). I will return to the dark matter component in more detail later, as it plays a crucial role in the formation of structures in the universe in general, as well as for the formation of galaxies.

An important, and often misunderstood concept in cosmology is the different measures of distance in an expanding universe. Thus I will briefly give an overview over those, as they play a role in the studies of distant galaxies which are presented in this thesis. It is often argued that the concept of distance would not make sense in an expanding universe. This is not true, one only has to take care which kind of distance definition is used. The type of distance which goes into the Hubble law is the so-called “proper

distance”, also known as “comoving distance”. This is the distance which could “in principle” be measured by a ruler, i.e. the current distance.

The “angular diameter distance” D_A is the (proper) distance the object had at the time of the emission of the light which we see today, i.e. by looking at the angular size, we see the object at the distance it had back then. In a flat universe (Ryden, 2003), the angular size distance relates to the proper distance by $D_p = (1 + z) \cdot D_A$.

The last important distance definition is the so-called “luminosity distance” D_L , which is not a real distance as such, but a consequence of the dimming of light by the redshift itself, which adds another factor $(1 + z)$. It’s rather the distance at which an object would have to be without the expansion effect to have the same luminosity as the one observed: $D_L = (1 + z)^2 \cdot D_A$ (valid in all Friedmann cosmologies, not only flat ones, Ryden, 2003).

Another useful fact is the relation between redshift and angular diameter distance: Due to the super-luminous expansion velocities on distances larger than the Hubble length ($D_H(z) = \frac{c}{H(z)}$), and the fact that the Hubble parameter was much higher at high redshifts ($H(z) \gtrsim 200 \frac{km}{s \cdot Mpc}$ for $z \gtrsim 2$ in the currently favored cosmology), the angular diameter distance peaks at $z = 1.64$ and declines for higher redshifts, with the slope for that being shallow, and it should be emphasized that for redshifts $z \geq 1.64$ we see objects which were receding at superluminal expansion velocities at the time of the emission of the light we observe (Davis & Lineweaver, 2004).

1.3 DARK MATTER AND THE BUILD-UP OF STRUCTURE

Further above, I mentioned the classical evidences for the existence of dark matter. Another very important piece of evidence comes from the study of the CMB anisotropies themselves, and the arising question how these led to the large scale structures we see today. This is a non-trivial question, because if only baryonic matter were involved, it would be difficult, if not impossible to explain how in the available time matter could collapse into the structures we observe. This is because (radiation) pressure in the hot plasma and particles moving at relativistic speeds would smooth out inhomogeneities by streaming out from over-dense regions and into under-dense regions (Silk, 1967).

Dark Matter has to be invoked to alleviate this problem. In principle, two appearances of Dark Matter can be distinguished, so-called Hot Dark Matter (HDM) and Cold Dark Matter (CDM). The former again means particles moving at relativistic velocities at the time it decoupled from other particles in the early universe, whereas CDM particles moved at non-relativistic velocities at that time (and now). If HDM would be the main form of dark matter, density perturbations would be washed away on small scales, instead in such a scenario structures would first form on large scales, a so-called top-down scenario. In contrast to that, what has been observed in the universe, rather points to a bottom-up scenario, where structures first formed on small scales, and larger structures like clusters of galaxies or even superclusters forming later in cosmic time. This scenario is also called hierarchical clustering. Fig. 1.4 shows two sketches which

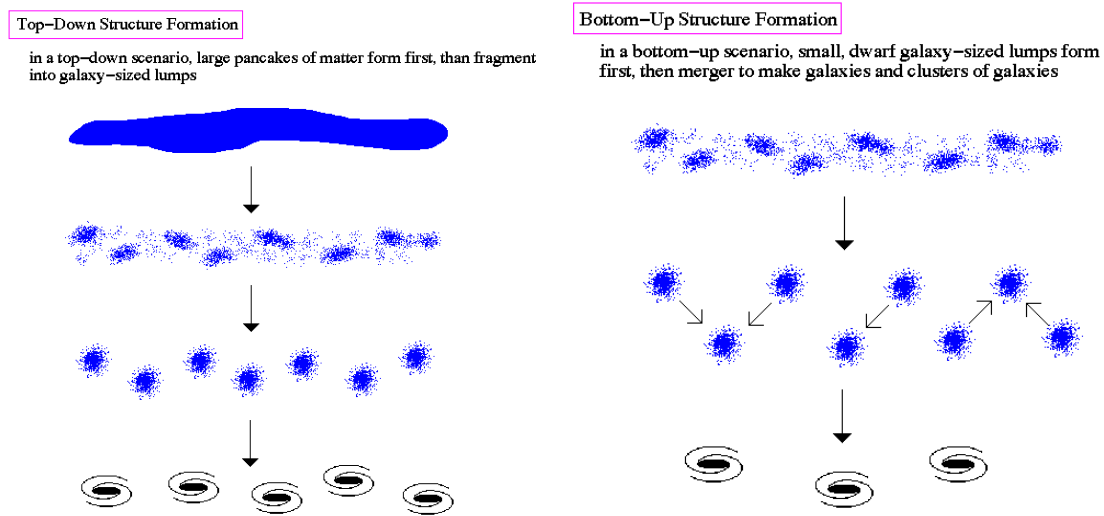


Figure 1.4 Left Panel: A sketch illustrating the top-down scenario of structure formation. Right Panel: An illustration of the bottom-up scenario, also called hierarchical structure formation.

illustrate these two scenarios.

Thus, most of the dark matter in the universe has to be in the form of cold dark matter. Detailed studies of large scale structures allow to independently gauge the amount of dark matter relative to baryonic matter, leading to the energy densities of these components quoted above. Sometimes people also consider so-called warm dark matter where the dark matter particles have some non-negligible velocities which cause perturbations to be washed out at some range of small scales, but less than for HDM.

The large scale structure can be regarded as the “skeleton” of the universe. Back-of-the-envelope calculations show that such structures evolve only slowly with time, hence they can be seen as “fossils” of the conditions in the early universe.

In light of that background, I will now briefly introduce the most important types of galaxies and then give an overview of the framework of galaxy formation and evolution, summarizing the current state of that field.

1.4 CLASSIFICATION AND MORPHOLOGIES OF GALAXIES

Even in the first half of the 20th century it was already clear from observations of “nebulae” (which were then shown to be galaxies) that they come in a huge diversity of appearances, i.e. shapes and forms. To put an order into this, a classification scheme was invented, based on those morphologies.

In his work “The Realm of the Nebulae” (Hubble, 1936), Edwin Hubble devised the so-called “Hubble Sequence”, in which two main types of galaxies are distinguished:

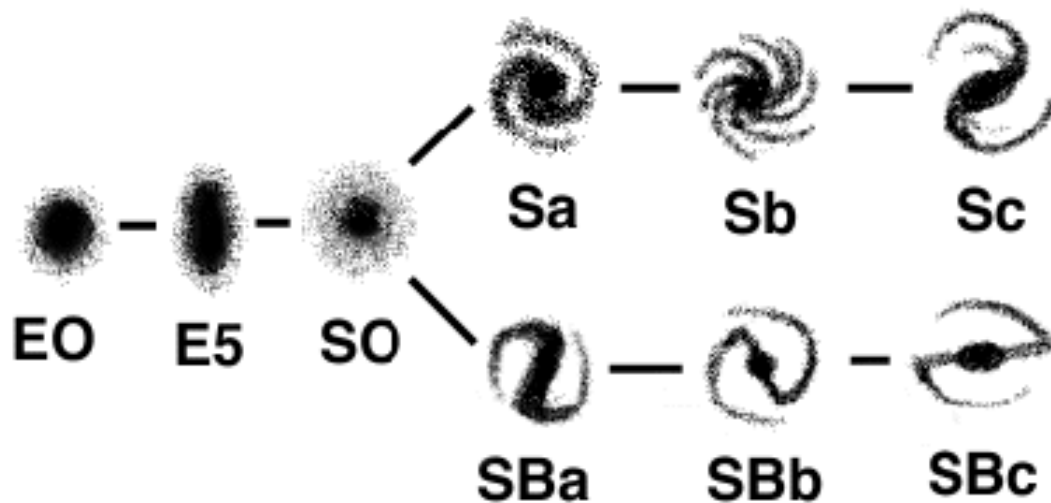


Figure 1.5 The classical Hubble “tuning fork” diagram.

“Elliptical galaxies” are named after their elliptical shapes, they appear to have little internal structure, and are denoted by the letter E followed by an indication of their ellipticity on the sky, between E0 and E7. The other big class of galaxies are “Spiral galaxies”, which are rather flat disks, and exhibit a distinct structure of spiral arms, which gave them their name. They are designated with the letter S followed by an index a, b, or c (Sa, Sb, Sc), according to the tightness of their spiral arms. Apart from the disk and spiral arms they exhibit a central bulge, which with their spheroid-like morphology resemble elliptical galaxies. This led Edwin Hubble to the hypothesis that elliptical galaxies might be an early stage of galaxy evolution, and spiral galaxies somehow developing out of those. Thus his classification is a continuous sequence beginning with elliptical galaxies (E0 to E7) and moving on with the spiral galaxies (Sa to Sc). Referring to Hubble’s idea, ellipticals are also called “early type galaxies”, whereas spiral galaxies are referred to as “late type galaxies”.

The part of the sequence containing spiral galaxies is actually two-fold, to account for the so-called “Barred spiral galaxies” which exhibit a bar-shaped structure in their centers which then merge into the spiral structure (in fact, today we know that our Milky Way is also a barred spiral galaxy, Gerhard, 2002). They’re denoted as SB, with subclasses SBa, SBb, and SBc, and depicted parallel to the “normal” spiral galaxies. The Hubble sequence thus forms a two-pronged fork, also dubbed “Hubble’s tuning fork”. I show a sketch of the classical Hubble fork in Fig. 1.5.

Today we know that galaxy evolution did not proceed from early type to late type galaxies (these historical terms are nevertheless still in use), it rather seems that elliptical galaxies can form when spiral galaxies merge. Indeed, in the centers of galaxy clusters, the fraction of early type galaxies is higher than at lower densities, which cor-

roborates that picture. This morphology-density relation (Dressler, 1980) is just one example how crucially the formation and evolution of galaxies depends on their environments.

At the point where the Hubble “fork” divides, a transitional type of object exists, the so-called “Lenticular Galaxies”, as an intermediate form which combines properties of both elliptical as well as spiral galaxies, as like the latter they’re composed of both a disk component and a central bulge. They’re denoted as S0, and their bulges are a more dominant component than in normal spiral galaxies, whereas the disk component lacks the distinct spiral structure. The basic properties of their stellar populations however resemble more those of elliptical galaxies, i.e. mostly the absence of active star formation and lack of gas.

Along the Hubble sequence, key galaxy properties show certain trends, i.e. change systematically: Early type galaxies contain mostly old stellar populations and form virtually no new stars, whereas late type galaxies have both younger stellar populations and actively form stars. Also, the amount of gas and dust increases along the Hubble sequence. These correlations between morphological classes and other galaxy properties can be described as relations between morphology and other observable quantities, especially the (integrated) colors, which (as will be elaborated later) reflect both the composition and age of the stars they contain.

Also, the environmental dependence of galaxy properties and their evolution has left its imprint in the form of a change of the “composition” of galaxies with cosmic time, the so-called Butcher-Oemler effect: Only about 5% of galaxies in nearby clusters are late-type (and thus blue) galaxies (Butcher & Oemler, 1978b), whereas at $z \sim 0.4$, i.e. more than 4 billion years ago, the fraction of blue galaxies in clusters was still about 50% (Butcher & Oemler, 1978a, 1984).

The above-mentioned morphological classifications stem from a time before the invention of modern computers, when astronomers classified galaxies visually, i.e. simply “by eye”, this was however a very good method as the human brain is much more suitable for this task, and it’s extremely challenging to let a computer do the same. Nowadays however, where huge numbers of galaxies can and have been observed, their morphological analysis has to rely on computers.

An approach which is similar to the morphological classification turns out to be very helpful here: Instead of the shape of galaxies itself, one measures rather their light distributions. Spheroid-like systems (like bulges and elliptical galaxies) show different light profiles than disc-like systems (like spiral galaxies). De Vaucouleurs (1948) found an empirical law for the surface brightness profiles of elliptical galaxies and also the bulges of spiral galaxies, $\ln I(r) = \ln I_e - 7.669 \cdot (\frac{r}{r_e} - 1)$. r_e is defined as the radius within which half of the total luminosity is contained, it is called “half-light radius” or “effective radius” and I_e corresponds to the surface brightness at r_e . For disk galaxies, a different empirical law was found, which shows an exponential surface brightness profile: $I(r) = I_0 \cdot \exp(\frac{r}{r_e})$ (de Vaucouleurs, 1959; Freeman, 1970). Sersic (1968) general-

ized those laws, and devised the so-called Sersic profile $\ln I(r) = \ln I_0 - k \cdot r^{\frac{1}{n}}$, where n is the so-called Sersic index. Setting $n = 4$ gives a de Vaucouleurs profile, and the exponential law for disk galaxies corresponds to a Sersic profile with $n = 1$. The Sersic formalism can thus be used to distinguish disc-dominated and spheroid-dominated galaxies, with the “transition” typically taken at $n = 2$ (or $n = 2.5$).

When CCDs revolutionized observational astronomy from the 1980s onwards, large surveys became feasible, yielding catalogs with millions of galaxies. Two of the most important such surveys are the Sloan Digital Sky Survey (Stoughton et al., 2002, SDSS), and the Two Degree Field Galaxy Redshift Survey (Colless et al., 2001, 2dF). Early and late type galaxies are now rather separated by their Sersic indices, as this kind of analysis is the most effective for large digital datasets. Analyses of big samples of galaxies have revealed two “sequences”, the “red sequence” and “blue sequence”. The red sequence corresponds to early type, i.e. passive (not starforming) elliptical galaxies with higher masses, whereas the blue sequence comprises more star-forming galaxies at lower masses, and they more resemble disk galaxies. These sequences can be clearly seen in “color-magnitude diagrams” (where color is plotted against magnitude), showing a clear “bimodality” (red galaxies are most luminous, and blue galaxies form most of the lower luminosity galaxies). Due to the correlation between morphology and Sersic index, the latter is also correlated with colors: The red sequence is populated by spheroid-dominated galaxies which mostly have Sersic indices around $n = 4$, whereas the blue sequence comprises of disk-like galaxies which have Sersic indices around $n = 1$ (however, dwarf elliptical galaxies often also have low Sersic indices). Thus we see two clearly separated populations of galaxies. The red sequence in the color-magnitude diagrams of galaxy clusters also provides a means to identify clusters. The slope of the red sequence (more luminous galaxies on it are tendentially redder) is a manifestation of the known correlation between luminosity and color (Visvanathan & Sandage, 1977) (actually the correlation with mass is stronger than that with luminosity). It is also closely related to the luminosity-metallicity relation (Faber, 1973).

The environmental dependence of galaxy properties can clearly be seen in rich clusters, where in the densest regions mostly red spheroid-like galaxies are found and almost no blue disk galaxies, whereas the latter dominate in low-density environments (Hogg et al., 2004).

The number density of galaxies in a certain population in terms of their luminosities, the so-called luminosity function, can be very well described by a power law with an exponential cut-off at high luminosities: $\phi(L)dL = \phi^* \left(\frac{L}{L^*}\right)^\alpha \cdot \exp\left(-\frac{L}{L^*}\right) \frac{dL}{L^*}$. This so-called Schechter function (Schechter, 1976) is characterized by two parameters, the slope α of the power law, and a characteristic luminosity L^* at the “break” between the two parts.

1.4.1 ACTIVE GALACTIC NUCLEI AND QUASARS

Although the classical classification scheme devised by Hubble is still the basis for bringing some order in the overwhelming diversity of galaxy types, it misses out on a

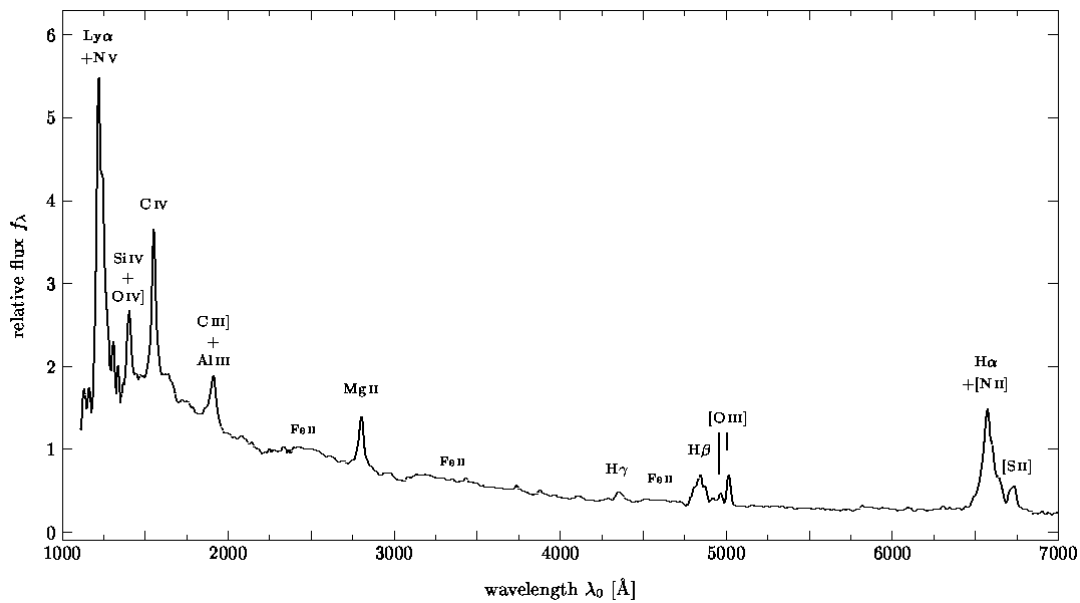


Figure 1.6 A composite spectrum (de-redshifted to rest-frame wavelengths) combined from low-resolution spectra of QSOs and Seyfert 1s, taken from Meusinger et al. (2003).

very significant phenomenon, the so-called “active galaxies”. This phenomenon, which plays an important role in the evolution of galaxies and which is not accounted for in the morphological classification, is better known as so-called “active galactic nuclei” (AGN). An active galaxy is thus simply a galaxy with an active galactic nucleus. Phenomenologically, an AGN is a very compact region in the centre of a galaxy which has an “abnormally” high luminosity over large parts (or even the whole) electromagnetic spectrum.

Probably the most well-known kind of active galaxies are quasars (which is short for “quasi-stellar radio source”), which were discovered as radio-sources whose optical counterparts (those were not always found right away) appear as point-sources which at first glance look like stars, but by redshift measurements it became clear that they are in fact very distant objects, and must therefore have huge intrinsic luminosities (Schmidt, 1963). They are the most luminous galaxies in the universe.

At first the nature of those sources was a big mystery, especially the intriguing question which physical mechanism is behind the release of such vast energies. The explanation which came up soon after and is still the widely accepted model, is the accretion of mass onto a supermassive black hole (with masses between $10^6 M_{\odot}$ and $10^{10} M_{\odot}$) in the centre of a galaxy (Lynden-Bell, 1969). The accreted material forms a so-called “accretion disk”. The accretion disk is heated up by dissipation, which in turn gets angular momentum out of the disk and thus enables material to fall onto the black hole. These processes can indeed very efficiently convert gravitational potential energy and kinetic

energy into radiation.

Nowadays it has been established that probably most (or even all) massive galaxies host a black hole at their centers. All galaxies with a supermassive black hole have probably been active at some point in their history. Typically those phases last for several millions of years. Accretion disks often also feature so-called “jets”, which are very fast outflows of material out of the disk. Jets go in both directions perpendicular to the plane of the disk, and are highly collimated and move at relativistic velocities. The radio-emission which is observed from quasars originates from those jets, via synchrotron radiation. A detailed review of this field can be found in Blandford (2001). Active galaxies showing this radio emission are also called “radio galaxies” and are thus a population which overlaps with quasars in general (the latter can also simply be described as high redshift radio galaxies). If the jet is not pointed “in the right direction”, no radio emission from a jet can be observed. In fact, most active galaxies do not exhibit strong radio emission, and thus the term “quasar” was supplemented by the more general concept of “quasi-stellar objects” (QSOs). Quasars are in this terminology also called “radio-loud QSOs”, whereas the rest (actually the majority) is referred to as “radio-quiet QSOs”. The use of all these terms is not unique in the literature, as sometimes the term QSO is reserved for radio-quiet QSOs, but it is also used as an umbrella term for both quasars and radio-quiet QSOs.

A handful more types of AGN are distinguished, such as Seyfert galaxies, LINERS, BL Lacertae objects, and Blazars, their treatment is however beyond the scope of this thesis which is more concentrated on non-active galaxies. Nevertheless, AGN play an important role in the evolution of galaxies in general, as via feedback mechanisms they for example have an influence on the star formation in a galaxy, which they can shut down very efficiently (also called “quenching of star formation”). There is a strong change in the number density of AGN with redshift, i.e. cosmic time. The peak of AGN activity occurred in the redshift range $2 < z < 3$ (Blandford, 2001). Interestingly, this coincides with the epoch when the overall star formation rate in the universe had its peak. Both are probably connected, which is also corroborated by the relation between black hole masses and the masses of the spheroidal components (bulges), the so-called $M - \sigma$ relation (Gebhardt et al., 2000).

Although QSOs are not directly subject of the studies which are presented here, they play a role in a phenomenon which I treat in the second paper of this thesis, the so-called “Damped Lyman α Absorbers”, and which I am going to introduce in the next section.

1.5 DAMPED LYMAN α ABSORBERS

A Damped Lyman α Absorbing system (DLA) is not really an object in itself, but rather a phenomenon which occurs when a galaxy with a gaseous halo happens to be in the sightline to a luminous QSO at larger distance (i.e. “in the background”). The spectrum of light from the QSO gets characteristic imprints when it passes through the clouds

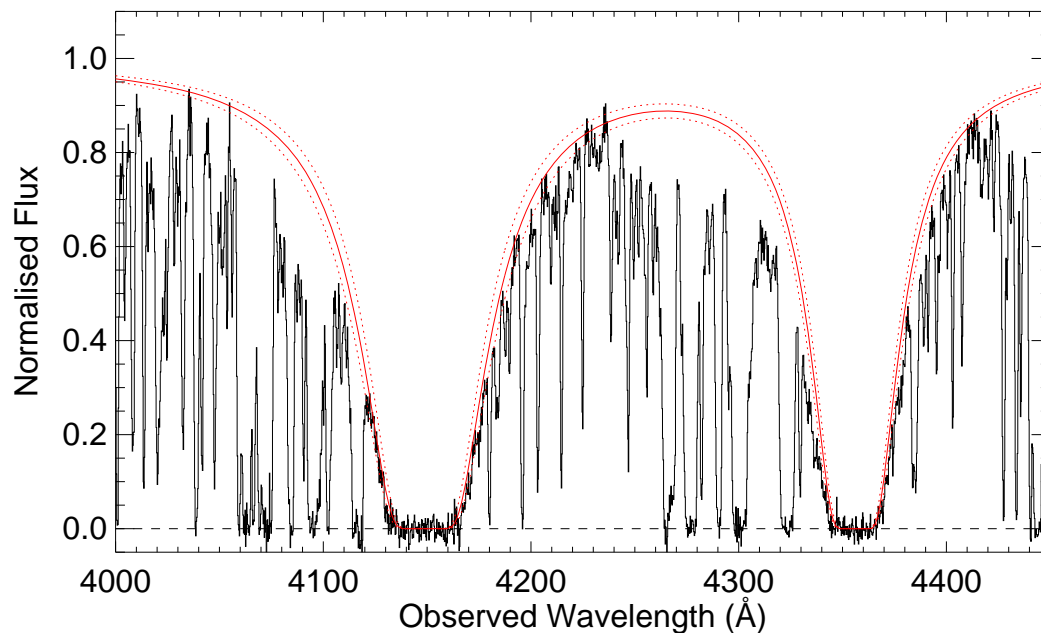


Figure 1.7 The $Ly\alpha$ absorption profiles of the two DLAs imprinted in the spectrum of Q0918+1636 from Fynbo et al. (2013b).

(which are mostly made of hydrogen). The most prominent feature is a broad absorption band from the Lyman α line at the redshift of the intervening absorber galaxy. The broadening of the Lyman α absorption is mostly due to radiation damping. The general method for finding such systems consists of fitting a continuum to the entire QSO spectrum blue-ward of its own $Ly\alpha$ emission, and then identifying damped $Ly\alpha$ candidates as absorption features with rest-frame equivalent widths W_r exceeding $W_{thresh} = 5\text{\AA}$.

Such systems provide an unparalleled means of insight in the neutral gas reservoirs which were the origin of galaxies at high redshifts. Damped Lyman α absorption occurs when the gas clouds have sufficient column densities (which is the density projected onto the cross-section of the line of sight to the quasar), i.e. $N(HI) \geq 10^{20} \text{cm}^{-2}$. Most known DLAs are at redshifts higher than $z > 1.6$ because around $z \sim 1.6$ the redshifted $Ly\alpha$ line enters the UV wavelength range which is observable from the ground, i.e. $> 300\text{nm}$. The hydrogen in DLAs is mostly neutral. (There are other classes of absorbing systems which all consist of an ionized medium.) The fact that it is neutral hydrogen gas suggests that it is raw material for star formation, so when looking at DLAs at high redshifts we see the precursors of a significant fraction of the stars in galaxies in today's universe. Furthermore, the hydrogen clouds which cause DLA absorption also contain metals and are thus interesting probes to study the chemical evolution of galaxies over cosmic time. Another aspect which makes DLAs very useful as a tool to study high redshift galaxies in general, is the difficulty to study the ISM at high redshifts directly. The clouds which we see against the backlight of background

QSOs provide unique laboratories for the ISM in the early universe.

The original case for the first damped Ly α survey was to find the neutral-gas disks of galaxies at high redshifts (Wolfe, 1986.) It turned out to be a way more efficient method for finding neutral gas reservoirs than the search for absorption of the 21cm radio line of hydrogen. With a rest-frame wavelength of $\lambda_{Ly\alpha} = 121.567\text{nm}$, optical bandpasses cover damped Lyman α absorption for a large range of redshifts.

Around that time (at the beginning of the 1980s) only four damped Ly α systems had been found. They were all systems with a high column-density, i.e. $N(HI) > 10^{21}\text{cm}^{-2}$ (Beaver et al., 1972; Carswell et al., 1975; Smith et al., 1979; Wright et al., 1979). Nine major surveys for DLAs have been conducted since then (Ellison et al., 2001; Lanzetta et al., 1991, 1995; Péroux et al., 2003; Prochaska & Herbert-Fort, 2004; Prochaska et al., 2005; Rao & Turnshek, 2000; Storrie-Lombardi & Wolfe, 2000; Wolfe et al., 1995). Additionally boosted by new data releases from the SDSS in recent years, the number of known DLAs has up to now reached the order of 10000 (Prochaska et al., 2005; Noterdaeme et al., 2012a).

Damped Ly α systems can be regarded as a cross-section selected population of neutral gas clouds at high redshifts and therefore the results will be sensitive to the gas distribution at large impact parameters. The “impact parameter” is the technical term for the projected distance of the background QSO to the centre of the galaxy whose gaseous halo is responsible for the absorption. Those galaxy counterparts are very difficult to find, as projected on the sky they are close to bright background QSOs. Note that 1” corresponds to a projected proper distance of 8.5kpc at $z = 2$. For impact parameters below that, the background QSO and the DLA galaxy will very often be blended due to the size of the seeing disc. Subtraction of the point spread function (PSF) of the QSO may help to identify the galaxy counterpart of a DLA, but this is a tricky business as it always costs signal-to-noise.

A technique which has often been used is to search for a Ly α emission line at the absorption redshift. One problem that may arise with this is that if the impact parameter is too large then the DLA galaxy will be outside the slit. As a way to circumvent this issue, Smith et al. (1989); Deharveng et al. (1990); Wolfe et al. (1992) carried out narrow-band surveys for Ly α emission. Early attempts to detect Ly α in emission were not successful, it turned out later that this was largely due to the lower sensitivity of 4-m class telescopes which were used, after Møller et al. (2002, 2004) reported detections of Ly α emission from 2 out of 18 damped Ly α systems surveyed using 8- to 10-m class telescopes.

Damped Ly α systems resemble randomly selected Ly α emitters (Rauch & Haehnelt, 2011) by the similarity in Ly α luminosity and in the compact size of the emission regions. As a counter example, DLA2206-19A is a luminous Lyman Break Galaxy, which was first found on NIR images obtained with NICMOS (Warren et al., 2001). There seems to be only little overlap between damped Lyman α systems and the population of Lyman Break Galaxies. More precisely, whereas DLA galaxies and Lyman Break Galaxies are probably both mainly star-forming galaxies, the DLA galaxies are typically

fainter than Lyman Break Galaxies in current surveys (Fynbo et al., 1999; Møller et al., 2002).

Star-formation rates can be inferred from the $H\alpha$ emission line (if detected) via the Kennicutt (1989) relation, and only lower limits on it can be inferred from $Ly\alpha$ emission because the latter is strongly influenced by dust extinction.

The current list of DLA galaxies which have been detected directly can be found in Krogager et al. (2012), additionally there is one known double DLA system (Fynbo et al., 2013b).

Most of the known Damped $Ly\alpha$ systems at all redshifts are metal poor.

When a spectrum of a galaxy counterpart of a DLA is observed (Prochaska et al., 2003; Krogager et al., 2012), it is very interesting to determine the velocities with which gas flows out of the galaxy, contributing to the halo. This is done via the redshift difference between the DLA absorption and emission lines of the galaxy counterpart and may give vital clues on the origin of the metals (see Fynbo et al., 2013b, as a nice example).

DLAs thus play an important role in study of the formation of galaxies, as they give information which could not be made available by other means. For more details about DLA research, I refer to Wolfe et al. (2005).

1.6 GALAXY FORMATION

In the scenario outlined in Sect. 1.1 and Sect. 1.3 lie the roots of the appearance of the one type of astrophysical object which can be plainly regarded the constituents which the universe is made of today: galaxies. A thorough treatment of this utmost complex field can hardly be condensed into the volume of one book. A nice overview of all the framework and background is given in the book by Longair (2008).

After recombination (the process from which the CMB originates), with the expanding universe further cooling down ($T(t) \propto a(t)$), the stage was set for the various and complex processes which occur on the way to building up galaxies. Dark matter and gas were attracted by the denser areas originating from the growth of primordial density fluctuations, forming the first proto-galaxies. These processes took place within a few hundred million years after the Big Bang. In the first decades of research on galaxies, since they were shown to be of “extragalactic” nature, it was impossible to probe this cosmic epoch observationally, simply because telescopes and detectors were not sensitive enough to show galaxies in the early universe (Partridge & Peebles, 1967).

1.6.1 GROWTH OF PERTURBATIONS

The general question how out of small density perturbations due to quantum fluctuations can transform into distinct objects mainly under the influence of gravity, was first treated by Jeans (1902) who introduced the so-called Jeans length $\lambda_J = c_s \cdot (G \cdot \rho_0 \cdot \pi^{-1})^{-\frac{1}{2}}$,

where c_s is the sound speed and ρ_0 the initial density of the medium. The physical meaning of this length is that the density contrast grows exponentially on scales greater than the Jeans length, where internal pressure gradients can no more compensate the gravitational attraction. This holds for the static case, but taking into account that galaxies form(ed) in an expanding universe, Lemaître (1933), Tolman (1934), and Lifshitz (1946) calculated that the Jeans criterion itself still holds but not the exponential growth of density contrasts, the latter rather grows with time according to $\frac{\delta\rho}{\rho} \propto t^{\frac{2}{3}}$ in an expanding universe with critical density. As the amplitudes of density fluctuations had, independently of the encompassed masses, to be of order $\frac{\delta\rho}{\rho} \sim 10^{-4}$, they could not have their origin in statistical fluctuations, and for this reason the above-mentioned authors questioned the gravitational collapse as the way galaxies could form. It was only when the idea of an inflationary phase right after the Big Bang emerged, that a viable physical mechanism was conceived, i.e. quantum fluctuations during inflation. Harrison (1970) and Zeldovich (1972) explored the spectrum of fluctuations on all scales and inferred a power spectrum of the form $|\Delta_k|^2 \propto k^n$, with $n = 1$. This scale-free power spectrum is consistent with what is measured in the CMB.

Once the density contrast has grown to $\Delta = \frac{\delta\rho}{\rho} \sim 1$, the further evolution becomes non-linear and the formation of galaxies can proceed with the formation of stars as one of the main processes. Galaxies themselves constitute over-densities relative to the average density of the universe of about six orders of magnitude, and clusters of galaxies still about a factor of ~ 1000 . Calculating back in time it can thus be estimated that, because the matter density changes with redshift according to $\rho \propto (z + 1)^3$, the density contrast for galaxies in the making must have been unity around $z \sim 100$, and for galaxy clusters around $z \sim 10$. Note that these were only rough estimations, with the real formation redshifts being rather lower, as will be outlined later. However, it can be safely concluded that $\frac{\delta\rho}{\rho} \sim 1$ was only achieved well after the time of recombination ($z \sim 1090$), when the universe was already matter-dominated. As after recombination space became transparent and photons could travel longer distances, another conclusion is that it must be in principle possible to access the early stages of galaxy formation observationally.

Furthermore, it follows that at higher redshifts, i.e. close to the era of recombination, the density perturbations were still in the linear regime, making theoretical predictions about large-scale structure more reliable and comparable with observations. Calculations of small perturbations under the influence of gravity by Lifshitz (1946) showed that, in case that the perturbations are within the horizon, both the gravitational potential and pressure gradients lead to a de-coupling from uniform and isotropic expansion, and the density contrast can be linked to the wavenumbers of the power spectrum by $\frac{d^2\Delta}{dt^2} + 2\left(\frac{\dot{a}}{a}\right)\frac{d\Delta}{dt} = \Delta(4 \cdot \pi \cdot G \cdot \rho_0 - k^2 \cdot c_s^2)$.

In a static medium (which is not the case for galaxy formation in an expanding universe, but for example valid for star formation), waves of the form $\Delta = \Delta_0 \cdot \exp i(\vec{k} \cdot \vec{r} - \omega \cdot t)$ fulfill a dispersion relation $\omega^2 = c_s^2 \cdot k^2 - 4 \cdot \pi \cdot G \cdot \rho$ (Jeans, 1902), which shows that pressure can keep stable oscillations for $c_s^2 \cdot k^2 > 4 \cdot \pi \cdot G \cdot \rho$, or rewritten in terms of wave-

length, for lengths smaller than the Jeans length $\lambda_J = c_s \cdot (G \cdot \rho_0 \cdot \pi^{-1})^{-\frac{1}{2}}$. On the other hand, for wavelengths above the Jeans length, the right-hand side of the dispersion relation becomes negative, leading to instability and exponential collapse. For $\lambda \gg \lambda_J$ the characteristic time for collapse of mass with density ρ is $\tau = (4 \cdot \pi \cdot G \cdot \rho)^{-\frac{1}{2}}$. Thus the Jeans length is simply the scale below which perturbations are still stable against gravitational collapse, or in other words it is the distance which sound waves in the medium can travel within the collapse time.

Let us now turn to the case of an expanding medium. At the early eras, where the origin of galaxies lies, dark energy did not play a major role, so that the cosmological model can be approximated by an Einstein-de Sitter universe, with $H(t) = \frac{\dot{a}}{a} \propto \frac{2}{3 \cdot t}$ and $a \propto t^{\frac{2}{3}}$, density contrasts did not grow exponentially like in the static case, but rather according to $\Delta \propto (z + 1)^{-1}$, i.e. linearly with scale factor a .

In the general case of Friedman models with zero pressure (i.e. a matter-dominated universe), Heath (1977) and Carroll et al. (1992) derived a general solution where $\Delta(a) = \frac{5 \cdot \Omega_0}{2} \cdot \left(\frac{1}{a} \cdot \frac{da}{dt}\right) \cdot \int_0^a \frac{da'}{\left(\frac{da'}{dt}\right)^3}$. Also in this case, the density contrast scales as $\Delta \propto a$ for $\Omega_0 \gg 1$ and grows only very little at small redshifts, especially as the dark energy term begins to dominate over gravitational attraction. Peculiar velocities, which stem from gradients in gravitational attraction due to perturbations on large scales, grow in an expanding universe with cosmic time according to $v \propto t^{\frac{1}{3}}$ in a flat universe. The highest peculiar velocities actually occur at the redshift where dark energy begins to dominate, i.e. relatively recently in cosmic history. The slow growth of density perturbations shows us that structures both on large scales as well as on galaxy scales did not form out of primordial plasma. Because the perturbations grew only by small factors once they were within the horizon, they form a direct probe of the early universe. On scales larger than the horizon, perturbations are independent of scale factor, i.e. "frozen", this is because there is no causal connection. The horizon itself evolves with $r_H(t) = 3 \cdot c \cdot t$ in the matter-dominated phase, but with $r_H(t) = 2 \cdot c \cdot t$ in radiation-dominated phase (where $a \propto t^{\frac{1}{2}}$).

Although in reality both baryonic as well as dark matter play important roles (especially as the latter makes up a clear majority in mass), let us have a look at adiabatic baryonic fluctuations (this means that fluctuations in matter and energy density are the same) alone, as valuable insights can be derived from those: For wavelengths smaller than the Jeans wavelength, perturbations propagate as sound waves, whereas for wavelengths larger than the Jeans wavelength, perturbations are unstable, and for $\lambda \gg \lambda_J$ perturbations grow as $\Delta \propto a^2 = (z + 1)^{-2}$ in the radiation dominated era, and as $\Delta \propto a = (z + 1)^{-1}$ in the matter-dominated era (when $\Omega_\Lambda \sim 0$ and $(z + 1) > \Omega_0^{-\frac{1}{3}}$), and finally growth tends towards zero for small redshifts.

Now the question is which baryonic mass M_J corresponds to the Jeans length. The answer is $M_J = \left(\frac{\pi \cdot \lambda^3}{6}\right) \cdot \rho_B$. In the radiation-dominated era, the perturbations were rather in the energy density of radiation, which thus determines the Jeans length, but the mass of baryons on this scale was $M_J = 8.5 \cdot 10^{28} \cdot a^3 \cdot \Omega_B \cdot h^2 \cdot M_\odot$. This depen-

dence of the Jeans mass on a^3 means that M_J reached the mass of a massive galaxy (i.e. $M \sim 10^{11} \cdot M_\odot$) at a redshift around $z \sim 10^6$. Comparing the cosmological horizon during the radiation-dominated era ($r_H = 2 \cdot c \cdot t = c \cdot (\frac{3}{8\pi \cdot G \cdot \rho})^{\frac{1}{2}}$) with the Jeans length ($\lambda_J = c \cdot (\frac{3\pi}{24 \cdot G \cdot \rho})^{\frac{1}{2}}$) we see that both are of the same order of magnitude during that era. It means that around $z \sim 10^6$, perturbations enter the horizon and the Jeans length becomes larger than the size of the perturbations, i.e. they were stable at that time. Then let us have a look at the transition to the matter-dominated era. First, matter and radiation were still coupled as long as the plasma was ionized. Around the epoch of recombination, matter and radiation were decoupled and this changed the evolution of the Jeans mass. It depends on the variation of the sound speed with redshift (i.e. cosmic time). At the time of transition, the sound speed dropped below the relativistic sound speed $\frac{c}{\sqrt{3}}$. The Jeans mass is now derived to be $M_J = \frac{3.75 \cdot 10^{15}}{(\Omega_B \cdot h^2)^2} \cdot M_\odot$, i.e. it is independent of the scale factor a . Perturbations with masses bigger than that grew proportionally to the scale factor after they entered the horizon.

Oscillating perturbations within the horizon in the matter-dominated era decreased, as they lost energy with expansion. At the time of recombination ($z \sim 1090$), the Jeans mass was $M_J = (\frac{\pi \cdot \lambda^3}{6}) \cdot \rho_B = 1.6 \cdot 10^5 \cdot (\Omega_0 \cdot h^2)^{-\frac{1}{2}} \cdot M_\odot$, i.e. the Jeans mass became much less than the mass of typical galaxies, it rather resembled the typical masses of globular clusters. These masses began to collapse. Even in the era when matter and radiation were coupled, photons could escape out of the density perturbations, thus taking energy out of the radiation that provided the pressure for the sound waves. Those were subsequently damped. This process is referred to as ‘‘Silk damping’’ (Silk, 1968). In the 1980s, baryonic matter was constrained to make up considerably less than the critical density in the universe, and as a consequence it was inferred that perturbations of the size of typical galaxy masses would have been damped out before recombination, and only very big structures, on the scale of today’s galaxy clusters, would have survived. This scenario (top-down) is inconsistent with the observed build-up of structure (which rather goes bottom-up). This is one of the reasons why the existence of non-baryonic cold dark matter (CDM) has to be assumed.

In the CDM scenario, perturbations also on small scales (like galaxies’ sizes) survived at early epochs. Dark matter does not interact with radiation and so does not suffer damping. After the radiation-dominated phase, dark matter governs dynamics, and forms structures independently of the plasma. Baryonic perturbations, also on small scales, collapsed into the cold dark matter perturbations after recombination, when matter and radiation had decoupled. Because of the different physical properties of baryonic and dark matter (the latter does not interact with radiation!), their perturbations evolve separately.

In the CDM scenario, relatively low-mass objects formed soon after recombination, and then clustered/merged influenced by perturbations on larger scales. This is the so-called bottom-up scenario. Another consequence of this scenario is that stars can begin to form early enough to account for the observationally inferred re-ionization of the

IGM and its early enrichment by products of stellar nucleosynthesis. As dark matter can be thought as collisionless particles, dissipative processes did not play a role, so in order to fulfill the virial theorem, dark matter perturbations rather lost kinetic energy by a process called “violent relaxation” (Lynden-Bell, 1967). As dark matter clustered into “halos” baryonic matter could collapse onto them.

Discrepancies between the observed large scale distribution of galaxies and the predictions of the CDM scenario can be alleviated by the concept of “biasing”, i.e. that the assumption that light traces (dark) mass is not valid: Galaxies are rather more likely to form in the highest peaks of density fluctuations (Kaiser, 1984), i.e. they are biased towards the highest-density perturbations. Observational evidence is that galaxy clusters are more strongly clustered than galaxies themselves. Another biasing mechanism might be that gas in the voids might be too hot so no stars and galaxies could form there. Biasing is described by the bias parameter b which is defined by $\Delta_{gal} = b \cdot \Delta_D$. On large scales there is no bias, but on small scales biases like the morphology-density relation are obvious. For a description of the variation of the bias parameter with luminosity, see Norberg et al. (2001).

1.6.2 OBJECT FORMATION

When looking at the collapse of density perturbations, one might ask what prevents the collapse to go on until eventually a black hole would form. The simple answer is that via violent relaxation (Lynden-Bell, 1967), the virial theorem will be finally satisfied, i.e. that the internal kinetic energy will be half of the (negative) potential energy of gravity (which is achieved by a collapse by a factor of two). In practice, systems are considered virialized (or in dynamical equilibrium) after a few times the crossing time. Coles & Lucchin (1995) worked out that those conditions require densities which are by a factor of a few hundred higher than the background density of the universe, in order to make distinct objects which are gravitationally bound. Out of the typical peculiar velocities and masses of galaxies, upper limits to their formation redshifts can be estimated. The same estimation for clusters of galaxies show that they become gravitationally bound objects only relatively late in the history of the universe, i.e. around $z \sim 1$.

The baryonic component of galaxies is “what is visible”, and this fact, i.e. that it gives off radiation, shows us that dissipation occurs here, i.e. that the system loses thermal energy. These radiative losses let the baryonic matter contract within the dark matter haloes, i.e. they overcome the internal thermal pressure. This plays also a major role for the formation of stars in galaxies (be it in today’s universe or at early times when the first stars and galaxies emerged), where protostellar clouds radiate gravitational energy away, until they become optically thick. Rees & Ostriker (1977) investigated the role of this process for the formation of galaxies, for the two most important elements, hydrogen and helium, and Silk & Wyse (1993) extended their analysis including heavier elements. At temperatures above $T > 10^6 K$, Bremsstrahlung is the dominant mech-

anism which radiates energy away, while around $T \sim 10^4 K$ transitions in hydrogen atoms (either free bound or bound-bound) play an important role, and ionized helium around $T \sim 10^5 K$.

If the cooling time is shorter than the collapse time, dissipative processes play a more important role than pure dynamics, which interestingly is the case for the typical range of galaxy masses. This shows us that those processes determine the masses of galaxies more decisively than the power spectrum of the primordial fluctuations, i.e. cooling plays an important role in the formation of galaxies. These results hold although the above-mentioned studies did not include non-baryonic dark matter. A seminal paper by White & Rees (1978) outlined a two-stage scenario of galaxy formation, in which baryonic matter is assumed to constitute only about 20% of the total mass and halos of dark matter constitute the gravitational potential wells, where baryonic matter could then fall into and cool. The process just mentioned is also known as hierarchical clustering.

Press & Schechter (1974) worked out a formalism (the so-called Press-Schechter formalism) to theoretically predict the mass function. Their approach has shown to fit reality surprisingly well and shall thus be described here. They assumed that the primordial density fluctuations were Gaussian. Furthermore, they assumed an Einstein-de Sitter cosmological model, i.e. that density perturbations grew according to $\Delta \propto a \propto t^{\frac{2}{3}}$. Their mass function can be expressed as $n(M) = \frac{\rho \cdot \gamma}{\sqrt{\pi} \cdot M^2} \cdot \left(\frac{M}{M^*}\right)^{\frac{\gamma}{2}} \cdot \exp\left[-\left(\frac{M}{M^*}\right)^\gamma\right]$ with $\gamma = 1 + \left(\frac{n_s}{3}\right)$ and $M^* = M^*(t_0) \cdot \left(\frac{t}{t_0}\right)^{\frac{4}{3\gamma}}$. The mass spectrum is a power-law with an exponential cut-off at high masses. It agrees well with the observed mass function of galaxy clusters (Schechter, 2002).

Recalling Rees & Ostriker (1977) one sees that for very large masses at relatively low densities, cooling times can exceed the age of the universe, which results in the exponential cut-off of the luminosity function for galaxies, and also explains why the most massive systems (i.e. superclusters) formed quite late in the history of the universe. Efsthathiou & Rees (1988) argued that, because very massive galaxies ($M \sim 10^{12} M_\odot$) only enter the stage below redshifts of $z \leq 4$, quasars (which are amongst the most massive galaxies) must be much more rare at $z \geq 4$, as it takes black holes with masses of the order $M \sim 10^9 M_\odot$ to power such luminous AGN and those can probably only form in such massive galaxies, given the finding that among present-day galaxies black hole masses are less than 1% of the halo mass. In fact, large surveys (Schmidt et al., 1995; Fan et al., 2001, 2004) have shown that the (comoving) number density of quasars peaks in the redshift interval $2 < z < 3$ and decreases above that redshift. In fact, the dramatic changes in the number densities of quasars with redshift is one of the most compelling pieces of evidence that there is a strong evolution of the populations of galaxies in cosmic history. This is also a direct sign that the universe is not homogeneous with respect to time (it is only homogeneous and isotropic with respect to space). One can roughly distinguish between the evolution of galaxies with active galactic nuclei on the one hand, and the evolution of the stellar content of galaxies on the other hand. Both areas

obviously overlap and have to be considered together to put together a more complete picture of the co-evolution of supermassive black holes in the centers of galaxies, and the galaxies and their stellar populations as a whole.

1.6.3 MAKING REAL GALAXIES

Now, after this relatively quick overview over the framework of galaxy formation in the early universe, let us turn to the question what a realistic picture of galaxy formation might look like. What I discussed up to here concerned processes on large scales and left out aspects like the formation of stars and feedback, which are however very important in explaining galaxy population, like the red and blue sequences. Although over the decades, astronomers have put together quite an amount of knowledge and insights, many details and also big issues are still not really understood. Among those are the environmental dependences of star formation, the mechanisms of supernova explosions (see below) and how supermassive black holes influence or even govern the evolution of galaxies.

One aspect which provides important constraints is the history of star formation in the universe, i.e. the changes in star formation rates with cosmic time. This does not only tell us about the build-up of stellar mass, but is also important for the enrichment of the interstellar medium (ISM) with heavy elements (i.e. their production in massive stars and distribution in subsequent supernova explosions).

Global star formation rates were for example derived from UV/optical observations of star forming galaxies. Lilly & Cowie (1987) and Cowie et al. (1988) determined those from the flat blue continuum in the spectra (flat, because on the one hand massive luminous blue stars are short-lived but on the other hand are “replaced” by on-going star formation).

Another method to find star-forming galaxies at high redshifts $z > 3$ is the Lyman-Break technique, and the thereby found galaxies are dubbed “Lyman-Break Galaxies” (Steidel et al., 1996b,a).

But star-forming galaxies are not the only populations of galaxies at high redshifts. It was found that some galaxies already had old stellar populations by $z \sim 2$, i.e. must have stopped forming stars at considerably earlier times, and built up most of their stellar mass already at high redshifts, a process which must have been finished by $z \sim 2$ as evidence shows that they did not grow significantly in mass since then (McCarthy et al., 2004; Cimatti et al., 2004). This somewhat contradicts the expectations of hierarchical clustering. Also it does not fit very well into the global evolution of star-formation rates, which seems to have peaked around $z \sim 2$. The just outlined phenomenon that there are massive galaxies which formed most of their stellar mass very early, whereas for lower-mass galaxies star-formation seems to continue to later eras, has been called “downsizing” (Juneau et al., 2005). It will not be easy to incorporate this scenario into the general picture of galaxy formation and evolution.

In summary let us recapitulate that dark matter haloes in the early universe provide the seeds into which gas can collapse and form a protogalaxy. Star formation leads to UV radiation from blue stars heating up gas, and explosions of supernovae further support the build-up of halos of hot gas by blowing gas out of the star-forming regions. Cold gas on the contrary forms disks, which are rotationally supported. Kennicutt (1989) found empirically that star formation proceeds with about 10% efficiency on the dynamical timescale. Spheroid-like objects like the bulges of spiral galaxies can form either via secular instabilities in discs or via mergers of galaxies. The latter are also behind the growth of massive black holes in the centers of galaxies, with their tidal forces attracting cold gas onto the black holes, the latter also building up stellar mass in the bulge in so-called “nuclear starbursts”.

1.7 STELLAR POPULATIONS AS MAIN CONSTITUENTS OF GALAXIES

The light which we observe from galaxies originates mostly from stars and gas (as long as there is no active galactic nucleus). For this reason, using the knowledge about the formation and evolution of stars themselves (which we know mostly from stars in our own galaxy), is a key ingredient for the investigation of the nature of individual galaxies, as only this way we can infer properties like the (stellar) mass of a whole galaxy, the rates at which new stars form in them, and even how star formation itself proceeded with time, i.e. the so-called star formation histories.

In a very simple picture, stars form by the gravitational collapse of clouds which consist mostly of molecular hydrogen, but also heavier elements, and even more complex molecules. The latter, even though they make up only a very tiny fraction of mass, play an important role as “catalyzers”, which facilitate the condensation process and enable the collapse of smaller masses than what would be possible if gravitation was the only relevant force. The latter was the case in the very early universe, where there was only hydrogen, helium, and some traces of lithium. The very first stars (so-called Population III) must have been very massive, i.e. more than several tens of times the mass of our Sun, and likely contained no metals at all (Clark et al., 2011; Greif et al., 2011). However, so far they have not been observed directly (as they must have disappeared long ago, and must only appear at very high redshifts). Stars which formed after population III stars exploded as supernovae were enriched with the thereby produced heavier elements (metals), such still relatively metal-poor stars are also called population II stars. Finally, more metal-rich stars are classified as the so-called population I. In our galaxy as well as other spiral galaxies we see stars from both populations, with population I being the younger generation of stars in the disk and spiral arms, whereas population II stars are mostly found in their halos and also bulges.

The most important parameter of any star is its (initial) mass, which mostly due to its gravitational force determines most properties of a star, i.e. its radius, (surface) temper-

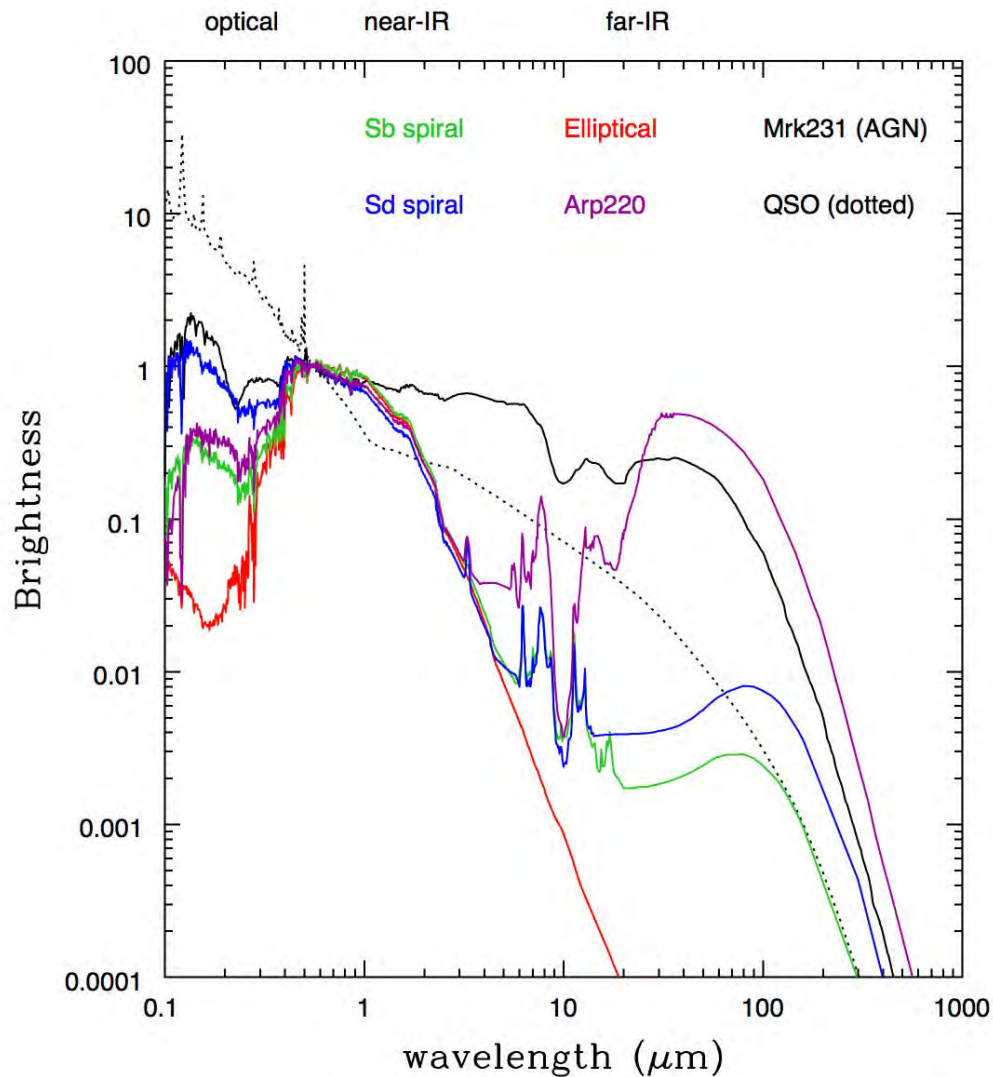


Figure 1.8 Examples of spectral energy distributions for typical galaxies: An old elliptical galaxy (red line), two types of spiral galaxies (Sb in green and Sd in blue), an AGN (Markarian 231, solid black line), a QSO (dotted black line), and a merging star-bursting galaxy (Arp 220, violet line). The spectra are taken from Polletta et al. (2007).

ature, and thus luminosity and, also very important, its lifetime, as well as the different stages of its evolution. During the main phase of their life, all stars release the energy which makes them shine by nuclear fusion of hydrogen into helium in their cores, a phase which is named “main sequence” after the region they occupy in the color-magnitude diagram (the so-called Hertzsprung-Russel Diagram, HRD). The observed color of a star reflects its surface temperature, they can approximately be regarded as black bodies (although this is strictly speaking not valid).

Depending on the mass, stars remain on the main sequence for between a few million years (for the most massive stars) up to many billions of years (for stars close to solar mass and below), during which the star's luminosity remains roughly constant. As the luminosity of a main sequence star scales roughly with $L \propto M^{3.5}$, higher mass stars live much shorter than lower mass stars. Once for lack of hydrogen in the core this phase is over, a complex evolution begins, which again depends on the mass of the star. In the helium burning phase, more energy is released because of gravitational contraction and thus higher pressures and temperatures, and the star becomes larger and more luminous. With expansion the star's surface temperature decreases, with colors becoming redder: the star evolves to a so-called red giant (stars which have evolved to red giants are located on the so-called Red Giant Branch, RGB). From this stage onwards, heavier elements are produced in the core (the so-called triple- α process plays an important role in this). Once the helium in the core is "used up", the star follows the so-called Asymptotic Giant Branch (AGB) in the HRD. Fusion in such stars is going on in shells around the core (which itself consists of carbon and oxygen), where helium and also hydrogen are burned. The energy output from these processes leads to so-called thermal pulses. Stars undergoing this phase emit a substantial fraction of the light of a stellar population at near-infrared wavelength and thus have to be taken into account in the studies of the SEDs of galaxies. The exact evolution of a star is, as mentioned before, highly dependent on the mass. The lowest mass stars don't go through a red giant phase but simply "fade away" after their main sequence phase. Stars around the solar mass lose their outer envelopes due to the thermal pulses at the end of their red giant (and AGB) phase, forming the so-called planetary nebulae, while the former core contracts and ends up as a "white dwarf".

Stars with initial masses above about 8 solar masses (corresponding to about 1.4 solar masses in the core) take a different evolution at the end of their lives: In their cores and outer shells, heavier elements up to iron are produced, after which the chain of fusion ends. They explode as a supernova, ejecting loads of heavy elements into the interstellar medium. Elements which are heavier than iron can in fact only be produced in supernova explosions.

Above I mentioned that the surface temperature of a star can be inferred from the continuum emission under the assumption that it is a black body, this temperature which is inferred from continuum parts is also called the "effective temperature". They range from about 3000K for the lowest mass stars to about 50000K for the most massive and luminous stars. An ideal black body would only emit continuum light, but in reality the atoms around the surface of a star (the so-called photosphere) absorb (and reemit) light from the thermal emission in lower layers, thus imprinting their spectral lines onto the spectrum. By absorbing light with the wavelengths of transitions between energy levels in the atoms, characteristic absorption lines appear in the spectrum of a star. The presence and abundance of heavy elements ("metals") can thus be inferred from the presence and strength of their characteristic absorption lines. Different excitation levels in the atoms are populated depending on the surface temperature of a star, which has

a direct influence on which absorption lines of a certain element appear in the spectrum. In total, the spectrum of a star is composed of continuum emission which can be approximated by the emission of a black body with the effective temperature of the star, and the characteristic absorption lines of hydrogen, helium and metals. As a result, stars with different masses and thus temperatures and luminosities, can be classified by their spectra, in so-called spectral classes. For historical reasons, these spectral classes are named O, B, A, F, G, K, and M. This sequence (which also contains finer divisions within each spectral class) goes from highest mass and bluest colors to lowest mass and red colors. Each of the classes is characterized by the surface temperatures of its stars and the absorption lines they exhibit. A very prominent set of absorption lines is the Balmer series of neutral hydrogen, transitions between the second energy level in hydrogen atoms and higher levels, with the most important Balmer lines being the $H\alpha$ and $H\beta$ lines with rest-frame wavelengths of $\lambda_{H\alpha} = 656.28\text{nm}$ and $\lambda_{H\beta} = 486.1\text{nm}$, respectively. I here use these as an example how the strength of absorption lines depends on the temperature and thus spectral type of a star. As the Balmer lines originate from the second energy level in hydrogen atoms, this level has to be populated with electrons to allow for Balmer absorption to occur. The maximum of this occurs for temperatures around 9000K which corresponds to stars of spectral type A. Spectra of A-stars thus exhibit the strongest Balmer absorption lines, whereas they are significantly weaker for other spectral types.

As long as a galaxy does not host an active galactic nucleus, the (ultraviolet ,visible and infrared) continuum light emitted by a galaxy originates from stars, either directly from the stars themselves or indirectly as emission from heated dust. Furthermore, gas atoms in the clouds from which stars form get excited by high-energy photons from young stars, and as a consequence they reradiate the energy as emission lines from the cascades of transitions between energy levels. All those contributions together make up the spectrum of a galaxy, also named the spectral energy distribution (SED). The SED of a galaxy contains key informations about its content of stars, i.e. how much mass is contained in stars (the so-called stellar mass) and the relative fractions of the different (spectral) types of stars. The latter mainly depends on two things: One of them is the relative distribution of stars of different masses, the so-called initial mass function (IMF). The IMF gives the dependence of the number density of stars on their masses. The other main factor is simply the age of the stellar population, as not only do “old” stars, which undergo their RGB and AGB phases, have a significant impact on the SED of a galaxy, but especially as the most massive stars disappear after a few millions of years (after exploding as supernovae) and with time more and more stars (moving on to lower masses) leave the main sequence, with only redder (and lower mass) stars remaining on the main sequence. As a consequence, the integrated spectrum of a stellar population (i.e. the sum of the light of its stars) becomes redder with time. With some assumptions, it is thus possible to infer the age of a stellar population from its spectrum. At this point it is worthwhile to explicitly mention a prominent feature in the spectrum of an evolved stellar population, the so-called “Balmer/4000Å break”, because it plays

an important role in the study of quiescent galaxies, which is the topic of the next chapter of this thesis. The Balmer/4000Å break occurs after a timespan of $> 10^8 yr$. It is a combined feature which on the one side originates from the short wavelength end of the Balmer series, and the 4000Å-break arises because of an accumulation of absorption lines of mainly ionized metals, and as the opacity increases with decreasing stellar temperature, the 4000Å-break gets larger with higher ages, and it is largest for old and metal-rich stellar populations. Let us now outline the application of the knowledge of stellar astrophysics which was summarized above, to the study of galaxies in terms of the light of the stars they contain.

The study of galaxy spectra to gain insights in their stellar populations is the subject of stellar population synthesis modeling. For this purpose, the knowledge about the spectra of stars of different spectral types and especially their evolution with time, is compiled in order to build stellar population synthesis models. These provide recipes for calculating the integrated spectrum of a stellar population in dependence of time and initial conditions. One of these initial conditions is the metallicity of the stellar population, which has a direct influence on absorption lines and also on colors in general.

The most important initial condition however is the stellar initial mass function. It can not be observed directly, especially for galaxies at high redshifts in which we can not resolve single stars, and so the IMF has to be put in as an assumption. However, the IMF for the Milky Way is well known observationally. These empirical results were first put in an analytical form by the seminal work of Salpeter (1955), who devised a power law of the form $N(M)\Delta M = N_0 \cdot (\frac{M}{M_\odot})^{-\alpha} \cdot (\frac{\Delta M}{M_\odot})$, with a dimensionless exponent α which he determined as $\alpha = 2.35$. This is the so-called Salpeter IMF. With decreasing mass the number of stars in each mass interval ΔM increases heavily. It is clear that this “law” must have a “cut-off” at low masses, as otherwise the number of stars would increase endlessly with decreasing mass, which is unrealistic. In fact, the lowest mass which is possible for stars is about $0.08 \cdot M_\odot$, as below this limit no hydrogen fusion can be ignited. Objects below this mass but above typical masses of planets are called “brown dwarfs”, because of their deep red colors due to their low surface temperatures (which are between 500K and 2200K). They emit most of their light at near-infrared wavelengths, which at redshifts of $z \sim 2$ (the range which I explore in the studies in this thesis) is redshifted to mid-infrared wavelengths (furthermore, their intrinsic luminosity is very low), and thus not accessible with optical and NIR observations. Nevertheless, a substantial amount of mass might be “hidden” in brown dwarfs. As it is clear that the Salpeter IMF can not be a realistic description of the number density of stars at the lower end of the mass range, it is normally assumed that it is valid only for $M \gtrsim 0.5 \cdot M_\odot$. For the mass range below one solar mass, a “flattening” of the power law for the IMF was suggested (Miller & Scalo, 1979), i.e. that in the lower mass limit α should approach 0. Kroupa (2001) devised broken power law as IMF, where the exponent for the mass range $M \geq 0.5 \cdot M_\odot$ is almost identical to the Salpeter form (with $\alpha = 2.3$), and $\alpha = 1.3$ for $0.08 \cdot M_\odot < M \leq 0.5 \cdot M_\odot$, and $\alpha = 0.3$ for $M \leq 0.08 \cdot M_\odot$.

Another form of the IMF which nowadays is very often used in stellar population synthesis modeling, is the Chabrier (2003) IMF, which has a log-normal form.

Stellar population synthesis modeling is nowadays the standard way to infer the stellar properties of galaxies at high redshifts. The most widely used models for this purpose are the those developed by Bruzual & Charlot, which are often simply dubbed “BC03 and BC07 models” after the years in which they were devised (Bruzual & Charlot, 2003a). The other set of stellar population synthesis models are those devised by Maraston (2005), also dubbed “M05 models”. The basic “ingredients” for all those models are recipes for the evolution of stars of different initial masses, an IMF, and an extinction law which describes dust extinction. Examples for the latter are the Milky Way (MW) extinction law and the Calzetti law (Calzetti et al., 1994, 2000).

The technique of matching stellar population synthesis models to the SEDs of galaxies is called “SED fitting”. In this procedure, a grid of models is computed. This grid is made of several parameters which are varied, such as the star formation timescales τ , the age of the stellar population, and the extinction coefficient E_{B-V} . Out of this grid of theoretical models, the best fit model is determined and its associated physical parameters. This procedure can be applied for both spectroscopic data as well as (broad-band) photometric SEDs. For the latter case, the (theoretical) magnitudes of the models in the used filters are computed (by convolving the model spectra with the filter transmission curves). Outputs from the fitting procedure include the age of the stellar population, the dust extinction, and the inferred total stellar mass, as well as an estimate of the ongoing (specific) star-formation rate.

At this point the definition of the age needs to be addressed, as this is a non-trivial question. On the one hand, one could regard the age simply as the time since the formation of the first stars of a stellar population began, i.e. its “real age”. The determination of this age requires knowledge about the star formation history (SFH), which is difficult to gain independently. Motivated from studies of our own Milky Way, many models simply assume an exponentially declining star formation history, with a range of e-folding timescales. Other commonly used star-formation histories are a constant star formation rate which is truncated after a certain amount of time, and delayed exponential SFHs. Many authors determine the so-called “luminosity weighted age” instead of the real age. This does not reflect the formation time of the stellar population, but has the advantage that it is more closely related to the observed SED. It is rather the mean age of the stars in the population, with the most luminous stars having the highest impact, i.e. the presence of newly formed high-mass stars lowers the luminosity-weighted age significantly. The exact star formation history does not need to be known to infer a luminosity weighted age from an SED, i.e. the SED of any stellar population with arbitrary SFH is identical to that of a stellar population with the same luminosity weighted age which formed its stars in an instant.

Note that a redshift for the object also has to be taken into account to obtain a meaningful fit. Either this redshift is already known from spectroscopy, or it has to be determined as an additional parameter in the SED fitting procedure. The latter method,

which is used to determine redshifts for objects without spectroscopic redshift measurements, from (broad-band) photometric data alone. Redshifts which are determined by this method, are called “photometric redshifts” (or short “photo-z”), as opposed to spectroscopic redshifts which are mostly inferred from spectral lines.

1.8 GAMMA RAY BURSTS AND THEIR HOST GALAXIES

Gamma-ray bursts (GRBs) are outbursts of gamma rays on the sky. They were first discovered by the Vela satellites in 1967 and it was only in the years from 1969 to 1972 that they were found to be of extraterrestrial origin. Because of the military background of the mission, it was only in 1973 that these observations were published (Klebesadel et al., 1973), which then opened up a new field of astrophysical research.

Especially theorists were very eager to come up with many models to explain the phenomenon of GRBs in the years after their first detection, and most of them proposed their sources to be located within the Milky Way or even our solar system (see Hurley, 2003, for an overview of early publications on that subject). Nevertheless, for three decades there was only little progress, due to a lack of real data from observations. As gamma rays are absorbed by the Earth’s atmosphere it is only possible to detect the outbursts with satellites, and for this purpose the Compton Gamma Ray Observatory (CGRO) was launched in 1991, which had the Burst and Transient Source Explorer (BATSE) instrument on board. A larger number of GRBs could be detected, leading to the insight that the GRBs do not originate from special locations on the sky, they are rather distributed very isotropically (Piran, 1992). Another satellite, the Italian-Dutch BeppoSAX mission, was capable of providing for the first time positions which were accurate enough to allow for follow-up observations.

Finally, in 1997 an afterglow of a GRB was detected in X-rays (Costa et al., 1997) and also in optical wavelengths (van Paradijs et al., 1997). Via spectroscopy it was possible to measure redshifts, and so their distances and, more important, the amount of energy they radiate off, could be inferred. It became clear that GRBs are of extragalactic origin (the first hint to that was their uniform distribution over the whole sky), and must thus be very energetic and luminous events. The observation of supernovae occurring together with GRBs, and the discovery of host galaxies of GRBs, made it clear that the observed GRBs originated in very distant galaxies, and the apparent connection to supernovae indeed provided plausible source for the vast energy outputs. For a general overview over the so called “SN / GRB connection”, I refer to Hjorth & Bloom (2012). The two most important current missions dedicated to GRBs are the Fermi (with the Gamma-Ray Burst Monitor and Large Area Telescope) and Swift (with the Burst Alert Telescope) satellites. The total number of GRBs which have ever been detected, has risen to a few thousands thanks to those satellites. For a review on GRBs in general, see Gehrels et al. (2009).

In fact, the GRBs which originate in supernova explosions form a subclass of GRBs which are called “long GRBs” (with a duration of the gamma-ray emission of more

than 2 seconds), as opposed to the so-called short GRBs with durations shorter than 2 seconds. The latter seem to have a completely different origin, they are likely the result of mergers of neutron stars (Nakar, 2007; Tanvir et al., 2013). Most observed gamma-ray burst events belong to the Long GRB class.

They do not only make up a research field in its own right (the physical mechanisms by which they release the huge energy outputs are not understood yet), but can also serve as a tool to study the history of star formation in the early universe: Because stars which explode as supernovae have only very short lifetimes (a few millions of years), gamma-ray bursts and their associated supernovae are a telltale sign of recent star formation activity in their host galaxy. In fact, all observed GRB host galaxies are star-forming galaxies. A current overview on the connection between GRB rate and star-formation rates is given by Robertson & Ellis (2012) and Kistler et al. (2013). This will be useful for inferring constraints on star formation at very high redshifts ($z > 7$), where it is difficult to be determined via spectroscopy of emission lines. Studying the host galaxies of GRBs (also possible through absorption spectroscopy of the much brighter afterglows) will thus be a good proxy for high redshift star forming galaxies in general.

1.9 GALAXY POPULATIONS AT HIGH REDSHIFTS

In the previous sections, some important types of galaxies at high redshifts, i.e. in the early universe, were already mentioned, namely the Lyman Break Galaxies (LBGs), galaxies which give rise to the phenomenon of Damped Lyman α Absorbers (DLAs), and galaxies which were selected as host galaxies of gamma-ray bursts. They all belong to the star-forming galaxies, i.e. to the above-mentioned “blue sequence”.

A more specific characterization of Lyman Break Galaxies (LBGs) will be briefly outlined here. As their name indicates they are selected by the presence of the so-called “Lyman Break” in their spectra. Star-forming galaxies harbor young stars, which means that there is substantial emission at UV wavelengths from hot blue stars. At wavelengths below the short wavelength end of the Lyman series (which occurs at $\lambda = 91\text{nm}$) there is a sharp drop-off in luminosity. This feature can be used to identify candidates for star-forming galaxies at $z > 3$ (Steidel et al., 1996b,a). The simple technique makes use of the fact that at those redshifts the wavelength at which the Lyman Break occurs is redshifted out of the wavelength range of the U -band. Thus these galaxies are very faint in the observed U -band, but significantly brighter in longer wavelength bands, and can therefore be identified as detections in those bands while being undetected in U . For this reason they are also called “drop-outs”. Applying the same principle to other optical and even near-infrared bandpasses, this technique can be extended to higher redshifts. For the determination of the exact redshift of galaxies selected by the Lyman Break technique, spectroscopic follow-up observations are needed.

Another technique to identify star-forming galaxies in the same redshift range, is to look for their emission in the Lyman α line. This can in principle be done by spectroscopy, however one has to find good candidates first. The two main techniques for

that are color selections (based on similar criteria as for Lyman Break Galaxies), and narrow-band imaging. These so-called “Lyman α emitters (LAE)” form a population which is not identical to LBGs although they both belong to the star-forming galaxies. LAE typically have relatively low stellar masses, typically up to several times $10^7 \cdot M_{\odot}$ and they have relatively young stellar ages of up to several hundred Myr. LBGs seem to be a class of galaxies which encompass specimens which have properties similar to LAE but do not exhibit Ly α emission. This is mostly because the Ly α emission line is a resonant line and thus highly susceptible to extinction.

So far, mostly star-forming galaxies have been described, but as already indicated above, even at the early epochs in cosmic history which correspond to redshifts $z > 2$ there was already a significant population of quiescent galaxies, which already built up their stellar masses early and stopped star-formation well ahead of the point in cosmic history at which we observe them at those redshifts. As they do not form stars, their spectra do not exhibit emission lines, and thus they can not be identified by any of the above-mentioned methods. Furthermore, because of the absence of young blue stars they are intrinsically very faint at rest-frame UV wavelengths, i.e. below the the above-mentioned Balmer/4000Å break which is probably the most important feature in spectra of galaxies with (mostly) old stellar populations. Color indices which comprise one band at shorter wavelengths and one band at longer wavelengths, will be red, a very straightforward way to find candidates for such galaxies in surveys. For example, red sequence galaxies at redshifts around 0.5 have the Balmer/4000Å break redshifted into the range in between the g - and i -bands and are thus conveniently identified by their red $g - i$ colors. At redshifts around $z \sim 2$, this spectral feature is redshifted to near-infrared (NIR) wavelengths. With its observed wavelength being around $1.2\mu\text{m}$, it is encompassed by the J -band in the NIR, even moving out of that band at $z > 2.3$. As a consequence, passive $z \sim 2$ galaxies are considerably fainter in the observed J -band than in the K_s -band (which roughly corresponds to the rest-frame R -band), which results in very red $J - K_s$ colors. Franx et al. (2003) used this feature to develop a simple color selection criterion solely based on the $J - K_s$ color. Their calculations based on stellar population synthesis models showed that when one employs a color cut of $J - K_s > 2.3$ (in the Vega magnitude system) one can very effectively single out such galaxies at $z \gtrsim 2$.

Galaxies fulfilling this criterion are called Distant Red Galaxies (DRGs). The first observational sample was discovered first in the Faint Infrared Extragalactic Survey (FIRES; Franx et al., 2003). Further observational studies showed that DRGs “come in two flavors”: Truly passively evolving galaxies without on-going star-formation, and star-forming galaxies whose spectra are reddened by heavy dust extinction, with both types making up roughly half of the total number of DRGs, respectively.

Quiescent DRGs are relatively massive galaxies with stellar masses of the order of $10^{10} - 10^{11} M_{\odot}$. Massive quiescent galaxies have been shown to be extremely compact $r_e \sim 1\text{kpc}$, with mean sizes about 3-6 times smaller than local elliptical galaxies of the same stellar mass (Toft et al., 2007, 2009; Kriek et al., 2009; Zirm et al., 2007). Galaxies

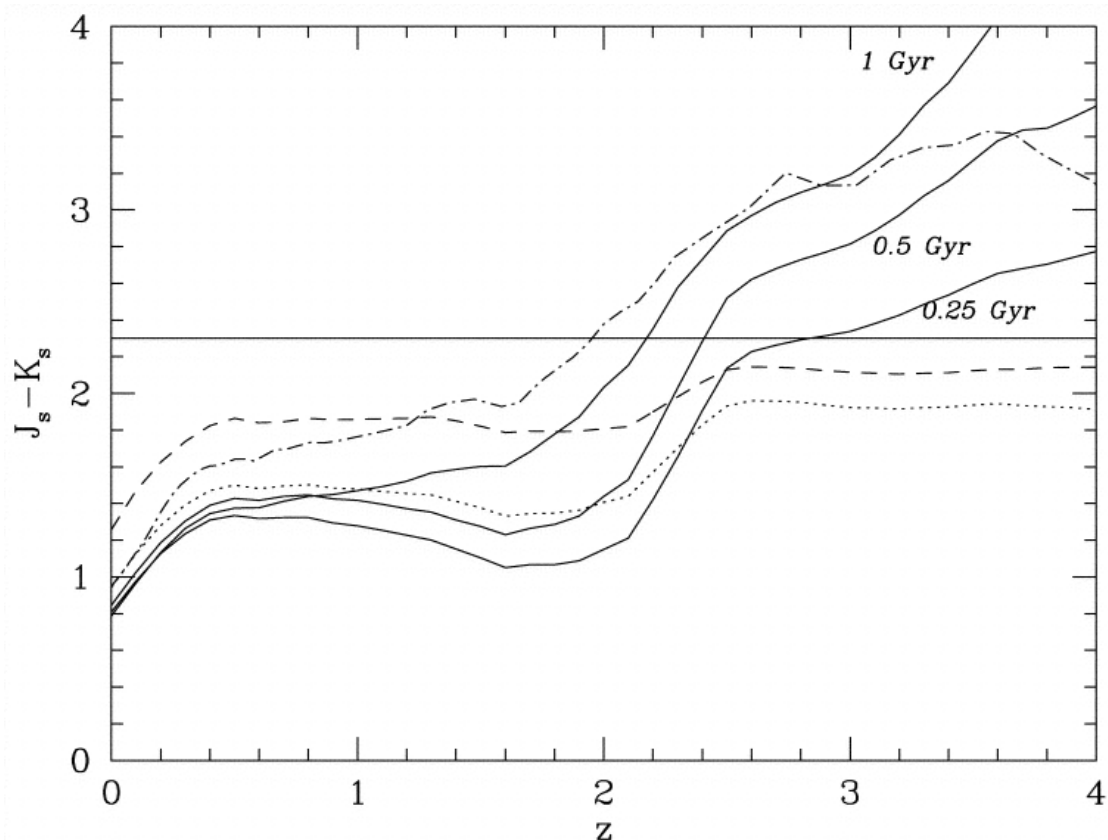


Figure 1.9 $J_s - K_s$ colors as a function of redshift for single-age stellar populations with ages of 0.25, 0.5, and 1 Gyr are shown as solid lines. It can be seen that the Balmer/4000Å break causes very red colors of $J - K_s > 2.3$ exclusively for $z > 2$. Dotted and dashed lines show models with on-going star-formation with ages of 1 Gyr and 100 Myr and reddenings of $E_{B-V} = 0.15$ and $E_{B-V} = 0.5$, respectively. The dash-dotted line demonstrates the color evolution of a single-burst stellar population with a formation redshift of $z_f = 5$, which also satisfies the DRG color cut for redshifts $z > 2$. Figure taken from Franx et al. (2003).

with such properties were originally not expected by galaxy formation models, which had predicted massive galaxies to be much larger and assemble at later times.

1.10 GRAVITATIONAL LENSING AS A TOOL TO STUDY QUIESCENT HIGH REDSHIFT GALAXIES

Spectroscopic observations of quiescent galaxies at $z \sim 2$ require very long exposure times even on the largest telescopes (i.e. 8m class telescopes like the ESO VLTs). Previous studies, such as GMASS (Cimatti et al., 2008; Kurk et al., 2008), have used $> 20h$ of 8m-telescope time to measure redshifts. With recent developments in instrumenta-

tion these very high numbers have been somewhat reduced. As an example, Toft et al. (2012) used 5 hours of integration time with the X-Shooter spectrograph (Vernet et al., 2011a) at the VLT to obtain a spectrum of a massive compact quiescent galaxy with a K_s -band magnitude of $K_s \sim 18.5$.

The need for long exposure times in order to gain spectra with sufficient signal-to-noise ratios has several reasons: Galaxies with no on-going star formation typically do not exhibit emission lines (which originate from excited gas in star forming regions), so their spectra only consist of (mainly stellar) continuum and absorption lines. The latter are not only needed to determine redshifts but can be also used to measure the velocity dispersion along the line-of-sight and as indicators of metallicities and other parameters. Furthermore, because of the absence of recent star formation (where “recent” means at least several tens of millions of years), there are no young stars and thus especially the short-lived high-mass blue stars are missing, which means that there are only stars of later types which are redder and fainter. Below (rest-frame) wavelengths of 4000\AA (where the Balmer/ 4000\AA break occurs), quiescent galaxies with old stellar populations emit considerably less light than actively star-forming galaxies. Instead, they emit most of their light at the red end of the (rest-frame) visible spectrum and longer wavelengths. At redshifts $z \sim 2$ (which means that wavelengths are stretched by a factor of ~ 3) this means that “old” galaxies are best observable at near-infrared (NIR) wavelengths, around $\lambda \sim 2\mu\text{m}$, whereas at (observed) optical wavelengths they are very faint ($I > 25$). Observations thus have to concentrate on NIR wavelengths, but for a good sampling of important features like the Balmer/ 4000\AA break also shorter wavelengths should be covered.

At NIR wavelengths, emission from the night sky is much higher than at optical wavelengths, thus heavily increasing the exposure times needed for sufficient signal-to-noise ratios. To illustrate the enormous impact of the high sky-background let me mention the K_s -band wavelength region as illustration, where the sky-background has a typical brightness of $K_s \sim 13$ (Vega), but our objects of interest have magnitudes between 18 and 21, which means that they’re at least 100 times, and even up to 1000 times fainter than the sky-background.

The above-mentioned example from Toft et al. (2012) was a study of a very bright example of a quiescent $z \sim 2$ galaxy, which in terms of the above-mentioned luminosity function corresponds to a $15L^*$ galaxy. Looking at the luminosity function we see that galaxies with such high luminosities are very rare, they’re the most massive specimens of their class, and they are so extreme that they may not be representative of more typical fainter galaxies in terms of their formation history. The change in number density at the bright end of the luminosity function is exponential, which means that the difference in number density between the brightest examples and L^* is a factor of more than one million. The typical luminosity L^* DRG corresponds to a $K_s \sim 21.4$ (Marchesini et al., 2007). As this is about 3 magnitudes fainter than the bright examples mentioned above, it is clear that with the presently available instrumentation it is not feasible within reasonable amounts of observing time (i.e. not more than a few

hours) per object to obtain spectra with sufficient S/N. In the completely background-dominated regime (which for these objects is the case at NIR wavelengths), required exposure times scale with the (inverse) square of the object's brightness, this illustrates clearly why we hit the limits of currently available telescopes and instruments here. Fortunately, another astrophysical phenomenon can be used (and has in fact been used) to alleviate that problem: The Gravitational Lensing effect of massive galaxy clusters can significantly boost the observed brightness of galaxies in the line-of-sight "behind" them.

Gravitational lensing is one of the predictions of General Relativity: As masses curve space, not only do bodies move along the geodesics of curved space-time, but also photons have to follow those paths, meaning that light paths are bent when they pass near massive objects. First this was observed during a solar eclipse in 1919 that light of stars which were actually "hidden" behind the sun, close to its edge, was deflected such that they appeared next to the sun (Eddington, 1919; Crommelin, 1919; Coles, 2001). The gravitational lensing effect has its name from the fact that, similar to optical lenses, large masses can deflect and also focus light, and as a consequence can also "magnify" the images of the background object whose light gets deflected. Despite these similarities to lenses made of glass, gravitational lenses deflect light in a different manner, as their maximum effect occurs close to the centre of the lens, and the minimum far away from it. The shape of an optical lens which would have the same effect as a gravitational lens resembles that of the bottom of a cut-off wine glass. In principle, any massive body can act as a gravitational lens. It was discussed in detail by Einstein in 1936, who however believed that it would not be possible to observe this effect. Zwicky predicted in 1937 that also whole galaxies and even galaxy clusters as a whole can lens other galaxies and concluded that it should be feasible to observe this phenomenon. It took until 1979 that this was seen for the first time.

Chwolson (1924) and Einstein (1936) predicted another effect caused by gravitational lensing: If the background object is located directly behind the "lens" as seen from the observers point of view, the lensed image of the background source can be seen as a ring, the so-called "Einstein ring". In reality the alignment is mostly not as symmetric as in this ideal case, so in most cases not a full ring can be seen, but only parts of a ring, the so-called "arcs".

The gravitational lensing effect, and especially observations of such arcs, can be used to measure masses of objects which act as lenses. This is particularly important because, as outlined in the previous sections, most of the mass in galaxies and clusters is in the form of dark matter which does not emit or otherwise interact with light.

Apart from these applications of the gravitational lensing effect as a tool to study astrophysical phenomena, it can also be used as a tool which solves the problem which was outlined at the beginning of this section. Due to their strong gravitational lensing effect, massive galaxy clusters can act as "gravitational telescopes", and as such can be seen as the biggest telescopes in the universe at all. It is a relatively straightforward idea to make use of this effect, to look for galaxies at high redshifts which are behind

massive galaxy clusters which are known to show the strong gravitational lensing effect. The highest possible magnification occurs in the case that the “lens” is at half the distance of the “lensed” background object, in terms of the angular diameter distance. This means that for $z \sim 2$ galaxies, the ideal redshift of a lensing clusters is $z \sim 0.3$. For several dozen of strong lensing clusters in the redshift range $0.1 < z < 0.8$, via spectroscopic observations of arcs from background galaxies at $z \sim 1$, models of their mass distributions have been derived, which can be used to predict the lensing magnifications for objects at higher redshifts. During the last decade, this method has been used to facilitate studies of galaxies up to very high redshifts. Those are summarized in Sect. 2.1. Apart from the boosting of the flux, it also has an additional advantage: Strong lensing can also magnify the observed size of a background object, which is especially useful for such distant objects which otherwise appear mostly unresolved, i.e. as point-sources. This makes morphological analyses of them easier than without this magnification. In Geier et al. (2013) I present a first application of this method to compact quiescent $z \sim 2$ galaxies.

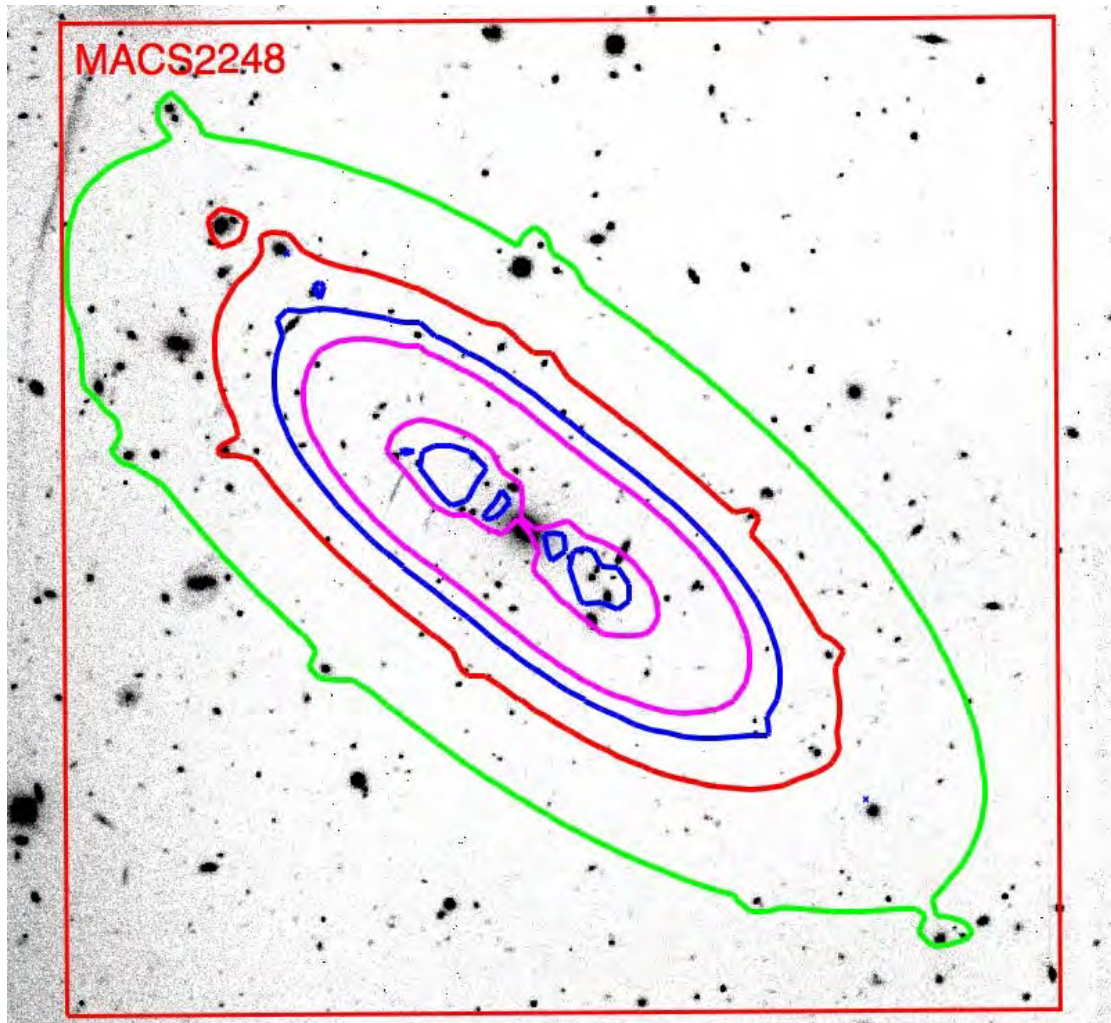


Figure 1.10 HST image of the strong lensing cluster MACS2248 with the overlaid FoV of SOFI (red square) and the 0.5mag magnification contour (green). The inner contours indicate magnifications of 1mag (red), 1.5mag (blue) and 2mag (magenta).

This chapter is based on: Stefan Geier, Johan Richard, Allison W.S. Man, Thomas Krühler, Sune Toft, Danilo Marchesini, & Johan P.U. Fynbo – *VLT/X-Shooter Near-Infrared Spectroscopy and HST Imaging of Gravitationally-Lensed $z \sim 2$ Compact Quiescent Galaxies*, Published in *The Astrophysical Journal*, 777, 87 (2013).

2

VLT/X-SHOOTER NEAR-INFRARED SPECTROSCOPY AND HST IMAGING OF GRAVITATIONALLY-LENSED $z \sim 2$ COMPACT QUIESCENT GALAXIES

ABSTRACT – *Quiescent massive galaxies at $z \sim 2$ are thought to be the progenitors of present-day massive ellipticals. Observations revealed them to be extraordinarily compact. The determination of stellar ages, star formation rates and dust properties via spectroscopic measurements has up to now only been feasible for the most luminous and massive specimens ($\sim 3 \times M_\star$). Here we present a spectroscopic study of two near-infrared selected galaxies which are close to the characteristic stellar mass M_\star ($\sim 0.9 \times M_\star$ and $\sim 1.3 \times M_\star$) and whose observed brightness has been boosted by the gravitational lensing effect. We measure the redshifts of the two galaxies to be $z = 1.71 \pm 0.02$ and $z = 2.15 \pm 0.01$. By fitting stellar population synthesis models to their spectro-photometric SEDs we determine their ages to be $2.4^{+0.8}_{-0.6}$ Gyr and 1.7 ± 0.3 Gyr, respectively, which implies that the two galaxies have higher mass-to-light ratios than most quiescent $z \sim 2$ galaxies in other studies. We find no direct evidence for active star-formation or AGN activity in either of the two galaxies, based on the non-detection of emission lines. Based on the derived redshifts and stellar ages we estimate the formation redshifts to be $z = 4.3^{+3.4}_{-1.2}$ and $z = 4.3^{+1.0}_{-0.6}$, respectively. We use the increased spatial resolution due to the gravitational lensing to derive constraints on the morphology. Fitting Sersic profiles to the de-lensed images of the two galaxies confirms their compactness, with one of them being spheroid-like, and the other providing the first confirmation of a passive lenticular galaxy at a spectroscopically derived redshift $z \sim 2$.*

2.1 INTRODUCTION

The study of galaxy formation and evolution has taken giant leaps forward in the last 15 years. In particular the use of the Lyman-break (or drop-out) selection technique has revealed large numbers of star-forming galaxies over a wide range of redshifts all the way back to $z \approx 10$ (e.g., Steidel et al., 2003; Bouwens et al., 2011). The current overall stellar mass density is about $5 \times 10^8 \text{ M Mpc}^{-3}$ (Fukugita et al., 1998; Dickinson

et al., 2003; Bell et al., 2003; Baldry et al., 2012) and the early build-up of this mass is now becoming observationally accessible (only accurate to a factor of a few at the highest redshifts) from roughly $z = 9$ (0.1% of the present value) to $z = 2.5$ (10–20% of the present value) (Labbé et al., 2010). Roughly 80–90% of present day stars must have formed at $z < 2.5$ (Marchesini et al., 2009). The cosmic star-formation history at $z < 2.5$ seems to proceed in a manner that has been referred to as “Downsizing”, i.e. proceeding from high- to low-mass systems as a function of cosmic time (e.g. Juneau et al., 2005). A similar picture emerges from the morphological evolution of galaxies at different stellar masses (Cameron et al., 2011).

It has become evident that the redshift interval $1.5 < z < 4$ constitutes the most important phase in the formation and evolution of massive ($\gtrsim 10^{11}$ M) galaxies. This is the cosmic era when massive galaxies had the peak of their star-formation and AGN activity and when their morphologies began to be transformed from being disk-like into being dominated by spheroids, and even having their star formation quenched (Lilly et al., 1996; Madau et al., 1996, 1998; Hopkins, 2004; Stockton et al., 2005; Hopkins & Beacom, 2006; Kodama et al., 2007; Zirm et al., 2008; Cano-Díaz et al., 2012). These processes are probably connected, with massive star-forming galaxies building up their stellar mass, subsequent mergers igniting nuclear starbursts, transforming the morphology from disks to spheroids, and finally ignition of the AGN shutting down star-formation. Furthermore, it appears that the mass-metallicity and color-magnitude relations we observe at lower redshifts were most likely established in that era (Mannucci et al., 2010).

The advent of deep near-infrared (NIR) surveys revealed a population of massive $z \sim 2$ galaxies that seem to have had their star-formation quenched already at $z \gtrsim 3$ (Franx et al., 2003; van Dokkum et al., 2003). These must have been the first massive galaxies that stopped forming stars. Many of these galaxies have been shown to be extremely compact (effective radii $r_e \sim 1$ kpc), with mean sizes of about one sixth to one third of that of local elliptical galaxies of the same stellar mass (Trujillo et al., 2006b,a; Toft et al., 2007; Zirm et al., 2007; Kriek et al., 2009; Toft et al., 2009; Newman et al., 2012). This probably reflects their very early formation epochs, when the Universe was much denser than today. Trujillo et al. (2009) and Taylor et al. (2010) find that in the local Universe this type of galaxies is extremely rare, which means that the massive compact galaxies we see at $z \sim 2$ must have experienced significant structural evolution since then. The picture that has been put together in the last few years is that of inside-out growth due to mostly minor merging (Bezanson et al., 2009; Naab et al., 2009; van Dokkum et al., 2010; Newman et al., 2012; Oogi & Habe, 2013). Quiescent galaxies contain a large fraction of the total stellar mass at $z \sim 2$, and need to be studied in greater detail in order to obtain a complete picture of all types of galaxy populations at $z \sim 2$. Our understanding of these distant massive quiescent galaxies is still limited, as redshifts and stellar population studies have been mainly based on broad-band photometry. Spectroscopic confirmation of their redshifts and stellar properties is very important but also very challenging, as these objects are extremely faint in the observed

optical wavelength range ($I > 25.5\text{mag}$) and in the absence of star formation do not exhibit emission lines. Up to now spectroscopic investigations have only been possible for the brightest galaxies of this class which may not be representative for the overall population. Previous spectroscopic studies, such as GMASS (Cimatti et al., 2008; Kurk et al., 2008), have used ~ 32 hours of 8-m telescope time (per MOS mask) to obtain redshifts. To push from mere redshift determinations to stellar population studies and stellar velocity dispersions, higher signal-to-noise ratios are required, which reduces the target sample size even further and renders statistical studies challenging with currently available instrumentation.

As a way to circumvent this problem we select massive quiescent galaxies that have been strongly lensed by intermediate redshift ($0.1 < z < 0.8$) galaxy clusters. Gravitational lensing can boost the observed magnitudes to a level at which spectroscopy of continuum and absorption lines becomes feasible within a reasonable amount of observing time, even for galaxies with luminosities around L_\star . The approach to make use of the strong gravitational lensing effect of galaxy clusters to identify galaxies at high redshifts (Pelló et al., 1998; Richard et al., 2004) for easier photometric (Pelló et al., 1999, 2007) and spectroscopic follow-up studies (Campusano et al., 2001; Lemoine-Busserolle et al., 2003) has been in use for more than a decade and has been proven a very powerful method for many types of high-redshift objects (Richard et al., 2006; Schaerer et al., 2007; Hempel et al., 2008; Maizy et al., 2010; Richard et al., 2011; Christensen et al., 2012a,b). We now extend this method to the above-described population of distant massive quiescent galaxies. With the help of already available mass-models (Ebeling et al., 2007; Richard et al., 2010) for clusters in which strong lensing is observed, we can determine the intrinsic luminosities of distant massive quiescent galaxies identified in the high-magnification regions of the cluster images.

In this way we have identified significantly magnified distant massive quiescent galaxies with intrinsic luminosities (assuming $z \approx 2$) around L_\star with observed Ks -band (Vega) magnitudes $\lesssim 19\text{mag}$. These galaxies are within reach of spectrographs like X-Shooter on the VLT with total exposure times of 5–10h, as has been shown in recent studies (van de Sande et al., 2011, 2012; Toft et al., 2012).

In this paper we present NIR spectra of two gravitationally-lensed distant massive quiescent galaxies obtained with VLT/X-Shooter, combined with broad-band photometry from the *Hubble Space Telescope* (HST) and ground-based facilities. In the next section we describe how the targets were selected from imaging data, and how the spectroscopic data were reduced. Sect. 2.3 contains the analysis of the spectra, with the obtained redshifts, stellar population synthesis models, constraints on potentially on-going star formation, and a structural analysis for the galaxies with resolved imaging from HST. In Sect. 2.4 we discuss the interpretation of these results with respect to currently discussed paradigms of galaxy formation and evolution. We adopt a flat ΛCDM cosmology with $H_0 = 70.4 \text{ km s}^{-1} \text{ Mpc}^{-1}$, $\Omega_M = 0.272$ and $\Omega_\Lambda = 0.728$, according to Komatsu et al. (2011). Magnitudes and colors in this paper are given in the Vega magnitude system, except where they are explicitly marked to be in the AB system.

2.2 OBJECT SELECTION, DATA REDUCTION AND SEDS

2.2.1 TARGET SELECTION

The two candidate $z \sim 2$ massive quiescent galaxies which we present in this article were identified behind the strong lensing clusters Abell 1413 ($z = 0.14$, Böhringer et al., 2000) and MACS2129-0741 ($z = 0.59$, Ebeling et al., 2007). For A1413 J - and K_s -band images were available from the WIRC instrument (Wilson et al., 2003) on the Palomar 200-inch telescope, with 5σ depths of 22.1mag in J and 20.5mag in K_s , respectively (see also Richard et al., 2010, for details on the data reduction). Near-Infrared imaging data of MACS2129-0741 was available from VLT/ISAAC (with 5σ depths of 22.9mag and 20.8mag in J and K_s , respectively). We adopt *MAGAUTO* in SExtractor (Bertin & Arnouts, 1996) for total magnitudes and determine the photometric zeropoints using bright (< 15 mag in each band) stars from the 2MASS catalog (Skrutskie et al., 2006) within the same field. For both clusters, $J - K_s$ colors were obtained by using the dual mode of SExtractor with the K_s -band image as detection image and measuring fluxes in small circular apertures of about the size of the seeing disc. To account for seeing differences, the WIRC J -band image of A1413 was Gaussian-convolved to the K_s -band seeing. In both the ISAAC images of MACS2129-0741, we measure seeing FWHMs of $0''.5$, thus no convolution was necessary. Galactic extinction corrections were applied according to the Schlegel et al. (1998) extinction maps.

One of the red galaxies, which we identified in the A1413 field, and which we refer to as A1413-1, was selected as one of the spectroscopic targets. Out of the lensed sources identified in the field of MACS2129-0741, we present spectroscopy for the brightest one which we refer to as MACS2129-1. Both were selected mainly for their relatively bright apparent magnitudes and the lensing magnification. The color-criterion of $J_s - K_s > 2.3$, originally proposed by Franx et al. (2003) was used as a guideline, but given that the brightest lensed red galaxy in the field of A1413 exhibits a color of $J - K_s \sim 2.15$, this was not followed strictly. A short summary of the two objects is given in Table 2.1.

At the time of target selection we assumed a redshift of the sources of $z \sim 2$ and using the mass models from Richard et al. (2010), we estimated the lensing magnifications to be 0.8mag for A1413-1 and 1.87mag for MACS2129-1, respectively. Later we will refine the de-lensing, based on more accurate redshifts, to be described in the following chapters.

In Fig. 2.1 we show cutout images of the two galaxies. It is clearly visible that the image of MACS2129-1 is stretched to an arc with an extension of about $1''.6$ (FWHM) by the strong lensing effect of the foreground cluster. We will discuss its morphology later in more detail, where MACS2129-1 turns out to be a disk-like galaxy in the source-plane at $z \sim 2$.

Table 2.1. Coordinates, magnitudes and colors of the two target galaxies. ^(a) Observed magnitude. ^(b) Estimated intrinsic magnitude inferred from the lensing magnification at $z \approx 2$.

Name	Facility	$Ks_{obs}^{(a)}$	$J - Ks$	$Ks_{int}^{(b)}$	RA	DEC
A1413-1	WIRC	19.01 ± 0.06	2.15	19.81	$11^h 55^m 15.4^s$	$+23^\circ 24' 52''.7'$
MACS2129-1	ISAAC	17.81 ± 0.01	2.42	19.68	$21^h 29^m 22.2^s$	$-07^\circ 41' 31''.2'$

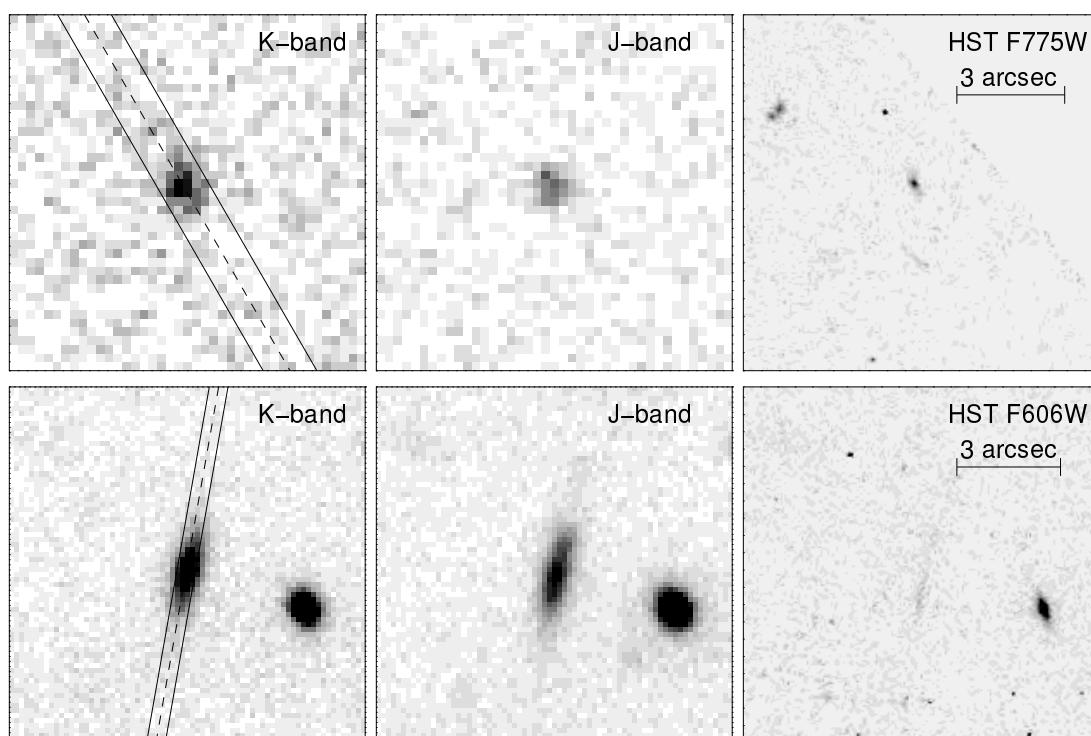


Figure 2.1 Upper panel: Cutout images of the gravitationally-lensed galaxy A1413-1 in the (WIRC) Ks - and J -bands, and in the HST/ACS F775W band. Lower panel: Cutout images of the gravitationally-lensed galaxy MACS2129-1 in the (ISAAC) Ks - and J -bands, and in the HST/ACS F606W band.

2.2.2 SPECTROSCOPIC DATA

Both targets (A1413-1 and MACS2129-1) were observed as part of the ESO program 087.B-0812 (PI: Toft) with the X-shooter spectrograph (D’Odorico et al., 2006) on VLT/UT2. This instrument is a medium-resolution Echelle spectrograph capable of obtaining spectra from the UV ($\sim 300nm$) to the NIR ($\sim 2500nm$) simultaneously. The data were

collected with a generic offset template that obtained six 480s long exposures per observation block in the NIR arm, using the $0''.9$ slit. The total exposure times in the NIR arm were 3.2h for both A1413-1 and MACS2129-1, in seeing conditions which varied between $0''.6$ and $1''.5$.

2.2.3 SPECTROSCOPIC DATA REDUCTION

For the reduction of the spectroscopic data the ESO X-shooter pipeline version 1.3.7 (Modigliani et al., 2010) was used. The calibration steps (master darks, order prediction, flat fields, and the 2d maps for later rectification of the spectra) were run for each night separately, with the default parameters in the pipeline (Goldoni, 2011).

With the output from these five calibration steps the scientific raw frames are reduced: The Echelle spectra get dark-subtracted, flatfielded, and rectified. We experiment with different pipeline recipes and parameter settings for the reduction of the science frames. It turned out that reducing them in “stare-mode”, where the sky-background for a given object frame is estimated from that same object frame, results in poor sky-subtraction and large skyline-residuals, especially in the wavelength range of the K -band. Instead, using the nodding recipe, where dithered frames are used pairwise for subtraction of the sky-background, provides the best sky-subtraction and signal-to-noise ratio (SNR) for data from the NIR arm. Thus we decided to use this method for the reduction of the object frames, which results in one reduced 2d image for each adjacent pair of raw object frames, which comprises 16min of exposure time. For consistency, the data from the UV and optical arms were also reduced with the nodding recipe and sampled onto the same grid.

2.2.4 FLUX CALIBRATION, COMBINATION AND 1D EXTRACTION

For flux calibration, standard stars were observed in each night in which the data were obtained. They are taken from a list of eight white dwarfs, the intrinsic spectra of which have been modeled very accurately. Each standard star observation is reduced with the same calibration data as the science frames from the same night and the same pipeline parameters are employed for the reduction of the raw standard frames. From the observed shape of the flux standard spectrum we derive the spectral response curve: the 1d extracted spectrum of the standard star is divided by the tabulated known intrinsic spectrum (which is first interpolated and re-gridded to the same pixel binning on the wavelength axis) and the resulting curve is smoothed with a kernel of 15 pixels to obtain a smooth response curve and to minimize artificial effects introduced by pixels with abnormal values. We apply the flux calibration by first dividing the 2d spectra of our science targets as well as the 1d response curve by the respective exposure times (thus normalizing them to 1s exposure time) and then dividing the normalized 2d spectra along the wavelength axis by the normalized response curve for the respective night. In the NIR, atmospheric extinction is negligible, and no atmospheric extinction table is available for that wavelength range in the pipeline release. Telluric absorption

is accounted for by the flux standard, as we apply only little smoothing to the overall response curve.

By collapsing and weighting the spectrum along the wavelength axis, we determine the shapes of the spectral point spread function (SPSF) on the individual 2d spectra which we get as output from the pipeline, and thus determine the shifts to register and co-add the 2d spectra, which is done as a mean combination with rejection of outliers, which we define as pixel values which deviate from the mean by more than 10σ . We apply the same calibrations to the error maps as well, and combine them according to

$$Err_{combined} = \frac{\sqrt{\sum_{i=1}^n Err_i^2}}{n} \quad (2.1)$$

The final SPSF is determined by collapsing the weighted 2d stack along the wavelength axis in the H -band wavelength range (where the SNR per pixel is highest) and the 1d spectrum is extracted by applying the corresponding normalized weights, a procedure which is similar to the optimal extraction procedure described in Horne (1986). The extraction window spans a spatial extension of $1''.8$ around the centre of the trace for the point-source-like A1413-1, and for MACS2129-1, which is extended to an arc with a FWHM of $1''.6$, we extract the 1d spectrum in a $2''.6$ window. A 1d error spectrum is extracted the following way: with NSP being the normalized SPSF along the extraction window, the 1d variance is calculated as

$$Var(\lambda) = \frac{\sum_{y=y_1}^{y_2} Err(\lambda, y)^2 * NSP(y)^2}{(\sum_{y=y_1}^{y_2} NSP(y)^2)^2} \quad (2.2)$$

and the 1d errors are then the square root of that variance.

Galactic extinction corrections are taken from Schlegel et al. (1998) and implemented with the *fm_unred* code in IDL.

To check the flux level we integrate the extracted 1d spectra over the transmission curves of the Ks -band filters of the instrument from which the imaging data originate and compare with the photometric measurement. We subsequently scale both 1d spectra to match the Ks -band photometry, thus correcting for slit losses.

2.2.5 HST IMAGING DATA

To add further information to the SEDs of the two galaxies we include photometry from publicly available *HST* images of the two galaxies. For A1413-1 we use images obtained with the Advanced Camera for Surveys (ACS) in the $F775W$ and $F850LP$ bands as part of program 9292 (PI: Holland Ford). For MACS2129-1 we use images obtained with ACS in the $F606W$ band and with Wide Field Camera 3 (WFC3) in the $F105W$, $F110W$, $F125W$, $F140W$ and $F160W$ bands. These images were obtained as part of the CLASH Survey (program 12100, PI: Marc Postman). Photometry for A1413-1 is done with circular apertures (diameter 2). For MACS2129-1, which is extended to an arc, we use SExtractor (Bertin & Arnouts, 1996) to define elliptical apertures and

measure the total counts using *MAGAUTO*. For the *F606W* image of MAC2129-1 we used the *F110W* image (re-binned and rotated to the *F606W* pixel size and orientation) to define the aperture as the source is very faint in this band. We adopt zeropoints and aperture corrections from the ACS and WFC3 instrument handbooks. The Schlegel et al. (1998) maps again provide the galactic extinction corrections. The error bars on the photometry are conservative estimations, in order to account for cross-calibration issues when used together with the X-Shooter spectra to construct the SEDs of the two galaxies. We check the accuracy of the relative flux-calibration in both spectra by overplotting the HST photometry and conclude from the good agreement that no further flux correction of the spectra is necessary.

2.2.6 SPITZER IMAGING DATA

Both MACS2129 and A1413 had also been observed with the Multiband Imaging Photometer (MIPS) on the Spitzer Space Telescope, in the 24μ -band. 1320s of integration time were obtained on MACS2129 as part of program 50610 (PI: Yun) and 480s on A1413 as part of program 41011 (PI: Egami). Both galaxies in our study are undetected on these images. Because of noise structures in the images it was also not possible to derive upper limits on their fluxes.

2.3 DATA ANALYSIS

The signal-to-noise ratio in the spectra of both targeted galaxies is relatively low. We estimated the S/N in bins of several nm along the wavelength axis, where we sum up the flux in the object trace in a spatial window of about one seeing FWHM, and estimated the noise from the regions of the same size without object flux below and above the trace. For MACS2129-1 we thus estimate a mean $S/N/$ of ~ 1.3 , ~ 2.5 , and ~ 2.1 in the *J*-, *H*-, and *Ks*-band wavelength regions, respectively. For the spectrum of the significantly fainter A1413-1 the values are ~ 0.9 , ~ 1.2 , and ~ 1.0 for *J*, *H*, and *Ks*, respectively.

2.3.1 REDSHIFT DETERMINATION AND SPECTRAL ENERGY DISTRIBUTION ANALYSIS

Emission and absorption lines

The NIR 2d spectra of both galaxies were examined visually to search for emission lines and absorption features. Visualizations of both the NIR 2d and 1d spectra are shown in Figures 2.4, 2.5, and 2.6. For better visibility, we also smooth them along the wavelength axis. We do not detect emission lines in the spectra of any of the two galaxies. At several positions we see hints of absorption lines, but we did not consider these significant and reliable enough for an independent robust redshift measurement. Instead we proceed with an analysis of the spectral energy distributions and photometric red-

shift measurements in Sect. 2.3.1 and Sect. 2.3.1. Guided by those we then in Sect. 2.3.1 return to the issue of the nature of the tentative spectral lines.

We do not find any trace in the UV arm data for both objects. Over the whole optical wavelength range, a trace is detected from MACS2129-1, and partly from A1413-1. Even in big bins, however, we only find very low S/N. As a consequence we will later rely on the HST broad-band magnitudes for this wavelength range.

Construction of spectro-photometric Spectral Energy Distributions

Although the potential absorption lines in the NIR spectra of both galaxies are not significant enough to reliably determine independent spectroscopic redshifts, there is still the possibility to determine their redshifts (although with higher uncertainties than for line measurements) from the shape of the NIR spectrum, i.e. mainly the position of the Balmer/4000Å-break which both are distinctive (but partly overlapping) features in stellar populations with ages of several hundred Myrs and above.

In order to have a well-sampled Spectral Energy Distribution (SED) with sufficient S/N in each data point, we bin the NIR spectrum, with bin sizes ranging between 15nm and 70nm.

For each bin we regard the wavelength range as the transmission curve $T_{synth}(\lambda)$ of a “synthetic filter” with cut-on and cut-off wavelengths λ_1 and λ_2 and mean wavelength λ_{mean} , which we all define below. Furthermore, the combined fluxes and errors in each bin are calculated from the original fluxes and errors as follows:

$$weight(\lambda) = \frac{1}{err(\lambda)^2} \quad (2.3)$$

$$T_{synth}(\lambda) = \frac{weight(\lambda)}{max(weight(\lambda))} \quad (2.4)$$

$$\lambda_{mean} = \frac{\int_{\lambda_1}^{\lambda_2} \lambda \cdot T_{synth}(\lambda) \cdot d\lambda}{\int_{\lambda_1}^{\lambda_2} T_{synth}(\lambda) \cdot d\lambda} \quad (2.5)$$

$$F_{\lambda,bin} = \frac{\sum_{\lambda_1}^{\lambda_2} F_{\lambda}(\lambda) \cdot T_{synth}(\lambda)}{\sum_{\lambda_1}^{\lambda_2} T_{synth}(\lambda)} \quad (2.6)$$

$$Err_{bin} = \frac{\sqrt{\sum_{\lambda_1}^{\lambda_2} Err(\lambda)^2 \cdot T_{synth}(\lambda)^2}}{\sum_{\lambda_1}^{\lambda_2} T_{synth}(\lambda)} \quad (2.7)$$

One can see from the above formulae that the relative weights of each contributing wavelength pixel are used as “transmission” of our individually defined “synthetic filters”.

To obtain reliable constraints on the redshifts via the position of the Balmer/4000Å-break we want to sample this region with several data points on each side of the feature. From visual inspection of the shape of both spectra we conclude that the Balmer/4000Å-break is located in the range of the Y- and J-bands. We thus manually define 10 bins

in this wavelength region, which turn out to exhibit S/N ratios between 5.5 and 16 for the A1413-1 spectrum and between 13 and 32 for the MACS2129-1 spectrum. We then divide the *H*-band wavelength region into two parts, one ranging from 1440nm to 1521nm with lower S/N, and one from 1521nm to 1798nm, where the S/N ratio reaches its highest values across the whole NIR wavelength range. Both of them are binned by an algorithm which sets the bin sizes such that they result in a certain S/N ratio. We thus bin the short wavelength region of the H-band with S/N per bin of 20 for the A1413-1 spectrum and 50 for MACS2129-1, and for the longer wavelength range of the *H*-band we bin up to a S/N per bin of 35 for A1413-1 and 75 for MACS2129-1. For the K_s -band wavelength range from 1970nm to 2300nm we again define bins manually: we exclude noisy regions (where absorption is high) and split the rest into 7 bins, with S/N ratios between 6 and 24 for A1413-1 and 22 and 49 for MACS2129-1. Wavelengths beyond the end of the K_s -band at $2.3\mu m$ were excluded as the sky-subtraction here was not sufficiently good to allow robust measurements.

In addition to the SEDs constructed out of the NIR spectra, we add the above-mentioned HST photometry in the *F606W* band for MACS2129-1 and in the *F775W* and *F850LP* bands for A1413-1, in order to extend the SEDs of the two galaxies also to optical wavelengths.

A complete overview of the SEDs is given in Tables 2.4 and 2.5, where we include the quasi-photometric magnitudes of the binned NIR spectra, and the broad-band magnitudes from the HST images described in section 2.2.5.

Stellar population synthesis fits to the SEDs

We use the multi-wavelength SEDs, described in section 2.3.1, to fit stellar population synthesis models, in order to determine photometric redshifts as well as stellar ages, masses, and dust extinctions from them. Given the limited SNR of the available spectra and the low significance of absorption lines, it is not possible to place robust constraints on the metallicities. We fit the data using the LePhare code (Arnouts et al., 1999; Ilbert et al., 2006) and galaxy models from Bruzual & Charlot (2003a, BC03 hereafter), based on the Chabrier initial mass function (IMF) (Chabrier, 2003), and the Calzetti extinction law (Calzetti et al., 1994, 2000). The assumed star formation histories in the BC03 models follow an exponential declining rate, $SFR \propto e^{-\frac{t}{\tau}}$, with 9 different e-folding timescales τ , ranging from 0.1 Gyr to 30 Gyr. Furthermore, they come with three different metallicities, $Z = 0.02$ (solar value), $Z = 0.008$ and $Z = 0.004$. LePhare is based on a χ^2 template-fitting procedure (Arnouts et al., 1999, 2002), with an input grid comprising of the above-mentioned list of 27 BC03 models, a range of redshifts z in steps Δz , extinction coefficients E_{B-V} , and a list of ages for the models. A library of theoretical magnitudes is built by redshifting each SED in steps of Δz and convolving them with the transmission curves of the filters. In our case, these filters are those defined synthetically by the binning procedure described in Sec. 2.3.1. LePhare also takes into account the opacity of the inter-galactic medium as described in Madau (1995, see also

Møller & Jakobsen 1990). After the determination of the z value taken from the input grid which minimizes the merit function χ^2 , the best fitting redshift is derived with a parabolic interpolation of the redshift probability distribution. Following Ilbert et al. (2006, 2009) the 1σ level errors obtained from the probability distribution function are a reliable estimate of the actual photo- z accuracy. In the computation of the library of theoretical galaxy magnitudes, we follow an iterative approach: we first adopt a wide-spaced grid covering a large range of input values to obtain first estimates on the (photometric) redshift, the range of possible stellar ages, and the extinction coefficient E_{B-V} . With the help of those, we narrow down the range of redshifts, ages and E_{B-V} values used in a second iteration of the LePhare fitting procedure, enabling us to use smaller steps and thus a finer input grid for z and E_{B-V} . The main motivation for this approach is the technical limitation of the libraries to a maximum of $9 \cdot 10^5$ entries, i.e. the product of number of input BC03 models, extinction laws, and the numbers of entries on the grids of ages, Δz steps and E_{B-V} values. The finer sampling on the redshift grid allows us to reduce the systematics and obtain more detailed insights in the shape of the redshift probability distribution, especially about potential secondary or double peaks. The lower uncertainties in the redshift due to the finer redshift grid and the smaller steps in the used E_{B-V} values allow us to obtain a more accurate estimation of the latter and thus result in more reliable constraints on the stellar ages. The best fit models for both galaxies are overplotted in Fig. 2.2 and Fig. 2.3, and the results for the derived physical parameters are summarized in Table 2.2. It has to be emphasized here that the stellar masses are subject to systematic uncertainties (which can easily exceed a factor of 2) which are not included in the quoted error budget but originate in the uncertainty on the initial mass function (IMF) which is not well constrained at high redshifts. It turns out that the input SEDs are best fit by the BC03 models with an e-folding timescale for star formation of 0.1 Gyr (A1413-1) and 0.3 Gyr (MACS2129-1), respectively. The model fit for A1413-1 indicates no on-going star formation (with an upper limit of $\sim 0.2 M_{\odot} \text{yr}^{-1}$), and for MACS2129-1 the fit allows for a star formation rate of $2 \pm 2 M_{\odot} \text{yr}^{-1}$ which according to the resulting specific star formation rate of $(1.8 \pm 1.8) \cdot 10^{-11} \text{yr}^{-1}$ means that MACS2129-1 can be regarded as a passively evolving galaxy. We emphasize that this value for star formation is solely based on the best-fit model with the assumption of an exponentially declining star formation rate. This approximation does most likely not represent reality (Anderson & Soto, 2012) and as a consequence the computed star formation rates should not be taken too literally. Given the non-detection of emission lines we conclude that the MACS2129-1 spectrum is still consistent with no ongoing star formation.

Nature of tentatively detected spectral lines

Guided by the photometric redshifts found above we now return to the issue of tentative absorption lines in the spectrum. As can be seen in Fig. 2.4 and Fig. 2.5 there are indications of very broad $H\beta$ absorption at the expected positions dictated by the

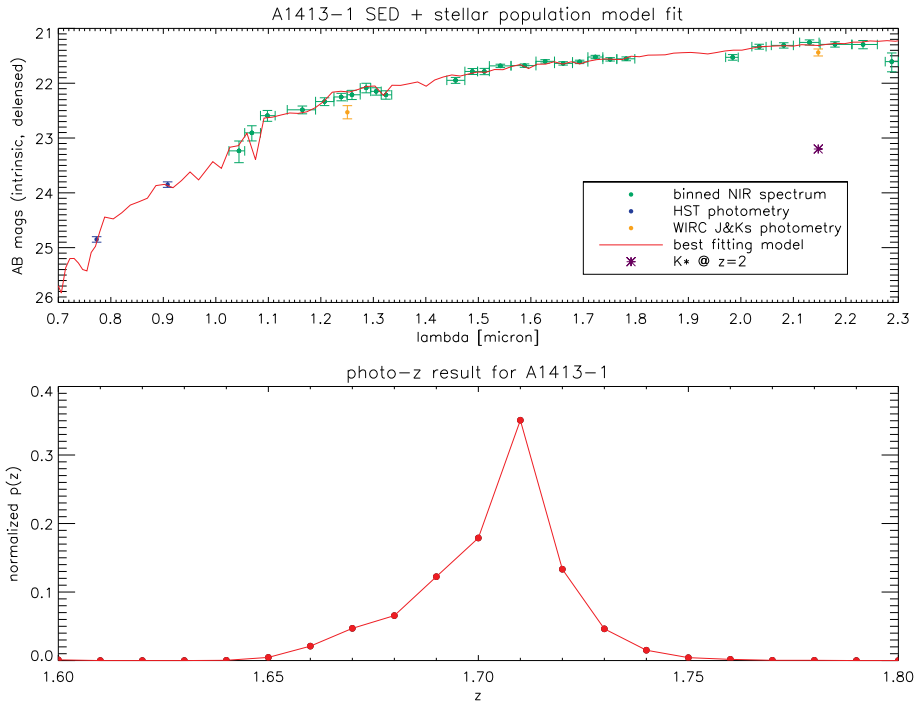


Figure 2.2 Upper panel: Spectro-photometric SED of the gravitationally-lensed galaxy A1413-1, together with HST/ACS and Palomar/WIRC photometry. Overplotted is the best-fit BC03 model, a 2.4 Gyr passively evolving population with little dust and a stellar mass of $M_{\star} = 7.6 \cdot 10^{10} M_{\odot}$. Lower Panel: Probability distribution of the photometric redshift for A1413-1.

photometric redshifts for both MACS2129-1 ($S/N \sim 3.5$) and A1413. For MACS2129-1 there are also hints of absorption at the expected position of CaII + H δ . Based on the position of the tentative H β lines we infer spectroscopic redshifts of $z = 2.1477 \pm 0.0007$ and $z = 1.707 \pm 0.002$, which are fully consistent with the photometric redshifts. We defer further analysis of these tentative features (e.g. velocity dispersions) to a future study. To double-check the SED fitting performed in Sect. 2.3.1 we re-ran the same procedure, but this time with the redshifts fixed to the spectroscopic redshifts inferred from the H β lines. The results from the new LePhare fits show no significant changes with respect to the results reported in Table 2.2.

2.3.2 PROFILE FITS TO THE DE-LENSED IMAGES

Of the two targets in this study, MACS2129-1 shows a clearly extended morphology, which is most prominent on the HST F160W image. We use this image to reconstruct the shape of the object in the source plane, based on the determined redshift. We show

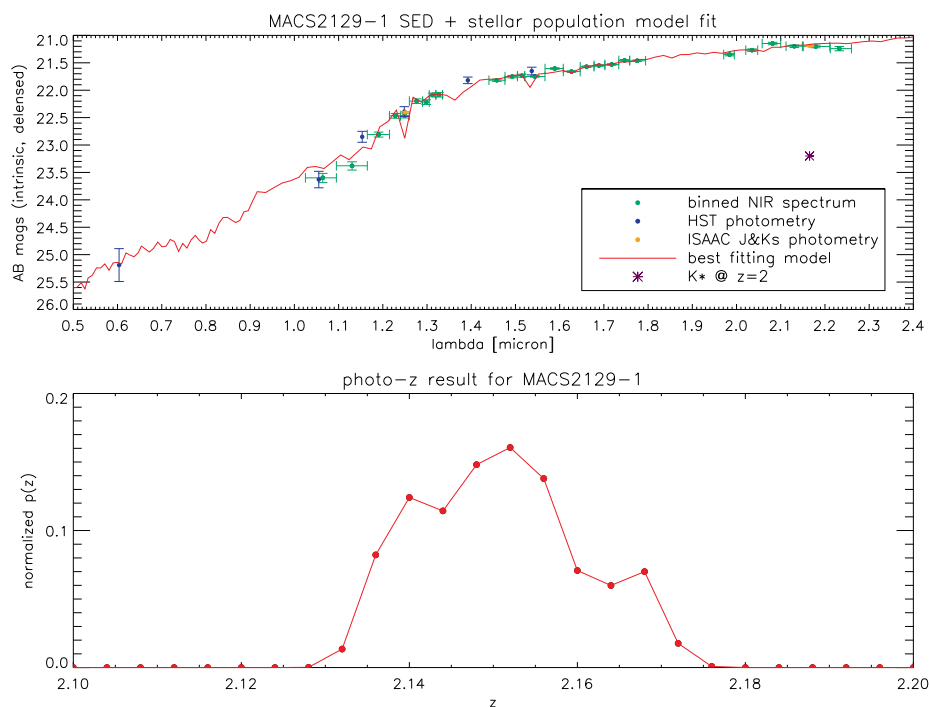


Figure 2.3 Upper panel: Spectro-photometric SED of the gravitationally-lensed galaxy MACS2129-1. Overplotted in red is the best-fit BC03 model with a Chabrier IMF, a 1.7 Gyr population with a stellar mass of $M_{\star} = 1.1 \cdot 10^{11} M_{\odot}$. Lower panel: Probability distribution of the photometric redshift for MACS2129-1.

Table 2.2. LePhare fitting results for the lensed galaxies A1413-1 and MACS2129-1

Parameter	A1413-1	MACS2129-1
z_{phot}	1.71 ± 0.02	2.15 ± 0.01
Age [Gyr]	$2.4^{+0.8}_{-0.6}$	1.7 ± 0.3
E_{B-V} [mag]	0.02 ± 0.01	0.1 ± 0.02
A_V [mag]	0.08 ± 0.08	0.41 ± 0.28
M_{\star} [$10^{10} M_{\odot}$]	7.6 ± 1.1	11.0 ± 2.8
SFR [$M_{\odot} yr^{-1}$]	0	2 ± 2
sSFR [yr^{-1}]	0	$(1.8 \pm 1.8) \cdot 10^{-11}$
z_{form}	$4.3^{+3.4}_{-1.2}$	$4.3^{+1.0}_{-0.6}$

Table 2.3. GALFIT fitting results for the reconstructed images of the lensed galaxies A1413-1 and MACS2129-1

Parameter	A1413-1	MACS2129-1
n	3.25 ± 0.02	0.88 ± 0.01
r_e	$2.38 \pm 0.01 kpc$	$2.60 \pm 0.29 kpc$
$\frac{b}{a}$	0.50 ± 0.01	0.47 ± 0.03
r_c	$1.68 \pm 0.01 kpc$	$1.78 \pm 0.14 kpc$
PA	14° E of N	-34° E of N

the resulting de-lensed image in Fig. 2.8. Similarly, we use the HST F850LP image of A1413 to reconstruct the unlensed image of A1413-1, which is shown in Fig. 2.7.

We use GALFIT version 3.0 (Peng et al., 2002; Peng, 2010) to fit a 2D Sersic model convolved with the reconstructed PSF, to the de-lensed F160W image of MACS2129-1, and to the F850LP image of A1413-1. The code is run on 100 Monte Carlo realizations of the reconstructions. In the case of MACS2129-1, three of the 100 realizations give highly deviant results with very high χ^2 , which we subsequently discard. Uncertainties are computed as the standard deviation of all (remaining) results. The best-fit parameters (effective half-light radius r_{eff} , Sersic index n , and axis ratio $\frac{b}{a}$) are then used to quantify the structure of the galaxies. We compute the circularized radii as $r_c = r_{eff} \cdot \sqrt{\frac{b}{a}}$. The Sersic index provides an indication whether the light profile resembles more an exponential disk profile ($n = 1$) or an elliptical galaxy ($n = 4$). The results are summarized in Table 2.3 and visualized in Fig. 2.7 and Fig 2.8. As can be seen in the upper half of Fig. 2.8, the one-component Sersic fit to MACS2129-1 leaves two residuals, one in the core and one in the northern part of the galaxy. To account for these deviations from a simple Sersic profile, we produced a second fit, which models the two extra components with a psf, i.e. a point-source-like component. The lower half of Fig. 2.8 shows the residuals of this better fit. We note that the multi-component fit does not significantly alter the result for the Sersic index and effective radius of MACS2129-1.

We use the definition of Barro et al. (2012) of compactness (at $z \sim 2$)

$$\log M_\star[M_\odot] \cdot R[kpc]^{-1.5} > 10.3 \quad (2.8)$$

to assess how compact the two galaxies in our study are. Here R corresponds to the circularized effective radius. It is thus confirmed that MACS2129-1 is indeed a compact galaxy according to that definition, with $\log M_\star[M_\odot] \cdot r_c[kpc]^{-1.5} = 10.67 \pm 0.28$. The compactness of A1413-1 is computed as $\log M_\star[M_\odot] \cdot r_c[kpc]^{-1.5} = 10.54 \pm 0.14$ and thus also fulfills the criterion for compactness.

2.4 DISCUSSION AND CONCLUSIONS

In this article we analyzed the spectra of two gravitationally-lensed distant compact quiescent galaxies and derived their redshifts, stellar masses and ages, as well as constraints on dust extinction and potential star formation, from SED fitting. We also analyzed their morphologies based on HST images which we de-lensed with available mass-models for the lensing clusters. Interpretations of the results are presented below.

2.4.1 REDSHIFTS AND DERIVATION OF INTRINSIC MAGNITUDES

In the SED fitting procedure, the Balmer/4000Å-break is the feature which enables a reliable and robust determination of the redshifts of galaxies with evolved stellar populations. The resulting redshifts are $z = 1.71 \pm 0.02$ for A1413-1 and $z = 2.15 \pm 0.01$ for MACS2129-1. The respective error bars are taken from the 68% confidence intervals of the best fits. To visualize where spectral lines are expected to be at these redshifts, we overplot their positions at those redshifts in Figures 2.4, 2.5, and 2.6. We also use the derived redshifts to determine the magnifications according to the available mass models for both clusters. The resulting lensing magnifications are 1.73 ± 0.05 for A1413-1 and 3.95 ± 0.95 for MACS2129-1 and thus lower than the initial estimations based on the assumption of $z \sim 2$. Adopting $K_{\star} \sim 21.4$ as the typical luminosity (L_{\star}) of red galaxies at $z \sim 2$ (Marchesini et al., 2007), the two galaxies in this study exhibit luminosities of $\sim 5.2 \times L_{\star}$ (A1413-1) and $\sim 6.3 \times L_{\star}$ (MACS2129-1). Their stellar masses correspond to $\sim 0.9 \times M_{\star}$ and $\sim 1.3 \times M_{\star}$ (Marchesini et al., 2009). The de-lensed magnitudes according to the lensing magnifications were used to scale the stellar masses and star formation rates of the SED fits.

2.4.2 CONSTRAINTS ON LINE-FLUXES AND STAR FORMATION

In Fig. 2.6 we demonstrate the non-detectability of potential $H\alpha$ emission by zooming in on the wavelength regions where $H\alpha$ is expected at the redshifts of the two galaxies. In both the 1D and 2D spectral cutouts it is clearly visible that there is no detectable emission line. In order to constrain the amount of star formation which might have been still on-going in the two galaxies, despite the lack of detectable emission lines, we determined upper limits on potential $H\alpha$ line emission in the spectra. For that purpose, we subtracted the continuum around the positions where we would expect the $H\alpha$ line at the respective redshifts and added artificial emission lines. In this way, we infer 3σ limits on $H\alpha$ line emission of $2 \cdot 10^{17} \text{ erg} \cdot \text{s}^{-1} \cdot \text{cm}^{-2}$ and $2.4 \cdot 10^{17} \text{ erg} \cdot \text{s}^{-1} \cdot \text{cm}^{-2}$ for A1413-1 and MACS2129-1, respectively. Converting into intrinsic potential $H\alpha$ luminosities (taking also the lensing magnification into account) and applying the Kennicutt (1998a) relation, the 3σ upper limits on star formation rates in A1413-1 and MACS2129-1 turn out to be $< 1.8 \cdot M_{\odot} \cdot \text{yr}^{-1}$ and $< 1.7 \cdot M_{\odot} \cdot \text{yr}^{-1}$, respectively. The Kennicutt relation is based on the assumption of a Salpeter (1955) IMF and solar metallicities. Converting to the assumed Chabrier IMF via division by a factor of 1.58 (Treyer et al., 2007), the

3σ upper limits are of the order of $1M_{\odot} \cdot yr^{-1}$. These are the best limits on potentially on-going star-formation in quiescent $z \sim 2$ galaxies so far, even compared to the most recent similar studies (Kriek et al., 2009; Onodera et al., 2010; van de Sande et al., 2011; Toft et al., 2012).

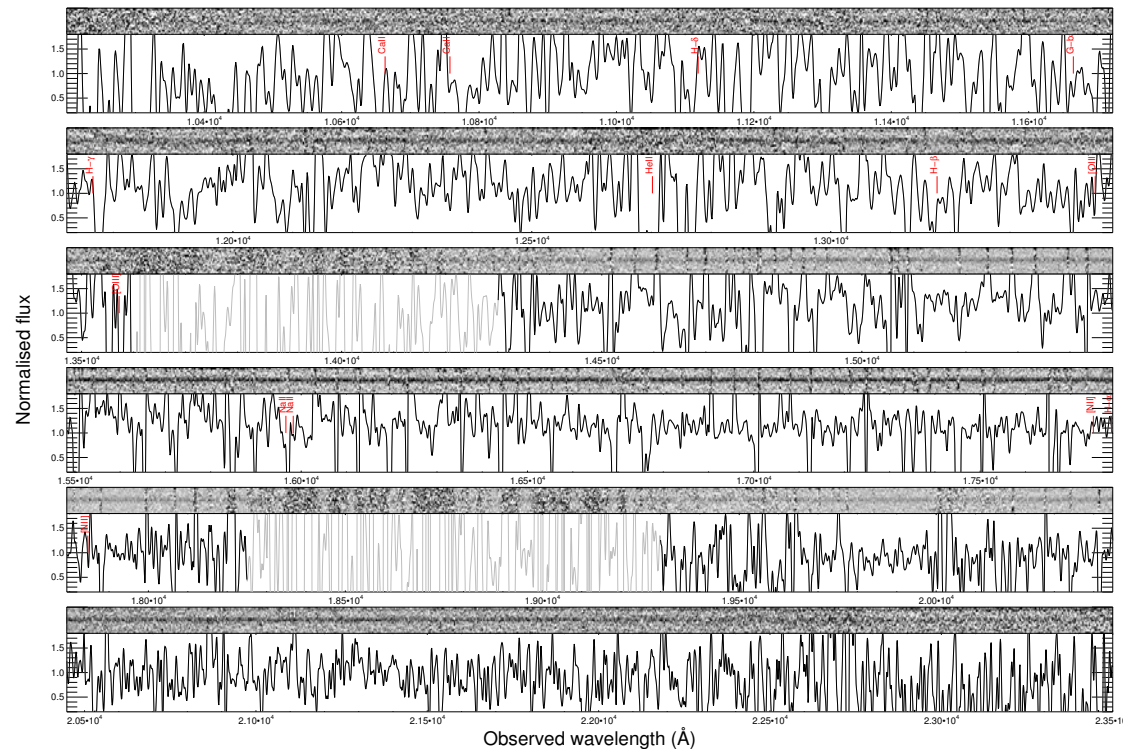


Figure 2.4 The 2D and 1D X-Shooter NIR spectrum of A1413-1. We overplot the expected positions of several spectral lines at the redshift of $z = 1.71$. Little black lines above the 1D spectrum indicate skylines. The wavelength regions in the gaps between the J- and H-bands and the H- and K-bands are plotted in grey to avoid distraction by the high noise (and absence of information) there.

2.4.3 STELLAR POPULATION PROPERTIES

From SED modeling, we derived the ages of the stellar populations to be in the range of $2.4^{+0.8}_{-0.6}$ Gyr (A1413-1) and 1.7 ± 0.3 Gyr (MACS2129-1). This is an intriguing result, as they turn out to be older and thus exhibit higher mass-to-light ratios than most galaxies from other studies (Kriek et al., 2008, 2009; van Dokkum & Brammer, 2010; van de Sande et al., 2011; Toft et al., 2012; van de Sande et al., 2012). This is mostly due to the fact that younger galaxies are easier to detect. van de Sande et al. (2012) indeed argue that their sample is biased towards young galaxies, compared to a mass-limited sample. By scaling to the intrinsic luminosities, taking into account the enhancement of the observed brightness by the lensing effect, and including the uncertainty on the

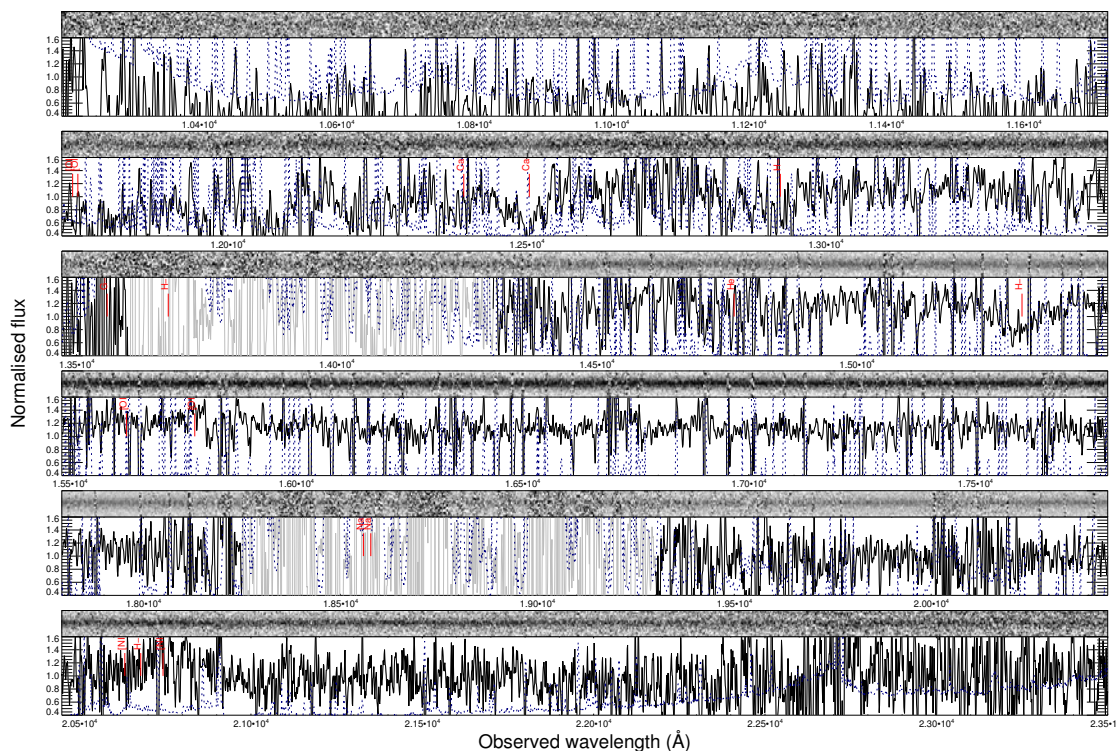


Figure 2.5 The 2D and 1D X-Shooter NIR spectrum of MACS2129-1. We overplot the expected positions of several spectral lines at the redshift of $z = 2.15$. The blue line indicates the error spectrum. Little black lines above the 1D spectrum indicate skylines. The wavelength regions in the gaps between the J- and H-bands and the H- and K-bands are plotted in grey to avoid distraction by the high noise (and absence of information) there.

lensing magnification in quadrature into the error budget, we infer their stellar masses to be $(7.6 \pm 1.1) \cdot 10^{10} M_{\odot}$ (A1413-1) and $(1.1 \pm 0.28) \cdot 10^{11} M_{\odot}$ (MACS2129-1). This makes them two of the least (intrinsically) luminous quiescent high- z galaxies whose properties have been studied spectroscopically. As visualized in Fig. 2.9 this mass range has been probed before, which was however only possible with exorbitant use of telescope time ($\sim 500h$ for the GMASS sample). The lensing approach makes these studies much more feasible, and will in the future also give us the possibility to test the properties of larger samples of $z \sim 2$ quiescent M_{\star} (and even L_{\star}) galaxies, which are much more representative of the overall population than the brightest ones (see also van de Sande et al. (2012) for a more detailed discussion of this issue).

2.4.4 MORPHOLOGIES

In section 2.3.2 we described the fitting of surface brightness profiles with the GALFIT tool, the results of which we summarize in Table 2.3. For A1413-1 we find a relatively

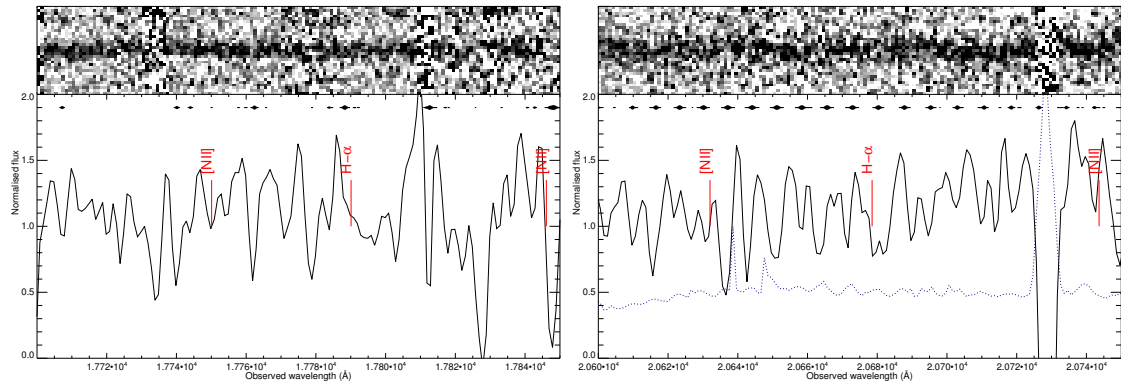


Figure 2.6 Left panel: Zoom-in on the wavelength region around the expected position of the $H\alpha$ line in the 2D and 1D spectrum of A1413-1. Right panel: Zoom-in on the wavelength region around the expected position of the $H\alpha$ line in the 2D and 1D spectrum of MACS2129-1. The cutouts show that there is no detectable emission line.

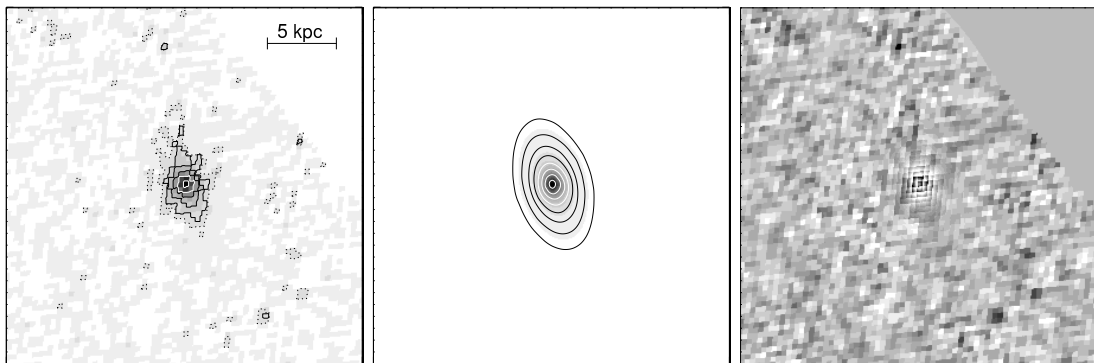


Figure 2.7 Left panel: The de-lensed image of the gravitationally-lensed distant massive quiescent galaxy A1413-1, reconstructed from the HST F850LP image, based on the derived redshift of $z = 1.71$. Middle panel: A Sersic profile fit to the de-lensed image, obtained with GALFIT. For further information about the fit results, see Table 2.3. Right panel: Residuals from the Sersic fit.

high Sersic index of $n \sim 3.3$ which resembles an early-type galaxy. The structural analysis of galaxy MACS2129-1 reveals a profile which is more disk-like than an exponential disk with $n = 0.88$. This shape classifies it as an S0 like galaxy. Only relatively recently it has been possible to identify disk-like galaxies around $z \sim 2$ (e.g. Genzel et al., 2006; van der Wel et al., 2011; Chang et al., 2013). Combined with the constraints on potentially on-going star formation it constitutes the first spectroscopically confirmed passive lenticular galaxy at $z > 2$.

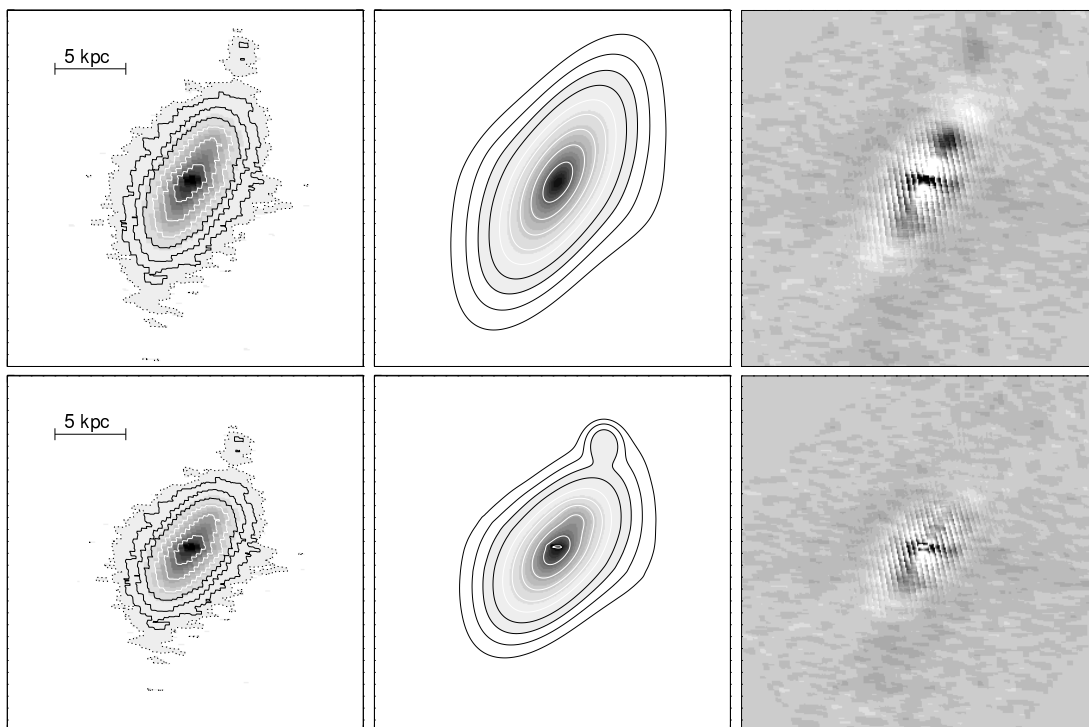


Figure 2.8 Left panel: The de-lensed image of the gravitationally-lensed distant massive quiescent galaxy MACS2129-1, reconstructed from the HST F160W image, based on the derived redshift of $z = 2.15$. Middle panel: A Sersic profile fit to the de-lensed image, obtained with GALFIT. For further information about the fit results, see Table 2.3. Right panel: Residuals from the Sersic fit. We recognize a bright core, which is not aligned with the disk and leaves a residual. Furthermore, there is another additional component in the northern part of the galaxy. In the lower panels we show the multi-component fit described in section 2.3.2 which include those extra components.

2.4.5 STELLAR MASSES AND SIZES

In order to compare the stellar masses and sizes of the two galaxies in our study, we compile a sample of passive galaxies in the redshift range $1.5 < z < 2.5$ from the literature. All these studies used the Chabrier IMF (Chabrier, 2003) and thus provide some useful comparison of stellar masses, and estimate their (circularized) half-light radii via Sersic profile fits. The 24 galaxies in this comparison sample are taken from Toft et al. (2012), van de Sande et al. (2011), Kriek et al. (2009); van Dokkum et al. (2009), van Dokkum & Brammer (2010), Onodera et al. (2010), Muzzin et al. (2012), Mancini et al. (2010), and Cimatti et al. (2008). For comparison with the typical properties of galaxies in today’s Universe, in Fig. 2.9 we plot the local stellar mass-size-relations for early-type (red color) and late-type (blue color) galaxies from Shen et al. (2003), with their intrinsic scatter plotted in dashed lines. The same color scheme is used to divide the $1.5 < z < 2.5$ galaxy sample into early-type ($n > 2.5$) and late-type ($n < 2.5$)

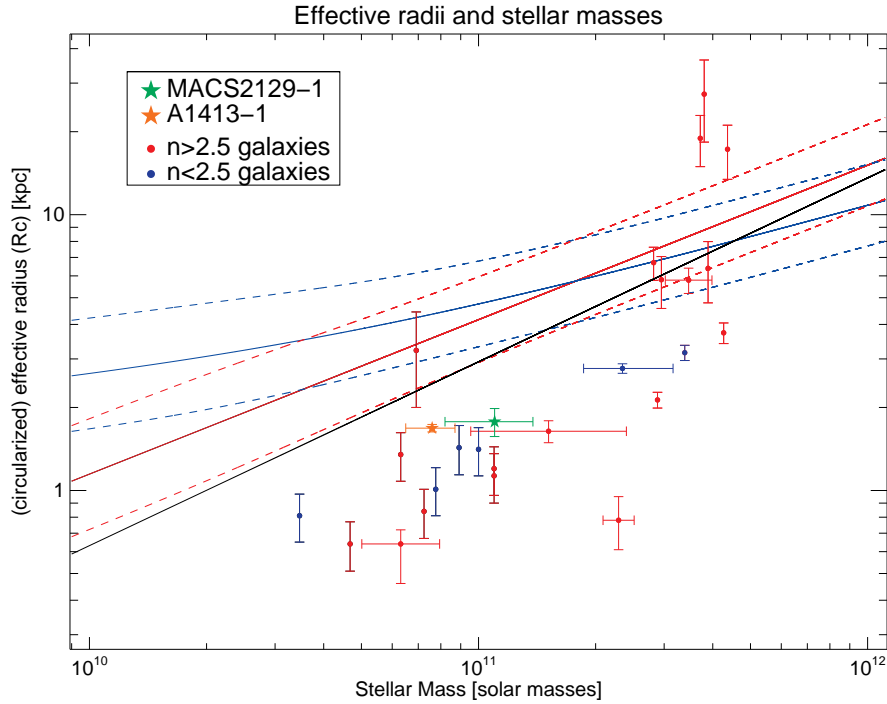


Figure 2.9 Effective (circularized) radii of the lensed $z \sim 2$ galaxies A1413-1 and MACS2129-1 plotted against their stellar masses. For comparison we overplot the values for a sample of 24 $1.5 < z < 2.5$ passive galaxies compiled from Toft et al. (2012), van de Sande et al. (2011), Kriek et al. (2009); van Dokkum et al. (2009), van Dokkum & Brammer (2010), Onodera et al. (2010), Muzzin et al. (2012), Mancini et al. (2010), and Cimatti et al. (2008). The local stellar mass-size-relations for early-type (red color) and late-type (blue color) galaxies from Shen et al. (2003) are also overplotted, with their intrinsic scatter in dashed lines. The compactness criterion of Barro et al. (2012) is indicated by the bold black line.

galaxies. The two galaxies from our galaxy are plotted in green (MACS2129-1) and orange (A1413-1) colors. As found in previous studies, quiescent galaxies at $1.5 < z < 2.5$ are significantly more compact than galaxies in today’s local Universe. The compactness criterion of Barro et al. (2012) is indicated by the bold black line.

The intriguing diversity of quiescent galaxies at $z \sim 2$ (see also Onodera et al., 2010) clearly indicates that the spectroscopic sample of quiescent $z \sim 2$ galaxies needs to be extended significantly to establish a robust picture of their role in the formation and evolution of early-type galaxies at all redshifts.

2.4.6 PROSPECTS FOR FUTURE DETAILED STUDIES

An additional advantage of observing lensed high-redshift galaxies is the increased spatial resolution due to the gravitational lensing effect. For unlensed compact $z \sim 2$ galaxies there is essentially no spatial information available in ground based observations, given the extreme compactness of these objects, (e.g. Toft et al., 2012). The additional spatial information is in particular striking for MACS2129-1 that is stretched along a caustic line resulting in an observed extension of almost 2. With a deeper observation using multiple slit positions it should be possible to determine both the dependence of the (line-of-sight) velocity dispersion on position within the galaxy as well as to establish if there is rotation of the overall system. We point out that the lensing approach will greatly increase the feasibility of continuum and absorption line spectroscopy of faint, i.e. $\sim L_*$ quiescent galaxies at high redshifts ($z \gtrsim 2$).

We emphasize the interesting finding that MACS2129-1 exhibits a surface brightness profile which strongly resembles a disk galaxy, which corroborates the existence of a significant fraction of massive passive disks at $z \sim 2$. The question whether disk-like galaxies dominate the passive galaxy population at $1.5 < z < 2.5$ is still a highly-debated topic, with no firm conclusion at hand yet (e.g. van der Wel et al., 2011; Wuyts et al., 2011).

In this current study, we have demonstrated that even in cases with limited S/N it is possible to use the continuum emission to derive useful constraints on important properties like redshifts, stellar masses and ages as well as the resulting formation redshifts. Subsequent studies of larger samples of quiescent $z \sim 2$ galaxies with intrinsic luminosities down to L_* will allow for statistically more robust insights into relationships between (stellar) masses, sizes, morphologies, and formation redshifts.

2.5 ACKNOWLEDGMENTS

We thank Teddy Frederiksen, Martin Sparre, Antonio de Ugarte Postigo, and Stefano Zibetti for helpful discussions. We thank the anonymous referee for constructive and helpful reviews. SG thanks Gottfried Beyvers for detailed proof-reading of the manuscript. We gratefully acknowledge support from the Lundbeck foundation, and the Dark Cosmology Centre which is funded by the Danish National Research Foundation. JR is supported by the EU Career Integration Grant 294074. TK acknowledges support by the European Commission under the Marie Curie Intra-European Fellowship Programme. JPUF acknowledges support from the ERC-StG grant EGG-278202.

2.6 APPENDIX MATERIAL

Table 2.4. Spectro-photometric measurements for A1413-1. ^(a) Effective wavelength calculated as in Eq. 3. ^(b) Short and long wavelength ends of the spectro-photometric bins. ^(c) Observed AB magnitude. ^(d) Intrinsic AB magnitude inferred from the lensing magnification.

Facility	Filter/ $\lambda_{eff}[nm]^{(a)}$	$cut - on^{(b)}$	$cut - off^{(b)}$	$mag_{obs}^{(c)}$	Δmag	$mag_{int}^{(d)}$
HST/ACS	F775W	-	-	24.25	0.05	24.85
HST/ACS	F850LP	-	-	23.25	0.05	23.85
XSH/NIR	1044.09	1025.0	1055.0	22.634	0.216	23.234
XSH/NIR	1068.59	1055.0	1085.0	22.306	0.147	22.906
XSH/NIR	1098.27	1085.0	1113.0	21.992	0.103	22.592
XSH/NIR	1164.83	1136.0	1190.0	21.885	0.073	22.485
XSH/NIR	1207.11	1190.0	1225.0	21.735	0.073	22.335
XSH/NIR	1238.78	1225.0	1250.0	21.651	0.068	22.251
WIRC	J	-	-	21.93	0.12	22.53
XSH/NIR	1259.32	1250.0	1275.0	21.611	0.087	22.211
XSH/NIR	1286.26	1275.0	1295.0	21.485	0.091	22.085
XSH/NIR	1305.40	1295.0	1315.0	21.548	0.069	22.148
XSH/NIR	1324.02	1315.0	1335.0	21.612	0.079	22.212
XSH/NIR	1456.64	1440.0	1474.3	21.347	0.056	21.947
XSH/NIR	1488.54	1474.4	1498.5	21.185	0.056	21.785
XSH/NIR	1511.31	1498.6	1521.0	21.185	0.059	21.785
XSH/NIR	1541.88	1521.0	1562.2	21.084	0.031	21.684
XSH/NIR	1587.96	1562.3	1609.7	21.079	0.031	21.679
XSH/NIR	1627.22	1609.8	1645.0	21.001	0.031	21.601
XSH/NIR	1661.47	1645.1	1679.3	21.038	0.031	21.638
XSH/NIR	1692.84	1679.4	1708.6	21.011	0.031	21.611
XSH/NIR	1722.86	1708.7	1737.1	20.922	0.031	21.522
XSH/NIR	1751.04	1737.2	1763.7	20.964	0.031	21.564
XSH/NIR	1781.63	1763.8	1798.0	20.955	0.035	21.555
XSH/NIR	1984.47	1971.0	1995.0	20.928	0.052	21.528
XSH/NIR	2035.02	2021.0	2048.0	20.733	0.046	21.333
XSH/NIR	2081.69	2058.0	2100.0	20.710	0.050	21.310
XSH/NIR	2130.80	2112.0	2149.0	20.656	0.048	21.256
WIRC	Ks (2147.40)	-	-	20.839	0.064	21.439
XSH/NIR	2179.26	2151.0	2211.0	20.692	0.050	21.292
XSH/NIR	2232.73	2212.0	2260.0	20.693	0.078	21.293
XSH/NIR	2287.43	2275.0	2300.0	21.006	0.186	21.606

Table 2.5. Spectro-photometric measurements for MACS2129-1. ^(a) Effective wavelength calculated as in Eq. 3. ^(b) Short and long wavelength ends of the spectro-photometric bins. ^(c) Observed AB magnitude. ^(d) Intrinsic AB magnitude inferred from the lensing magnification.

Facility	Filter/ $\lambda_{eff}[nm]^{(a)}$	$cut - on^{(b)}$	$cut - off^{(b)}$	$mag_{obs}^{(c)}$	Δmag	$mag_{int}^{(d)}$
HST/ACS	F606W	-	-	23.7	0.3	25.21
HST/WFC3	F105W	-	-	22.14	0.15	23.65
XSH/NIR	1064.01	1025.0	1095.0	22.108	0.087	23.618
HST/WFC3	F110W	-	-	21.36	0.10	22.87
XSH/NIR	1130.41	1095.0	1165.0	21.889	0.078	23.399
XSH/NIR	1190.63	1165.0	1215.0	21.319	0.046	22.829
HST/WFC3	F125W	-	-	20.90	0.09	22.41
XSH/NIR	1228.36	1215.0	1240.0	20.977	0.045	22.487
XSH/NIR	1249.32	1240.0	1260.0	20.973	0.044	22.483
ISAAC	J (1250.5)	-	-	20.914		22.424
XSH/NIR	1276.50	1260.0	1290.0	20.709	0.043	22.219
XSH/NIR	1298.29	1290.0	1305.0	20.727	0.044	22.237
XSH/NIR	1312.77	1305.0	1320.0	20.596	0.034	22.106
XSH/NIR	1327.19	1320.0	1335.0	20.593	0.041	22.103
HST/WFC3	F140W	-	-	20.33	0.06	21.84
XSH/NIR	1457.87	1440.0	1476.3	20.328	0.022	21.838
XSH/NIR	1492.49	1476.4	1504.4	20.262	0.022	21.772
XSH/NIR	1514.68	1504.5	1521.0	20.245	0.028	21.755
XSH/NIR	1544.03	1521.0	1566.8	20.259	0.015	21.769
XSH/NIR	1588.99	1566.9	1608.2	20.115	0.015	21.625
HST/WFC3	F160W	-	-	20.16	0.07	21.626
XSH/NIR	1626.76	1608.3	1646.4	20.170	0.015	21.680
XSH/NIR	1660.86	1646.5	1677.7	20.082	0.015	21.592
XSH/NIR	1688.87	1677.8	1702.2	20.059	0.015	21.569
XSH/NIR	1717.68	1702.3	1733.6	20.041	0.015	21.551
XSH/NIR	1746.74	1733.7	1758.4	19.965	0.015	21.475
XSH/NIR	1775.39	1758.5	1794.4	19.973	0.015	21.483
XSH/NIR	1984.37	1971.0	1995.0	19.860	0.023	21.370
XSH/NIR	2034.97	2021.0	2048.0	19.779	0.022	21.289
XSH/NIR	2081.61	2058.0	2100.0	19.658	0.022	21.168
XSH/NIR	2130.72	2112.0	2149.0	19.708	0.024	21.218
ISAAC	Ks (2165.2)	-	-	19.704	0.01	21.214
XSH/NIR	2179.10	2151.0	2211.0	19.712	0.024	21.222
XSH/NIR	2232.38	2212.0	2260.0	19.751	0.039	21.261
XSH/NIR	2287.42	2275.0	2300.0	19.443	0.049	20.953

This chapter is based on: Johan P. U. Fynbo, Stefan Geier, Lise Christensen, Anna Gallazzi, Jens-Kristian Krogager, Thomas Krühler, Cedric Ledoux, Justyn Maund, Palle Møller, Pasquier Noterdaeme, Thøger Rivera-Thorsen, & Marianne Vestergaard – *The Galaxy Counterparts of the two high-metallicity DLAs at $z = 2.412$ and $z = 2.583$ towards Q0918+1636*, Accepted for publication in Monthly Notices of The Royal Astronomical Society.

3

THE GALAXY COUNTERPARTS OF THE TWO HIGH-METALLICITY DLAs TOWARDS Q 0918+1636

ABSTRACT – *The quasar Q0918+1636 ($z = 3.07$) has two intervening high-metallicity Damped Lyman- α Absorbers (DLAs) along the line of sight, at redshifts of $z = 2.412$ and 2.583 . The $z = 2.583$ DLA is located at a large impact parameter of 16.2 kpc, and despite this large impact parameter it has a very high metallicity (consistent with solar), a substantial fraction of H_2 molecules, and it is dusty as inferred from the reddened spectrum of the background QSO. The $z = 2.412$ DLA has a metallicity of $[M/H] = -0.6$ (based on Zn II and Si II). In this paper we present new observations of this interesting sightline consisting of deep multi-band imaging and further VLT spectroscopy. By fitting stellar population synthesis models to the photometric SED we constrain the physical properties of the $z = 2.583$ DLA galaxy, and we infer its morphology by fitting a Sersic model to its surface brightness profile. We find it to be a relatively massive ($M_* \approx 10^{10} M_\odot$), strongly star-forming ($SFR \approx 30 M_\odot \text{ yr}^{-1}$), dusty ($E_{B-V} = 0.4$) galaxy with a disk-like morphology. We detect strong emission lines from the $z = 2.583$ DLA ([O II] $\lambda 3727$, [O III] $\lambda 4960$, [O III] $\lambda 5007$, $H\beta$, and $H\alpha$, albeit at low signal-to-noise (S/N) ratio except for the [O III] $\lambda 5007$ line). The metallicity derived from the emission lines is consistent with the absorption metallicity ($12 + \log(O/H) = 8.8 \pm 0.2$). We also detect [O III] $\lambda 5007$ emission from the galaxy counterpart of the $z = 2.412$ DLA at a small impact parameter (< 2 kpc). Overall our findings are consistent with the emerging picture that high-metallicity DLAs are associated with relatively luminous and massive galaxy counterparts, compared to typical DLAs.*

3.1 INTRODUCTION

For a long time the only available method for studying galaxies at redshifts $z > 1$ (barring QSO host galaxies) was to look at them in absorption against the light of background QSOs (e.g., Weymann et al., 1981; Wolfe et al., 2005). Then, from the second half of the 1990ies, the study of high- z galaxies in emission went through a breakthrough that is still unfolding (e.g., Giavalisco, 2002; Shapley, 2011). However, combining the

information from absorption and emission lines is still a poorly developed field. Although more than 10 000 of the so-called Damped Lyman- α Absorbers (DLAs) have been found so far (Noterdaeme et al., 2012a), and despite some progress (e.g., Møller et al., 2002) in finding their galaxy counterparts, we still have less than a dozen examples of such absorption selected galaxies (Krogager et al., 2012, see also Rauch et al. 2008, Rauch & Haehnelt 2011 and Schulze et al. 2012).

Expanding the sample is of great interest as we in this manner obtain unique information about the kinematics and chemical composition of gas surrounding the central ~ 1 kpc which are typically studied in emission. This information is vital for probing current ideas about the role of processes like inflow of pristine gas and outflow of enriched gas in galaxy formation and evolution (e.g., Dekel et al., 2009; Bouché et al., 2010; Fumagalli et al., 2011; Dekel & Krumholz, 2013; Crighton et al., 2013, and references therein).

The $z = 3.07$ quasar SDSSJ 091826.16+163609.0 was selected in the survey for high-metallicity DLAs described in Fynbo et al. (2010) and Fynbo et al. (2011). It was selected due to the presence of a DLA at $z = 2.412$ with strong Fe II lines. After obtaining deep X-Shooter spectroscopy of the QSO, Fynbo et al. (2011) serendipitously discovered a second DLA at $z = 2.583$ along the line of sight with even stronger metal lines. Fynbo et al. (2011) detected the forbidden [O II] and [O III] emission lines of the galaxy counterpart of this second DLA. The galaxy is located at an impact parameter of 2, corresponding to ~ 16 kpc at $z = 2.583$. The $z = 2.412$ DLA was not detected in emission in that study.

In this paper, we present new results based on new observations of this sightline obtained with the Hubble Space Telescope (*HST*), ESO Very Large Telescope (VLT) and Nordic Optical Telescope (NOT). In Sect. 3.2 we give an overview of the observations and data reduction, and describe the data analysis and the results in Sect. 3.3 and Sect. 3.4. Finally, Sect. 3.5 contains a discussion of our findings and their implications for the field.

Throughout this paper, we use a flat Λ CDM cosmology with $\Omega_\Lambda = 0.728$, $\Omega_m = 0.272$ and a Hubble constant of $H_0 = 70.4 \text{ km s}^{-1} \text{ Mpc}^{-1}$ (Komatsu et al., 2011). All magnitudes are given in the AB system.

3.2 OBSERVATIONS AND DATA REDUCTION

3.2.1 HST IMAGING

The field of Q 0918+1636 was observed with the Wide Field Camera 3 (WFC3) on the *HST* on two epochs in November 2011 (with the NIR detector in the F105W and F160W filters) and on April 18 2012 (with the UVIS detector in the F606W filter). The roll-angle of the telescope was set such that the $z = 2.583$ DLA galaxy falls between the diffraction spikes of the Point Spread Function (PSF) of the QSO. The two observations with the NIR detector were taken using the WFC3-IR-DITHER-BOX-MIN pattern providing an

Table 3.1 Log of observations

Band	Obs. Date	Exp. Time (sec)
<i>HST</i> /WFC3/F105W	Nov 9 2011	2612
<i>HST</i> /WFC3/F160W	Nov 9 2011	2612
<i>HST</i> /WFC3/F606W	Apr 9 2011	2523
NOT/Alfosc/ <i>g</i>	Jan 25–26 2012	8400
NOT/Alfosc/ <i>u</i>	Jan 25–26 2012	11500
NOT/NOTCam/ <i>K_s</i>	Mar 3 2012	7830
VLT/X-Shooter ¹ stare PA=0°	Feb 16 2010	3600
VLT/X-Shooter ¹ stare PA=60°	Feb 16 2010	3600
VLT/X-Shooter ¹ stare PA=−60°	Feb 16 2010	3600
VLT/X-Shooter nod PA=−66°	Apr 15 2012	2920
VLT/X-Shooter stare PA=162°	Apr 15 2012	6400
VLT/X-Shooter nod PA=66°	Mar 15–16 2013	10800

⁽¹⁾ Already published in Fynbo et al. (2011).

optimal 4-point sampling of the PSF. The UVIS observation was taken using the WFC3-UVIS-DITHER-BOX pattern.

We have reduced and combined the images using the software package `multidrizzle` provided by the STScI. By shifting and combining the images taken with sub-pixel offsets one achieves a better sampling of the PSF, which in the case of the IR observations is crucial as the PSF is poorly sampled in the native $0''.13 \text{ px}^{-1}$ images. For this work we have set the parameter `pixfrac` to 0.7 in all reductions and used a final pixel scale of $0''.06 \text{ px}^{-1}$ for IR and $0''.024 \text{ px}^{-1}$ for UVIS. For a detailed description of the parameters in the software we refer to the `multidrizzle` user manual.

3.2.2 NOT IMAGING

On the nights of Jan 25–26 2012 and March 3 2012 Q 0918+1636 was observed with the Andalucia Faint Object Spectrograph and Camera (ALFOSC) and with the Nordic Optical Telescope near-infrared Camera and spectrograph (NOTCam) at the NOT. A total of 8400 s, 11500 s and 7830 s of exposure time was obtained in the *g*-band, *u*-band, and *K_s*-band, respectively (see Table 3.1). Observing conditions were clear, with an average seeing FWHM of $\sim 1''$ in the January 2012 nights, and clear and sub-arcsec seeing on March 3rd 2012. The optical images were reduced using IRAF¹ standard procedures.

¹IRAF is distributed by the National Optical Astronomy Observatory, which is operated by the Association of Universities for Research in Astronomy (AURA) under cooperative agreement with the National Science Foundation.

The NOTCam images were reduced with custom IDL scripts, using a running-median for sky-subtraction, and an object mask for 2nd pass sky-subtraction. The NOTCam distortion correction was applied using the IRAF/`geotran` task.

3.2.3 VLT/X-SHOOTER SPECTROSCOPY

Q 0918+1636 was observed with VLT/X-Shooter on April 15 2012. Both a stare observation at a position angle of 162° East of North and a nodding observation at a position angle of -66° East of North were obtained. The observation at position angle -66° East of North was a mistake: it should have been at 66° East of North with the purpose of covering the $z = 2.583$ DLA galaxy and the QSO. In a stare observation the target is kept at a fixed position on the slit throughout the observation, whereas in a nodding observation an observing block consists of four exposures between which the target is moved in an ABBA pattern along the slit. A deeper observation was obtained on March 15–16 2013 at the correct position angle of 66° East of North for covering the $z = 2.583$ DLA galaxy and the QSO using the nodding template with a nod-throw of $4''$. In Fig. 3.1 we show the orientation of the slits in all the X-Shooter observations, both the new observations reported here and the previous observations of Fynbo et al. (2011). The purpose of the stare observation at position angle of 162° East of North was to determine the redshift of the galaxy seen in the bottom of Fig. 3.1 in order to establish if this could be the galaxy counterpart of the $z = 2.412$ DLA. For the full log of observations we refer to Table 3.1.

The spectra from March 2013 were reduced with the ESO X-Shooter pipeline 2.0 (Modigliani et al., 2010; Goldoni, 2011). We use the default parameters for the first five recipes which perform the basic calibrations (master darks, order prediction, flat fields, and the 2D maps for later rectification of the spectra). For the reduction of the object frames we use the corresponding pipeline recipes for the stare and nodding modes, with parameters optimized to provide the best possible sky-subtraction. The flux standard star LTT3218 was observed in both nights. Those spectra were reduced with the same calibration data as the spectra of the QSO/DLA system, and sampled onto the same spatial and wavelength grid. The extracted 1-dimensional (1D) standard star spectra were divided by the known tabulated spectrum of the standard star (which is first interpolated to the same wavelength grid), and the result smoothed with a kernel of 30 pixels to obtain a clean response curve. Each individual 2D spectrum was first normalized to an integration time of 1s, and then divided by the also normalized response curve from the corresponding night. The resulting flux-calibrated spectra from the 3 individual observing blocks (each comprising one hour of integration time) were collapsed along the wavelength axis to determine the peak positions of their spectral PSFs (SPSFs), and subsequently aligned on the spatial axis. Thereafter, they were stacked by means of a median combination. Galactic extinction corrections were taken from Schlafly & Finkbeiner (2011)² and implemented with the `fm_unred`

²provided by <http://ned.ipac.caltech.edu/>

code in IDL. The final SPSF was determined by collapsing the error-weighted 2D stack along the wavelength axis in the H -band wavelength range and the 1D spectrum of the quasar itself was extracted by applying the corresponding normalized weights, similar to the optimal extraction procedure described in Horne (1986). To check the flux level we integrated the 1D spectrum over the transmission curves of the NOTCam J - and H -band filters, and compared with the photometry from Fynbo et al. (2013a). The measurements agree within the errorbars, thus no correction of the flux level was necessary. With a gaussian fit to the SPSF we determined the seeing of the combined spectrum to be $\sim 0''.8$ in the H -band.

3.3 THE $z = 2.583$ DLA GALAXY

3.3.1 HST IMAGING

Based on the high resolution HST imaging we can now improve the relative astrometry over that presented in Fynbo et al. (2011). We find that the DLA galaxy is located at an impact parameter of $1''.98 \pm 0''.02$ from the QSO at a position angle of -115° East of North, consistent with the earlier measurements. This impact parameter corresponds to a proper distance of 16.2 kpc at $z = 2.583$.

We used the GALFIT tool (Peng et al., 2002; Peng, 2010) to fit 2D Sersic models, convolved with the PSF, to the HST images of the DLA galaxy. The Point Spread Functions (PSFs) for the *HST* images were simulated using the software TINYTIM. We chose to simulate the PSFs instead of using an empirical PSF as the model PSF has higher S/N ratio in the outer parts, where the PSFs from the data have high noise due to the background. We did the PSF simulation by first creating models using TINYTIM for each position of the target in the four-point dither pattern, assuming a QSO spectrum for the wavelength dependent PSF modeling, and taking into account the aberrations of the telescope as specified in the auxiliary data files. The models were sub-sampled by a factor of 5 compared to the native pixel scale of the detectors in order to position the model PSF more accurately. We then re-sampled the model PSF images to the native sampling and convolved them with the appropriate filter-specific Charge Diffusion Kernel. The four “raw” PSF images were then combined by the pipeline task `multidrizzle` in IRAF using the same parameters as for the data reduction. This allows us to mimic the effects of the reduction procedures. The results from GALFIT are the best-fit values for the effective half-light radius r_{eff} , the Sersic index n , and the axis ratio ($\frac{b}{a}$), which quantify the structure of the galaxy. The circularized radius is calculated as $r_c = r_{\text{eff}} \cdot \sqrt{\frac{b}{a}}$.

GALFIT also delivered photometry in all three bands, summarized in Table 3.2. Galactic extinction corrections are taken from the Schlafly & Finkbeiner (2011) maps.

The $z = 2.583$ DLA galaxy has a disk-like morphology with a Sersic index consistent with 1. The galaxy is compact with a circularized radius of only $0''.11$ corresponding to 0.9 kpc.

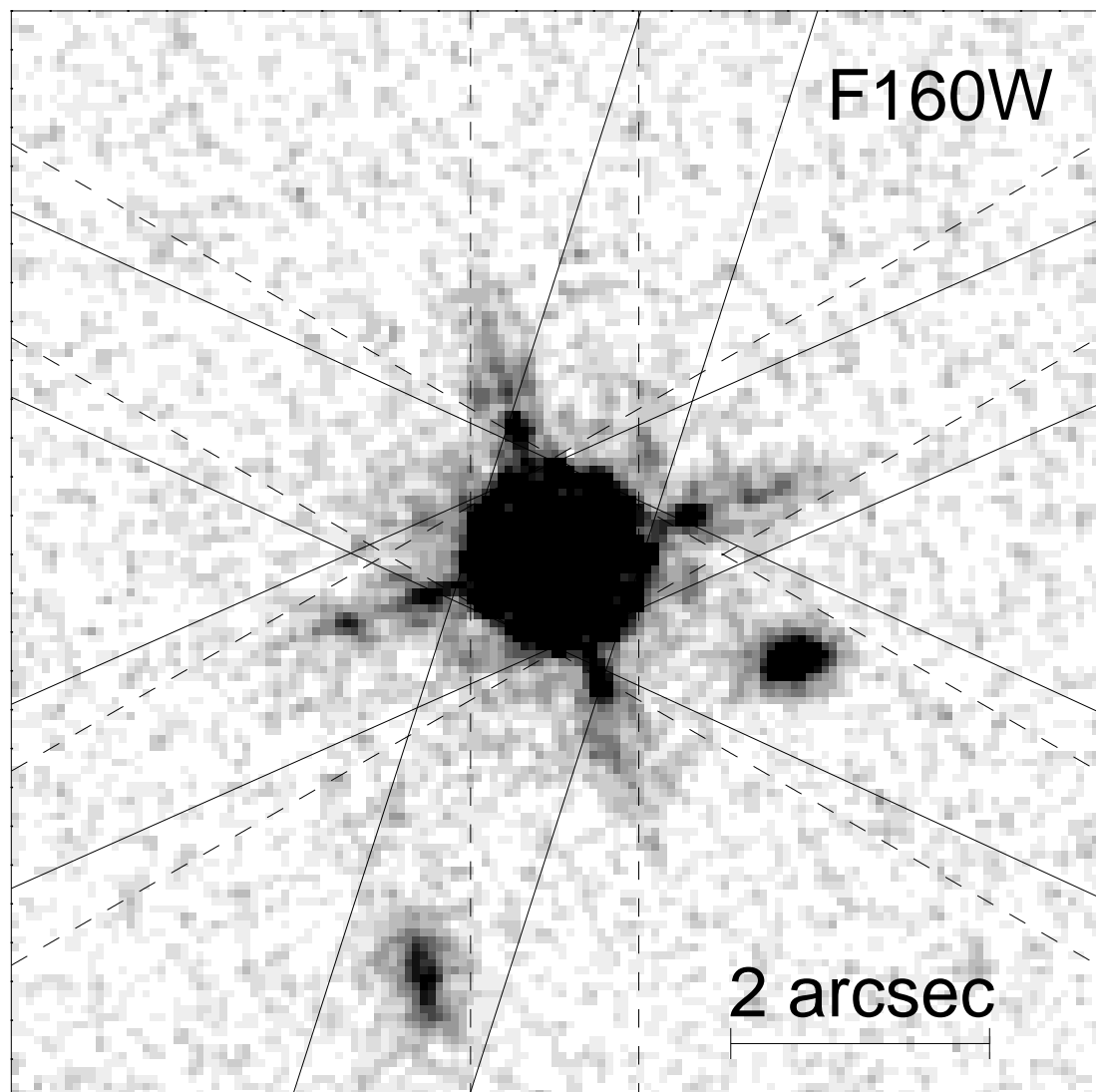


Figure 3.1 The *HST*/WFC3 F160W image and with all the X-Shooter slit orientations indicated with dashed lines for the observations presented in Fynbo et al. (2011) and full-drawn lines for the new observations presented here (see also Table 3.1).

3.3.2 NOT/ALFOSC IMAGING

We use *mag_{auto}* in SExtractor (Bertin & Arnouts, 1996) to measure the total fluxes of SDSS stars in the u- and g-band images of the field of Q 0918+1636, which we use to derive the zeropoints. In order to do photometry of the DLA galaxy counterpart we first did PSF subtraction using the same procedure as in similar previous studies (e.g., Møller & Warren, 1993; Fynbo et al., 1999, 2000). Magnitudes were measured in circular apertures. Again, Galactic extinction corrections are taken from the Schlafly & Finkbeiner (2011) maps. In the g-band we measure an AB magnitude of 25.9 ± 0.3 and

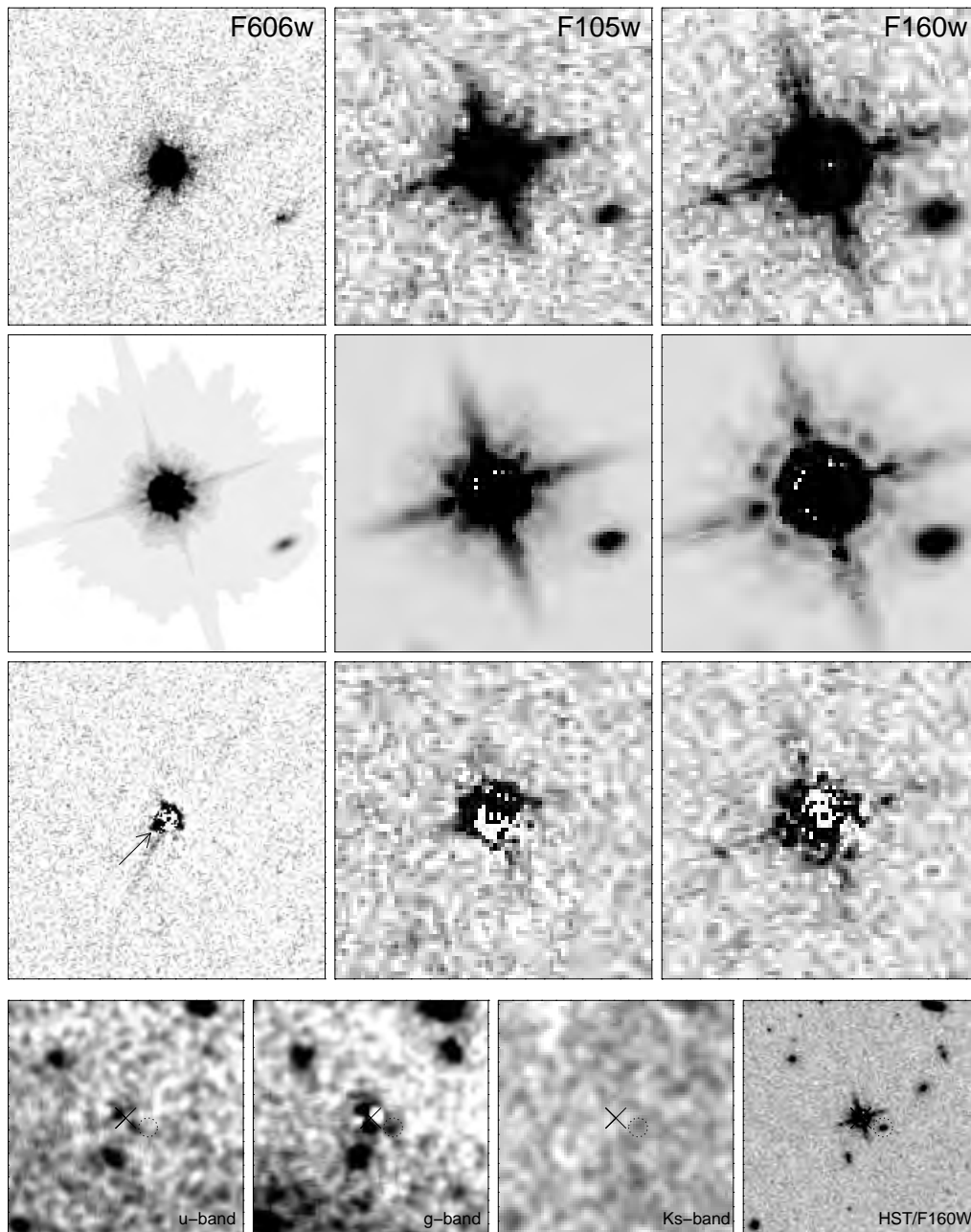


Figure 3.2 Top 9 panels: 5×5 arcsec² sections centred on the QSO in F606W, F105W and F160W (from left to right). The DLA galaxy is seen south-west of the QSO at an impact parameter of $2''.0$. The top row shows the science images, the middle row shows the GALFIT model and the bottom row shows the residuals after subtracting the model (QSO PSF and galaxy models) from the science images. The field size is 5×5 arcsec² and the images are oriented with North up and East to the left. The arrow in the lower left panel indicates the possible signature of the $z = 2.412$ DLA galaxy. The tail extending below the QSO is a result of Charge Transfer Inefficiency. Bottom panel: 19×19 arcsec² sections centred on the QSO in the u-, g-, and Ks-bands after PSF-subtraction. Also shown to the right is the *HST*/F160W band image on the same scale for comparison. The position of the $z = 2.583$ DLA galaxy is marked with a dotted circle. Again the images are oriented with North up and East to the left.

Table 3.2 Results from the GALFIT fits and NOT photometry. b/a is the ratio of the minor and major axis radii and n is the Sersic index. The magnitudes in the HST filters were computed by GALFIT, whereas aperture photometry was done on the NOT images.

Band	mag (AB)	r_{eff} (kpc)	PA (deg)	b/a	n	r_c (kpc)
F606W	25.46 ± 0.13	1.2 ± 0.2	-37 ± 6	0.4 ± 0.1	0.8 ± 0.4	0.73
F105W	24.61 ± 0.09	1.3 ± 0.3	-44 ± 9	0.3 ± 0.2	0.1 ± 0.7	0.69
F160W	23.68 ± 0.06	1.4 ± 0.1	-47 ± 6	0.4 ± 0.1	1.1 ± 0.4	0.93
u	$> 26.5(3\sigma)$					
g	25.9 ± 0.3					
K_s	$> 23.3(3\sigma)$					

in the u-band we do not detect the DLA galaxy down to a 3σ detection limit of 26.5 (in a $2''.0$ diameter aperture).

3.3.3 NOT/NOTCAM IMAGING

For the NOTCam/ K_s -band we determined the zeropoint with stars from the 2MASS catalog (Skrutskie et al., 2006). On the combined image in the K_s -band we again subtracted the PSF of the QSO using a PSF determined from stars in the field. The residual image does not contain significant emission at the position of the $z = 2.583$ DLA galaxy. There is residual flux at the expected position at the 2σ significance level, but we conservatively report a 3σ detection limit of 23.3 (on the AB system) measured in a $2''.0$ diameter aperture.

3.3.4 SED FITTING

We fit stellar population synthesis models to the six broad-band photometric points from the *HST* and NOT imaging listed in Table 3.2, to derive the stellar mass, age and star formation rate with the same procedure as in Krogager et al. (2013). In summary the fitting code uses the stellar population templates from Bruzual & Charlot (2003b) convolved with a large Monte Carlo library of star formation histories (exponential plus random bursts) assuming a Chabrier (2003) IMF. Dust is added following the two-component model of Charlot & Fall (2000), with the parameters being the total optical depth, τ_v , and the fraction of dust³ contributed by the ISM, μ . The metallicity is restricted to solar as inferred from the absorption analysis, but we find consistent results when using the full range of the models between 20% and 2.5 times solar. We then adopt a Bayesian approach by comparing the observed magnitudes to the ones predicted by

³For details on the prior distribution of the SFH and dust parameters see Salim et al. (2005)

Table 3.3 Results from the SED fitting

Parameter	Value
Age [Myr]	233^{+268}_{-125}
E_{B-V} [mag]	$0.38^{+0.16}_{-0.12}$
A_V [mag]	$1.54^{+0.72}_{-0.56}$
M_\star [$10^9 M_\odot$]	$12.6^{+6.1}_{-2.9}$
SFR [$M_\odot yr^{-1}$] ¹	27^{+20}_{-9}

¹ Averaged over 1 Gyr, but averaged over a shorter timescale of 10 Myr we get a similar value within the errors.

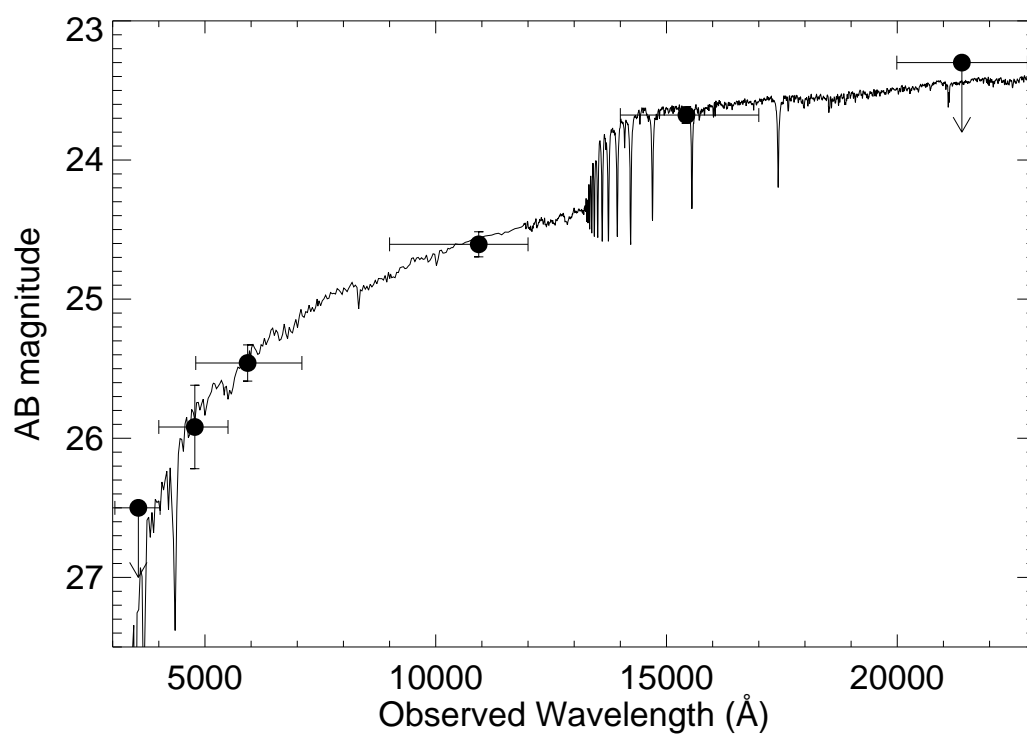


Figure 3.3 The broad-band SED of the $z = 2.583$ DLA galaxy, comprising of the Alfosc u- and g-bands, HST/WFC3 F606W-, F105W- and F160W-bands and the NOTCam K_s -band, is shown as black points. The best-fit model is shown with a full-drawn line.

all the models in the library, and we construct the probability density functions of stellar mass, mean luminosity-weighted stellar age, and star formation rate. Fortunately, none of the filters contains any of the strong emission line and hence we do not include emission lines in the fits. The results of the SED-fits are provided in Table 3.3.

3.3.5 VLT/X-SHOOTER SPECTROSCOPY

The galaxy which is responsible for the $z = 2.583$ DLA is located at a projected distance of $1''.98$ from the QSO, which corresponds to 10 pixels on the spatial axis of the 2D spectrum. Given the good seeing of $0''.8$ the two objects are well separated. Thus, we do not need to subtract the continuum of the QSO. At the spatial position where the DLA galaxy is located, there is very little continuum flux, but the [O III] $\lambda 5007$ emission line of the $z = 2.583$ DLA galaxy is clearly visible. The [O III] $\lambda 5007$ line is typically the line detected at highest S/N ratio for galaxies at similar redshifts (e.g., Fynbo et al., 2011). We then extract a 1D spectrum of the $z = 2.583$ DLA galaxy similarly as for the QSO spectrum, but this time using a gaussian SPSF with a FWHM of $0''.8$, as there is not enough continuum signal to determine the SPSF. The [O III] $\lambda 5007$ emission line is clearly located in wavelength regions without sky-line residuals. For this line the flux is determined by summing up the flux in the 1D spectrum. In Fig 3.4 we show the [O III] $\lambda 5007$ line in 1 and 2 dimensions. The redshift determined from the [O III] $\lambda 5007$ line is $z = 2.58277 \pm 0.00010$, which is $36 \pm 20 \text{ km s}^{-1}$ (where the uncertainty also includes the uncertainty on the absorption redshift) blueshifted compared to the centre of the low-ionization absorption lines (Fynbo et al., 2011).

To search for emission at lower impact parameter we subtract the QSO continuum following the procedure described in Fynbo et al. (2010). In Fig. 3.5 we show a wider region around the [O III] $\lambda 5007$ line from the $z = 2.583$ DLA galaxy after subtraction of the SPSF of the QSO. There is no evidence for emission at smaller impact parameters.

The $H\alpha$, $H\beta$, [O III] $\lambda 4960$, and [O II] $\lambda 3727$ lines are visible but detected at lower S/N ratio. We derive fluxes for these lines by fixing the redshift and width from the [O III] $\lambda 5007$ line. The resulting line fluxes are provided in Table 3.5. In particular $H\alpha$ is very uncertain as it is located far in the red end of the K-band where the sky-background is very high. We use the emission-line ratio R_{23} (originally defined by Pagel et al. (1979a)) to derive the oxygen abundance for the system. The index is defined as the ratio of [O II] $\lambda 3727$ and [O III] $\lambda\lambda 4959, 5007$ to $H\beta$. The R_{23} metallicity indicator is double-valued. Moreover, the calibration of the line ratio depends on the ionization parameter, which also depends on metallicity. We therefore solve the problem iteratively by use of the line ratio O_{32} as an indicator of the ionization parameter. By using the calibration of Kobulnicky & Kewley (2004a) to infer the metallicity, we obtain the following two values: the upper branch solution is $12 + \log(O/H) = 8.8 \pm 0.2$, and the lower branch solution is $12 + \log(O/H) = 8.2 \pm 0.2$. We consider the upper branch solution most likely in this case given the other properties of the system (absorption metallicity, luminosity, mass), but we cannot establish this on the basis of the emission lines alone.

For the $H\alpha$ emission line the observed line flux corresponds to a luminosity of $L_{H\alpha} = 1.5 \pm 0.5 \times 10^{42} \text{ erg s}^{-1}$. Converting the luminosity into SFR using Kennicutt (1998b) gives $\text{SFR}_{H\alpha} = 13 \pm 5 M_{\odot} \text{ yr}^{-1}$. Converting to the assumed Chabrier IMF (Treyer et al., 2007) we find $\text{SFR}_{H\alpha} = 8 \pm 3 M_{\odot} \text{ yr}^{-1}$. Correcting for the extinction in-

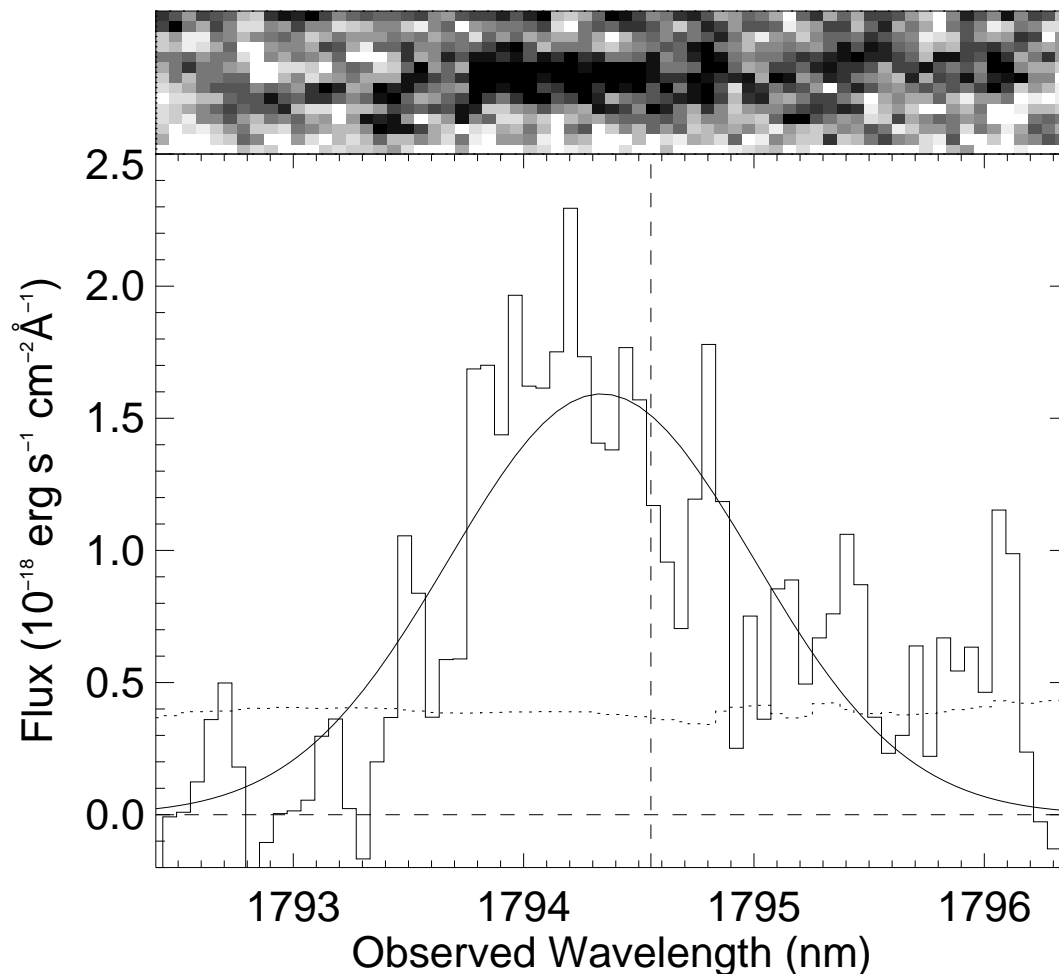


Figure 3.4 The $[\text{O III}] \lambda 5007$ emission line of the $z = 2.583$ DLA galaxy. The top panel shows the 2D spectrum and the bottom panel shows the 1D spectrum. The vertical dashed line indicates the predicted position of the line based on the absorption line redshift of the DLA. The observed line has a centroid that is blue shifted by 36 km s^{-1} relative to the absorption redshift. The FWHM of the line based on a Gaussian fit is $256 \pm 23 \text{ km s}^{-1}$ (uncorrected for the spectroscopic resolution of 45 km s^{-1}).

ferred from the SED fitting this corresponds to $22 \pm 7 M_{\odot} \text{ yr}^{-1}$ for the Chabrier IMF, consistent with the SFR derived from the SED fitting in Table 3.3.

Due to the increased S/N ratio of the spectrum of Q0918+1636 we are also able to detect much weaker absorption lines than in Fynbo et al. (2011). An example is $\text{Ti II } \lambda 1910$ for which we measure an observed equivalent width of $0.102 \pm 0.014 \text{ \AA}$ corresponding to a metallicity of -0.98 ± 0.05 implying that Titanium is depleted by close to 1 dex. This is consistent with observations of Titanium in the local group where Titanium is found to be highly depleted onto dust grains (e.g., Welty & Crowther, 2010). It is also consistent

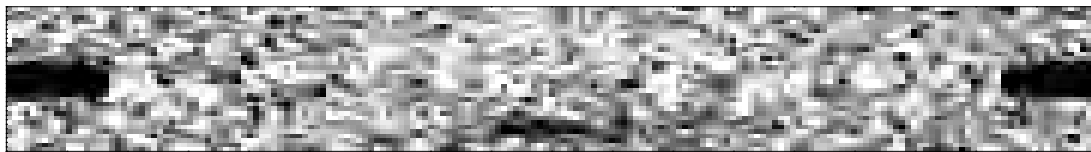


Figure 3.5 A wider region around the [O III] $\lambda 5007$ line of the $z = 2.583$ DLA galaxy after subtraction of the QSO SPSF (the boundaries of where the QSO continuum has been subtracted can be seen at each end of the figure). As seen here, there is no evidence for [O III] $\lambda 5007$ emission at small impact parameter. A [O III] $\lambda 5007$ line 3 times fainter than the detected line would have been detected even if superposed on the QSO trace.

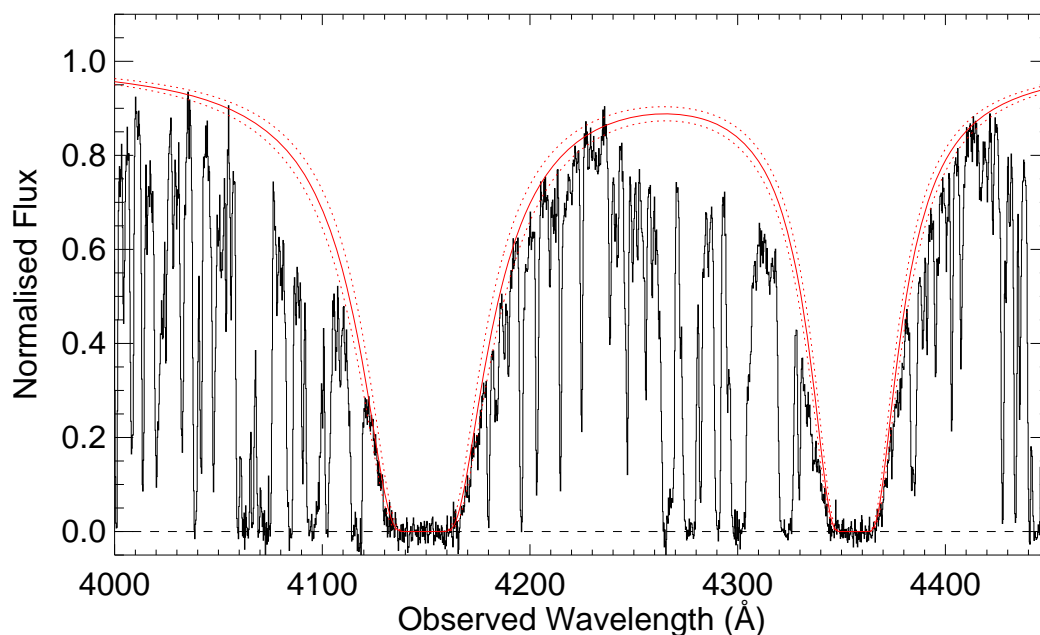


Figure 3.6 Voigt profile fits to the two DLA lines. For the $z = 2.583$ DLA at $\lambda = 4355$ Å the fit is from Fynbo et al. (2011). The derived column density for the $z = 2.412$ DLA is $\log N/\text{cm}^{-2} = 21.26 \pm 0.06$.

with the large depletion of Fe, Mn and Cr (Fynbo et al., 2011).

3.4 THE $z = 2.412$ DLA GALAXY

3.4.1 ABSORPTION LINE ANALYSIS

The original reason for targeting this QSO was the presence of a metal-strong DLA at $z = 2.412$. To characterize the absorption line properties of the $z = 2.412$ DLA we performed Voigt-profile fitting of the H I and metal absorption lines. For the DLA we derive an H I column density of $\log N/\text{cm}^{-2} = 21.26 \pm 0.06$ (Fig. 3.6).

Voigt-profiles were fitted to several metal lines using the VPfit software⁴, assuming turbulence-dominated internal motion in the system. The redshift measured from the low-ionization (Si II, Fe II, Zn II, Cr II, Mn II) absorption lines is $z = 2.4121 \pm 0.0002$. Redshifts and velocity dispersions were tied for each of the individual components of the low-ionization lines. High-ionization lines were fitted independently. The low-ionization absorption was found to be best fitted by six distinct components. A plot of the fit results is shown in Fig. 3.7, and inferred column densities are shown in Table 3.4. Integrated metallicities [M/H] based on low-ionization absorption are -0.6 ± 0.2 , -0.6 ± 0.2 , -1.2 ± 0.2 , -1.2 ± 0.2 and -1.3 ± 0.2 for Zn II, Si II, Cr II, Fe II and Mn II, respectively. In Fig. 3.7 we also show the intermediate and high-ionization lines from Al III and C IV. These lines are fitted independently and in this case only 5 sub-components suffice. It is striking that the $v < 0 \text{ km s}^{-1}$ absorption is strongest for Al III and C IV whereas the strongest low-ionization absorption is at $v > 0 \text{ km s}^{-1}$.

The resolution of X-Shooter is, as discussed in several earlier works, not ideal for robust Voigt-profile fitting (e.g., Fynbo et al., 2010; Noterdaeme et al., 2012b; Krühler et al., 2013), but for our purposes of establishing that the system is metal-rich and for inferring the velocity width of the absorption, the data are sufficient.

We also determine the velocity width of the low-ionization absorption following the prescription of Ledoux et al. (2006). Here we find $\Delta v = 349 \text{ km s}^{-1}$ and 352 km s^{-1} for Fe II, λ 2260 and Si II, λ 1808, respectively.

In conclusion, the metallicity of the system is well above our target selection criterion of 0.1 Z and there is evidence for substantial depletion of refractory elements on dust grains.

Further details on the analysis of this system can be found in Thorsen (2011).

3.4.2 THE GALAXY COUNTERPART

In Fynbo et al. (2011) no emission was found from the galaxy counterpart of this absorber. From the spectrum taken with the slit at the position angle of 162° East of North we find that the galaxy seen at the bottom of Fig. 3.1 is at a lower redshift of $z = 0.987$ based on the detection of the [O II] λ 3727 doublet and the [O III] λ 5007 line. In Fig. 3.2 there is no obvious other source at smaller impact parameters except the counterpart of the $z = 2.583$ DLA. One possibility is that the source is a faint galaxy at a small impact parameter. In the lower left sub-panel of the upper panel in Fig. 3.2 there is a hint of a source at a position angle of about 130° East of North (marked with an arrow). Opposite to this is a ring-like residual consistent with what one would expect if the centroid of the PSF has been shifted slightly to the lower left by the presence of the foreground galaxy. We have attempted to include such an additional source in the GALFIT modeling, but without success. We have done one test to gauge the reality of this potential source. Using GALFIT with rotated PSFs (45° , 90° , 135° , etc.), we find that the dimples surrounding the PSF core are either well subtracted or poorly subtracted (or, in general,

⁴<http://www.ast.cam.ac.uk/rfc/vpfit.html>

Table 3.4 Ionic column densities in the 6 individual line components of the DLA system at $z_{\text{abs}} = 2.412$.

Ion	Transition lines used	$\log N \pm \sigma_{\log N}$	$b \pm \sigma_b$ (km s ⁻¹)
$z_{\text{abs}} = 2.41033$			
MgI	2026,2852	12.60±0.05	38±1
SiII	1808	15.40±0.05	38±1
MnII	2576,2594,2606	12.79±0.05	38±1
FeII	1608,1611,2249,2260	14.70±0.05	38±1
ZnII	2026, 2062	12.77±0.05	38±1
CrII	2056,2062,2066	12.80±0.10	38±1
$z_{\text{abs}} = 2.41179$			
MgI	2026,2852	12.34±0.07	20±3
SiII	1808	15.0±0.1	20±3
MnII	2576,2594,2606	11.9±0.2	20±3
FeII	1608,1611,2249,2260	14.29±0.08	20±3
ZnII	2026, 2062	12.3±0.1	20±3
CrII	2056,2062,2066	12.3±0.4	20±3
$z_{\text{abs}} = 2.41231$			
MgI	2026,2852	12.1±0.1	22±6
SiII	1808	15.3±0.7	22±6
MnII	2576,2594,2606	12.6±0.7	22±6
FeII	1608,1611,2249,2260	14.8±0.7	22±6
ZnII	2026, 2062	12.4±0.7	22±6
CrII	2056,2062,2066	12.9±0.8	22±6
$z_{\text{abs}} = 2.41289$			
MgI	2026,2852	12.4±0.5	37±11
SiII	1808	15.4±0.5	37±11
MnII	2576,2594,2606	12.6±0.6	37±11
FeII	1608,1611,2249,2260	14.9±0.5	37±11
ZnII	2026,2062	12.5±0.5	37±11
CrII	2056	13.2±0.3	37±11
$z_{\text{abs}} = 2.4134$			
MgI	2026,2852	12.4±0.6	45±28
SiII	1808	15.3±0.7	45±28
MnII	2576,2594,2606	12.6±0.7	45±28
FeII	1608,1611,2249,2260	14.8±0.7	45±28
ZnII	2026, 2062	12.4±0.7	45±28
CrII	2056,2062,2066	12.9±0.8	45±28
$z_{\text{abs}} = 2.41404$			
MgI	2026,2852	11.5±1.0	28±3
SiII	1808	15.2±0.2	28±3
MnII	2576,2594,2606	12.5±0.2	28±3
FeII	1608,1611,2249,2260	14.7±0.2	28±3
ZnII	2026, 2062	11.9±0.4	28±3
CrII	2056,2062,2066	13.0±0.1	28±3

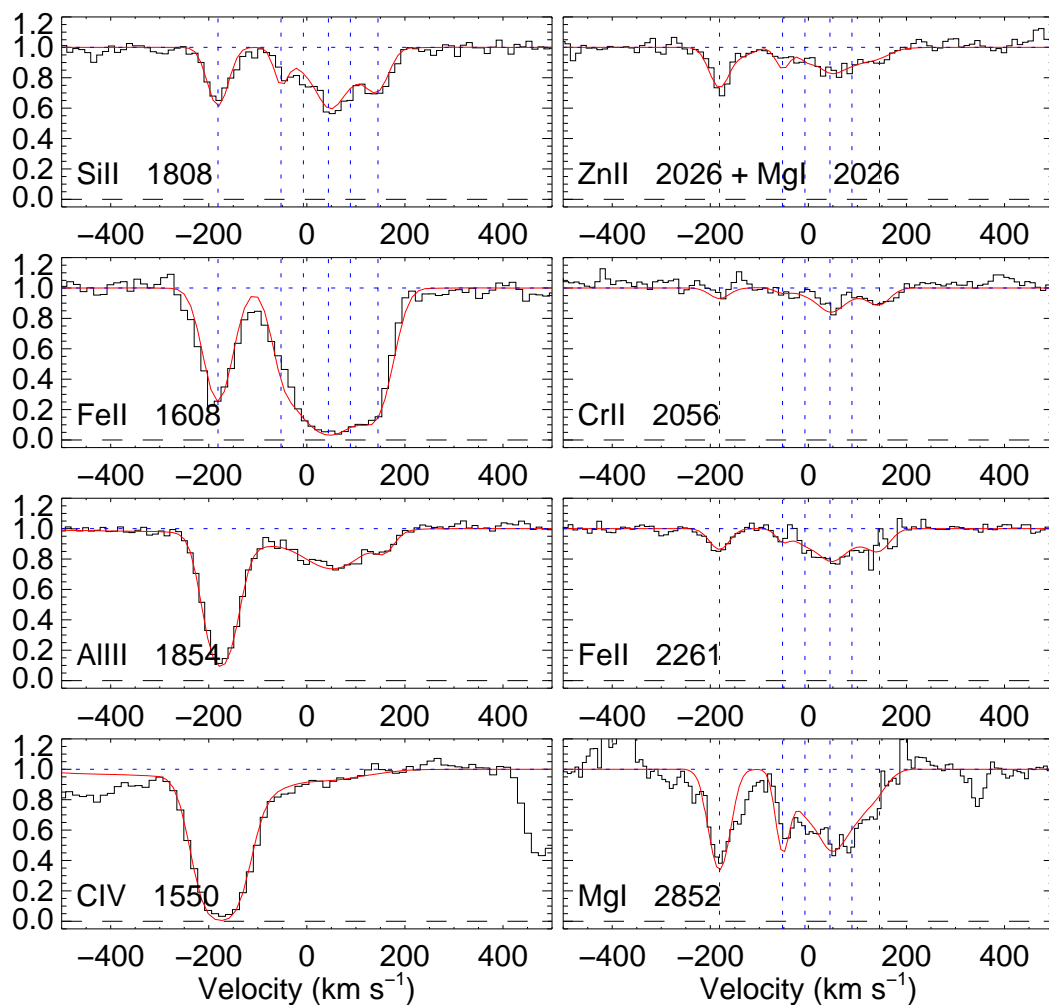


Figure 3.7 Voigt-profile fits to metal lines from the $z = 2.412$ DLA. The zero-point for the velocity scale is defined from the centroid of the [OIII] $\lambda 5007$ emission line. Data are shown in black and the model-fits in red. In the left column we list a weak and a strong low-ionization line (Si II and Fe II) and a medium- and high-ionization line (Al III and C IV) to illustrate the very different ionization states of the different sub-components. The vertical dotted lines mark the velocities for the sub-components in the fit to the low-ionization lines. In the right column we show the low-ionization lines from Zn II, Cr II, Fe II and Mg I. The zeropoint for the velocity scale is defined by the centroid (first moment) of the Si II 1808 line.

partially subtracted) depending on the angle of rotation. Obviously, the main effect is that the diffraction spikes change such that with a rotation one sees the original spikes as a positive residual and a negative residual oriented along the diffraction spikes of the rotated PSF. However, the residual to the south-east, labeled in the image, remains

Table 3.5 Measured emission line fluxes

Transition	Wavelength ⁽¹⁾	Flux ⁽²⁾	FWHM ⁽³⁾
$z = 2.412$ DLA			
[O III]	5006.84	4.1 ± 1.1	50 ± 12
$z = 2.583$ DLA			
[O II]	3726.03, 3728.82	25 ± 4	
[O III]	4958.92	11 ± 3	
[O III]	5006.84	25 ± 3	252 ± 23
H β	4861.325	13 ± 3	
H α	6562.80	27 ± 10	

(1) Transition rest frame wavelength in \AA .

(2) Flux in units of $10^{-18} \text{erg s}^{-1} \text{cm}^{-2}$.

(3) Line width at FWHM in units of km s^{-1} corrected for the instrumental resolution of 45 km s^{-1} .

fixed with roughly the same shape and brightness. In the end we are convinced that the residual is due to a real source and not an artifact from poor PSF subtraction. We note that the residual could also be related to the host galaxy of the QSO. The tail extending below the QSO is a result of Charge Transfer Inefficiency.

In the case of a very small impact parameter we expect potential emission lines from the galaxy to be included in all the slits shown in Fig. 3.1. We therefore co-added all the 2-dimensional spectra obtained up to 2012 and performed a SPSF-subtraction as described in Fynbo et al. (2010). In the upper panel of Fig. 3.8 we show the region around the position in the spectrum where the [O III] $\lambda 5007$ emission line is expected to fall. We tentatively, at about 3.5σ significance, detect an emission line at the expected position. The spectrum we obtained in March 2013 is substantially better due to better observing conditions and the use of the nodding observing template. In the lower panel of Fig. 3.8 we show the [O III] $\lambda 5007$ emission line from the $z = 2.412$ DLA now at a higher S/N ratio. The line is very narrow with a FWHM of $67 \pm 12 \text{ km s}^{-1}$, which is only slightly larger than the resolution of 45 km s^{-1} . Corrected for the resolution the FWHM is 50 km s^{-1} . The redshift determined from the line is $z = 2.4128 \pm 0.0002$, which is redshifted $38 \pm 25 \text{ km s}^{-1}$ relative to the mean absorption redshift, but of course well within the full $\sim 350 \text{ km s}^{-1}$ velocity extent of the low-ionization absorption.

We do not detect other lines, but [O III] $\lambda 5007$ is the line expected to be detected at highest significance at these redshifts (e.g., Fynbo et al., 2010; Krühler et al., 2012, 2013) and the non-detection of the other lines is expected on S/N grounds.

The impact parameter is consistent with 0 and a conservative upper limit is $0''.25$ corresponding to 2.0 kpc.

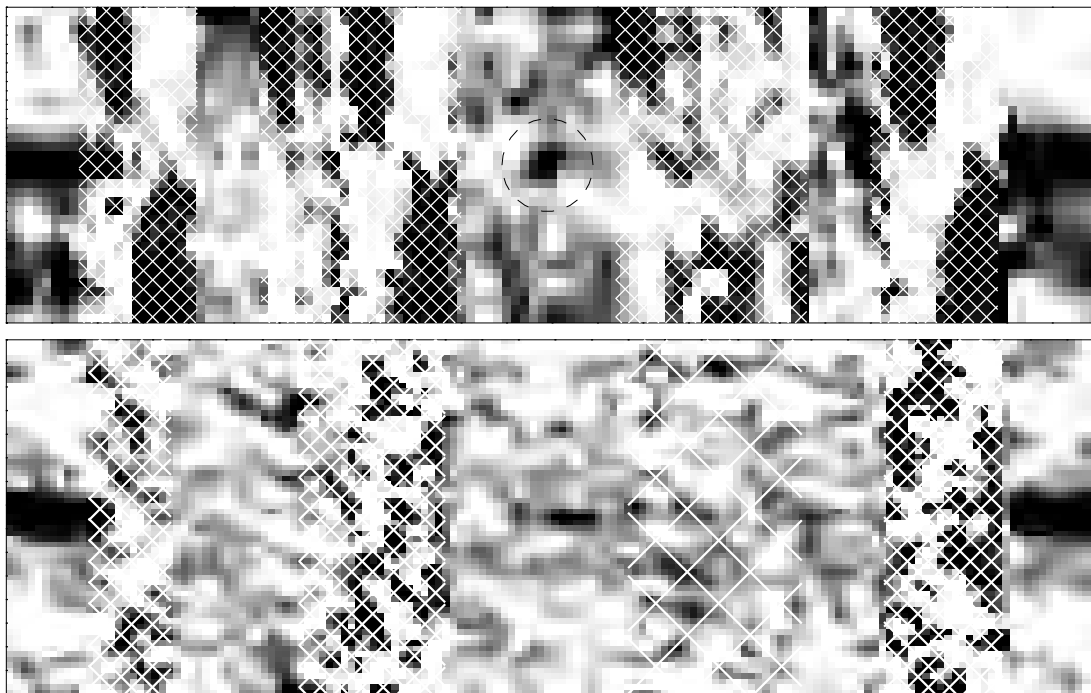


Figure 3.8 The region around the position in the spectrum where the [O III] $\lambda 5007$ emission line from the $z = 2.412$ DLA galaxy is expected to be observed. The upper panel is based on a stack of all the data taken up to and including 2012 and the lower panel is based on the 3 hr observation from March 2013. The QSO continuum can be seen in the left and right extremes of the figures, but in between it has been subtracted. Regions with sky-lines from airglow have been marked with a double-hatched pattern. The [O III] $\lambda 5007$ emission line from the $z = 2.412$ DLA galaxy is marked with a dashed circle in the upper panel.

3.5 DISCUSSION

In this paper we have presented new observations of the two DLAs towards Q 0918+1636 and their galaxy counterparts. The galaxy counterpart of the $z = 2.583$ DLA was discovered previously (Fynbo et al., 2011), whereas the discovery of the counterpart of the $z = 2.412$ DLA is first reported here.

3.5.1 THE $z = 2.583$ DLA GALAXY

For the $z = 2.583$ DLA Galaxy we have the largest amount of information: detection of several strong emission lines and a clear detection of the galaxy in the *HST* images. We can use our information about the size of the galaxy and the kinematics, as probed by the [O III] $\lambda 5007$ emission line of the $z = 2.583$ DLA galaxy to get an estimate of the dynamical mass of the system. As in Krogager et al. (2013) we follow the method described in Rhoads et al. (2013) to estimate the dynamical mass given the measured

size and velocity dispersion:

$$M_{\text{dyn}} \approx \frac{4\sigma^2 r_{\text{eff}}}{G \sin^2(i)},$$

where i denotes the inclination of the system with $i = 90^\circ$ being edge on and G is the gravitational constant. In order to estimate the velocity dispersion of the system we use the FWHM of the emission lines as a probe of the integrated gas-kinematics of the system. We then use the width of the [O III] $\lambda 5007$ line to estimate the velocity dispersion to be $\sigma = 107 \pm 10 \text{ km s}^{-1}$, and we adopt the size from the GALFIT analysis: $r_{\text{eff}} = 1.4 \text{ kpc}$ (see Table 3.2).

From the GALFIT analysis we infer a (projected) axis ratio of the galaxy of $b/a = 0.43$. The system may be described as disc-like, given the elongated shape, and the fact that we see a value of Sérsic n close to 1. We thus adopt a value of $\sin(i) = 0.5$ and use the fitted half-light semi-major axis for our estimate of the dynamical mass of the system: $M_{\text{dyn}} \approx 6.0 \pm 1.3 \times 10^{10} M_\odot$. This estimate should only be considered a rough approximation given the assumptions.

From our SED fit to the broad band imaging data, we obtain a stellar mass of $M_\star \gtrsim 10^{10} M_\odot$. We can use this measurement to test the mass-metallicity relation for DLA systems (Ledoux et al., 2006; Møller et al., 2013). Using the relation in Møller et al. (2013, their eq. 6) using as input solar metallicity (i.e., assuming that $C_{[M/H]} = 0$) we predict a stellar mass of $M_\star = 3 \times 10^{10} M_\odot$. Given the substantial (~ 0.38 dex) scatter in their relation, the agreement between the prediction and our best fit stellar mass from the SED fit is good.

3.5.2 THE NATURE OF DLA GALAXIES

The two DLA systems studied here are, as other systems in our survey (Fynbo et al., 2010, 2011; Krogager et al., 2012), drawn from the extreme high-metallicity end of the distribution and hence should not be considered typical examples of DLA galaxies. In Table 3.6 we compare the two systems and include also DLA galaxies from the literature for comparison (Weatherley et al., 2005; Fynbo et al., 2010, 2011; Bouché et al., 2012; Noterdaeme et al., 2012b; Krogager et al., 2013). For consistency we re-calculate the velocity shifts for N-14-1C and N-14-2C using the centroids of the low-ionization lines corresponding to $z_{\text{abs}} = 1.9205$. The galaxy counterpart of the $z = 2.412$ DLA is the system with the highest velocity extent of the low-ionization absorption. However, the FWHM of its [O III] emission is the lowest in the sample. This indicates that additional influences than mass must be important in determining the velocity width of the low-ionization absorption. One such possible influence is of course outflows. Another important reason for this may be the low impact parameter, which implies that a larger fraction of the gravitational potential is probed by the line-of-sight. We also observe here, as in Krogager et al. (2012), that the systems with the highest HI column densities have the smallest impact parameters. It would be interesting to carry out detailed

Table 3.6 Comparison of the two DLA galaxies studied here with DLA galaxies at similar redshifts from the literature. In the table we refer to the $z = 2.412$ and $z = 2.583$ DLA galaxies as DLA0918+1636-1 and DLA0918+1636-2, respectively.

DLA galaxy	z_{abs}	$\log N/\text{cm}^{-2}$	[M/H]	b^{\dagger} (kpc)	FWHM([O III]) (km s^{-1})	Δv_{90} (km s^{-1})	$\Delta v(\text{DLA-[O III]})$ (km s^{-1})	ref
DLA0918+1636-1	2.412	21.26	-0.6	< 2	50	350	-38 ± 25	(1)
DLA0918+1636-2	2.583	20.96	0.0	16.2	252	295	-36 ± 20	(1)
DLA1135-0010	2.207	22.10	-1.1	0.9	120	186	9 ± 10	(2)
DLA2222-0946	2.353	20.65	-0.5	6.2	115	185	25 ± 20	(3)
N-14-1C	1.920	20.67	-0.4	8.3	220	136	-150 ± 20	(4)
N-14-2C	1.920	20.67	-0.4	10.6	180	136	80 ± 9	(4)
DLA2243-60	3.330	20.65	-0.7	22.9	320	173	200 ± 20	(5)

(1) This work, Fynbo et al. (2011); (2) Noterdaeme et al. (2012b); (3) Fynbo et al. (2010); Krogager et al. (2013); (4) Weatherley et al. (2005); Ledoux et al. (2006); (5) Bouché et al. (2012); Ledoux et al. (2006); Bouché et al. (2013), Noterdaeme, private communication.

[†] Recalculated from the values in the original references to be consistent with the assumed cosmology.

comparisons of the quantities in Table 3.6 with simulations, e.g., similar to the works of Pontzen et al. (2008) and Rakic et al. (2013).

For the galaxy counterpart of the $z = 2.583$ we can establish further properties: It is a compact ($r_{\text{eff}} = 1$ kpc), strongly star-forming galaxy with a centroid 16.2 kpc away from the line-of-sight to the background QSO. The galaxy photometry is well fitted by galaxy templates with ages up to several 100 Myr. The ratio between the HI gas scale length of this DLA galaxy, as measured by its impact parameter, and the light scale length, as measured by its half-light radii, is of order 10 as seen in previous cases of DLA galaxy counterparts (Møller et al., 2002; Krogager et al., 2013). This is very different from the situation in local galaxies, where the gas only extends up to a few times the extension of the light (Bosma, 1981). Our data are deep, but the $(1 + z)^4$ dimming of surface brightness with redshift is a very strong effect. Hence, an important question is whether the measured compact morphology is only due to central high surface brightness regions embedded in lower surface brightness regions with extension more similar to the HI gas, but below the surface brightness detection limit of our data. Such HI central high surface brightness regions are also seen in local spiral galaxies (e.g., Carollo et al., 1997). The issue of morphology of star-forming galaxies at these redshifts as inferred from WFC3/IR data has been studied intensively by Law et al. (2012a,b) who find that these systems are not rotationally supported disk galaxies. Rather, they appear to be predominantly unstable, dispersion-dominated, systems fueled by rapid gas accretion which presumably later form extended rotationally supported disks. They also argue that all these galaxies drive strong outflows with more massive galaxies driving less highly ionized outflows. Compared to their sample the $z = 2.583$ DLA galaxy is in the upper third of the mass distribution. For the $z = 2.583$ galaxy the distances and ages are also consistent with a wind scenario: for an age of 233 Myr a mean speed of ~ 70 km s $^{-1}$ is required to reach 16 kpc. Such winds speeds are well below what is seen in nearby (more modest) winds (e.g., Melioli et al., 2013).

Bouché et al. (2013) argue for a similar system of a galaxy counterpart to a DLA at an even larger impact parameter (DLA2243-60 in Table 3.6) that the gas causing the DLA absorption is in a cold inflow. In their case the DLA metallicity is -0.72 , which is too high to be pristine gas. Hence, also in this case, an outflow must have been important for determining the properties of the system.

Rafelski et al. (2011) use statistical arguments to show that most DLAs must probe atomic gas with very low star-formation efficiencies. This would be consistent with a picture where metals in this gas originates from a wind rather than having been formed in situ.

The large impact parameter of the $z = 2.583$ galaxy could also be related to other processes like tidal stripping similar to what is seen in the Magellanic stream (Misawa et al., 2009). As DLAs are HI cross-section selected such systems will have a higher probability of being selected (see also Rauch et al., 2011, 2013). However, we note that the correlation between metallicity and impact parameter found by Krogager et al. (2012) would not obviously result from such a scenario and we do not see evidence for

a nearby galaxy that could have caused tidal stripping.

We note that none of the two galaxies have $\text{Ly}\alpha$ in emission. This may help explain the many non-detections resulting from searches for DLA galaxies in the previous few decades (Lowenthal et al., 1995; Møller et al., 2004; Fynbo et al., 2010, and references therein).

A coherent picture of DLAs and their relation to emission selected galaxies could be the following: DLAs originate from the outskirts of galaxies with properties (i.e., sizes, luminosities, stellar masses, metallicities) within the range of star-forming Lyman-break galaxies at similar redshift, but due to their cross-section selection they are more likely to be drawn from the fainter end of the luminosity function than emission selected galaxies (Fynbo et al., 1999; Møller et al., 2002; Fynbo et al., 2008; Rauch et al., 2008; Rauch & Haehnelt, 2011). There is evidence that DLA galaxies fulfill a metallicity-luminosity relation (Møller et al., 2004; Ledoux et al., 2006; Fynbo et al., 2008; Møller et al., 2013) and therefore high-metallicity DLAs are expected to have galaxy counterparts more similar to typical emission-selected galaxies (i.e., Lyman-break galaxies seen in ground-based surveys) than DLAs in general which probably have extreme galaxy counterparts (Fynbo et al., 1999; Haehnelt et al., 2000; Rauch et al., 2008). The galaxy counterparts of the two DLAs towards Q0918+1636 are consistent with this picture.

3.5.3 OUTLOOK

Thanks to new sensitive near-IR spectrographs the study of galaxy counterparts of $z > 2$ DLAs has now opened (Weatherley et al., 2005; Fynbo et al., 2010, 2011; Bouché et al., 2012; Noterdaeme et al., 2012b; Krogager et al., 2013). The identification of intervening DLAs towards transient sources like Gamma-Ray Burst afterglows have also led to the detection of a galaxy counterpart and this approach hence also appears promising for the future (Schulze et al., 2012). At the moment observations like these are limited to the bright counterparts of the highest metallicity DLAs. With the advent of extremely large telescopes equipped with advanced adaptive optics in the next decade, however, such studies can be extended to the galaxy counterparts of more typical DLAs and hence a more complete unification of absorption and emission studies of high- z galaxies is within reach.

3.6 ACKNOWLEDGMENTS

We thank the anonymous referee for a very helpful report and Steve Schulze for comments on an earlier version of the manuscript. The Dark Cosmology Centre is funded by the DNRF. JPUF acknowledges support from the ERC-StG grant EGGs-278202. LC acknowledges the support of the EU under a Marie Curie Intra-European Fellowship, contract GA-2010-247117. AG acknowledges support from the EU FP7/2007-2013 under grant agreement n. 267251 AstroFit. The research of JRM is supported through a Royal Society University Research Fellowship. TK acknowledges support by the Eu-

ropean Commission under the Marie Curie Intra-European Fellowship Programme in FP7.

4

THE METAL-ENRICHED HOST OF AN ENERGETIC γ -RAY BURST AT $z \approx 1.6$

ABSTRACT – *Context: The star-forming nature of long γ -ray burst (GRB) host galaxies provides invaluable constraints on the progenitors of GRBs and might open a shortcut to the characteristics of typical star-forming galaxies throughout the history of the Universe. Due to the absence of near-infrared (NIR) spectroscopy, however, detailed investigations, specifically a determination of the gas-phase metallicity of gamma-ray burst hosts, was largely limited to redshifts $z < 1$ to date. We observed the galaxy hosting GRB 080605 at $z = 1.64$ using optical/NIR spectroscopy and high-resolution HST/WFC3 imaging in the rest-frame wavelength range between 1150 and 8700Å. These data allow us to study a $z > 1$ GRB host in unprecedented detail and investigate the relation between GRB hosts and field galaxies. We avail of VLT/X-shooter optical/NIR spectroscopy to measure the metallicity, electron density, star-formation rate (SFR), and reddening of the host of GRB 080605. Specifically, we use different strong-line diagnostics to robustly measure the gas-phase metallicity within the interstellar medium (ISM) for the first time based on [N II] at this redshift. The host of the energetic ($E_{\gamma, \text{iso}} \sim 2 \times 10^{53}$ erg) GRB 080605 at $z \sim 1.64$ is a morphologically complex, vigorously star-forming galaxy with an H α -derived SFR of $31_{-6}^{+12} M_{\odot} \text{ yr}^{-1}$. Its ISM is significantly enriched with metals. Specifically, [N II]/H $\alpha = 0.14 \pm 0.02$ which yields an oxygen abundance $12 + \log(\text{O}/\text{H})$ between 8.3 and 8.6 depending on the adopted strong-line calibrator. This corresponds to values in the range of $0.4 - 0.8 Z_{\odot}$. For its measured stellar mass ($M_{*} = 8.0_{-1.6}^{+1.3} \times 10^9 M_{\odot}$) and SFR this value is consistent with the fundamental metallicity relation defined by star-forming field galaxies. The absence of strong Ly α emission constrains the escape fraction of resonantly-scattered Ly α photons to $f_{\text{esc}} \lesssim 0.08$. Our observations provide a detailed picture of the conditions in the ISM of a highly star-forming galaxy with irregular morphology at $z \sim 1.6$. They include the first robust metallicity measurement based on [N II] for a GRB host at $z > 1$ and directly illustrate that GRB hosts are not necessarily metal-poor, both on absolute scales as well as relative to their stellar mass and SFR. GRB hosts could thus be fair tracers of the population of ordinary star-forming galaxies at high redshift.*

4.1 INTRODUCTION

The violent stellar explosion that gives rise to long γ -ray bursts (see e.g., Piran, 2004; Gehrels et al., 2009, for reviews) and their multi-wavelength afterglows has been firmly related to broad-line supernovae (SNe) of type Ic, and hence star-formation (SF), via the core-collapse of massive stars (e.g., Galama et al., 1998; Hjorth et al., 2003; Stanek et al., 2003; Malesani et al., 2004; Pian et al., 2006; Campana et al., 2006). The GRB's high-energy signature is very luminous, and unaffected by dust and therefore pin-points regions of star-formation irrespective of galaxy brightness, dust obscuration and redshift. GRB-selected galaxies hence provide a sample of high-redshift, star-forming galaxies that is fully complementary to conventional survey studies.

The luminous afterglows furthermore facilitate redshift measurements, and detailed investigation about the chemical composition (e.g., Savaglio et al., 2003; Prochaska et al., 2006, 2009; de Ugarte Postigo et al., 2010) and the dust properties of the host (e.g., Galama & Wijers, 2001; Kann et al., 2006; Schady et al., 2007, 2010; Zafar et al., 2011). GRB hosts can hence be targeted with a known redshift, position and information about the galaxy's interstellar medium (ISM) at hand, providing an independent diagnostic of galaxy evolution and star-formation.

Notably at the highest redshifts (Greiner et al., 2009; Tanvir et al., 2009; Salvaterra et al., 2009; Cucchiara et al., 2011), GRBs allow us to set observational constraints on the history of star-formation (e.g., Kistler et al., 2009; Robertson & Ellis, 2012; Elliott et al., 2012), the galaxy luminosity function (Tanvir et al., 2012; Basa et al., 2012) as well as on the nature of young and star-forming galaxies (e.g., Christensen et al., 2004; Chen et al., 2009; Watson et al., 2011) beyond the detection limit of state-of-the-art surveys.

To represent a robust tool for cosmology and probe of star-formation, the physical conditions that lead to the formation of the GRB progenitor must be understood. As direct observations of GRB progenitors akin to those of some SNe remain impossible due to the cosmological distances, afterglow sight-line (e.g., Fynbo et al., 2009), spatially-resolved (e.g., Christensen et al., 2008; Thöne et al., 2008; Levesque et al., 2011) or galaxy-integrated measurements (e.g., Graham et al., 2009; Chen, 2012) provide the most constraining information on the kind of galactic environments GRBs occur in.

However, the properties of an unbiased sample of long GRBs hosts are still largely unknown, and selection effects due to optically-dark bursts (Groot et al., 1998; Fynbo et al., 2001; Perley et al., 2009) arguably play a crucial role (e.g., Krühler et al., 2011; Perley et al., 2011a). Consequently, the conditions for the formation of GRBs, the relation between GRB hosts and field galaxies and the extent to which GRBs trace the cosmic SFR remain highly debated (e.g., Jakobsson et al., 2005; Fruchter et al., 2006; Kocevski et al., 2009; Campisi et al., 2011; Kocevski & West, 2011).

Local galaxies hosting long GRBs tend to be of low stellar mass and metal content with respect to SDSS galaxies (Levesque et al., 2010a) as well as the hosts of core-collapse SNe (Fruchter et al., 2006; Modjaz et al., 2008), which has been interpreted as support for a limited chemical evolution of the GRB host - seemingly in line with

metallicity constraints on the GRB progenitor from theoretical calculations based on the collapsar model (Woosley, 1993; MacFadyen & Woosley, 1999). These properties, however, are not indicative per-se of GRBs preferring low-metallicity environments, but instead could be the result of low-mass, low-metallicity galaxies dominating the local star-formation rate (Mannucci et al., 2011). In fact, at higher redshifts (see e.g., Levan et al., 2006; Berger et al., 2007) and in *Swift* GRB host samples with a better controlled selection a population of red, luminous, high-mass hosts emerges (Rossi et al., 2011; Hunt et al., 2011; Chen et al., 2011; Svensson et al., 2012).

A fundamental characteristic of (GRB-selected) galaxies is their gas-phase metallicity, and in particular whether they follow the relation between stellar mass (M_*), metallicity (Z) and SFR defined by local field galaxies (Mannucci et al., 2010; Lara-López et al., 2010). However, observational access to the metallicity of GRB hosts remained largely elusive, and robust constraints are only available up to $z \sim 1$ (Savaglio et al., 2009; Levesque et al., 2010a). This is largely due to the absence of efficient NIR spectrographs, as important tracers of metallicity (such as [N II] ($\lambda 6584$) and $H\alpha$), are redshifted into the NIR wavelength regime above $z \sim 0.5$.

Here we present optical/NIR observations of the galaxy hosting GRB 080605 at $z = 1.64$ obtained with the X-shooter spectrograph at the Very Large Telescope (VLT), and NIR imaging with HST/WFC3 and LIRIS mounted at the William Herschel Telescope (WHT). The spectroscopic observations probe the rest-frame wavelength range between 1150 and 8700 Å and reveal a wealth of emission lines including $H\beta$, [O III], $H\alpha$ and [N II] ($\lambda 6584$).

GRB 080605 (Sbarufatti et al., 2008) was initially detected by the *Swift* satellite (Gehrels et al., 2004), and its optical/NIR afterglow was readily identified (Kann et al., 2008; Clemens et al., 2008). Spectroscopy of the afterglow was obtained with FORS2 at the VLT which yields a redshift of $z = 1.6403$ (Jakobsson et al., 2008; Fynbo et al., 2009). The optical/NIR afterglow is characterized by the presence of significant amounts of dust with $A_V \sim 0.5$ mag (Greiner et al., 2011; Zafar et al., 2011), including evidence of a 2175 Å feature (Zafar et al., 2012). The 2175 Å dust bump is a common characteristic observed along sight-lines through the Milky-Way. It becomes weaker in the Large Magellanic Cloud, and is absent from most sight-lines through the Small Magellanic Cloud. It is only rarely observed towards high-redshift environments such as quasars or absorbing systems, but common along sight-lines to highly extinguished afterglows (e.g. Krühler et al., 2008; Elíasdóttir et al., 2009; Zafar et al., 2011; Perley et al., 2011b). The carrier of the bump is currently not fully understood with graphite and polycyclic aromatic hydrocarbons being primary candidates (see e.g., Draine, 2003, for a review).

We adopt the concordance ($\Omega_M = 0.27$, $\Omega_\Lambda = 0.73$, $H_0 = 71 \text{ km s}^{-1} \text{ Mpc}^{-1}$) Λ CDM cosmology. All errors are given at 1σ confidence levels. All magnitudes are given in the AB system and are corrected for the Galactic reddening of $E_{B-V} = 0.137$ mag (Schlegel et al., 1998). The solar oxygen abundance is assumed to be $12 + \log(\text{O}/\text{H}) = 8.69$ (Asplund et al., 2009) throughout this work. Wavelengths are given in vacuum and the redshifts in the heliocentric system.

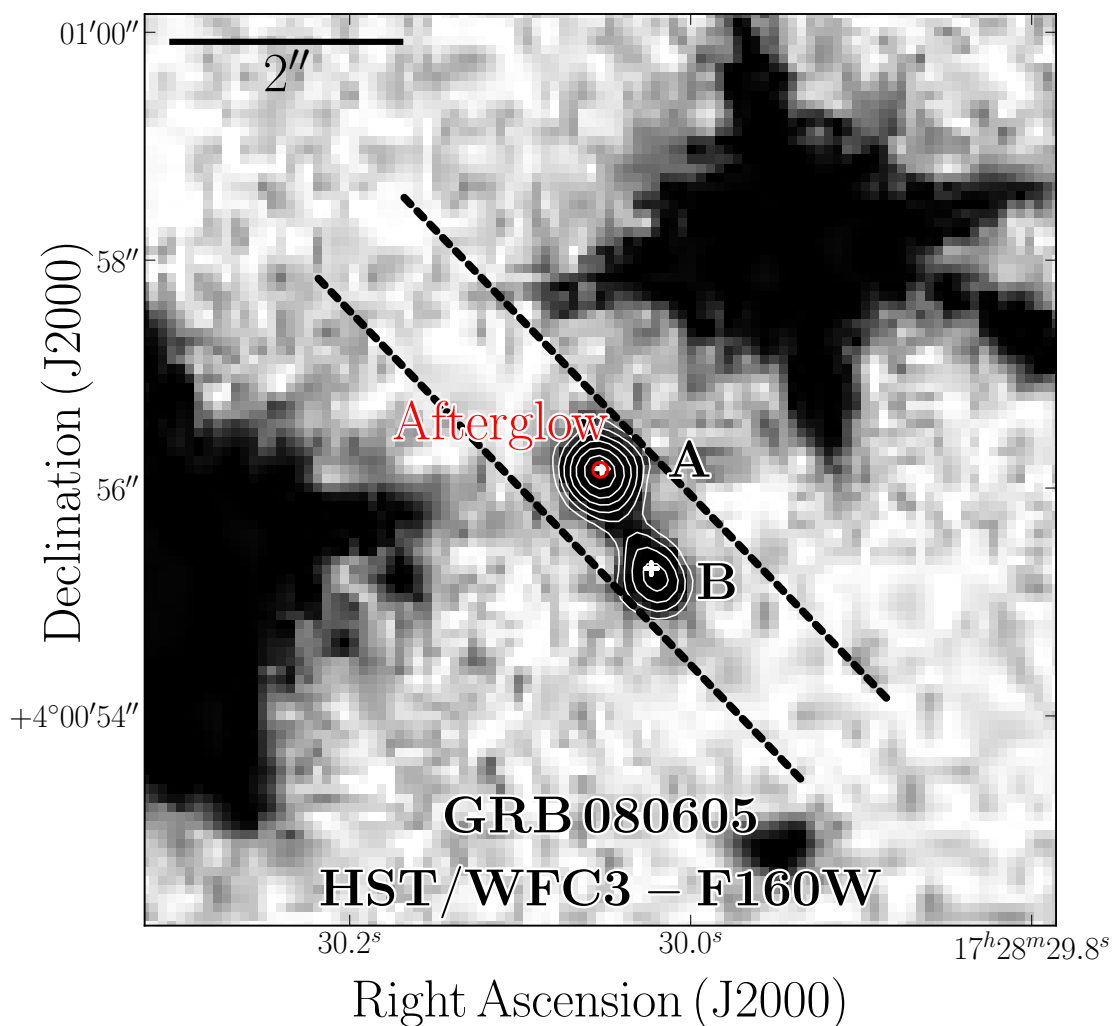


Figure 4.1 Finding chart (8×8) for the host of GRB 080605 as imaged with HST/WFC3. The afterglow position and its uncertainty are indicated by a red circle, and the different components are labeled A and B. The barycenter of each component is indicated by a white cross. The geometry of X-shooter’s UVB slit with width of $1''.0$ is illustrated by dashed black lines. The VIS and NIR slit have the same orientation but a width of $0''.9$. Logarithmically spaced contours are shown in white lines.

4.2 OBSERVATIONS AND DATA REDUCTION

4.2.1 SPACE-BASED IMAGING

The host of GRB 080605 was observed with the Hubble Space Telescope (HST) and Wide Field Camera 3 (WFC3) as part of a snapshot program targeting GRB hosts (PI: A. J.

Levan, Proposal ID: 12307) on 2012-02-22. HST imaging (see Figure 4.1) was obtained in the F160W filter in a three-point dither pattern resulting in a total exposure time of 1209 s. Individual images (pixel scale $0''.128/\text{px}$.) were drizzled to an output image with a pixel scale of $0''.08$ per pixel. Using several unsaturated stars in the field of view we measure a FWHM of the stellar PSF of $2.6 \pm 0.1 \text{ px}$, which is $0''.21 \pm 0''.01$.

To accurately locate the position of the afterglow within its host, we first used a GROND afterglow image from Greiner et al. (2011) and calibrated it astrometrically against ~ 80 sources from the USNO catalog. This sets the absolute astrometric scale with an accuracy of around $0''.4$ in each coordinate. The uncertainty introduced by centroiding errors of the afterglow is $\approx 15 \text{ mas}$. Afterwards, we registered a deeper GROND host image (Krühler et al., 2011) against the afterglow image using common field stars. The mapping uncertainty between the two GROND images is 20 mas . Finally, we used fainter stars from the host image that are unsaturated in the WFC3 frame to tie the space- to the ground-based imaging. In the last step the RMS-scatter of stellar positions is 60 mas in each coordinate, which dominates the total relative accuracy (65 mas) of the position of the afterglow within its host.

The host of GRB 080605 is clearly extended in the N/E direction in the HST imaging, and consists of two, somewhat blended components A and B (Fig. 4.1) with a projected distance of $1''.0$ between the brightest pixel of each component (corresponding to 8.6 kpc at $z = 1.641$). Photometry (see Table 4.1) was derived using elliptical Kron magnitudes via SExtractor (Bertin & Arnouts, 1996), an aperture correction of $6 \pm 4\%$ to the total flux (Graham & Driver, 2005) and the tabulated HST/WFC3 zeropoints¹ from March 06, 2012. Deblending parameters were set one time to measure the integrated flux of the both components to be comparable to the ground based imaging, and a second time to measure the flux contribution of the individual host components (see also Table 4.1). Given the small angular separation, the two components are not resolved in our ground-based imaging.

4.2.2 GROUND-BASED IMAGING

The field of the host of GRB 080605 was also imaged with the LIRIS instrument (Manchado et al., 2004) mounted at the 4.2 m WHT. We obtained a total of 0.55 hr of exposures in the J (average FWHM of the stellar PSF is $1''.4$), and 0.70 hr in the K_s -band (average FWHM of the stellar PSF is $1''.0$) at airmasses between 1.3 and 2.0. The data were reduced and photometry was performed within pyraf/IRAF (Tody, 1993) in a standard manner. Absolute calibration was obtained against roughly 40 field stars with magnitudes from the 2MASS catalog. This procedure resulted in an absolute photometric accuracy of around 0.05 mag in the J , and 0.07 mag in the K band, which is negligible compared to the error introduced by photon statistics. The LIRIS photometry is summarized in Table 4.1.

¹http://www.stsci.edu/hst/wfc3/phot_zp_lbn

Table 4.1 Photometric measurements.

Instrument	Filter	Exposure (s)	Brightness (mag) ^(a)
HST/WFC3	F160W	1209	(A) 22.38 ± 0.05
"	"	"	(B) 23.13 ± 0.06
"	"	"	(A & B) 21.96 ± 0.04
WHT/LIRIS	J	1980	(A & B) 22.2 ± 0.3
WHT/LIRIS	K_s	2520	(A & B) 21.8 ± 0.3

^(a) All magnitudes are in the AB system and corrected for a Galactic foreground extinction corresponding to a reddening of $E_{B-V} = 0.137$ mag (Schlegel et al., 1998).

4.2.3 X-SHOOTER OPTICAL/NIR SPECTROSCOPY

X-shooter (D’Odorico et al., 2006; Vernet et al., 2011b) at the VLT observed the host of GRB 080605 starting at 08:22 UT on 2011-04-26 for a total exposure time of 0.98 hr in the ultra-violet/blue (UVB), 1.01 hr in the visual (VIS), and 1.00 hr in the NIR arm, respectively. Spectroscopy was obtained with slit widths of $1''0$ (UVB), and $0''9$ (VIS and NIR), which results in resolving powers of $\lambda/\Delta\lambda \approx 5100$, 8800 and 5100 for the three arms. The geometry of the slit is illustrated in Figure 4.1.

Sky conditions were clear with an average seeing of $1''2$. In total, four nodded exposures in the sequence ABBA were obtained. In each nodding position a single UVB and VIS frame (885 and 910 s exposure time each), and three NIR frames (300 s exposure time each) were taken. Data were reduced with the X-shooter pipeline v. 1.5.0 (Goldoni et al., 2006) in physical mode, and the spectra were extracted using an optimal, variance-weighted method in IRAF (Tody, 1993).

The wavelength-solution was obtained against ThAr arc-lamp frames leaving residuals of around 0.2 pixel which corresponds to 6 km s^{-1} at $10\,000 \text{ \AA}$. Flux-calibration was performed against the spectro-photometric standard LTT7987² observed during the same night at 09:46 UT, immediately after the science exposures.

The stellar continuum of the host of GRB 080605 is detected in the X-shooter spectrum with a S/N ≈ 0.3 - 0.9 per pixel in parts of the UVB (3600 \AA to 5500 \AA) and VIS (5600 \AA to 9800 \AA). Within the NIR arm the continuum is only marginally seen in the J and H bands with S/N ~ 0.1 - 0.2 per pixel due to X-shooter’s lower sensitivity in this wavelength range. The host is undetected in the wavelength range of the K -band with a S/N smaller than ~ 0.1 per pixel.

A robust flux-calibration within the broad wavelength range of X-shooter’s sensitivity is challenging. We hence further corrected the flux-calibrated X-shooter spectrum in the UVB and VIS arms by integrating it over the filter curves of GROND (Greiner et al., 2008) and HST and matching it to the available host photometry (Krühler et al., 2011).

²http://www.eso.org/sci/facilities/paranal/instruments/xshooter/tools/specphot_list.html

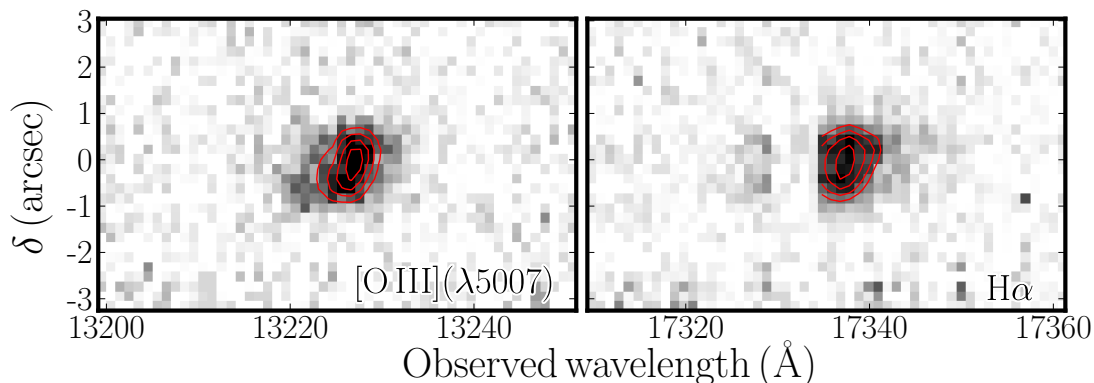


Figure 4.2 Two-dimensional cutouts of the X-shooter NIR spectrum centered on the observed wavelength of [O III](λ 5007) and H α . Skylines are indicated with grey shading. Linearly spaced contours are shown in red lines.

This procedure results in scaling factors of around 1.63 ± 0.09 for the g' -band in the UVB arm ($\approx 4590 \text{ \AA}$), and 1.56 ± 0.13 , 1.35 ± 0.12 and 1.26 ± 0.14 for the r' , i' and z' band at 6220, 7640 and 8990 \AA , respectively. For the NIR arm, we derive factors of 1.4 ± 0.4 for the J -band and 1.4 ± 0.2 for the F160W-band. Due to the non-detection of the continuum in the K -band, no correction can be obtained between 18 000 and 23 000 \AA , but no emission lines are detected in this wavelength regime.

We further tested the absolute flux calibration and its inter- and intra-arm continuity via observations of telluric standard stars taken on the same night. We find that the absolute flux of the telluric is typically recovered within uncertainties of 30%, while its spectral shape is robust to an accuracy better than 15% within each arm.

4.3 RESULTS

4.3.1 HOST GALAXY SYSTEM AND AFTERGLOW POSITION

The system hosting GRB 080605 consists of two components A and B (see Fig. 4.1) with barycentric coordinates of RA (J2000) = 17:28:30.05, decl. (J2000) = +04:00:56.2 for component A and RA (J2000) = 17:28:30.02, decl. (J2000) = +04:00:55.3 for component B, respectively. The half-light radii r_e in the observed F160W-band (rest-frame $\sim 5800 \text{ \AA}$) for the two components are marginally resolved ($r_{e,5800}^A \sim 0''.19$ or 1.6 kpc, $r_{e,5800}^B \sim 0''.26$ or 2.2 kpc). The half-light radius for the total host complex is $r_{e,5800} = 0''.41$ or 3.5 kpc.

The afterglow position coincides with the center of component A (Figure 4.1). Within our astrometric accuracy of 65 mas, no significant offset is detected and we conclude that the GRB exploded within a projected distance of 900 pc (90% confidence) to the central region of component A.

Table 4.2 Host parameters from stellar population synthesis modeling.

Absolute magnitude M_B (mag _{AB})	-22.4 ± 0.1
Age (Gyr)	$0.19^{+0.09}_{-0.10}$
Effective reddening E_{B-V}^{stars} (mag)	$0.10^{+0.05}_{-0.08}$
M_* ($10^9 M$)	$8.0^{+1.3}_{-1.6}$
SFR _{SED} ($M \text{ yr}^{-1}$)	49^{+26}_{-13}
sSFR _{SED} (Gyr^{-1})	6^{+5}_{-2}

4.3.2 EMISSION LINE PROFILE

The X-shooter spectrum of the host galaxy of GRB 080605 covers the wavelength range between 3050 and 23 000 Å (rest-frame 1150 and 8700 Å) and is rich in emission lines. The emission lines are identified as the doublets of [O II], [O III], [S II], [N II], as well as $H\alpha$, $H\beta$, and [O I]. The significance of the detection of the Balmer lines, [O III], [O II] and [N II] (λ 6584) is $> 8\sigma$, while it is between 2 and 4σ for [N II] (λ 6548), the [S II] doublet, and [O I] (λ 6366).

The two emission lines detected at the highest S/N ([O III] (λ 5007) and $H\alpha$, see also Section 4.3.4) are marginally tilted, reflecting the contributions of component A and B. Figure 4.2 shows the two-dimensional cutouts centered at the wavelength of the [O III] (λ 5007) and $H\alpha$ lines. They define heliocentric³ redshifts of $z_A = 1.64104 \pm 0.00004$ and $z_B = 1.64083 \pm 0.00007$ measured from the peak of the emission lines. These values correspond to a separation of $\Delta v \sim 20 \text{ km s}^{-1}$ (Figures 4.1 and 4.2).

For the fainter emission lines, we lack signal-to-noise ratio in our X-shooter spectrum and individual contributions of components A and B are strongly blended and can not be resolved. Similar to the ground-based photometry, we will thus report line-fluxes integrated over the complete host galaxy complex (Section 4.3.4) in the following.

4.3.3 HOST SED

Fitting the HST and LIRIS NIR photometry of the entire host system together with published broad-band magnitudes (see Krühler et al., 2011, for details) in LePhare⁴ (Arnouts et al., 1999; Ilbert et al., 2006) yields the galaxy parameters listed in Table 4.2. Here we assumed models from Bruzual & Charlot (2003a) based on an initial mass function (IMF) from Chabrier (2003) and a Calzetti dust attenuation law (Calzetti, 2001). Given that both method and data are largely unchanged, these values are only slightly refined with respect to those computed by Krühler et al. (2011).

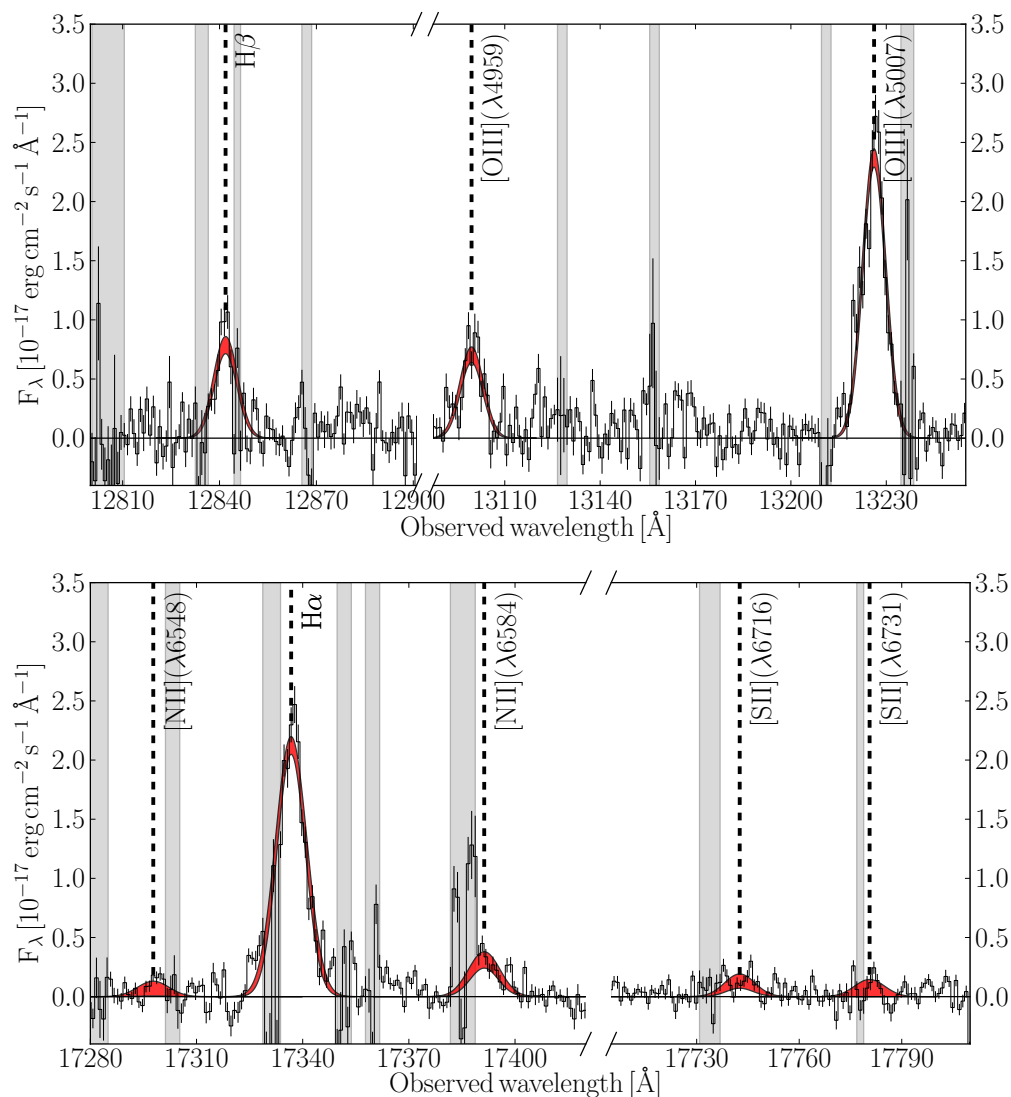


Figure 4.3 Continuum-subtracted emission lines used to determine the gas-phase metallicity in the X-shooter spectrum, as well as the [S II] doublet. The black line shows the raw spectrum including errors, and the red-shaded areas denote the 90% confidence region of the fit of the emission lines using Gaussians. Grey shaded areas denote wavelength regions that have been omitted in the fitting due to skyline contamination.

4.3.4 EMISSION LINE FLUXES

In the measurement of emission line fluxes (Table 4.3), the redshift (i.e., line centroids) and line widths were fitted simultaneously by tying weak emission lines to those detected at high S/N. In detail, we linked the parameters of the two components of the

³The heliocentric correction in the direction of GRB 080605 is 19 km s^{-1} for our observations.

⁴<http://www.cfht.hawaii.edu/~arnouts/lephare.html>

[O II] doublet in the visual arm, as well as the Gaussian widths and centroids of the various emission lines in the NIR arm. Although the emission of the forbidden and recombination lines does not necessarily arise from the same physical components, the assumption of a common redshift and line width provides a fair approximation and a good fit to the data (Fig. 4.3). The robustness of the procedure is further supported by, within errors, unchanged line parameters, fluxes and flux ratios when using different combination of ties (i.e., free FWHM, tying $H\beta$ to [O III] ($\lambda 5007$) or all lines except [O II] to each other) or allowing for multiple Gaussians components in the individual lines.

In addition, we cross-checked our method by numerically integrating the flux of the emission lines. Here, errors were estimated via Monte-Carlo techniques. This results in values that are consistent with those of the Gaussian fitting at 2σ confidence, but is more sensitive to skylines and small-scale irregularities in the data. It further disregards the physical information of a common redshift, and hence results in larger errors than the Gaussian fitting in particular for lines with low S/N, or those affected by skylines. We thus report fit-based values in Table 4.3. Our conclusions remain unchanged when using different Gaussian fitting methods or numerical integration techniques for the line flux measurements.

From the observed FWHM of the [O II] doublet ($\approx 5 \text{ \AA}$), and assuming a resolving power of 8800 of X-shooter's VIS arm, we derive a measured velocity dispersion σ of around $\sigma \sim 50 \text{ km s}^{-1}$ for the host galaxy complex, comparable to star-forming systems of similar mass observed through gravitational lenses (e.g., Christensen et al., 2010).

We do not detect significant emission from the resonant $\text{Ly}\alpha$ transition. Using the redshift, and assuming an intrinsic FWHM of twice the recombination lines (e.g., Fynbo et al., 2010), we set a limit on the $\text{Ly}\alpha$ flux of $4.7 \times 10^{-17} \text{ erg cm}^{-2} \text{ s}^{-1}$ ($7.6 \times 10^{-17} \text{ erg cm}^{-2} \text{ s}^{-1}$ after matching the spectrum to photometry) at the redshifted $\text{Ly}\alpha$ wavelength of 3210 \AA . It is estimated from an artificial emission line added on top of the sky contribution at the respective wavelength range, folded with the error spectrum and represents the flux that is detected at a combined S/N > 3 in 99% of all iterations. Similar limits are obtained when allowing for an offset of several ten to few hundreds of km s^{-1} for $\text{Ly}\alpha$ with respect to the recombination lines (Milvang-Jensen et al., 2012a). The non-detection of $\text{Ly}\alpha$ is further discussed in Section 4.4.4.

In the further analysis, we matched the spectrum to broad-band photometry (see Section 4.2.3), and applied when appropriate the correction for an average stellar Balmer absorption using a rest-frame equivalent width of 1 \AA (Cowie & Barger, 2008; Zahid et al., 2011), and for host galaxy extinction using the Balmer decrement (see Section 4.3.5). The corresponding wavelength-dependent factors are shown in Table 4.3.

Comparing the emission line ratios of [O III]/ $H\beta$ versus [N II] ($\lambda 6584$)/ $H\alpha$ against standard diagnostic relations (e.g., Kewley et al., 2001; Kauffmann et al., 2003), a significant contribution of an AGN to the host emission of GRB 080605 is readily excluded. Measurements of emission line fluxes and upper limits are reported in Table 4.3.

Table 4.3 Emission lines in the X-shooter spectrum.

Transition	Wavelength ^(a)	Flux ^(b)	Correction ^(c)
Ly α	1215	< 4.7	3.2 ^{+7.8} _{-1.6}
[O II]	3727	10.6 \pm 0.6	1.7 ^{+1.3} _{-0.5}
[O II]	3730	12.2 \pm 0.9	1.7 ^{+1.3} _{-0.5}
H β	4863	7.2 \pm 0.5	1.8 ^{+1.1} _{-0.6}
[O III]	4960	6.5 \pm 0.4	1.8 ^{+1.0} _{-0.6}
[O III]	5008	21.6 \pm 0.6	1.8 ^{+1.0} _{-0.6}
[O I]	6366	1.6 \pm 0.4	1.7 ^{+0.7} _{-0.4}
[N II]	6550	0.8 \pm 0.4	1.6 ^{+0.6} _{-0.3}
H α	6565	22.4 \pm 1.0	1.6 ^{+0.6} _{-0.3}
[N II]	6585	3.2 \pm 0.4	1.6 ^{+0.6} _{-0.3}
[S II]	6718	1.2 \pm 0.4	1.6 ^{+0.6} _{-0.3}
[S II]	6733	0.9 \pm 0.4	1.6 ^{+0.6} _{-0.3}

^(a) Rest-frame vacuum wavelength in units of Å.

^(b) Galactic extinction corrected flux in units of 10^{-17} erg s $^{-1}$ cm $^{-2}$. The flux is quoted as measured in the X-shooter spectrum (without correction). The flux error is statistical only, and does not contain the error of the absolute flux calibration.

^(c) The given correction includes the matching factor to broad-band photometry, stellar Balmer absorption if applicable, and reddening according to the Balmer line ratio. These factors are not independent. In particular it was assumed that [N II] and H α , for example, have identical values (except for the Balmer absorption).

4.3.5 BALMER DECREMENT

The ratio between the Balmer lines H α and H β is a tracer of the visual extinction towards the H II regions. We used the respective photometry-matched and stellar Balmer absorption corrected line fluxes to derive the intrinsic Balmer ratio, which is a direct measure of the selective reddening, or the total visual extinction under the assumption of a specific extinction law (and treating the H II regions as point-like). This probes a different physical quantity than the reddening value inferred from fitting the galaxy's SED from Table 4.2, as the SED modeling is sensitive to the attenuation of the stellar component which depends on the topology of the ISM and dust and galaxy geometry (e.g., Pierini et al., 2004).

Under standard assumptions of electron density (10^2 cm $^{-3}$ \lesssim n_e \lesssim 10^4 cm $^{-3}$, see also Sect. 4.3.6) and temperature ($T_e \sim 10^4$ K) for case B recombination (Osterbrock, 1989), the Balmer ratio indicates an average reddening towards the H II regions of $E_{B-V}^{\text{gas}} = 0.07^{+0.13}_{-0.07}$ mag. This corresponds to $A_V^{\text{gas}} = 0.22^{+0.40}_{-0.22}$ mag when assuming a MW-type extinction law with $R_V = 3.1$ (Cardelli et al., 1989). The reddening corrections according to the Balmer decrement for all emission lines except Ly α are fairly

robust and independent on the assumption of a specific extinction law, as there is little difference within the wavelength range of the Balmer lines between sight-lines through local galaxies (e.g., Pei, 1992) or with respect to extra-galactic extinction laws derived from GRB afterglows (Schady et al., 2012).

4.3.6 ELECTRON DENSITY

The flux ratio between the two components of the [O II] doublet is sensitive to the electron density (Osterbrock & Ferland, 2006). Individual components are resolved and well detected because of the high spectral resolution of X-shooter (see Fig. 4.4). Assuming an electron temperature T_e of 10^4 K, we derive an electron density of $n_e \sim 200 \text{ cm}^{-3}$. This value is typical for Galactic H II regions (e.g., Copetti et al., 2000). The low significance of the detection of the [S II] doublet (see Fig. 4.3) prevents meaningful constraints on the electron density based on [S II].

4.3.7 STAR-FORMATION RATE

Emission line fluxes of $H\alpha$ and [O II], as well as the UV continuum flux trace the unobscured star-formation within a galaxy (Kennicutt, 1998a; Kewley et al., 2004). The $H\alpha$ -derived value presents the most reliable optical indicator of a galaxy's SFR, as it is independent of metal abundances, and less sensitive to the uncertainties in the visual extinction than the other methods. SFR values depend quite strongly on the assumption of the IMF. In the following, we report values based on the initial formulation of the SFR from Kennicutt (1998a), but converted to a Chabrier IMF (Chabrier, 2003)⁵. Based on $H\alpha$, the SFR of the host of GRB 080605 is $\text{SFR}_{H\alpha} = 31_{-6}^{+12} M_{\odot} \text{ yr}^{-1}$. Here we used correction-factor and its error (see Tab. 4.3), and thus include the uncertainty in the flux calibration and host-intrinsic reddening. SFRs from [O II] ($\text{SFR}_{[\text{O II}]} = 55_{-22}^{+55} M_{\odot} \text{ yr}^{-1}$) and the SED modeling ($\text{SFR}_{\text{SED}} = 49_{-13}^{+26} M_{\odot} \text{ yr}^{-1}$) are within the larger uncertainties in good agreement with the $H\alpha$ -derived value.

Optically derived SFRs do not provide a full picture of the total (obscured and unobscured) star-formation in a galaxy. Based on sub-mm and radio measurements, there is evidence that the total SFR of few GRB-selected galaxies can be around or even higher than $100 M_{\odot} \text{ yr}^{-1}$ (e.g., Berger et al., 2003; Tanvir et al., 2004; Michałowski et al., 2012). The sample of sub-mm detected GRB hosts, however, is still very limited (e.g., Michałowski et al., 2008), and a full census of the actual SFR of GRB hosts will have to await the advent of statistically representative samples observed with sensitive far-infrared, sub-mm or radio observatories such as *Herschel*, ALMA or the eVLA.

Despite these limitations, optically-derived SFRs are well-established tools for the characterization of galaxies. We will thus put the host of GRB 080605 into the context of SFRs from field galaxies derived in a similar manner, with the caveat that the reported

⁵ Assuming a Salpeter IMF would increase all SFR estimates by a factor of ≈ 1.7 (e.g., Förster Schreiber et al., 2009).

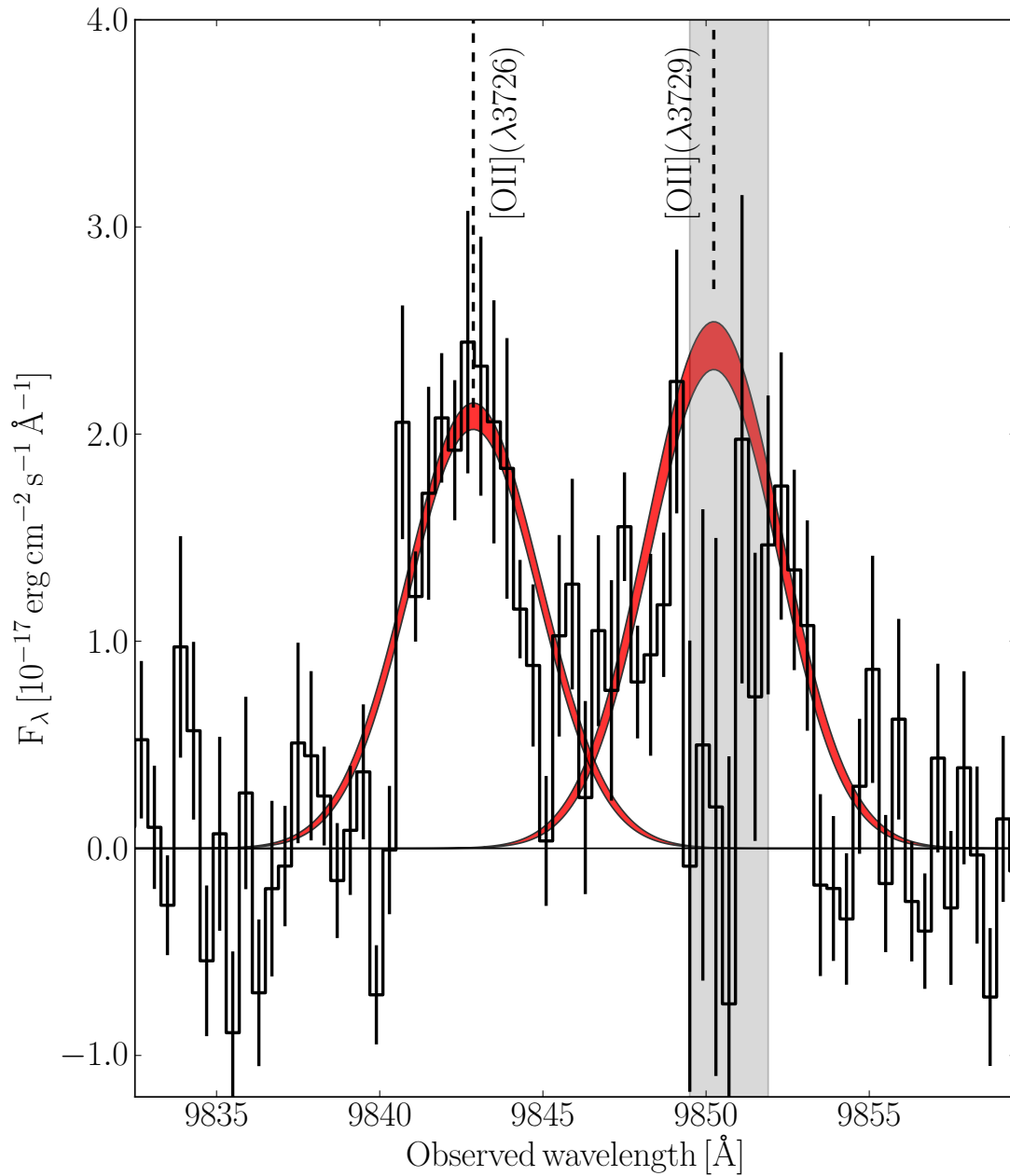


Figure 4.4 The continuum-subtracted [O II] ($\lambda\lambda$ 3726 3729) doublet. Lines and shadings are the same as in Fig. 4.3.

SFRs might trace only a fraction of the total SFR of a given galaxy.

Together with the stellar mass measurement of $M_* = 8.0_{-1.6}^{+1.3} \times 10^9 M_\odot$, the specific SFR ($\text{sSFR}_{\text{H}\alpha} = \text{SFR}_{\text{H}\alpha} / M_*$) and growth timescale $\tau = 1/\text{sSFR}_{\text{H}\alpha}$ are 4 Gyr^{-1} and 260 Myr, respectively, making the host of GRB 080605 a highly active and star-bursting

galaxy.

4.3.8 METALLICITY

The gas-phase metallicity of galaxies is typically measured using different diagnostic ratios of emission lines originating in H II regions (see e.g., Kewley & Ellison, 2008, and references therein). Most commonly used are the R_{23} calibrator, that requires measurements of line fluxes from [O II], [O III] and $H\beta$ (Pagel et al., 1979b; McGaugh, 1991; Kobulnicky & Kewley, 2004b), the O3N2 and N2 diagnostics which uses ratios of [O III], and $H\beta$, and/or [N II] and $H\alpha$ (Alloin et al., 1979; Pettini & Pagel, 2004), and the N2O2 indicator via [O II] and [N II] (Kewley & Dopita, 2002). For a detailed description on the individual strong-line diagnostics we refer to Kewley & Ellison (2008).

The R_{23} method is double-valued but its degeneracy can be broken via the line ratios of [N II]/ $H\alpha$ or [N II]/[O II]. In our case, [N II]/ $H\alpha$ = 0.14 ± 0.02 and [N II]/[O II] = 0.10 ± 0.04 . The significant flux detected in [N II] strongly points to the upper branch solution. Similarly, the N2O2 ratio is only applicable for high metallicities with $\log([\text{N II}]/[\text{O II}]) > -1.2$. Due to the large difference in wavelength of the lines used by N2O2 and R_{23} , their values are sensitive to the reddening in the host and wavelength-dependent errors in the flux calibration.

Both the O3N2 (see Eq. 1) and N2 methods, however, use flux ratios of adjacent emission lines, which are relatively close in wavelength space, and in our case are all within the NIR arm. The observed lines of [O III] and $H\beta$ are located in the J , and [N II] and $H\alpha$ in the H -band. Errors in the flux calibration or systematic uncertainties due to flat-fielding, slit-losses, intrinsic host extinction or reddening in the Galaxy are hence not going to affect the overall metallicity measurement in this case.

Based on O3N2, for example, the oxygen abundance is (Pettini & Pagel, 2004):

$$12 + \log(\text{O}/\text{H}) = 8.73 - 0.32 \times \log \left(\frac{F_{[\text{O III}](\lambda 5007)}/F_{H\beta}}{F_{[\text{N II}](\lambda 6584)}/F_{H\alpha}} \right) \quad (4.1)$$

which is $12 + \log(\text{O}/\text{H}) = 8.31 \pm 0.02$ for GRB 080605. Using the N2, R_{23} and N2O2 strong-line indicators, the oxygen abundance is $12 + \log(\text{O}/\text{H}) = 8.36 \pm 0.03$ for N2, $12 + \log(\text{O}/\text{H}) = 8.45^{+0.09}_{-0.12}$ for R_{23} , and $12 + \log(\text{O}/\text{H}) = 8.60^{+0.11}_{-0.19}$ for N2O2. Here, all errors are based on the uncertainties of the line flux measurement and the correction factor only (see Table 4.3), and do not include the systematic error inherent to the calibrator. Errors correctly reflect the larger uncertainty in the strong-line diagnostics that include flux ratios between lines in different wavelength regimes (R_{23} and N2O2). Oxygen abundances based on different indicators are further summarized in Table 4.4. We use the appropriate diagnostics when comparing to literature values.

Table 4.4 Oxygen abundances based on different strong-line indicators

Indicator	Lines / Methods	$12 + \log(\text{O}/\text{H})$	Z/Z	Uncertainty ^(a) (dex)	References ^(b)
R_{23}	[O II] (3727), H β , [O III] (5007)	$8.45^{+0.09}_{-0.12}$	0.63 ± 0.15	0.15	(1), (2), (3)
	[O II] (3727), H β , [O III] (5007)	$8.50^{+0.10}_{-0.13}$	0.64 ± 0.17	~ 0.1	(4, 6)
O3N2	H β , [O III] (5007), H α , [N II] (6584)	8.31 ± 0.02	0.42 ± 0.02	0.14	(5)
	[O III] (5007), [N II] (6584)	8.46 ± 0.10	$0.59^{+0.15}_{-0.12}$	0.24	(6)
N2	H α , [N II] (6584)	8.36 ± 0.03	0.47 ± 0.04	0.18	(5)
	H α , [N II] (6584)	8.52 ± 0.06	$0.68^{+0.09}_{-0.08}$	0.12	(6)
N2O2	[O II] (3727), [N II] (6584)	$8.60^{+0.11}_{-0.19}$	$0.82^{+0.24}_{-0.29}$	~ 0.1	(7)
	[O II] (3727) [N II] (6584)	$8.53^{+0.14}_{-0.24}$	$0.69^{+0.27}_{-0.30}$	0.10	(6)
Combined fit	R_{23} , O3N2, N2, N2O2	8.52 ± 0.09	$0.68^{+0.15}_{-0.13}$	included	(4), (6), (8)

^(a) Systematic 1σ scatter inherent to the diagnostic line ratio.

^(b) References for the indicator: (1) Pagel et al. (1979b); (2) McGaugh (1991); (3) Kobulnicky & Kewley (2004b); (4) Maiolino et al. (2008); (5) Pettini & Pagel (2004); (6) Nagao et al. (2006); (7) Kewley & Dopita (2002); (8) Mannucci et al. (2011).

4.4 DISCUSSION

The metallicity of GRB hosts is measured either directly in absorption using the bright afterglow emission, or, as in this work, in emission via host galaxy spectroscopy and strong-line diagnostics. In the former case, measurements are typically restricted to $z \gtrsim 2$ (e.g., Jakobsson et al., 2006; Savaglio, 2006), while the latter case requires NIR spectroscopy for $z \gtrsim 1$. Emission line metallicities are calibrated on local samples, and hence depend on the assumption that the physical processes underlying these diagnostic ratios are still valid at high redshift. There is hence considerable systematic uncertainty between metallicities derived directly in absorption or through emission lines. Furthermore, metallicity measurements at high-redshift via the different techniques are available for only a few objects. They tend to agree reasonably well (see e.g., Dessauges-Zavadsky et al., 2010), but systematic effects in a direct comparison remain hard to quantify until larger samples of objects with both, ISM as well as gas-phase metallicities, become available.

Our measurement of the gas-phase metallicity of the host of GRB 080605 represents a first view into the metal abundances of GRB hosts in the redshift range $1 \lesssim z \lesssim 2$ (Fig. 4.5). Generally, the distribution in metallicity as inferred from GRB-DLAs shows a large dispersion with values $0.01 \lesssim Z/Z_{\odot}$ (Vreeswijk et al., 2004; Prochaska et al., 2008; Rau et al., 2010) to solar or even super-solar (Prochaska et al., 2009; Savaglio et al., 2003, 2012). A similar spread in metallicities is also found in hydrodynamical solutions of individual sight-lines through GRB hosts (Pontzen et al., 2010). The metallicity derived from afterglow spectroscopy could be dominated by sight-line effects, and large samples might be required to assess the general properties of GRB hosts via afterglow spectroscopy in a statistical approach.

Host-integrated metallicities via emission lines should therefore give a more self-contained picture of the metal-enrichment of the ISM in high-redshift GRB hosts. Galaxy metallicity measurements are however challenging observationally in a stellar mass range around or below $10^{10} M_{\odot}$, and thus still sparse, in particular at $z > 1$. Current GRB host samples are furthermore subject to complex selection biases (Krühler et al., 2011), which are only resolved through statistical samples of high completeness (e.g., Fynbo et al., 2009; Cenko et al., 2009; Greiner et al., 2011; Salvaterra et al., 2011; Hjorth et al., 2012). Consequently, a consistent picture of the relation between galaxies selected through GRBs and normal field galaxies is not yet reached.

4.4.1 THE HOST OF GRB 080605 WITHIN THE SAMPLE OF GRB HOSTS

With respect to previous GRB host galaxies, the metallicity, stellar mass and star-formation rate of the host of GRB 080605 are relatively high (see Fig. 4.5). With a metallicity around half solar, a stellar mass of $8 \times 10^9 M_{\odot}$ and $\text{SFR} \sim 30 M_{\odot} \text{ yr}^{-1}$, it is significantly enriched with metals and vigorously forming stars. This contradicts the suggestion, that an up-

per metallicity limit⁶ for cosmological, $z \gtrsim 1$, GRBs of $Z \lesssim 0.2 Z_{\odot}$ exists (Stanek et al., 2006).

The substantial gas-phase metallicity of the host is even more intriguing, as GRB 080605 itself is energetic. The inferred isotropic-equivalent energy release in γ -rays is $E_{\gamma, \text{iso}} \sim 2.2 \times 10^{53}$ erg as calculated from the prompt emission data from Golenetskii et al. (2008). This value puts GRB 080605 within the most-energetic 15% of all *Swift* bursts (Butler et al., 2007, 2010).

A connection between host metallicity and γ -ray energy release of the GRB, or a metallicity cut-off might be expected in the collapsar scenario (Woosley, 1993; MacFadyen & Woosley, 1999), for example. Progenitor stars with lower metallicities are likely to have higher angular momentum due to smaller wind losses, and thus result in a more energetic explosion (e.g., Hirschi et al., 2005; Yoon & Langer, 2005). An energetic burst such as GRB 080605 would hence be more likely in a low-metallicity environment, in contrast to our observations. Our observations are, however, in line with the work of Wolf & Podsiadlowski (2007) and Levesque et al. (2010b), who find no correlation between $E_{\gamma, \text{iso}}$ and host metallicity in 18 GRBs at $z < 1$.

The role of metallicity in long GRB progenitors is thus far from being understood. The metallicity distribution of a representative GRB host sample will indirectly also allow us to put constraints on the metal content of the progenitor. For example, complex scenarios of stellar evolution, or binary models for the formation of long GRBs (e.g., Fryer et al., 1999) can both relax the constraints on progenitor metallicity. In addition, even within a metal-rich galaxy a metal-poor progenitor could in principle form in specific regions of fairly primordial chemical composition such as gas inflows or in (merging) galaxies with substantial diversity in their metal enrichment. To first order, however, the gas-phase, i.e., H II-region averaged, metallicity should provide a fair representation of the chemical evolution of the galaxy as a whole.

The galaxy hosting GRB 080605 has indeed a disturbed morphology, indicative of an early merger or intrinsically clumpy structure. A merger could have also triggered the enhanced star formation of the host of GRB 080605 when compared to GRB hosts at low redshift (e.g., Savaglio et al., 2009; Levesque et al., 2010a). GRB hosts with similar SFR, however, might not be uncommon at $z > 1$. A good fraction of X-ray selected GRB hosts at $1 < z < 2$ has observed *R*-band brightnesses (probing the rest frame UV) in a range between 24 mag and 22.5 mag (Malesani et al., 2009) indicating dust uncorrected SFRs up to $10 M_{\odot} \text{yr}^{-1}$. Already mild dust-attenuation in the host can easily increase this to values of $50 M_{\odot} \text{yr}^{-1}$ or even higher, illustrating that GRB hosts with SFRs significantly above $10 M_{\odot} \text{yr}^{-1}$ are not an exceptionally rare phenomenon at $z > 1$ (see also e.g., Fynbo et al., 2005; Chen et al., 2011; Krühler et al., 2011; Savaglio et al., 2012).

⁶Adopted to our reference solar oxygen abundance.

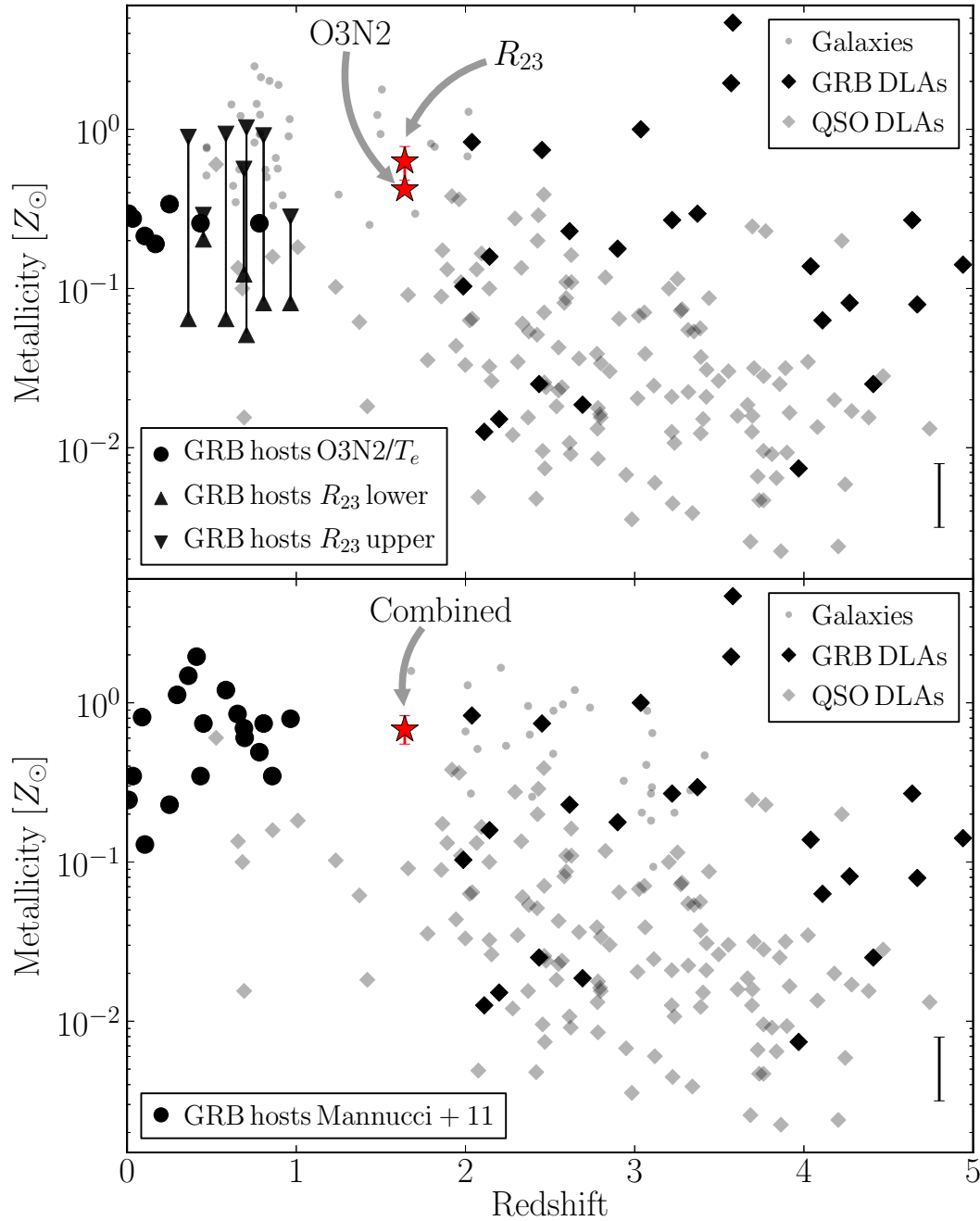


Figure 4.5 Metallicity of the host of GRB 080605 (star). Other GRB host metallicities are shown with black circles and upward/downward triangles as compiled and in the scale of Savaglio et al. (2009) (top panel) and Mannucci et al. (2011) (bottom panel). Field galaxies are shown as grey dots (Savaglio et al., 2005; Pérez-Montero et al., 2009; Mannucci et al., 2009; Hayashi et al., 2009; Richard et al., 2011), and in similar metallicity scales as the GRB measurements. Absorption metallicities from GRB afterglows (Rau et al., 2010; D’Elia et al., 2010; Savaglio et al., 2012; Thöne et al., 2011, and references therein) and QSOs (Prochaska et al., 2003) are plotted as black and grey diamonds, respectively. Errorbars for individual events in the comparison samples are omitted to enhance clarity. The error bars at the bottom right corner of each panel illustrate uncertainties of 0.2 dex., which are typical for both, GRB-DLA (e.g., Rau et al., 2010; Thöne et al., 2011) and GRB host metallicity (e.g., Mannucci et al., 2011) measurements.

4.4.2 AFTERGLOW VERSUS HOST PROPERTIES

The substantial gas-phase metallicity of $Z \sim Z_{\odot}/2$ might directly relate to the substantial $A_V \sim 0.5$ mag including the presence of the 2175 Å dust feature as observed in the afterglow SED (Greiner et al., 2011) and spectrum (Zafar et al., 2012). A metallicity of around solar was also inferred from GRB-DLAs for GRBs 070802 and 080607, both of which were substantially reddened, and had 2175 Å dust features (Elíasdóttir et al., 2009; Prochaska et al., 2009; Perley et al., 2011b) as well. This seems to support the association between the 2175 Å bump and chemically evolved galaxies (e.g., Noll et al., 2009). With only a small handful of such events, however, no strong conclusions can be drawn, yet.

4.4.3 THE MASS-METALLICITY RELATION AT $z \sim 2$

Having the key parameters of stellar mass, metallicity and SFR of the host of GRB 080605 at hand, we can now investigate its relation to the mass-metallicity (M_* - Z) relation at $z \sim 2$ (e.g., Erb et al., 2006). A further basic property is the host's location with respect to the fundamental metallicity relation (FMR) defined by SDSS galaxies in a mass range between $9.2 \lesssim \log(M_*) \lesssim 11.4$. The FMR connects M_* , $12 + \log(\text{O}/\text{H})$, and SFR (Mannucci et al., 2010) via:

$$12 + \log(\text{O}/\text{H}) = 8.90 + 0.47 \times (\mu_{0.32} - 10) \quad (4.2)$$

where $\mu_{0.32} = \log(M_* [M_{\odot}]) - 0.32 \times \log(\text{SFR}_{\text{H}\alpha} [M_{\odot} \text{ yr}^{-1}])$. The oxygen abundance for GRB 080605 on the Mannucci et al. (2010, 2011) scale is $12 + \log(\text{O}/\text{H}) = 8.52 \pm 0.09$. The value derived from M_* and SFR via Eq. 4.2 is consistent with it ($12 + \log(\text{O}/\text{H}) = 8.63 \pm 0.08$). Errors are again based on the statistical uncertainty of line-flux measurement, correction factor and stellar mass only⁷.

This establishes the host of GRB 080605 as a star-forming galaxy which has no significant deficit of metals with respect to star-forming galaxies at low redshift for its given mass and SFR. Or, conversely, the selection through the energetic GRB 080605 does not lead to its host being metal-poor with respect to field galaxies of comparable stellar mass and SFR.

The host of GRB 080605 hence provides the opportunity to probe the mass-metallicity relation at $z \sim 2$ (e.g., Erb et al., 2006) at lower stellar masses (Fig. 4.6). If populated with more events, GRB hosts can thus provide unique constraints on the low-mass end of the $M_* - Z$ relation (see also e.g., Vergani et al., 2011) similar to measurements via gravitationally lensed objects (e.g., Wuyts et al., 2012) but without the need for (and uncertainty of) a detailed lens model (Fig. 4.6).

⁷A systematic error on the stellar mass estimate of ± 0.2 dex., for example, would translate into additional systematic errors of ± 0.12 on the derived metallicity.

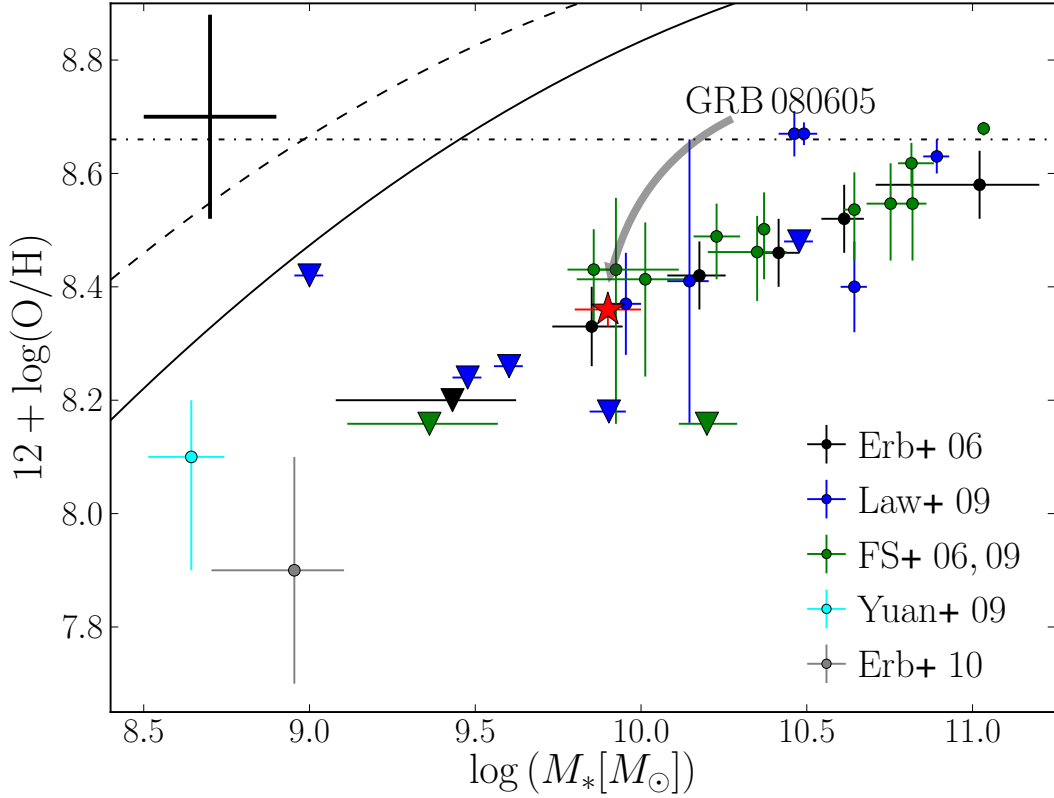


Figure 4.6 The host of GRB 080605 with respect to the mass-metallicity relation at $z \sim 2$. Different colored symbols represent the averaged galaxy distribution from Erb et al. (2006) in black, as well as individual sources from Förster Schreiber et al. (2006, 2009) in green, from Law et al. (2009) in blue and gravitationally lensed galaxies from Yuan & Kewley (2009) and Erb et al. (2010) in cyan and grey, respectively. Upper limits are shown with downward triangles with the same color-coding. All measurements are in the N2 scale of Pettini & Pagel (2004). The horizontal dashed-dotted line marks the solar oxygen abundance. The dashed line is the local $M - Z$ relation (Tremonti et al., 2004), which is also shown shifted (solid line) to the observations at $z \sim 0.7$ (Savaglio et al., 2005). Approximate systematic errors on the N2 metallicity scale and the mass determination are indicated in the top left corner.

4.4.4 THE NON-DETECTION OF $\text{Ly}\alpha$

The luminosity-independent selection of star-forming galaxies through GRBs offers a unique probe of the escape fraction (f_{esc}) of $\text{Ly}\alpha$ photons. The path length of resonantly scattered $\text{Ly}\alpha$ photons depends on the geometry and kinematics of H I within a galaxy, and could thus be greatly enhanced as compared to, for example, the path length of photons from recombination lines such as $\text{H}\alpha$. The longer path length directly translates into a higher dust absorption probability for $\text{Ly}\alpha$ photons and hence f_{esc} might end up anywhere below unity (e.g., Atek et al., 2009).

$\text{Ly}\alpha$ emission from GRB hosts was detected in both narrow-band imaging and afterglow/host spectroscopy (e.g., Fynbo et al., 2003; Jakobsson et al., 2005; D’Avanzo et al., 2010; Milvang-Jensen et al., 2012a). The broad wavelength coverage of X-shooter extending down to the UV ($\text{Ly}\alpha$ line at $z \sim 1.64$ is redshifted to 3210 Å) coupled with the tight constraints on the galaxies reddening and extreme luminosity of $\text{H}\alpha$, makes the host of GRB 080605 an ideal test case for the escape fraction in a high-redshift environment.

At $f_{\text{esc}} = 1$, the intrinsic ratio between $\text{Ly}\alpha$ and $\text{H}\alpha$ is 8.7 (Brocklehurst, 1971). Consequently, $\text{Ly}\alpha$ is expected to be a factor 12 more luminous than our non-detection implies. This corresponds to an escape fraction of $f_{\text{esc}} < 0.08$, which was estimated in the same way as the flux limit but using the photometry-matched spectrum and its errors as discussed in Section 4.2.3.

While the evidence for reddening from the recombination lines and the stellar continuum is weak, the properties of the afterglow (Zafar et al., 2012) provide compelling evidence that there is enough dust in the ISM to absorb the scattered $\text{Ly}\alpha$ photons efficiently.

Our limit is consistent with previous estimates using narrow-band surveys targeting both $\text{Ly}\alpha$ and $\text{H}\alpha$ (Hayes et al., 2010) or measured from the column density distribution of GRB-DLAs (Fynbo et al., 2009). A larger sample of hosts observed in similar fashion can provide competitive constraints on the average escape fraction in high-redshift environments at $1.6 < z < 2.5$. These measurements would be completely independent on conventional selection techniques, and representative of young, star-forming galaxies common in the early Universe. Establishing the average escape fraction at cosmological distances and for typical star-forming galaxies has strong implications for the use of $\text{Ly}\alpha$ emission as a tracer of star-formation and luminosity functions derived from $\text{Ly}\alpha$ galaxies at the highest redshifts.

4.5 CONCLUSIONS

We presented medium-resolution optical/NIR spectroscopy and ground and space-based imaging of the galaxy selected through GRB 080605 at $z = 1.64$. Our HST imaging probes and resolves the large-scale structure of the host, and shows it to be a morphologically complex system that consists of two components separated by 8.6 kpc. An X-shooter spectrum covering its rest-frame UV-to optical wavelength range (1150 to 8700 Å) reveals a wealth of emission lines, including [O II], [O III], $\text{H}\beta$ as well as [N II] and $\text{H}\alpha$. These recombination and forbidden lines allow us to put unique constraints on the conditions of the ISM in the host. It is in particular the first robust measurement of the gas-phase metallicity of a GRB host at $z > 1$ using strong-line indicators based on [N II] ($\lambda 6584$).

The host of GRB 080605 is significantly enriched with metals with an oxygen abundance $12 + \log(\text{O}/\text{H})$ between 8.3 and 8.6 ($0.4 Z_{\odot} < Z < 0.8 Z_{\odot}$) for several different strong-line diagnostics. In addition, its stellar mass is $M_* = 8.0_{-1.6}^{+1.3} \times 10^9 M_{\odot}$ and the

galaxy is extremely star-forming ($\text{SFR}_{\text{H}\alpha} = 31_{-6}^{+12} M_{\odot} \text{ yr}^{-1}$, $\text{sSFR}_{\text{H}\alpha} = 4 \text{ Gyr}^{-1}$). With a gas-phase metallicity above 40% of the solar value and luminosity above L^* (Krühler et al., 2011), it contrasts many observation of GRBs at lower redshift, which typically showed their hosts to be sub-luminous and metal-poor galaxies. Coupled with the high energy-release in γ -rays of $E_{\gamma, \text{iso}} \sim 2.2 \times 10^{53} \text{ erg}$, it challenges those GRB progenitor models in which the formation of energetic GRBs requires very low metallicities.

The metallicity measurement of the host of GRB 080605 directly shows that GRB hosts at $z > 1$ are not necessarily metal-poor, both on absolute scales as well as relative to their stellar mass and SFR. Our detailed spectroscopic observations in fact suggest that the hosts of GRBs in general might provide a fair representation of the high-redshift, SFR-weighted population of ordinary star-forming galaxies.

GRB hosts thus offer a selection of star-forming galaxies at high redshifts, including objects in the low-mass ($M_* \lesssim 10^{10} M_{\odot}$) regime, which are challenging to study otherwise. Targeted spectroscopic investigation become feasible through the afterglow's redshift, its sub-arcsec position and the substantial star-formation within GRB-selected galaxies.

Similar data for a representative and statistically significant sample of GRB hosts hold the key for understanding the nature of GRB hosts in particular and give important insights into the high-redshift population of star-forming galaxies in general. Furthermore, they yield the fundamental information to establish GRBs as probes of the star-formation up to the era of re-ionization. With the availability of highly redshift-complete GRB, afterglow and host samples such as TOUGH⁸ (Hjorth et al., 2012; Jakobsson et al., 2012; Milvang-Jensen et al., 2012b; Krühler et al., 2012; Michałowski et al., 2012, Malesani et al., in prep.) and NIR spectroscopy with X-shooter these studies are now feasible for the first time, and will continue to open the window with respect to the properties of GRB hosts in the previously unexplored redshift range $1 \lesssim z \lesssim 3$.

4.6 ACKNOWLEDGEMENTS

We thank L. Christensen and S. Savaglio for important insights and valuable discussion, and A. Rau for providing data for Figure 5 in machine-readable format. We also thank the referee for constructive comments, that helped to improve the quality of the manuscript. TK acknowledges support by the European Commission under the Marie Curie Intra-European Fellowship Programme in FP7. JPUF acknowledges support from the ERC-StG grant EGG-278202. The Dark Cosmology Centre is funded by the Danish National Research Foundation. Based on observations made with the NASA/ESA Hubble Space Telescope, obtained from the data archive at the Space Telescope Institute.

⁸<http://www.dark-cosmology.dk/TOUGH>

COAUTHORSTATEMENTS

Paper I

NIR spectroscopy and imaging of gravitationally-lensed quiescent $z \sim 2$ galaxies.

Stefan Geier, Johan Richard, Allison W.S. Man, Thomas Krühler, Sune Toft, Danilo Marchesini, & Johan P. U. Fynbo
The Astrophysical Journal, 2013, 777, 87

Chapter 2 is based on this paper.

SG as the lead author did the majority of the analysis and wrote most of the paper, including the figures. ST wrote the proposal which led to the spectroscopic data, and contributed to the introduction. SG contributed to that by doing the ISAAC photometry and selection of targets. SG reduced the X-Shooter spectra, including flux calibration and extractions. He also did the analysis of the spectra, i.e. the binning and SED fitting. JR provided the lensing magnifications, de-lensed the images of the galaxies, and provided the paragraph on Spitzer data. AM did the morphological analysis of the de-lensed images with the GALFIT tool and provided the text for the corresponding paragraph in the paper. TK assisted SG in the use of the LePhare SED fitting tool. JPUF helped with the HST photometry, supervised the work done by SG, and contributed ideas to the background of the introduction. All co-authors read the manuscript at each stage of revision and provided comments.

Paper II

The Galaxy Counterparts of the two high-metallicity DLAs at $z=2.412$ and $z=2.583$ towards Q0918+1636

*Johan P. U. Fynbo, Stefan Geier, Lise Christensen, Anna Gallazzi,
Jens-Kristian Krogager, Thomas Krühler, Cedric Ledoux, Justyn
Maund, Palle Møller, Pasquier Noterdaeme, Thøger Rivera-Thorsen, &
Marianne Vestergaard*

**Accepted for publication in Monthly Notices of The Royal
Astronomical Society**

Chapter 3 is based on this paper.

JPUF wrote the HST proposal which led to the HST imaging data, and obtained the X-Shooter spectroscopy, as well as the ALFOSC images. SG reduced the X-Shooter spectra, including flux calibration and extraction. SG also reduced the NOTCam imaging data, and did the photometry on the HST and NOT images. SG wrote part of the introduction, and the sections about reduction of the X-Shooter and NOTCam data. SG also did independent SED fitting of the $z = 2.583$ galaxy counterpart (AG did the SED-fitting included in the paper). Together with TK and LC, SG did the line-flux measurements. TRT and JPUF did the absorption line analysis for the $z = 2.412$ DLA. JKK and JM did the PSF-subtraction of the HST images. JPUF did the PSF subtraction of the ground-based images. All co-authors provided comments and suggestions for the paper.

Paper III

The metal-enriched host of an energetic γ -ray burst at $z \approx 1.6$

Thomas Krühler, Johan P. U. Fynbo, Stefan Geier, Jens Hjorth, Daniele Malesani, Bo Milvang-Jensen, Andrew Levan, Martin Sparre, Darach Watson, & Tayyabba Zafar

Astronomy and Astrophysics, 2012, 546, 8

Chapter 4 is based on this paper.

TK reduced and analyzed the X-shooter spectroscopy, as well as HST, and ground-based imaging, and he wrote most of the text of the paper. JPUF led the X-shooter proposal and helped in the X-shooter data reduction and analysis. SG led and obtained the ground-based LIRIS imaging, and helped in the X-shooter data reduction and analysis, the ground-based photometry and the photometric SED. DM helped in the X-shooter data reduction and analysis and provided a very thorough proof reading of the manuscript. AJL led the HST proposal, helped in the HST data reduction and performed an independent analysis of the HST photometry. JPUF, JH and DM provided insights into the X-shooter flux calibration. JPUF, JH, DM and DJW provided advice in various stages during the work and creation of the manuscript. JPUF, SG, JH, DM, BMJ, AJL, MS, DJW and TZ contributed to the observing proposals, provided constructive discussion and valuable comments and feedback - either in oral and/or written form - on all parts of the manuscript, but mainly to the results and their scientific interpretation. Contributions by non-coauthors and supporting institutions are mentioned in the acknowledgments of the article. This co-author statement was written by the first author of the article (TK). Co-authors do not have exact knowledge of the contributions of the other co-authors.

From: Johan Fynbo <jfynbo@dark-cosmology.dk>
Subject: **Fwd: <http://arxiv.org/abs/1306.2496> - coauthor statement**
Date: September 3, 2013 7:53:47 AM GMT+02:00
To: Stefan Geier <sgeier@dark-cosmology.dk>

FYI

----- Forwarded message -----

From: **RICHARD JOHAN** <joan.richard@univ-lyon1.fr>
Date: Tue, Aug 27, 2013 at 9:53 AM
Subject: Re: <http://arxiv.org/abs/1306.2496> - coauthor statement
To: Johan Fynbo <jfynbo@dark-cosmology.dk>
Cc: Allison Man <allison@dark-cosmology.dk>, Thomas Kruehler <tom@dark-cosmology.dk>, Sune Toft <sune@dark-cosmology.dk>, Danilo Marchesini <Danilo.Marchesini@tufts.edu>

ok :)

Congrats Stefan on the submission

Johan

On 27 Aug 2013, at 09:49, Johan Fynbo wrote:

Dear all,

Stefan is about to submit his PhD thesis. For this he needs coauthor statements for all included papers. For his main paper - on which you all coauthors - his proposed statement is this:

"Chapter 2 is based on this paper. SG as the lead author did the majority of the analysis and wrote most of the paper and made the figures. ST wrote the proposal which led to the spectroscopic data. SG contributed to that by doing the ISAAC photometry and selection of targets. SG reduced the X-Shooter spectra, including flux calibration and extractions. He also did the analysis of the spectra, i.e. the binning and SED fitting. JR provided the lensing magnifications and de-lensed the images of the galaxies, provided the paragraph on Spitzer data. AM did the morphological analysis of the de-lensed images with the GALFIT tool and provided the text for the corresponding paragraph in the paper. TK assisted SG in the use of the LePhare SED fitting tool. JPUF helped with the HST photometry, supervised the work done by SG, and contributed ideas to the background of the introduction. All co-authors read the manuscript at each stage of revision and provided comments."

Is this statement ok with you? We basically need a "ok" - and then that can be included in the thesis or otherwise adjustments for the statement that can then be approved and included in the thesis.

Best wishes and thanks,
Johan

CRAL, Observatoire de Lyon
9, avenue Charles André
69561 Saint Genis Laval cedex, France
Tél: +33 478 868 381
E-mail: joan.richard@univ-lyon1.fr

From: Johan Fynbo <jfynbo@dark-cosmology.dk>
Subject: **Fwd: <http://arxiv.org/abs/1306.2496> - coauthor statement**
Date: September 3, 2013 7:55:10 AM GMT+02:00
To: Stefan Geier <sgeier@dark-cosmology.dk>

FYI

----- Forwarded message -----

From: **Allison Man** <allison@dark-cosmology.dk>
Date: Tue, Aug 27, 2013 at 1:45 PM
Subject: Re: <http://arxiv.org/abs/1306.2496> - coauthor statement
To: Johan Fynbo <jfynbo@dark-cosmology.dk>
Cc: Stefan Geier <stefan@not.iac.es>

Hi Johan,

Yes, that's fine by me.

Cheers,
Allison

On Aug 27, 2013, at 9:49 AM, Johan Fynbo wrote:

Dear all,

Stefan is about to submit his PhD thesis. For this he needs coauthor statements for all included papers. For his main paper - on which you all are coauthors - his proposed statement is this:

"Chapter 2 is based on this paper. SG as the lead author did the majority of the analysis and wrote most of the paper and made the figures. ST wrote the proposal which led to the spectroscopic data. SG contributed to that by doing the ISAAC photometry and selection of targets. SG reduced the X-Shooter spectra, including flux calibration and extractions. He also did the analysis of the spectra, i.e. the binning and SED fitting. JR provided the lensing magnifications and de-lensed the images of the galaxies, provided the paragraph on Spitzer data. AM did the morphological analysis of the de-lensed images with the GALFIT tool and provided the text for the corresponding paragraph in the paper. TK assisted SG in the use of the LePhare SED fitting tool. JPUF helped with the HST photometry, supervised the work done by SG, and contributed ideas to the background of the introduction. All co-authors read the manuscript at each stage of revision and provided comments."

Is this statement ok with you? We basically need a "ok" - and then that can be included in the thesis or otherwise adjustments for the statement that can then be approved and included in the thesis.

Best wishes and thanks,
Johan

From: Johan Fynbo <jfynbo@dark-cosmology.dk>
Subject: **Fwd: <http://arxiv.org/abs/1306.2496> - coauthor statement**
Date: September 3, 2013 8:36:50 AM GMT+02:00
To: Stefan Geier <sgeier@dark-cosmology.dk>

FYI

----- Forwarded message -----

From: **Sune Toft** <sune@dark-cosmology.dk>
Date: Tue, Sep 3, 2013 at 8:36 AM
Subject: Re: <http://arxiv.org/abs/1306.2496> - coauthor statement
To: Johan Fynbo <jfynbo@dark-cosmology.dk>

Ja

On 03/09/2013, at 07.56, Johan Fynbo <jfynbo@dark-cosmology.dk> wrote:

Hej Sune,

Var dette statement ok med dig?

Bedste hilsener,
Johan

----- Forwarded message -----

From: **Johan Fynbo** <jfynbo@dark-cosmology.dk>
Date: Tue, Aug 27, 2013 at 9:58 AM
Subject: Re: <http://arxiv.org/abs/1306.2496> - coauthor statement
To: RICHARD JOHAN <johan.richard@univ-lyon1.fr>, Allison Man <allison@dark-cosmology.dk>, Thomas Kruehler <tom@dark-cosmology.dk>, Sune Toft <sune@dark-cosmology.dk>, Danilo Marchesini <Danilo.Marchesini@tufts.edu>

Dear all,

Here are new statement. We need an ok to this so please ignore the previous version:

"Chapter 2 is based on this paper. SG as the lead author did the majority of the analysis and wrote most of the paper and made the figures. ST wrote the proposal which led to the spectroscopic data. SG contributed to that by doing the ISAAC photometry and selection of targets. SG reduced the X-Shooter spectra, including flux calibration and extractions. He also did the analysis of the spectra, i.e. the binning and SED fitting. JR provided the lensing magnifications and de-lensed the images of the galaxies, provided the paragraph on Spitzer data. AM did the morphological analysis of the de-lensed images with the GALFIT tool and provided the text for the corresponding paragraph in the paper. TK assisted SG in the use of the LePhare SED fitting tool. JPUF helped with the HST photometry, supervised the work done by SG, and contributed ideas to the background of the introduction. ST also contributed a lot to the introduction. All co-authors read the manuscript at each stage of revision and provided comments."

Is this statement ok with you? We basically need a "ok" - and then that can be included in the thesis or otherwise adjustments for the statement that can then be approved and included in the thesis.

Best wishes and thanks,
Johan

From: Johan Fynbo <jfynbo@dark-cosmology.dk>
Subject: **Fwd: <http://arxiv.org/abs/1306.2496> - coauthor statement**
Date: September 3, 2013 7:54:56 AM GMT+02:00
To: Stefan Geier <sgeier@dark-cosmology.dk>

FYI

----- Forwarded message -----

From: **Marchesini, Danilo** <Danilo.Marchesini@tufts.edu>
Date: Tue, Aug 27, 2013 at 12:39 PM
Subject: Re: <http://arxiv.org/abs/1306.2496> - coauthor statement
To: Johan Fynbo <jfynbo@dark-cosmology.dk>
Cc: "Marchesini, Danilo" <Danilo.Marchesini@tufts.edu>, RICHARD JOHAN <johan.richard@univ-lyon1.fr>, Allison Man <allison@dark-cosmology.dk>, Thomas Kruehler <tom@dark-cosmology.dk>, Sune Toft <sune@dark-cosmology.dk>

OK

Danilo

Dr. Danilo Marchesini
Assistant Professor in Astrophysics
Tufts University
Physics and Astronomy Department
Science and Technology Center (STC)
4 Colby Street
Medford, MA 02155 USA
Tel. [617-627-2756](tel:617-627-2756)
Fax [617-627-3878](tel:617-627-3878)
Danilo.Marchesini@tufts.edu<mailto:Danilo.Marchesini@tufts.edu>
<http://cosmos.phy.tufts.edu/~danilo/>

On Aug 27, 2013, at 3:58 AM, Johan Fynbo wrote:

Dear all,

Here are new statement. We need an ok to this so please ignore the previous version:

"Chapter 2 is based on this paper. SG as the lead author did the majority of the analysis and wrote most of the paper and made the figures. ST wrote the proposal which led to the spectroscopic data. SG contributed to that by doing the ISAAC photometry and selection of targets. SG reduced the X-Shooter spectra, including flux calibration and extractions. He also did the analysis of the spectra, i.e. the binning and SED fitting. JR provided the lensing magnifications and de-lensed the images of the galaxies, provided the paragraph on Spitzer data. AM did the morphological analysis of the de-lensed images with the GALFIT tool and provided the text for the corresponding paragraph in the paper. TK assisted SG in the use of the LePhare SED fitting tool. JPUF helped with the HST photometry, supervised the work done by SG, and contributed ideas to the background of the introduction. ST also contributed a lot to the introduction. All co-authors read the manuscript at each stage of revision and provided comments."

Is this statement ok with you? We basically need a "ok" - and then that can be included in the thesis or otherwise adjustments for the statement that can then be approved and included in the thesis.

Best wishes and thanks,
Johan

From: Johan Fynbo <jfynbo@dark-cosmology.dk>
Subject: **Fwd: <http://arxiv.org/abs/1306.2496> - coauthor statement**
Date: September 3, 2013 7:59:28 AM GMT+02:00
To: Stefan Geier <sgeier@dark-cosmology.dk>

This is ok with me!

----- Forwarded message -----

From: **Johan Fynbo** <jfynbo@dark-cosmology.dk>
Date: Tue, Aug 27, 2013 at 9:58 AM
Subject: Re: <http://arxiv.org/abs/1306.2496> - coauthor statement
To: RICHARD JOHAN <johan.richard@univ-lyon1.fr>, Allison Man <allison@dark-cosmology.dk>, Thomas Kruehler <tom@dark-cosmology.dk>, Sune Toft <sune@dark-cosmology.dk>, Danilo Marchesini <Danilo.Marchesini@tufts.edu>

Dear all,

Here are new statement. We need an ok to this so please ignore the previous version:

"Chapter 2 is based on this paper. SG as the lead author did the majority of the analysis and wrote most of the paper and made the figures. ST wrote the proposal which led to the spectroscopic data. SG contributed to that by doing the ISAAC photometry and selection of targets. SG reduced the X-Shooter spectra, including flux calibration and extractions. He also did the analysis of the spectra, i.e. the binning and SED fitting. JR provided the lensing magnifications and de-lensed the images of the galaxies, provided the paragraph on Spitzer data. AM did the morphological analysis of the de-lensed images with the GALFIT tool and provided the text for the corresponding paragraph in the paper. TK assisted SG in the use of the LePhare SED fitting tool. JPUF helped with the HST photometry, supervised the work done by SG, and contributed ideas to the background of the introduction. ST also contributed a lot to the introduction. All co-authors read the manuscript at each stage of revision and provided comments."

Is this statement ok with you? We basically need a "ok" - and then that can be included in the thesis or otherwise adjustments for the statement that can then be approved and included in the thesis.

Best wishes and thanks,
Johan

From: Johan Fynbo <jfynbo@dark-cosmology.dk>
Subject: **Fwd: MNRAS: MN-13-1414-MJ.R2 - Coauthor statement**
Date: September 3, 2013 8:00:35 AM GMT+02:00
To: Stefan Geier <sgeier@dark-cosmology.dk>

This is ok with me!

----- Forwarded message -----

From: **Johan Fynbo** <jfynbo@dark-cosmology.dk>
Date: Tue, Aug 27, 2013 at 9:30 AM
Subject: MNRAS: MN-13-1414-MJ.R2 - Coauthor statement
To: Johan Fynbo <jfynbo@dark-cosmology.dk>
Cc: Lise Christensen <lise@dark-cosmology.dk>, Anna Gallazzi <gallazzi@arcetri.astro.it>, Jens-Kristian Krogager <krogager@dark-cosmology.dk>, Thomas Kruehler <tom@dark-cosmology.dk>, Cédric Ledoux <clédoux@eso.org>, "J. Maund@qub.ac.uk" <j.maund@qub.ac.uk>, Palle Moller <pmoller@eso.org>, Pasquier Noterdaeme <noterdaeme@iap.fr>, Thøger Rivera-Thorsen <trive@astro.su.se>, Marianne Vestergaard <vester@dark-cosmology.dk>

Dear all,

Stefan includes this manuscript in his PhD thesis. For that reason he needs a coauthor statement. His co-author statement on this manuscript is this:

"JPUF wrote the HST proposal which led to the HST imaging data, and obtained the X-Shooter spectroscopy, as well as the Alfvén images. SG reduced the X-Shooter spectra, including flux calibration and extraction. SG also reduced the NOTCam imaging data, and did the photometry on the HST and NOT images. SG wrote part of the introduction, and the sections about reduction of the X-Shooter and NOTCam data. SG also did independent SED fitting of the $z=2.583$ galaxy counterpart (Anna Gallazzi did the SED-fitting included in the paper). Together with Thomas Kruehler and Lise Christensen SG did the line-flux measurements. Thøger Thorsen-Rivera and JPUF did the absorption line analysis for the $z=2.412$ DLA. Jens-Kristian Krogager and Justyn Maund did the PSF-subtraction of the HST images. JPUF did the PSF subtraction of the ground-based images. All co-authors provided comments and suggestions for the paper."

Is this statement ok with you? We basically need a "ok" - and then that can be included in the thesis or otherwise adjustments for the statement that can then be approved and included in the thesis.

Best wishes,
Johan

From: Johan Fynbo <jfynbo@dark-cosmology.dk>
Subject: **Fwd: MNRAS: MN-13-1414-MJ.R2 - Coauthor statement**
Date: August 30, 2013 4:05:18 PM GMT+02:00
To: Stefan Geier <sgeier@dark-cosmology.dk>

----- Forwarded message -----

From: **Lise Christensen** <lise@dark-cosmology.dk>
Date: Tue, Aug 27, 2013 at 10:27 AM
Subject: Re: MNRAS: MN-13-1414-MJ.R2 - Coauthor statement
To: Johan Fynbo <jfynbo@dark-cosmology.dk>

Dear Johan

The statement is ok with me.

Lise

On 27 Aug 2013, at 09:30, Johan Fynbo wrote:

Dear all,

Stefan includes this manuscript in his PhD thesis. For that reason he needs a coauthor statement. His co-author statement on this manuscript is this:

"JPUF wrote the HST proposal which led to the HST imaging data, and obtained the X-Shooter spectroscopy, as well as the Alfosc images. SG reduced the X-Shooter spectra, including flux calibration and extraction. SG also reduced the NOTCam imaging data, and did the photometry on the HST and NOT images. SG wrote part of the introduction, and the sections about reduction of the X-Shooter and NOTCam data. SG also did independent SED fitting of the $z=2.583$ galaxy counterpart (Anna Gallazzi did the SED-fitting included in the paper). Together with Thomas Kihler and Lise Christensen SG did the line-flux measurements. Thøger Thorsen-Rivera and JPUF did the absorption line analysis for the $z=2.412$ DLA. Jens-Kristian Krogager and Justyn Maund did the PSF-subtraction of the HST images. JPUF did the PSF subtraction of the ground-based images. All co-authors provided comments and suggestions for the paper."

Is this statement ok with you? We basically need a "ok" - and then that can be included in the thesis or otherwise adjustments for the statement that can then be approved and included in the thesis.

Best wishes,
Johan

From: Johan Fynbo <jfynbo@dark-cosmology.dk>
Subject: **Fwd: MNRAS: MN-13-1414-MJ.R2 - Coauthor statement**
Date: August 30, 2013 4:05:53 PM GMT+02:00
To: Stefan Geier <sgeier@dark-cosmology.dk>

----- Forwarded message -----

From: **Anna Gallazzi** <gallazzi@arcetri.astro.it>
Date: Tue, Aug 27, 2013 at 12:18 PM
Subject: Re: MNRAS: MN-13-1414-MJ.R2 - Coauthor statement
To: Johan Fynbo <jfynbo@dark-cosmology.dk>

Hi Johan

it's OK with me

Cheers
Anna

On Tue, Aug 27, 2013 at 9:30 AM, Johan Fynbo <jfynbo@dark-cosmology.dk> wrote:
Dear all,

Stefan includes this manuscript in his PhD thesis. For that reason he needs a coauthor statement. His co-author statement on this manuscript is this:

"JPUF wrote the HST proposal which led to the HST imaging data, and obtained the X-Shooter spectroscopy, as well as the Alfosc images. SG reduced the X-Shooter spectra, including flux calibration and extraction. SG also reduced the NOTCam imaging data, and did the photometry on the HST and NOT images. SG wrote part of the introduction, and the sections about reduction of the X-Shooter and NOTCam data. SG also did independent SED fitting of the $z=2.583$ galaxy counterpart (Anna Gallazzi did the SED-fitting included in the paper). Together with Thomas K(\\u)hler and Lise Christensen SG did the line-flux measurements. Th(\\o)ger Thorsen-Rivera and JPUF did the absorption line analysis for the $z=2.412$ DLA. Jens-Kristian Krogager and Justyn Maund did the PSF-subtraction of the HST images. JPUF did the PSF subtraction of the ground-based images. All co-authors provided comments and suggestions for the paper."

Is this statement ok with you? We basically need a "ok" - and then that can be included in the thesis or otherwise adjustments for the statement that can then be approved and included in the thesis.

Best wishes,
Johan

From: Johan Fynbo <jfynbo@dark-cosmology.dk>
Subject: **Fwd: MNRAS: MN-13-1414-MJ.R2 - Coauthor statement**
Date: August 30, 2013 4:06:13 PM GMT+02:00
To: Stefan Geier <sgeier@dark-cosmology.dk>

----- Forwarded message -----

From: **Jens-Kristian Krogager** <jkrogage@eso.org>
Date: Tue, Aug 27, 2013 at 2:31 PM
Subject: Re: MNRAS: MN-13-1414-MJ.R2 - Coauthor statement
To: Johan Fynbo <jfynbo@dark-cosmology.dk>

Ok with me



Johan Fynbo

27. aug 2013 03.30

Dear all,

Stefan includes this manuscript in his PhD thesis. For that reason he needs a coauthor statement. His co-author statement on this manuscript is this:

"JPUF wrote the HST proposal which led to the HST imaging data, and obtained the X-Shooter spectroscopy, as well as the Alifosc images. SG reduced the X-Shooter spectra, including flux calibration and extraction. SG also reduced the NOTCam imaging data, and did the photometry on the HST and NOT images. SG wrote part of the introduction, and the sections about reduction of the X-Shooter and NOTCam data. SG also did independent SED fitting of the $z=2.583$ galaxy counterpart (Anna Gallazzi did the SED-fitting included in the paper). Together with Thomas Köhler and Lise Christensen SG did the line-flux measurements. Thøger Thorsen-Rivera and JPUF did the absorption line analysis for the $z=2.412$ DLA. Jens-Kristian Krogager and Justyn Maund did the PSF-subtraction of the HST images. JPUF did the PSF subtraction of the ground-based images. All co-authors provided comments and suggestions for the paper."

Is this statement ok with you? We basically need a "ok" - and then that can be included in the thesis or otherwise adjustments for the statement that can then be approved and included in the thesis.

Best wishes,
Johan

From: Johan Fynbo <jfynbo@dark-cosmology.dk>
Subject: **Fwd: MNRAS: MN-13-1414-MJ.R2 - Coauthor statement**
Date: August 30, 2013 4:06:02 PM GMT+02:00
To: Stefan Geier <sgeier@dark-cosmology.dk>

----- Forwarded message -----

From: **Thomas Kruehler** <t.kruehler@gmail.com>
Date: Tue, Aug 27, 2013 at 1:47 PM
Subject: Re: MNRAS: MN-13-1414-MJ.R2 - Coauthor statement
To: Johan Fynbo <jfynbo@dark-cosmology.dk>

Hi Johan,

ok with me.

Cheers
Thomas

On 27.08.13 09:30, Johan Fynbo wrote:

Dear all,

Stefan includes this manuscript in his PhD thesis. For that reason he needs a coauthor statement. His co-author statement on this manuscript is this:

"JPUF wrote the HST proposal which led to the HST imaging data, and obtained the X-Shooter spectroscopy, as well as the Alfosc images. SG reduced the X-Shooter spectra, including flux calibration and extraction. SG also reduced the NOTCam imaging data, and did the photometry on the HST and NOT images. SG wrote part of the introduction, and the sections about reduction of the X-Shooter and NOTCam data. SG also did independent SED fitting of the $z=2.583$ galaxy counterpart (Anna Gallazzi did the SED-fitting included in the paper). Together with Thomas Kruehler and Lise Christensen SG did the line-flux measurements. Thøger Thorsen-Rivera and JPUF did the absorption line analysis for the $z=2.412$ DLA. Jens-Kristian Krogager and Justyn Maund did the PSF-subtraction of the HST images. JPUF did the PSF subtraction of the ground-based images. All co-authors provided comments and suggestions for the paper."

Is this statement ok with you? We basically need a "ok" - and then that can be included in the thesis or otherwise adjustments for the statement that can then be approved and included in the thesis.

Best wishes,
Johan

From: Johan Fynbo <jfynbo@dark-cosmology.dk>
Subject: **Fwd: MNRAS: MN-13-1414-MJ.R2 - Coauthor statement**
Date: August 30, 2013 4:06:25 PM GMT+02:00
To: Stefan Geier <sgeier@dark-cosmology.dk>

----- Forwarded message -----

From: **clédoux** <clédoux@eso.org>
Date: Tue, Aug 27, 2013 at 6:18 PM
Subject: Re: MNRAS: MN-13-1414-MJ.R2 - Coauthor statement
To: Johan Fynbo <jfynbo@dark-cosmology.dk>

Fine with me (of course!)

On 27/08/13 03:30, Johan Fynbo wrote:

Dear all,

Stefan includes this manuscript in his PhD thesis. For that reason he needs a coauthor statement. His co-author statement on this manuscript is this:

"JPUF wrote the HST proposal which led to the HST imaging data, and obtained the X-Shooter spectroscopy, as well as the Alfosc images. SG reduced the X-Shooter spectra, including flux calibration and extraction. SG also reduced the NOTCam imaging data, and did the photometry on the HST and NOT images. SG wrote part of the introduction, and the sections about reduction of the X-Shooter and NOTCam data. SG also did independent SED fitting of the $z=2.583$ galaxy counterpart (Anna Gallazzi did the SED-fitting included in the paper). Together with Thomas Kähler and Lise Christensen SG did the line-flux measurements. Thøger Thorsen-Rivera and JPUF did the absorption line analysis for the $z=2.412$ DLA. Jens-Kristian Krogager and Justyn Maund did the PSF-subtraction of the HST images. JPUF did the PSF subtraction of the ground-based images. All co-authors provided comments and suggestions for the paper."

Is this statement ok with you? We basically need a "ok" - and then that can be included in the thesis or otherwise adjustments for the statement that can then be approved and included in the thesis.

Best wishes,
Johan

From: Johan Fynbo <jfynbo@dark-cosmology.dk>
Subject: **Fwd: MNRAS: MN-13-1414-MJ.R2 - Coauthor statement**
Date: August 30, 2013 4:04:50 PM GMT+02:00
To: Stefan Geier <sgeier@dark-cosmology.dk>

----- Forwarded message -----

From: **Justyn Maund** <j.maund@qub.ac.uk>
Date: Tue, Aug 27, 2013 at 9:31 AM
Subject: Re: MNRAS: MN-13-1414-MJ.R2 - Coauthor statement
To: Johan Fynbo <jfynbo@dark-cosmology.dk>

Hi
fine with me!

Cheers
J

On 27/08/2013 08:30, Johan Fynbo wrote:
Dear all,

Stefan includes this manuscript in his PhD thesis. For that reason he needs a coauthor statement. His co-author statement on this manuscript is this:

"JPUF wrote the HST proposal which led to the HST imaging data, and obtained the X-Shooter spectroscopy, as well as the Alfosc images. SG reduced the X-Shooter spectra, including flux calibration and extraction. SG also reduced the NOTCam imaging data, and did the photometry on the HST and NOT images. SG wrote part of the introduction, and the sections about reduction of the X-Shooter and NOTCam data. SG also did independent SED fitting of the $z=2.583$ galaxy counterpart (Anna Gallazzi did the SED-fitting included in the paper). Together with Thomas Kihler and Lise Christensen SG did the line-flux measurements. Thøger Thorsen-Rivera and JPUF did the absorption line analysis for the $z=2.412$ DLA. Jens-Kristian Krogager and Justyn Maund did the PSF-subtraction of the HST images. JPUF did the PSF subtraction of the ground-based images. All co-authors provided comments and suggestions for the paper."

Is this statement ok with you? We basically need a "ok" - and then that can be included in the thesis or otherwise adjustments for the statement that can then be approved and included in the thesis.

Best wishes,
Johan

From: Johan Fynbo <jfynbo@dark-cosmology.dk>
Subject: **Fwd: MNRAS: MN-13-1414-MJ.R2 - Coauthor statement**
Date: August 30, 2013 4:05:43 PM GMT+02:00
To: Stefan Geier <sgeier@dark-cosmology.dk>

----- Forwarded message -----

From: **Palle Møller** <pmoller@eso.org>
Date: Tue, Aug 27, 2013 at 11:57 AM
Subject: RE: MNRAS: MN-13-1414-MJ.R2 - Coauthor statement
To: Johan Fynbo <jfynbo@dark-cosmology.dk>

OK :-)

noget nyt ang indskrivning af Maryam som PhD student?
jeg er paa vej til Chile nu. Connector igen i Paris lufthavn
om et par timer eller saa.

hvad er forresten status af Ia's paper. Regner vi stadig
med at goere det faerdigt eller er det blevet droppet?
Det er noget tid siden vi har hoert noget.

Cheers,
Palle

From: johan.dark@gmail.com [johan.dark@gmail.com] on behalf of Johan Fynbo [jfynbo@dark-cosmology.dk]
Sent: Tuesday, August 27, 2013 9:30 AM
To: Johan Fynbo
Cc: Lise Christensen; Anna Gallazzi; Jens-Kristian Krogager; Thomas Kruehler; Cédric Ledoux; j.maund@qub.ac.uk; Palle Møller; Pasquier Noterdaeme; Thøger Rivera-Thorsen; Marianne Vestergaard
Subject: MNRAS: MN-13-1414-MJ.R2 - Coauthor statement

Dear all,

Stefan includes this manuscript in his PhD thesis. For that reason he needs a coauthor statement. His co-author statement on this manuscript is this:

"JPUF wrote the HST proposal which led to the HST imaging data, and obtained the X-Shooter spectroscopy, as well as the Alfosc images. SG reduced the X-Shooter spectra, including flux calibration and extraction. SG also reduced the NOTCam imaging data, and did the photometry on the HST and NOT images. SG wrote part of the introduction, and the sections about reduction of the X-Shooter and NOTCam data. SG also did independent SED fitting of the $z=2.583$ galaxy counterpart (Anna Gallazzi did the SED-fitting included in the paper). Together with Thomas Kruehler and Lise Christensen SG did the line-flux measurements. Thøger Thorsen-Rivera and JPUF did the absorption line analysis for the $z=2.412$ DLA. Jens-Kristian Krogager and Justyn Maund did the PSF-subtraction of the HST images. JPUF did the PSF subtraction of the ground-based images. All co-authors provided comments and suggestions for the paper."

Is this statement ok with you? We basically need a "ok" - and then that can be included in the thesis or otherwise adjustments for the statement that can then be approved and included in the thesis.

Best wishes,
Johan

From: Johan Fynbo <jfynbo@dark-cosmology.dk>
Subject: **Fwd: MNRAS: MN-13-1414-MJ.R2 - Coauthor statement**
Date: August 30, 2013 4:05:29 PM GMT+02:00
To: Stefan Geier <sgeier@dark-cosmology.dk>

----- Forwarded message -----

From: **Thøger Emil Rivera-Thorsen** <trive@astro.su.se>
Date: Tue, Aug 27, 2013 at 10:34 AM
Subject: Re: MNRAS: MN-13-1414-MJ.R2 - Coauthor statement
To: Johan Fynbo <jfynbo@dark-cosmology.dk>

Mine efternavne skal lige byttes rundt til "Rivera-Thorsen" - ellers er det et klart OK fra mig! :-)

On 2013-08-27 09:30, Johan Fynbo wrote:

Dear all,

Stefan includes this manuscript in his PhD thesis. For that reason he needs a coauthor statement. His co-author statement on this manuscript is this:

"JPUF wrote the HST proposal which led to the HST imaging data, and obtained the X-Shooter spectroscopy, as well as the Alfosc images. SG reduced the X-Shooter spectra, including flux calibration and extraction. SG also reduced the NOTCam imaging data, and did the photometry on the HST and NOT images. SG wrote part of the introduction, and the sections about reduction of the X-Shooter and NOTCam data. SG also did independent SED fitting of the $z=2.583$ galaxy counterpart (Anna Gallazzi did the SED-fitting included in the paper). Together with Thomas Kähler and Lise Christensen SG did the line-flux measurements. Thøger Thorsen-Rivera and JPUF did the absorption line analysis for the $z=2.412$ DLA. Jens-Kristian Krogager and Justyn Maund did the PSF-subtraction of the HST images. JPUF did the PSF subtraction of the ground-based images. All co-authors provided comments and suggestions for the paper."

Is this statement ok with you? We basically need a "ok" - and then that can be included in the thesis or otherwise adjustments for the statement that can then be approved and included in the thesis.

Best wishes,
Johan

--

Thøger Emil Rivera-Thorsen
Ph.D. student
Stockholm University,
Department of Astronomy

From: Johan Fynbo <jfynbo@dark-cosmology.dk>
Subject: **Fwd: MNRAS: MN-13-1414-MJ.R2 - Coauthor statement**
Date: September 3, 2013 7:55:51 AM GMT+02:00
To: Stefan Geier <sgeier@dark-cosmology.dk>

FYI

Message -----

From: **Marianne Vestergaard** <vester@dark-cosmology.dk>
Date: Tue, Aug 27, 2013 at 10:36 AM
Subject: Re: MNRAS: MN-13-1414-MJ.R2 - Coauthor statement
To: Johan Fynbo <jfynbo@dark-cosmology.dk>

OK with me.

Marianne

On 27/08/13 09.30, Johan Fynbo wrote:

Dear all,

Stefan includes this manuscript in his PhD thesis. For that reason he needs a coauthor statement. His co-author statement on this manuscript is this:

"JPUF wrote the HST proposal which led to the HST imaging data, and obtained the X-Shooter spectroscopy, as well as the Alfosc images. SG reduced the X-Shooter spectra, including flux calibration and extraction. SG also reduced the NOTCam imaging data, and did the photometry on the HST and NOT images. SG wrote part of the introduction, and the sections about reduction of the X-Shooter and NOTCam data. SG also did independent SED fitting of the $z=2.583$ galaxy counterpart (Anna Gallazzi did the SED-fitting included in the paper). Together with Thomas Kihler and Lise Christensen SG did the line-flux measurements. Thøger Thorsen-Rivera and JPUF did the absorption line analysis for the $z=2.412$ DLA. Jens-Kristian Krogager and Justyn Maund did the PSF-subtraction of the HST images. JPUF did the PSF subtraction of the ground-based images. All co-authors provided comments and suggestions for the paper."

Is this statement ok with you? We basically need a "ok" - and then that can be included in the thesis or otherwise adjustments for the statement that can then be approved and included in the thesis.

Best wishes,
Johan

--

Marianne Vestergaard
Dark Cosmology Centre, The Niels Bohr Institute
Juliane Maries Vej 30, DK-2100 Copenhagen Ø, Denmark

Phone: +45 35 32 59 09 /59 91 (secretary)
Fax: +45 35 32 06 17
<http://www.dark-cosmology.dk/~vester>

From: Johan Fynbo <jfynbo@dark-cosmology.dk>
Subject: **Fwd: A&A 546, A8 (2012) - coauthor statement**
Date: September 3, 2013 8:01:33 AM GMT+02:00
To: Stefan Geier <sgeier@dark-cosmology.dk>

This is ok with me!

----- Forwarded message -----

From: **Johan Fynbo** <jfynbo@dark-cosmology.dk>
Date: Fri, Aug 30, 2013 at 1:09 PM
Subject: A&A 546, A8 (2012) - coauthor statement
To: Thomas Kruehler <tom@dark-cosmology.dk>, Jens Hjorth <jens@dark-cosmology.dk>, Daniele Malesani <malesani@dark-cosmology.dk>, Bo Milvang-Jensen <milvang@dark-cosmology.dk>, Andrew Levan <a.j.levan@warwick.ac.uk>, Martin Sparre <sparre@dark-cosmology.dk>, Darach Watson <darach@dark-cosmology.dk>, Tayyaba Zafar <tayyaba.dark@gmail.com>

Dear all,

Thomas Kruehler was kind to write this statement concerning A&A 546, A8 (2012) included in Stefan Geier's thesis.

"TK reduced and analyzed the X-shooter spectroscopy, as well as HST, and ground-based imaging, and he wrote most of the text of the paper. JPUF lead the X-shooter proposal and helped in the X-shooter data reduction and analysis. SG lead and obtained the ground-based LRIS imaging, and helped in the X-shooter data reduction and analysis, the ground-based photometry and the photometric SED. DM helped in the X-shooter data reduction and analysis and provided a very thorough proof reading of the manuscript. AJL lead the HST proposal, helped in the HST data reduction and performed an independent analysis of the HST photometry. JPUF, JH and DM provided insights into the X-shooter flux calibration. JPUF, JH, DM and DJW provided advice in various stages during the work and creation of the manuscript. JPUF, SG, JH, DM, BMJ, AJL, MS, DJW and TZ contributed to the observing proposals, provided constructive discussion and valuable comments and feedback - either in oral and/or written form - on all parts of the manuscript, but mainly to the results and their scientific interpretation. Contributions by non-coauthors and supporting institutions are mentioned in the acknowledgments of the article.

This co-author statement was written by the first author of the article (TK). Co-authors do not have exact knowledge of the contributions of the other co-authors."

Can the co-authors agree to this statement?

Best wishes and thanks,
Johan

From: Johan Fynbo <jfynbo@dark-cosmology.dk>
Subject: **Fwd: Kruehler statement**
Date: August 31, 2013 2:36:42 PM GMT+02:00
To: Stefan Geier <sgeier@dark-cosmology.dk>

fyi

----- Forwarded message -----

From: **Jens Hjorth** <jens@dark-cosmology.dk>
Date: Sat, Aug 31, 2013 at 1:40 PM
Subject: Re: Kruehler statement
To: Johan Fynbo <jfynbo@dark-cosmology.dk>
Cc: Darach Watson <darach@dark-cosmology.dk>

This statement is an accurate representation of my contribution to this paper, and I know of no reason that the statement is not accurate regarding the contributions of the other authors.

Jens

On 30 Aug 2013, at 12:20, Johan Fynbo <jfynbo@dark-cosmology.dk> wrote:

Thomas send me this. Would this be better to include?

"TK reduced and analyzed the X-shooter spectroscopy, as well as HST, and ground-based imaging, and he wrote most of the text of the paper. JPUF lead the X-shooter proposal and helped in the X-shooter data reduction and analysis. SG lead and obtained the ground-based LRIS imaging, and helped in the X-shooter data reduction and analysis, the ground-based photometry and the photometric SED. DM helped in the X-shooter data reduction and analysis and provided a very thorough proof reading of the manuscript. AJL lead the HST proposal, helped in the HST data reduction and performed an independent analysis of the HST photometry. JPUF, JH and DM provided insights into the X-shooter flux calibration. JPUF, JH, DM and DJW provided advice in various stages during the work and creation of the manuscript. JPUF, SG, JH, DM, BMJ, AJL, MS, DJW and TZ contributed to the observing proposals, provided constructive discussion and valuable comments and feedback - either in oral and/or written form - on all parts of the manuscript, but mainly to the results and their scientific interpretation. Contributions by non-coauthors and supporting institutions are mentioned in the acknowledgments of the article.

This co-author statement was written by the first author of the article (TK). Co-authors do not have exact knowledge of the contributions of the other co-authors."

From: Johan Fynbo <johan.dark@gmail.com>
Subject: **Fwd: A&A 546, A8 (2012) - coauthor statement**
Date: September 2, 2013 5:50:11 PM GMT+02:00
To: Stefan Geier <sgeier@astro.ku.dk>

FYI

Bedste hilsener,
Johan

Start på videresendt besked:

Fra: Daniele Malesani <malesani@dark-cosmology.dk>
Dato: 2. sep. 2013 17.03.39 CEST
Til: Johan Fynbo <jfynbo@dark-cosmology.dk>
Cc: Thomas Kruehler <t.kruehler@gmail.com>, Jens Hjorth <jens@dark-cosmology.dk>, Bo Milvang-Jensen <milvang@dark-cosmology.dk>, Andrew Levan <a.levan@warwick.ac.uk>, Martin Sparre <sparre@dark-cosmology.dk>, Darach Watson <darach@dark-cosmology.dk>, Tayyaba Zafar <tayyaba.dark@gmail.com>
Emne: Vedr.: **A&A 546, A8 (2012) - coauthor statement**

Hi.

Sorry for the delay: I agree with the statement below, and thank Thomas for his careful wording.

I have signed coauthorship statements for several theses during the past years, and it has usually taken of order one minute to agree on a sentence. I understand this debate comes from a new set of rules? If so, I agree with Darach that their applicaton seems problematic and puts unnecessary burden on everybody.

It has crossed my mind that the discussion has been particularly careful because of the specific candidate.

d

On 30/8/13 13:09 , Johan Fynbo wrote:

Dear all,

Thomas Kruehler was kind to write this statement concerning A&A 546, A8 (2012) included in Stefan Geier's thesis.

"TK reduced and analyzed the X-shooter spectroscopy, as well as HST, and ground-based imaging, and he wrote most of the text of the paper. JPUF lead the X-shooter proposal and helped in the X-shooter data reduction and analysis. SG lead and obtained the ground-based LRIS imaging, and helped in the X-shooter data reduction and analysis, the ground-based photometry and the photometric SED. DM helped in the X-shooter data reduction and analysis and provided a very thorough proof reading of the manuscript. AJL lead the HST proposal, helped in the HST data reduction and performed an independent analysis of the HST photometry. JPUF, JH and DM provided insights into the X-shooter flux calibration. JPUF, JH, DM and DJW provided advice in various stages during the work and creation of the manuscript. JPUF, SG, JH, DM, BMJ, AJL, MS, DJW and TZ contributed to the observing proposals, provided constructive discussion and valuable comments and feedback - either in oral and/or written form - on all parts of the manuscript, but mainly to the results and their scientific interpretation. Contributions by non-coauthors and supporting institutions are mentioned in the acknowledgments of the article.

This co-author statement was written by the first author of the article (TK). Co-authors do not have exact knowledge of the contributions of the other co-authors."

Can the co-authors agree to this statement?

Best wishes and thanks,
Johan

From: Johan Fynbo <jfynbo@dark-cosmology.dk>
Subject: **Fwd: A&A 546, A8 (2012) - coauthor statement**
Date: August 30, 2013 4:03:56 PM GMT+02:00
To: Stefan Geier <sgeier@dark-cosmology.dk>

----- Forwarded message -----

From: **Bo Milvang-Jensen** <milvang@astro.ku.dk>
Date: Fri, Aug 30, 2013 at 1:29 PM
Subject: Re: A&A 546, A8 (2012) - coauthor statement
To: Johan Fynbo <jfynbo@dark-cosmology.dk>

Yes, I agree with this statement.

mvh. Bo

On Fri, Aug 30, 2013 at 01:09:22PM +0200, Johan Fynbo wrote:

> Dear all,
>
> Thomas Kruehler was kind to write this statement concerning A&A 546, A8
> (2012) included in Stefan Geier's thesis.
>
> "TK reduced and analyzed the X-shooter spectroscopy, as well as HST, and
> ground-based imaging, and he wrote most of the text of the paper. JPUF lead
> the X-shooter proposal and helped in the X-shooter data reduction and
> analysis. SG lead and obtained the ground-based LRIS imaging, and helped in
> the X-shooter data reduction and analysis, the ground-based photometry and
> the photometric SED. DM helped in the X-shooter data reduction and analysis
> and provided a very thorough proof reading of the manuscript. AJL lead the
> HST proposal, helped in the HST data reduction and performed an independent
> analysis of the HST photometry. JPUF, JH and DM provided insights into the
> X-shooter flux calibration. JPUF, JH, DM and DJW provided advice in various
> stages during the work and creation of the manuscript. JPUF, SG, JH, DM,
> BMJ, AJL, MS, DJW and TZ contributed to the observing proposals, provided
> constructive discussion and valuable comments and feedback - either in oral
> and/or written form - on all parts of the manuscript, but mainly to the
> results and their scientific interpretation. Contributions by non-coauthors
> and supporting institutions are mentioned in the acknowledgments of the
> article.
>
> This co-author statement was written by the first author of the article
> (TK). Co-authors do not have exact knowledge of the contributions of the
> other co-authors."
>
> Can the co-authors agree to this statement?
>
> Best wishes and thanks,
> Johan

From: Johan Fynbo <johan.dark@gmail.com>
Subject: **Fwd: A&A 546, A8 (2012) - coauthor statement**
Date: September 2, 2013 5:50:29 PM GMT+02:00
To: Stefan Geier <sgeier@dark-cosmology.dk>

FYI

Bedste hilsener,
Johan

Start på videresendt besked:

Fra: "Levan, Andrew" <A.J.Levan@warwick.ac.uk>
Dato: 2. sep. 2013 17.15.18 CEST
Til: Johan Fynbo <jfnbo@dark-cosmology.dk>
Emne: **Vedr.: A&A 546, A8 (2012) - coauthor statement**

Hi Johan,

Yes, this is fine with me.

Cheers,
Andrew

From: johan.dark@gmail.com [johan.dark@gmail.com] on behalf of Johan Fynbo [jfnbo@dark-cosmology.dk]
Sent: 02 September 2013 13:15
To: Levan, Andrew
Subject: Fwd: A&A 546, A8 (2012) - coauthor statement

Hi Andrew,

I this statement also acceptable to you?

Best wishes,
Johan

----- Forwarded message -----

From: Johan Fynbo <jfnbo@dark-cosmology.dk<<mailto:jfnbo@dark-cosmology.dk>>>
Date: Fri, Aug 30, 2013 at 1:09 PM
Subject: A&A 546, A8 (2012) - coauthor statement
To: Thomas Kruehler <tom@dark-cosmology.dk<<mailto:tom@dark-cosmology.dk>>>, Jens Hjorth <jens@dark-cosmology.dk<<mailto:jens@dark-cosmology.dk>>>, Daniele Malesani <malesani@dark-cosmology.dk<<mailto:malesani@dark-cosmology.dk>>>, Bo Milvang-Jensen <milvang@dark-cosmology.dk<<mailto:milvang@dark-cosmology.dk>>>, Andrew Levan <a.j.levan@warwick.ac.uk<a.j.levan@warwick.ac.uk>>, Martin Sparre <sparre@dark-cosmology.dk<<mailto:sparre@dark-cosmology.dk>>>, Darach Watson <darach@dark-cosmology.dk<<mailto:darach@dark-cosmology.dk>>>, Tayyaba Zafar <tayyaba.dark@gmail.com<<mailto:tayyaba.dark@gmail.com>>>

Dear all,

Thomas Kruehler was kind to write this statement concerning A&A 546, A8 (2012) included in Stefan Geier's thesis.

"TK reduced and analyzed the X-shooter spectroscopy, as well as HST, and ground-based imaging, and he wrote most of the text of the paper. JPUF lead the X-shooter proposal and helped in the X-shooter data reduction and analysis. SG lead and obtained the ground-based LRIS imaging, and helped in the X-shooter data reduction and analysis, the ground-based photometry and the photometric SED. DM helped in the X-shooter data reduction and analysis and provided a very thorough proof reading of the manuscript. A.J.L lead the HST proposal, helped in the HST data reduction and performed an independent analysis of the HST photometry. JPUF, JH and DM provided insights into the X-shooter flux calibration. JPUF, JH, DM and DJW provided advice in various stages during the work and creation of the manuscript. JPUF, SG, JH, DM, BMJ, AJL, MS, DJW and TZ contributed to the observing proposals, provided constructive discussion and valuable comments and feedback - either in oral and/or written form - on all parts of the manuscript, but mainly to the results and their scientific interpretation. Contributions by non-coauthors and supporting institutions are mentioned in the acknowledgments of the article.

This co-author statement was written by the first author of the article (TK). Co-authors do not have exact knowledge of the contributions of the other co-authors."

Can the co-authors agree to this statement?

Best wishes and thanks,
Johan

From: Johan Fynbo <jfynbo@dark-cosmology.dk>
Subject: **Fwd: A&A 546, A8 (2012) - coauthor statement**
Date: August 30, 2013 4:03:36 PM GMT+02:00
To: Stefan Geier <sgeier@dark-cosmology.dk>

----- Forwarded message -----

From: **Martin Sparre** <martinsparre@gmail.com>
Date: Fri, Aug 30, 2013 at 1:57 PM
Subject: Re: A&A 546, A8 (2012) - coauthor statement
To: Johan Fynbo <jfynbo@dark-cosmology.dk>

ok!

2013/8/30 Johan Fynbo <jfynbo@dark-cosmology.dk>

Dear all,

Thomas Kruehler was kind to write this statement concerning A&A 546, A8 (2012) included in Stefan Geier's thesis.

"TK reduced and analyzed the X-shooter spectroscopy, as well as HST, and ground-based imaging, and he wrote most of the text of the paper. JPUF lead the X-shooter proposal and helped in the X-shooter data reduction and analysis. SG lead and obtained the ground-based LRIS imaging, and helped in the X-shooter data reduction and analysis, the ground-based photometry and the photometric SED. DM helped in the X-shooter data reduction and analysis and provided a very thorough proof reading of the manuscript. AJL lead the HST proposal, helped in the HST data reduction and performed an independent analysis of the HST photometry. JPUF, JH and DM provided insights into the X-shooter flux calibration. JPUF, JH, DM and DJW provided advice in various stages during the work and creation of the manuscript. JPUF, SG, JH, DM, BMJ, AJL, MS, DJW and TZ contributed to the observing proposals, provided constructive discussion and valuable comments and feedback - either in oral and/or written form - on all parts of the manuscript, but mainly to the results and their scientific interpretation. Contributions by non-coauthors and supporting institutions are mentioned in the acknowledgments of the article.

This co-author statement was written by the first author of the article (TK). Co-authors do not have exact knowledge of the contributions of the other co-authors."

Can the co-authors agree to this statement?

Best wishes and thanks,
Johan

From: Johan Fynbo <jfynbo@dark-cosmology.dk>
Subject: **Fwd: A&A 546, A8 (2012) - coauthor statement**
Date: August 30, 2013 4:04:11 PM GMT+02:00
To: Stefan Geier <sgeier@dark-cosmology.dk>

----- Forwarded message -----

From: **Darach Watson** <darach@dark-cosmology.dk>
Date: Fri, Aug 30, 2013 at 1:27 PM
Subject: Re: A&A 546, A8 (2012) - coauthor statement
To: Johan Fynbo <jfynbo@dark-cosmology.dk>

This statement is an accurate representation of my contribution to this paper, and I know of no reason that the statement is not accurate regarding the contributions of the other authors.

On 30 August 2013 13:09, Johan Fynbo <jfynbo@dark-cosmology.dk> wrote:

Dear all,

Thomas Kruehler was kind to write this statement concerning A&A 546, A8 (2012) included in Stefan Geier's thesis.

"TK reduced and analyzed the X-shooter spectroscopy, as well as HST, and ground-based imaging, and he wrote most of the text of the paper. JPUF lead the X-shooter proposal and helped in the X-shooter data reduction and analysis. SG lead and obtained the ground-based LRIS imaging, and helped in the X-shooter data reduction and analysis, the ground-based photometry and the photometric SED. DM helped in the X-shooter data reduction and analysis and provided a very thorough proof reading of the manuscript. AJL lead the HST proposal, helped in the HST data reduction and performed an independent analysis of the HST photometry. JPUF, JH and DM provided insights into the X-shooter flux calibration. JPUF, JH, DM and DJW provided advice in various stages during the work and creation of the manuscript. JPUF, SG, JH, DM, BMJ, AJL, MS, DJW and TZ contributed to the observing proposals, provided constructive discussion and valuable comments and feedback - either in oral and/or written form - on all parts of the manuscript, but mainly to the results and their scientific interpretation. Contributions by non-coauthors and supporting institutions are mentioned in the acknowledgments of the article.

This co-author statement was written by the first author of the article (TK). Co-authors do not have exact knowledge of the contributions of the other co-authors."

Can the co-authors agree to this statement?

Best wishes and thanks,
Johan

--

Dr. Darach Watson

Dark Cosmology Centre
Niels Bohr Institute
University of Copenhagen
Juliane Maries Vej 30
DK-2100 Copenhagen Ø
Denmark

Tel: [+45 - 353 25994](tel:+4535325994)
24 80 38 25
Fax: [+45 353 20 617](tel:+4535320617)

From: Johan Fynbo <jfynbo@dark-cosmology.dk>
Subject: **Fwd: A&A 546, A8 (2012) - coauthor statement**
Date: August 30, 2013 4:03:23 PM GMT+02:00
To: Stefan Geier <sgeier@dark-cosmology.dk>

----- Forwarded message -----

From: **Tayyaba** <tayyaba.dark@gmail.com>
Date: Fri, Aug 30, 2013 at 3:11 PM
Subject: Re: A&A 546, A8 (2012) - coauthor statement
To: Johan Fynbo <jfynbo@dark-cosmology.dk>

Hi Johan,

This is very precise. I agree with this statement. I dont know the policy of the University for contributions but this one explains all.

Best wishes,
Tayyaba

On 30 Aug 2013, at 16:09, Johan Fynbo wrote:

Dear all,

Thomas Kruehler was kind to write this statement concerning A&A 546, A8 (2012) included in Stefan Geier's thesis.

"TK reduced and analyzed the X-shooter spectroscopy, as well as HST, and ground-based imaging, and he wrote most of the text of the paper. JPUF lead the X-shooter proposal and helped in the X-shooter data reduction and analysis. SG lead and obtained the ground-based LRIS imaging, and helped in the X-shooter data reduction and analysis, the ground-based photometry and the photometric SED. DM helped in the X-shooter data reduction and analysis and provided a very thorough proof reading of the manuscript. AJL lead the HST proposal, helped in the HST data reduction and performed an independent analysis of the HST photometry. JPUF, JH and DM provided insights into the X-shooter flux calibration. JPUF, JH, DM and DJW provided advice in various stages during the work and creation of the manuscript. JPUF, SG, JH, DM, BMJ, AJL, MS, DJW and TZ contributed to the observing proposals, provided constructive discussion and valuable comments and feedback - either in oral and/or written form - on all parts of the manuscript, but mainly to the results and their scientific interpretation. Contributions by non-coauthors and supporting institutions are mentioned in the acknowledgments of the article.

This co-author statement was written by the first author of the article (TK). Co-authors do not have exact knowledge of the contributions of the other co-authors."

Can the co-authors agree to this statement?

Best wishes and thanks,
Johan

BIBLIOGRAPHY

- Alloin, D., Collin-Souffrin, S., Joly, M., & Vigroux, L. 1979, *A&A*, 78, 200
- Anderson, J. P., & Soto, M. 2012, *ArXiv e-prints*
- Arnouts, S., Cristiani, S., Moscardini, L., Matarrese, S., Lucchin, F., Fontana, A., & Giallongo, E. 1999, *MNRAS*, 310, 540
- Arnouts, S., et al. 2002, *MNRAS*, 329, 355
- Asplund, M., Grevesse, N., Sauval, A. J., & Scott, P. 2009, *ARA&A*, 47, 481
- Atek, H., Kunth, D., Schaerer, D., Hayes, M., Deharveng, J. M., Östlin, G., & Mas-Hesse, J. M. 2009, *A&A*, 506, L1
- Audouze, J. 1981, in *Cosmology and Particles - 16TH Moriond*, ed. J. Audouze, P. Crane, T. Gaisser, D. Hegyi, & J. Tran Thanh Van, 231–240
- Baldry, I. K., et al. 2012, *MNRAS*, 421, 621
- Barro, G., et al. 2012, *ArXiv e-prints*
- Basa, S., Cuby, J. G., Savaglio, S., Boissier, S., Clement, B., Flores, H., Le Borgne, D., & Mazure, A. 2012, *A&A* submitted, arXiv:1201.6383
- Beaver, E. A., Burbidge, E. M., McIlwain, C. E., Epps, H. W., & Strittmatter, P. A. 1972, *ApJ*, 178, 95
- Bell, E. F., McIntosh, D. H., Katz, N., & Weinberg, M. D. 2003, *ApJS*, 149, 289
- Berger, E., Cowie, L. L., Kulkarni, S. R., Frail, D. A., Aussel, H., & Barger, A. J. 2003, *ApJ*, 588, 99
- Berger, E., Fox, D. B., Kulkarni, S. R., Frail, D. A., & Djorgovski, S. G. 2007, *ApJ*, 660, 504
- Bertin, E., & Arnouts, S. 1996, *A&AS*, 117, 393
- Bezanson, R., van Dokkum, P. G., Tal, T., Marchesini, D., Kriek, M., Franx, M., & Coppi, P. 2009, *ApJ*, 697, 1290
- Blandford, R. D. 2001, *Progress of Theoretical Physics Supplement*, 143, 182
- Böhringer, H., et al. 2000, *ApJS*, 129, 435
- Bosma, A. 1981, *AJ*, 86, 1825

- Bouché, N., Murphy, M. T., Kacprzak, G. G., Péroux, C., Contini, T., Martin, C., & Dessauges-Zavadsky, M. 2013, *Science*, in press (arXiv:1306.0134)
- Bouché, N., et al. 2010, *ApJ*, 718, 1001
- . 2012, *MNRAS*, 419, 2
- Bouwens, R. J., et al. 2011, *Nature*, 469, 504
- Braun, R. 2013, *Nature*, 497, 191
- Brocklehurst, M. 1971, *MNRAS*, 153, 471
- Bruzual, G., & Charlot, S. 2003a, *MNRAS*, 344, 1000
- . 2003b, *MNRAS*, 344, 1000
- Butcher, H., & Oemler, Jr., A. 1978a, *ApJ*, 219, 18
- . 1978b, *ApJ*, 226, 559
- . 1984, *ApJ*, 285, 426
- Butler, N. R., Bloom, J. S., & Poznanski, D. 2010, *ApJ*, 711, 495
- Butler, N. R., Kocevski, D., Bloom, J. S., & Curtis, J. L. 2007, *ApJ*, 671, 656
- Calzetti, D. 2001, *PASP*, 113, 1449
- Calzetti, D., Armus, L., Bohlin, R. C., Kinney, A. L., Koornneef, J., & Storchi-Bergmann, T. 2000, *ApJ*, 533, 682
- Calzetti, D., Kinney, A. L., & Storchi-Bergmann, T. 1994, *ApJ*, 429, 582
- Cameron, E., Carollo, C. M., Oesch, P. A., Bouwens, R. J., Illingworth, G. D., Trenti, M., Labbé, I., & Magee, D. 2011, *ApJ*, 743, 146
- Campana, S., et al. 2006, *Nature*, 442, 1008
- Campisi, M. A., Tapparello, C., Salvaterra, R., Mannucci, F., & Colpi, M. 2011, *MNRAS*, submitted, arXiv:1105.1378
- Campusano, L. E., Pelló, R., Kneib, J.-P., Le Borgne, J.-F., Fort, B., Ellis, R., Mellier, Y., & Smail, I. 2001, *A&A*, 378, 394
- Cano-Díaz, M., Maiolino, R., Marconi, A., Netzer, H., Shemmer, O., & Cresci, G. 2012, *A&A*, 537, L8
- Cardelli, J. A., Clayton, G. C., & Mathis, J. S. 1989, *ApJ*, 345, 245
- Carollo, C. M., Stiavelli, M., de Zeeuw, P. T., & Mack, J. 1997, *AJ*, 114, 2366
- Carroll, S. M., Press, W. H., & Turner, E. L. 1992, *ARA&A*, 30, 499
- Carswell, R. F., Hilliard, R. L., Strittmatter, P. A., Taylor, D. J., & Weymann, R. J. 1975, *ApJ*, 196, 351

- Cenko, S. B., et al. 2009, *ApJ*, 693, 1484
- Chabrier, G. 2003, *PASP*, 115, 763
- Chabrier, G. 2003, *Publications of the Astronomical Society of the Pacific*, 115, 763
- Chang, Y.-Y., van der Wel, A., Rix, H.-W., Wuyts, S., Zibetti, S., Ramkumar, B., & Holden, B. 2013, *ApJ*, 762, 83
- Charlot, S., & Fall, S. M. 2000, *ApJ*, 539, 718
- Chen, H., et al. 2009, *ApJ*, 691, 152
- . 2011, *ApJL*, 727, L53
- Chen, H.-W. 2012, *MNRAS*, 419, 3039
- Christensen, L., D'Odorico, S., Pettini, M., Belokurov, V., Evans, N. W., Kellogg, M., & Vernet, J. 2010, *MNRAS*, 406, 2616
- Christensen, L., Hjorth, J., & Gorosabel, J. 2004, *A&A*, 425, 913
- Christensen, L., Vreeswijk, P. M., Sollerman, J., Thöne, C. C., Le Flo'ch, E., & Wiersema, K. 2008, *A&A*, 490, 45
- Christensen, L., et al. 2012a, *MNRAS*, 427, 1973
- . 2012b, *MNRAS*, 427, 1953
- Chwolson, O. 1924, *Astronomische Nachrichten*, 221, 329
- Cimatti, A., et al. 2004, *Nature*, 430, 184
- . 2008, *A&A*, 482, 21
- Clark, P. C., Glover, S. C. O., Klessen, R. S., & Bromm, V. 2011, *ApJ*, 727, 110
- Clemens, C., Krühler, T., Greiner, J., Kupcu Yoldas, A., Yoldas, A., & Szokoly, G. 2008, *GCN*, 7834
- Coles, P. 2001, in *Astronomical Society of the Pacific Conference Series*, Vol. 252, *Historical Development of Modern Cosmology*, ed. V. J. Martínez, V. Trimble, & M. J. Pons-Bordería, 21
- Coles, P., & Lucchin, F. 1995, *Cosmology. The origin and evolution of cosmic structure*
- Colless, M., et al. 2001, *MNRAS*, 328, 1039
- Copetti, M. V. F., Mallmann, J. A. H., Schmidt, A. A., & Castañeda, H. O. 2000, *A&A*, 357, 621
- Costa, E., et al. 1997, *Nature*, 387, 783
- Cowie, L. L., & Barger, A. J. 2008, *ApJ*, 686, 72
- Cowie, L. L., Lilly, S. J., Gardner, J., & McLean, I. S. 1988, *ApJL*, 332, L29
- Crighton, N., Hennawi, J. F., & Prochaska, J. X. 2013, submitted to *ApJL*

- Crommelin, A. C. D. 1919, *The Observatory*, 42, 368
- Cucchiara, A., et al. 2011, *ApJ*, 736, 7
- D'Avanzo, P., et al. 2010, *A&A*, 522, A20
- Davis, T. M., & Lineweaver, C. H. 2004, *PASA*, 21, 97
- de Ugarte Postigo, A., et al. 2010, *A&A*, 513, A42
- de Vaucouleurs, G. 1948, *Annales d'Astrophysique*, 11, 247
- . 1959, *Handbuch der Physik*, 53, 311
- Deharveng, J. M., Buat, V., & Bowyer, S. 1990, *A&A*, 236, 351
- Dekel, A., & Krumholz, M. R. 2013, *MNRAS*, 432, 455
- Dekel, A., et al. 2009, *Nature*, 457, 451
- D'Elia, V., et al. 2010, *A&A*, 523, A36
- Dessauges-Zavadsky, M., D'Odorico, S., Schaerer, D., Modigliani, A., Tapken, C., & Vernet, J. 2010, *A&A*, 510, A26
- Dicke, R. H., Peebles, P. J. E., Roll, P. G., & Wilkinson, D. T. 1965, *ApJ*, 142, 414
- Dickinson, M., Papovich, C., Ferguson, H. C., & Budavári, T. 2003, *ApJ*, 587, 25
- D'Odorico, S., et al. 2006, in *Society of Photo-Optical Instrumentation Engineers (SPIE) Conference Series*, Vol. 6269, Society of Photo-Optical Instrumentation Engineers (SPIE) Conference Series
- Draine, B. T. 2003, *ARA&A*, 41, 241
- Dressler, A. 1980, *ApJ*, 236, 351
- Ebeling, H., Barrett, E., Donovan, D., Ma, C.-J., Edge, A. C., & van Speybroeck, L. 2007, *ApJL*, 661, L33
- Eddington, A. S. 1919, *The Observatory*, 42, 119
- Efstathiou, G., & Rees, M. J. 1988, *MNRAS*, 230, 5P
- Einstein, A. 1936, *Science*, 84, 506
- Elíasdóttir, Á., et al. 2009, *ApJ*, 697, 1725
- Elliott, J., Greiner, J., Khochfar, S., Schady, P., Johnson, J. L., & Rau, A. 2012, *A&A*, in press, arXiv:1202.1225
- Ellison, S. L., Yan, L., Hook, I. M., Pettini, M., Wall, J. V., & Shaver, P. 2001, *A&A*, 379, 393
- Erb, D. K., Pettini, M., Shapley, A. E., Steidel, C. C., Law, D. R., & Reddy, N. A. 2010, *ApJ*, 719, 1168

Erb, D. K., Shapley, A. E., Pettini, M., Steidel, C. C., Reddy, N. A., & Adelberger, K. L. 2006, *ApJ*, 644, 813

Faber, S. M. 1973, *ApJ*, 179, 731

Fan, X., et al. 2001, *AJ*, 122, 2833

—. 2004, *AJ*, 128, 515

Förster Schreiber, N. M., et al. 2006, *ApJ*, 645, 1062

—. 2009, *ApJ*, 706, 1364

Franx, M., et al. 2003, *ApJL*, 587, L79

Freeman, K. C. 1970, *ApJ*, 160, 811

Fruchter, A. S., et al. 2006, *Nature*, 441, 463

Fryer, C. L., Woosley, S. E., & Hartmann, D. H. 1999, *ApJ*, 526, 152

Fukugita, M., Hogan, C. J., & Peebles, P. J. E. 1998, *ApJ*, 503, 518

Fumagalli, M., Prochaska, J. X., Kasen, D., Dekel, A., Ceverino, D., & Primack, J. R. 2011, *MNRAS*, 418, 1796

Fynbo, J. P. U., Krogager, J.-K., Venemans, B., Noterdaeme, P., Vestergaard, M., Møller, P., Ledoux, C., & Geier, S. 2013a, *ApJS*, 204, 6

Fynbo, J. P. U., Prochaska, J. X., Sommer-Larsen, J., Dessauges-Zavadsky, M., & Møller, P. 2008, *ApJ*, 683, 321

Fynbo, J. P. U., et al. 2001, *A&A*, 369, 373

—. 2003, *A&A*, 406, L63

—. 2005, *ApJ*, 633, 317

—. 2009, *ApJS*, 185, 526

—. 2010, *MNRAS*, 408, 2128

—. 2011, *MNRAS*, 413, 2481

—. 2013b, *ArXiv e-prints*

Fynbo, J. U., Burud, I., & Møller, P. 2000, *A&A*, 358, 88

Fynbo, J. U., Møller, P., & Warren, S. J. 1999, *MNRAS*, 305, 849

Galama, T. J., & Wijers, R. A. M. J. 2001, *ApJL*, 549, L209

Galama, T. J., et al. 1998, *Nature*, 395, 670

Gamow, G. 1948, *Nature*, 162, 680

- Gebhardt, K., et al. 2000, *ApJL*, 539, L13
- Gehrels, N., Ramirez-Ruiz, E., & Fox, D. B. 2009, *ARA&A*, 47, 567
- Gehrels, N., et al. 2004, *ApJ*, 611, 1005
- Geier, S., Richard, J., Man, A. W. S., Krühler, T., Toft, S., Marchesini, D., & Fynbo, J. P. U. 2013, *ApJ*, 777, 87
- Genzel, R., et al. 2006, *Nature*, 442, 786
- Gerhard, O. 2002, *Space Sci. Rev.*, 100, 129
- Giavalisco, M. 2002, *ARA&A*, 40, 579
- Goldoni, P. 2011, *Astronomische Nachrichten*, 332, 227
- Goldoni, P., Royer, F., François, P., Horrobin, M., Blanc, G., Vernet, J., Modigliani, A., & Larsen, J. 2006, in *SPIE Conf. Ser.*, Vol. 6269
- Golenetskii, S., Aptekar, R., Mazets, E., Pal'Shin, V., Frederiks, D., & Cline, T. 2008, *GCN*, 7854, 1
- Graham, A. W., & Driver, S. P. 2005, *PASA*, 22, 118
- Graham, J. F., Fruchter, A. S., Kewley, L. J., Levesque, E. M., Levan, A. J., Tanvir, N. R., Reichart, D. E., & Nysewander, M. 2009, in *AIPC Ser.*, Vol. 1133, 269–272
- Greif, T. H., Springel, V., White, S. D. M., Glover, S. C. O., Clark, P. C., Smith, R. J., Klessen, R. S., & Bromm, V. 2011, *ApJ*, 737, 75
- Greiner, J., et al. 2008, *PASP*, 120, 405
- . 2009, *ApJ*, 693, 1610
- . 2011, *A&A*, 526, A30
- Groot, P. J., et al. 1998, *ApJL*, 493, L27
- Haehnelt, M. G., Steinmetz, M., & Rauch, M. 2000, *ApJ*, 534, 594
- Harrison, E. R. 1970, *Phys. Rev. D*, 1, 2726
- Hayashi, M., et al. 2009, *ApJ*, 691, 140
- Hayes, M., et al. 2010, *Nature*, 464, 562
- Heath, D. J. 1977, *MNRAS*, 179, 351
- Hempel, A., Schaerer, D., Egami, E., Pelló, R., Wise, M., Richard, J., Le Borgne, J.-F., & Kneib, J.-P. 2008, *A&A*, 477, 55
- Hirschi, R., Meynet, G., & Maeder, A. 2005, *A&A*, 443, 581
- Hjorth, J., & Bloom, J. S. 2012, *The Gamma-Ray Burst - Supernova Connection*, 169–190

- Hjorth, J., et al. 2003, *Nature*, 423, 847
- . 2012, *ApJ*, 756, 187
- Hogg, D. W., et al. 2004, *ApJL*, 601, L29
- Hopkins, A. M. 2004, *ApJ*, 615, 209
- Hopkins, A. M., & Beacom, J. F. 2006, *ApJ*, 651, 142
- Horne, K. 1986, *PASP*, 98, 609
- Hubble, E. P. 1926, *ApJ*, 63, 236
- . 1936, *Realm of the Nebulae*
- Hunt, L., Palazzi, E., Rossi, A., Savaglio, S., Cresci, G., Klose, S., Michałowski, M., & Pian, E. 2011, *ApJL*, 736, L36
- Hurley, K. 2003, in *American Institute of Physics Conference Series, Vol. 662, Gamma-Ray Burst and Afterglow Astronomy 2001: A Workshop Celebrating the First Year of the HETE Mission*, ed. G. R. Ricker & R. K. Vanderspek, 153–155
- Ilbert, O., et al. 2006, *A&A*, 457, 841
- . 2009, *ApJ*, 690, 1236
- Izotov, Y. I., Stasinska, G., & Guseva, N. G. 2013, *ArXiv e-prints*
- Jakobsen, P. 1998, *A&A*, 331, 61
- Jakobsson, P., Vreeswijk, P. M., Xu, D., & Thöne, C. C. 2008, *GCN*, 7832
- Jakobsson, P., et al. 2005, *MNRAS*, 362, 245
- . 2006, *A&A*, 460, L13
- . 2012, *ApJ*, 752, 62
- Jarosik, N., et al. 2011, *ApJS*, 192, 14
- Jeans, J. H. 1902, *Royal Society of London Philosophical Transactions Series A*, 199, 1
- Juneau, S., et al. 2005, *ApJL*, 619, L135
- Kaiser, N. 1984, *ApJL*, 284, L9
- Kann, D. A., Klose, S., & Zeh, A. 2006, *ApJ*, 641, 993
- Kann, D. A., Laux, U., Klose, S., Ertel, S., & Greiner, J. 2008, *GCN*, 7829
- Kant, I. 1755, *Allgemeine Naturgeschichte und Theorie des Himmels*
- Kauffmann, G., et al. 2003, *MNRAS*, 346, 1055
- Kennicutt, Jr., R. C. 1989, *ApJ*, 344, 685

- . 1998a, *ARA&A*, 36, 189
- . 1998b, *ARA&A*, 36, 189
- Kewley, L. J., & Dopita, M. A. 2002, *ApJS*, 142, 35
- Kewley, L. J., Dopita, M. A., Sutherland, R. S., Heisler, C. A., & Trevena, J. 2001, *ApJ*, 556, 121
- Kewley, L. J., & Ellison, S. L. 2008, *ApJ*, 681, 1183
- Kewley, L. J., Geller, M. J., & Jansen, R. A. 2004, *AJ*, 127, 2002
- Kistler, M. D., Yüksel, H., Beacom, J. F., Hopkins, A. M., & Wyithe, J. S. B. 2009, *ApJL*, 705, L104
- Kistler, M. D., Yüksel, H., & Hopkins, A. M. 2013, ArXiv e-prints
- Klebesadel, R. W., Strong, I. B., & Olson, R. A. 1973, *ApJL*, 182, L85
- Kobulnicky, H. A., & Kewley, L. J. 2004a, *ApJ*, 617, 240
- . 2004b, *ApJ*, 617, 240
- Kocevski, D., & West, A. A. 2011, *ApJL*, 735, L8
- Kocevski, D., West, A. A., & Modjaz, M. 2009, *ApJ*, 702, 377
- Kodama, T., Tanaka, I., Kajisawa, M., Kurk, J., Venemans, B., De Breuck, C., Vernet, J., & Lidman, C. 2007, *MNRAS*, 377, 1717
- Komatsu, E., et al. 2011, *ApJS*, 192, 18
- Kriek, M., van Dokkum, P. G., Labbé, I., Franx, M., Illingworth, G. D., Marchesini, D., & Quadri, R. F. 2009, *ApJ*, 700, 221
- Kriek, M., et al. 2008, *ApJ*, 677, 219
- Krogager, J.-K., Fynbo, J. P. U., Møller, P., Ledoux, C., Noterdaeme, P., Christensen, L., Milvang-Jensen, B., & Sparre, M. 2012, *MNRAS*, 424, L1
- Krogager, J.-K., et al. 2013, *MNRAS*, 433, 3091
- Kroupa, P. 2001, *MNRAS*, 322, 231
- Krühler, T., et al. 2008, *ApJ*, 685, 376
- . 2011, *A&A*, 534, 108
- . 2012, *ApJ*, 758, 46
- . 2013, *A&A*, 557, A18
- Kurk, J. D., et al. 2008, in *Astronomical Society of the Pacific Conference Series*, Vol. 381, *Infrared Diagnostics of Galaxy Evolution*, ed. R.-R. Chary, H. I. Teplitz, & K. Sheth, 303–+
- Labbé, I., et al. 2010, *ApJL*, 716, L103

- Lanzetta, K. M., Wolfe, A. M., & Turnshek, D. A. 1995, *ApJ*, 440, 435
- Lanzetta, K. M., Wolfe, A. M., Turnshek, D. A., Lu, L., McMahon, R. G., & Hazard, C. 1991, *ApJS*, 77, 1
- Lara-López, M. A., et al. 2010, *A&A*, 521, L53
- Law, D. R., Steidel, C. C., Erb, D. K., Larkin, J. E., Pettini, M., Shapley, A. E., & Wright, S. A. 2009, *ApJ*, 697, 2057
- Law, D. R., Steidel, C. C., Shapley, A. E., Nagy, S. R., Reddy, N. A., & Erb, D. K. 2012a, *ApJ*, 759, 29
- . 2012b, *ApJ*, 745, 85
- Ledoux, C., Petitjean, P., Fynbo, J. P. U., Møller, P., & Srianand, R. 2006, *A&A*, 457, 71
- Lemaître, G. 1933, *Comptes Rendus de L'Academie des Sciences de Paris*, 196, 903
- Lemoine-Busserolle, M., Contini, T., Pelló, R., Le Borgne, J.-F., Kneib, J.-P., & Lidman, C. 2003, *A&A*, 397, 839
- Levan, A., et al. 2006, *ApJ*, 647, 471
- Levesque, E. M., Berger, E., Kewley, L. J., & Bagley, M. M. 2010a, *AJ*, 139, 694
- Levesque, E. M., Berger, E., Soderberg, A. M., & Chornock, R. 2011, *ApJ*, 739, 23
- Levesque, E. M., Soderberg, A. M., Kewley, L. J., & Berger, E. 2010b, *ApJ*, 725, 1337
- Lifshitz, E. 1946, *Journal of Physics, Academy of Sciences of the USSR*, 10, 116
- Lilly, S. J., & Cowie, L. L. 1987, in *Infrared astronomy with arrays*, ed. C. G. Wynn-Williams & E. E. Becklin, 473
- Lilly, S. J., Le Fevre, O., Hammer, F., & Crampton, D. 1996, *ApJL*, 460, L1
- Longair, M. S. 2008, *Galaxy Formation*
- Lowenthal, J. D., Hogan, C. J., Green, R. F., Woodgate, B., Caulet, A., Brown, L., & Bechtold, J. 1995, *ApJ*, 451, 484
- Lynden-Bell, D. 1967, *MNRAS*, 136, 101
- . 1969, *Nature*, 223, 690
- MacFadyen, A. I., & Woosley, S. E. 1999, *ApJ*, 524, 262
- Madau, P. 1995, *ApJ*, 441, 18
- Madau, P., Ferguson, H. C., Dickinson, M. E., Giavalisco, M., Steidel, C. C., & Fruchter, A. 1996, *MNRAS*, 283, 1388
- Madau, P., Pozzetti, L., & Dickinson, M. 1998, *ApJ*, 498, 106

- Maiolino, R., et al. 2008, *A&A*, 488, 463
- Maizy, A., Richard, J., de Leo, M. A., Pelló, R., & Kneib, J. P. 2010, *A&A*, 509, A105
- Malesani, D., Hjorth, J., Fynbo, J. P. U., Milvang-Jensen, B., Jakobsson, P., & Jaunsen, A. O. 2009, in *AIPC Ser.*, Vol. 1111, 513–519
- Malesani, D., et al. 2004, *ApJL*, 609, L5
- Manchado, A., et al. 2004, in *SPIE Conf. Ser.*, Vol. 5492, 1094–1104
- Mancini, C., et al. 2010, *MNRAS*, 401, 933
- Mannucci, F., Cresci, G., Maiolino, R., Marconi, A., & Gnerucci, A. 2010, *MNRAS*, 408, 2115
- Mannucci, F., Salvaterra, R., & Campisi, M. A. 2011, *MNRAS*, 414, 1263
- Mannucci, F., et al. 2009, *MNRAS*, 398, 1915
- Maraston, C. 2005, *MNRAS*, 362, 799
- Marchesini, D., van Dokkum, P. G., Förster Schreiber, N. M., Franx, M., Labbé, I., & Wuyts, S. 2009, *ApJ*, 701, 1765
- Marchesini, D., et al. 2007, *ApJ*, 656, 42
- McCarthy, P. J., et al. 2004, *ApJL*, 614, L9
- McGaugh, S. S. 1991, *ApJ*, 380, 140
- Melioli, C., de Gouveia Dal Pino, E. M., & Gerassate, F. G. 2013, *MNRAS*, 430, 3235
- Meusinger, H., Brunzendorf, J., & Laget, M. 2003, *Astronomische Nachrichten*, 324, 474
- Michałowski, M. J., Hjorth, J., Castro Cerón, J. M., & Watson, D. 2008, *ApJ*, 672, 817
- Michałowski, M. J., et al. 2012, *ApJ*, 755, 85
- Miller, G. E., & Scalo, J. M. 1979, *ApJS*, 41, 513
- Milvang-Jensen, B., Fynbo, J. P. U., Malesani, D., Hjorth, J., Jakobsson, P., & Møller, P. 2012a, *ApJ*, submitted
- . 2012b, *ApJ*, 756, 25
- Misawa, T., Charlton, J. C., Kobulnicky, H. A., Wakker, B. P., & Bland-Hawthorn, J. 2009, *ApJ*, 695, 1382
- Møller, P., & Warren, S. J. 1993, *A&A*, 270, 43
- Modigliani, A., et al. 2010, in *Society of Photo-Optical Instrumentation Engineers (SPIE) Conference Series*, Vol. 7737, Society of Photo-Optical Instrumentation Engineers (SPIE) Conference Series
- Modjaz, M., et al. 2008, *AJ*, 135, 1136

- Møller, P., Fynbo, J. P. U., & Fall, S. M. 2004, *A&A*, 422, L33
- Møller, P., Fynbo, J. P. U., Ledoux, C., & Nilsson, K. K. 2013, *MNRAS*, 430, 2680
- Møller, P., & Jakobsen, P. 1990, *A&A*, 228, 299
- Møller, P., Warren, S. J., Fall, S. M., Fynbo, J. U., & Jakobsen, P. 2002, *ApJ*, 574, 51
- Muzzin, A., et al. 2012, *ArXiv e-prints*
- Naab, T., Johansson, P. H., & Ostriker, J. P. 2009, *ApJL*, 699, L178
- Nagao, T., Maiolino, R., & Marconi, A. 2006, *A&A*, 459, 85
- Nakar, E. 2007, *Phys. Rep.*, 442, 166
- Newman, A. B., Ellis, R. S., Bundy, K., & Treu, T. 2012, *ApJ*, 746, 162
- Noll, S., et al. 2009, *A&A*, 499, 69
- Norberg, P., et al. 2001, *MNRAS*, 328, 64
- Noterdaeme, P., et al. 2012a, *A&A*, 547, L1
- . 2012b, *A&A*, 540, A63
- Onodera, M., et al. 2010, *ApJL*, 715, L6
- Oogi, T., & Habe, A. 2013, *MNRAS*, 428, 641
- Osterbrock, D. E. 1989, *Astrophysics of gaseous nebulae and active galactic nuclei*
- Osterbrock, D. E., & Ferland, G. J. 2006, *Astrophysics of gaseous nebulae and active galactic nuclei*
- Pagel, B. E. J., Edmunds, M. G., Blackwell, D. E., Chun, M. S., & Smith, G. 1979a, *MNRAS*, 189, 95
- . 1979b, *MNRAS*, 189, 95
- Partridge, R. B., & Peebles, P. J. E. 1967, *ApJ*, 147, 868
- Pei, Y. C. 1992, *ApJ*, 395, 130
- Pelló, R., Kneib, J.-P., Bolzonella, M., & Miralles, J. M. 1999, in *Astronomical Society of the Pacific Conference Series*, Vol. 191, *Photometric Redshifts and the Detection of High Redshift Galaxies*, ed. R. Weymann, L. Storrie-Lombardi, M. Sawicki, & R. Brunner, 241
- Pelló, R., Kneib, J. P., & Bruzual, G. 1998, *Ap&SS*, 263, 55
- Pelló, R., et al. 2007, *Highlights of Astronomy*, 14, 250
- Peng, C. 2010, in *Bulletin of the American Astronomical Society*, Vol. 42, *American Astronomical Society Meeting Abstracts #215*, 229.09
- Peng, C. Y., Ho, L. C., Impey, C. D., & Rix, H.-W. 2002, *AJ*, 124, 266

Penzias, A. A., & Wilson, R. W. 1965, *ApJ*, 142, 419

Pérez-Montero, E., et al. 2009, *A&A*, 495, 73

Perley, D. A., Bloom, J. S., Cenko, S. B., Levan, A. J., Chen, H., & Tanvir, N. R. 2011a, in *AAS Meeting Abstracts*, Vol. 217, 108.02

Perley, D. A., et al. 2009, *AJ*, 138, 1690

—. 2011b, *AJ*, 141, 36

Péroux, C., McMahon, R. G., Storrie-Lombardi, L. J., & Irwin, M. J. 2003, *MNRAS*, 346, 1103

Pettini, M., & Pagel, B. E. J. 2004, *MNRAS*, 348, L59

Pian, E., et al. 2006, *Nature*, 442, 1011

Pierini, D., Gordon, K. D., Witt, A. N., & Madsen, G. J. 2004, *ApJ*, 617, 1022

Piran, T. 1992, *ApJL*, 389, L45

—. 2004, *Reviews of Modern Physics*, 76, 1143

Planck Collaboration et al. 2013, *ArXiv e-prints*

Polletta, M., et al. 2007, *ApJ*, 663, 81

Pontzen, A., et al. 2008, *MNRAS*, 390, 1349

—. 2010, *MNRAS*, 402, 1523

Press, W. H., & Schechter, P. 1974, *ApJ*, 187, 425

Prochaska, J. X., Chen, H., & Bloom, J. S. 2006, *ApJ*, 648, 95

Prochaska, J. X., Dessauges-Zavadsky, M., Ramirez-Ruiz, E., & Chen, H.-W. 2008, *ApJ*, 685, 344

Prochaska, J. X., Gawiser, E., Wolfe, A. M., Cooke, J., & Gelino, D. 2003, *ApJS*, 147, 227

Prochaska, J. X., & Herbert-Fort, S. 2004, *PASP*, 116, 622

Prochaska, J. X., Herbert-Fort, S., & Wolfe, A. M. 2005, *ApJ*, 635, 123

Prochaska, J. X., et al. 2009, *ApJL*, 691, L27

Rafelski, M., Wolfe, A. M., & Chen, H.-W. 2011, *ApJ*, 736, 48

Rakic, O., Schaye, J., Steidel, C. C., Booth, C. M., Dalla Vecchia, C., & Rudie, G. C. 2013, *MNRAS*, 433, 3103

Rao, S. M., & Turnshek, D. A. 2000, *ApJS*, 130, 1

Rau, A., et al. 2010, *ApJ*, 720, 862

Rauch, M., Becker, G. D., Haehnelt, M. G., & Gauthier, J.-R. 2013, *ArXiv e-prints*

- Rauch, M., Becker, G. D., Haehnelt, M. G., Gauthier, J.-R., Ravindranath, S., & Sargent, W. L. W. 2011, *MNRAS*, 418, 1115
- Rauch, M., & Haehnelt, M. G. 2011, *MNRAS*, 412, L55
- Rauch, M., et al. 2008, *ApJ*, 681, 856
- Rees, M. J., & Ostriker, J. P. 1977, *MNRAS*, 179, 541
- Rhoads, J. E., Malhotra, S., Finkelstein, S. L., Fynbo, J. P. U., McLinden, E. M., Richardson, M. L. A., & Tilvi, V. S. 2013, *ArXiv e-prints*, 1301.3140
- Richard, J., Jones, T., Ellis, R., Stark, D. P., Livermore, R., & Swinbank, M. 2011, *MNRAS*, 413, 643
- Richard, J., Pelló, R., Kneib, J.-P., Schaerer, D., Santos, M. R., & Ellis, R. 2004, in *Astrophysics and Space Science Library*, Vol. 301, *Astrophysics and Space Science Library*, ed. M. Plionis, 27
- Richard, J., Pelló, R., Schaerer, D., Le Borgne, J.-F., & Kneib, J.-P. 2006, *A&A*, 456, 861
- Richard, J., et al. 2010, *MNRAS*, 404, 325
- Robertson, B. E., & Ellis, R. S. 2012, *ApJ*, 744, 95
- Rossi, A., et al. 2011, *A&A*, submitted, arXiv:1202.1434
- Rubin, V. C. 1983, *Science*, 220, 1339
- Rubin, V. C., Thonnard, N., & Ford, Jr., W. K. 1977, *ApJL*, 217, L1
- Ryden, B. 2003, *Introduction to cosmology*
- Salim, S., et al. 2005, *ApJL*, 619, L39
- Salpeter, E. E. 1955, *ApJ*, 121, 161
- Salvaterra, R., et al. 2009, *Nature*, 461, 1258
- . 2011, *ApJ* in press, arXiv:1112.1700
- Savaglio, S. 2006, *New Journal of Physics*, 8, 195
- Savaglio, S., Fall, S. M., & Fiore, F. 2003, *ApJ*, 585, 638
- Savaglio, S., Glazebrook, K., & Le Borgne, D. 2009, *ApJ*, 691, 182
- Savaglio, S., et al. 2005, *ApJ*, 635, 260
- . 2012, *MNRAS*, 420, 627
- Sbarufatti, B., et al. 2008, *GCN*, 7828, 1
- Schady, P., et al. 2007, *MNRAS*, 377, 273
- . 2010, *MNRAS*, 401, 2773

- . 2012, *A&A*, 537, A15
- Schaerer, D., et al. 2007, *A&A*, 469, 47
- Schechter, P. 1976, *ApJ*, 203, 297
- Schechter, P. L. 2002, in *Lighthouses of the Universe: The Most Luminous Celestial Objects and Their Use for Cosmology*, ed. M. Gilfanov, R. Sunyaev, & E. Churazov, 3–540
- Schlafly, E. F., & Finkbeiner, D. P. 2011, *ApJ*, 737, 103
- Schlegel, D. J., Finkbeiner, D. P., & Davis, M. 1998, *ApJ*, 500, 525
- Schmidt, M. 1963, *Nature*, 197, 1040
- Schmidt, M., Schneider, D. P., & Gunn, J. E. 1995, *AJ*, 110, 68
- Schulze, S., et al. 2012, *A&A*, 546, A20
- Sersic, J. L. 1968, *Atlas de galaxias australes*
- Shapley, A. E. 2011, *ARA&A*, 49, 525
- Shen, S., Mo, H. J., White, S. D. M., Blanton, M. R., Kauffmann, G., Voges, W., Brinkmann, J., & Csabai, I. 2003, *MNRAS*, 343, 978
- Silk, J. 1967, *Nature*, 215, 1155
- . 1968, *ApJ*, 151, 459
- Silk, J., & Wyse, R. F. G. 1993, *Phys. Rep.*, 231, 293
- Skrutskie, M. F., et al. 2006, *AJ*, 131, 1163
- Smith, H. E., Cohen, R. D., Burns, J. E., Moore, D. J., & Uchida, B. A. 1989, *ApJ*, 347, 87
- Smith, H. E., Margon, B., & Jura, M. 1979, *ApJ*, 228, 369
- Smith, R. W. 1982, *The expanding universe: astronomy's "Great Debate" 1900 - 1931.*
- Smoot, G. F., et al. 1992, *ApJL*, 396, L1
- Spite, M., Spite, F., & Bonifacio, P. 2012, *Memorie della Societa Astronomica Italiana Supplementi*, 22, 9
- Stanek, K. Z., et al. 2003, *ApJL*, 591, L17
- . 2006, , 56, 333
- Steidel, C. C., Adelberger, K. L., Shapley, A. E., Pettini, M., Dickinson, M., & Giavalisco, M. 2003, *ApJ*, 592, 728
- Steidel, C. C., Giavalisco, M., Dickinson, M., & Adelberger, K. L. 1996a, *AJ*, 112, 352
- Steidel, C. C., Giavalisco, M., Pettini, M., Dickinson, M., & Adelberger, K. L. 1996b, *ApJL*, 462, L17

- Stockton, A., McGrath, E., & Canalizo, G. 2005, in *Bulletin of the American Astronomical Society*, Vol. 37, American Astronomical Society Meeting Abstracts, 1293
- Storrie-Lombardi, L. J., & Wolfe, A. M. 2000, *ApJ*, 543, 552
- Stoughton, C., et al. 2002, *AJ*, 123, 485
- Svensson, K. M., et al. 2012, *MNRAS*, 421, 25
- Tanvir, N. R., Levan, A. J., Fruchter, A. S., Hjorth, J., Hounsell, R. A., Wiersema, K., & Tunncliffe, R. 2013, *ArXiv e-prints*
- Tanvir, N. R., et al. 2004, *MNRAS*, 352, 1073
- . 2009, *Nature*, 461, 1254
- . 2012, *MNRAS* submitted, arXiv:1201.6074
- Taylor, E. N., Franx, M., Glazebrook, K., Brinchmann, J., van der Wel, A., & van Dokkum, P. G. 2010, *ApJ*, 720, 723
- Thöne, C. C., Fynbo, J. P. U., Goldoni, P., et al. 2011, *A&A* submitted
- Thöne, C. C., et al. 2008, *ApJ*, 676, 1151
- Thorsen, T. J. 2011, Master's thesis, Niels Bohr Institute, Copenhagen University, Juliane Maries Vej 30, DK-2100 Copenhagen O, Denmark
- Tody, D. 1993, in *ASPC Ser.*, Vol. 52, *Astronomical Data Analysis Software and Systems II*, 173
- Toft, S., Franx, M., van Dokkum, P., Förster Schreiber, N. M., Labbe, I., Wuyts, S., & Marchesini, D. 2009, *ApJ*, 705, 255
- Toft, S., Gallazzi, A., Zirm, A., Wold, M., Zibetti, S., Grillo, C., & Man, A. 2012, *ApJ*, 754, 3
- Toft, S., et al. 2007, *ApJ*, 671, 285
- Tolman, R. C. 1934, *Proceedings of the National Academy of Science*, 20, 169
- Tremonti, C. A., et al. 2004, *ApJ*, 613, 898
- Treyer, M., et al. 2007, *ApJS*, 173, 256
- Trimble, V. 2013, *ArXiv e-prints*
- Trujillo, I., Cenarro, A. J., de Lorenzo-Cáceres, A., Vazdekis, A., de la Rosa, I. G., & Cava, A. 2009, *ApJL*, 692, L118
- Trujillo, I., et al. 2006a, *MNRAS*, 373, L36
- . 2006b, *ApJ*, 650, 18
- Tytler, D., O'Meara, J. M., Suzuki, N., & Lubin, D. 2000, *Physica Scripta Volume T*, 85, 12
- van de Sande, J., et al. 2011, *ApJL*, 736, L9

- . 2012, ArXiv e-prints
- van der Wel, A., et al. 2011, *ApJ*, 730, 38
- van Dokkum, P. G., & Brammer, G. 2010, *ApJL*, 718, L73
- van Dokkum, P. G., Kriek, M., & Franx, M. 2009, *Nature*, 460, 717
- van Dokkum, P. G., et al. 2003, *ApJL*, 587, L83
- . 2010, *ApJ*, 709, 1018
- van Paradijs, J., et al. 1997, *Nature*, 386, 686
- Vergani, S. D., et al. 2011, *A&A*, 535, A127
- Vernet, J., et al. 2011a, *A&A*, 536, A105
- . 2011b, *A&A*, 536, A105
- Visvanathan, N., & Sandage, A. 1977, *ApJ*, 216, 214
- Vreeswijk, P. M., et al. 2004, *A&A*, 419, 927
- Warren, S. J., Møller, P., Fall, S. M., & Jakobsen, P. 2001, *MNRAS*, 326, 759
- Watson, D., et al. 2011, *ApJ*, 741, 58
- Weatherley, S. J., Warren, S. J., Møller, P., Fall, S. M., Fynbo, J. U., & Croom, S. M. 2005, *MNRAS*, 358, 985
- Welty, D. E., & Crowther, P. A. 2010, *MNRAS*, 404, 1321
- Weymann, R. J., Carswell, R. F., & Smith, M. G. 1981, *ARA&A*, 19, 41
- White, S. D. M., & Rees, M. J. 1978, *MNRAS*, 183, 341
- Wilson, J. C., et al. 2003, in *Society of Photo-Optical Instrumentation Engineers (SPIE) Conference Series*, Vol. 4841, *Society of Photo-Optical Instrumentation Engineers (SPIE) Conference Series*, ed. M. Iye & A. F. M. Moorwood, 451–458
- Wolf, C., & Podsiadlowski, P. 2007, *MNRAS*, 375, 1049
- Wolfe, A. M. 1986, *Royal Society of London Philosophical Transactions Series A*, 320, 503
- Wolfe, A. M., Gawiser, E., & Prochaska, J. X. 2005, *ARA&A*, 43, 861
- Wolfe, A. M., Lanzetta, K. M., Foltz, C. B., & Chaffee, F. H. 1995, *ApJ*, 454, 698
- Wolfe, A. M., Lanzetta, K. M., Turnshek, D. A., & Oke, J. B. 1992, *ApJ*, 385, 151
- Woosley, S. E. 1993, *ApJ*, 405, 273
- Wright, A. E., Morton, D. C., Peterson, B. A., & Jauncey, D. L. 1979, *MNRAS*, 189, 611
- Wuyts, E., Rigby, J. R., Sharon, K., & Gladders, M. D. 2012, *ApJ* submitted, arXiv:1202.5267

- Wuyts, S., et al. 2011, *ApJ*, 742, 96
- Yoon, S., & Langer, N. 2005, *A&A*, 443, 643
- Yuan, T.-T., & Kewley, L. J. 2009, *ApJL*, 699, L161
- Zafar, T., Watson, D., Elíasdóttir, Á., Fynbo, J. P. U., et al. 2012, *ApJ*, submitted
- Zafar, T., Watson, D., Fynbo, J. P. U., Malesani, D., Jakobsson, P., & de Ugarte Postigo, A. 2011, *A&A*, 532, A143
- Zahid, H. J., Kewley, L. J., & Bresolin, F. 2011, *ApJ*, 730, 137
- Zeldovich, Y. B. 1972, *MNRAS*, 160, 1P
- Zirm, A. W., et al. 2007, *ApJ*, 656, 66
- . 2008, *ApJ*, 680, 224
- Zwicky, F. 1933, *Helvetica Physica Acta*, 6, 110